AD 923562

FG

Copy number 24

Report number (14) MDC-A2181

# (6) Comparison Of The Basic F-4E And The Slatted F-4E Stall/Near Stall/Spin Characteristics,

(1)

(12) 277p.

Revision date

Revision letter

Issue date (11) 1 August 1973

Contract number (15) N00019-71-~~0265~~ -C-0265 NEW

Prepared by Ralph J. Pelikan

(10) Ralph J. Pelikan
Aerodynamics Engineer

Approved by W. A. Rousseau

W. A. Rousseau
Project Aerodynamic Engineer

Distribution limited to U.S. Gov't. agencies only;
Test and Evaluation; 13 NOV 1974. Other requests
for this document must be referred to
ASD/SD4 W-P AFB, Ohio, 45433

COPY AVAILABLE TO DDC DOES NOT
PERMIT FULLY LEGIBLE PRODUCTION

MCDONNELL AIRCRAFT COMPANY
Box 516, Saint Louis, Missouri 63166 – Tel. (314)232-0232

MCDONNELL DOUGLAS
CORPORATION

DDC
RECEIVED
NOV 11 1974
B

U63 111

ACCESSION for
NTIS White Section ☐
DDC Buff Section ☑
UNANNOUNCED ☐
JUSTIFICATION ..............................
..............................
BY ..............................
DISTRIBUTION/AVAILABILITY CODES
Dist. AVAIL. and/or SPECIAL
B

IN CONCURRENCE

F. Laacke

F. Laacke
Branch Manager, Aerodynamics

C.W. Miller

C. W. Miller
Manager, Aerodynamics

# ABSTRACT

This report presents the results of a six-degree-of-freedom analytical study to examine the stall/near stall/spin characteristics of the slatted F-4E aircraft. The basic F-4E and the slatted F-4E are analyzed and compared. Primary emphasis was directed toward the stall/near stall characteristics. Some analyses of spin characteristics and recovery techniques were also accomplished.

Departure and post stall characteristics are analyzed in detail. The primary points of interest are: (1) types of entry into the stall, (2) the effect of lateral-directional control inputs on the departure characteristics, (3) recovery techniques, and (4) evaluation of five methods that predict the point at which the aircraft becomes lateral-directionally unstable. Included ~~is a new technique created by McDonnell Aircraft Company.~~ The previous F-4 spin evaluation developed a dynamic model whereby rotary balance and forced oscillation data are utilized to compute the spin and spin entry motions. Further development of this dynamic model has been accomplished so that it can be used in both the unstalled and stalled flight regimes. Transition between the two regimes can be smoothly accomplished. Based on the investigation, recommendations are made relative to the techniques for recovery from a departure and for preventing departures through the use of control surfaces. A comparison of the slatted F-4E flight test stall/near stall characteristics with the analytical characteristics are qualitatively evaluated.

The analytical study of the spin entry and developed spins were performed primarily to note any differences in spin characteristics between the basic F-4E and the slatted F-4E. The effect of three c.g. positions are studied along with the effect of using recovery controls in a spin.

TABLE OF CONTENTS

| Section | Title | Page |
|---|---|---|
| | INCONCURRENCE ........................................ | i |
| | ABSTRACT ........................................ | ii |
| | TABLE OF CONTENTS ........................................ | iii |
| | LIST OF PAGES ........................................ | v |
| | LIST OF TABLES ........................................ | vi |
| | LIST OF FIGURES ........................................ | vii |
| | LIST OF SYMBOLS & NOMENCLATURE ........................ | xiv |
| 1 | INTRODUCTION ........................................ | 1.1 |
| 2 | WIND TUNNEL AND FREE FLIGHT MODEL TEST RESULTS FOR THE BASIC AND SLATTED F-4E | 2.1 |
| | 2.1 Wind Tunnel Static and Dynamic Investigation | 2.1 |
| | 2.1.1 Static Force & Moment Wind Tunnel Results | 2.1 |
| | 2.1.1.1 Longitudinal Characteristics | 2.1 |
| | 2.1.1.2 Lateral-Directional Characteristics | 2.2 |
| | 2.1.2 Dynamic Wind Tunnel Test Results | 2.3 |
| | 2.2 Free Flight Model Test Results | 2.3 |
| | 2.2.1 Free Flight Test Results | 2.3 |
| | 2.2.2 Helicopter Drop Model Results | 2.4 |
| 3. | STALL/NEAR STALL/DEPARTURE CHARACTERISTICS | 3.1 |
| | 3.1 Effects of Flight Maneuver On Departures | 3.2 |
| | 3.2 Effect of Rate of Entry On Departure | 3.6 |
| | 3.3 Effect of Aircraft Weight, C.G., and Inertia on Departure | 3.9 |
| | 3.4 Effect of Lateral-Directional Control Inputs on Departure | 3.9 |
| | 3.5 Recovery From Departure | 3.13 |
| | 3.6 Flight Test Qualitative Results | 3.14 |

TABLE OF CONTENTS (Cont'd)

| Section | Title | Page |
|---|---|---|
| 4 | SPIN CHARACTERISTICS | 4.1 |
| | 4.1 Spin Entry and Spin Mode Characteristics | 4.1 |
| | 4.2 Spin Recovery Characteristics | 4.2 |
| 5 | DEPARTURE PREDICTION TECHNIQUES | 5.1 |
| | 5.1 Directional Divergence Parameter "Dynamic $C_{n_\beta}$" | 5.1 |
| | 5.2 Lateral Control Divergence Parameter | 5.1 |
| | 5.2.1 Aileron Alone Divergence Parameter | 5.2 |
| | 5.2.2 Aileron/Rudder Divergence Parameter | 5.3 |
| | 5.2.3 Aileron Proportional To Rudder Divergence Criterion | 5.3 |
| | 5.3 $\beta$ Plus $\delta$ Axis Stability Indicator | 5.4 |
| 6 | CONCLUSIONS | 6.1 |
| | 6.1 Stall/Near Stall/Departure | 6.1 |
| | 6.2 Spin Characteristics | 6.2 |
| | 6.3 Divergence Criteria | 6.2 |
| 7 | RECOMMENDATIONS | 7.1 |
| 8 | REFERENCES | 8.1 |
| | APPENDICES | |
| | Appendix A: Slatted F-4E Aerodynamic Data | A.1 |
| | Appendix B: Basic F-4E Aerodynamic Data | B.1 |
| | Appendix C: Equations of Motion | C.1 |
| | Appendix D: The Use of Forced Oscillation Derivatives To Generate Linear Rotary Balance Data Below 35° Angle of Attack | D.1 |

## LIST OF PAGES

Title Page

i thru xix

1.1 thru 1.4

2.1 thru 2.13

3.1 thru 3.77

4.1 thru 4.22

5.1 thru 5.12

6.1 thru 6.2

7.1

8.1

A.1 thru A.47

B.1 thru B.49

C.1 thru C.7

D.1 thru D.18

## LIST OF TABLES

| Table No. | Title | Page |
|---|---|---|
| 1 | Aircraft Weights and Inertias | 3.2 |
| 2 | Stall Time History Summary | 3.4 |
| 3 | Effect of 1g Stall and Constant Bank Angle Turn on Departure | 3.7 |
| 4 | Effect of Rate of Entry On Departure | 3.8 |
| 5 | Effect of Aircraft, C.G. and Inertias On Departure | 3.10 |
| 6 | Effect of Lateral-Directional Controls Inputs on Departure | 3.12 |
| 7 | Spin Time History Summary | 4.2 |
| 8 | Spin Characteristics Summary | 4.3 |

## LIST OF FIGURES

| Figure No. | Title | Page |
|---|---|---|
| 1.1 | Reference Axes Angle of Attack And Angle of Sideslip Definition | 1.2 |
| 1.2 | Euler Angle Sequence And Sign Convention for, Forces, Moments, and Velocities | 1.3 |
| 1.3 | Thrust Vector Orientation and Sign Convention | 1.4 |
| 2.1 | Pitching Moment Coefficient Versus Angle of Attack | 2.5 |
| 2.2 | Normal Force Coefficient Versus Angle of Attack | 2.6 |
| 2.3 | Variation of Axial Force Coefficient With Angle of Attack | 2.7 |
| 2.4 | Stabilator Effectiveness Versus Angle of Attack | 2.8 |
| 2.5 | Directional Stability Characteristics Versus Angle of Attack | 2.9 |
| 2.6 | Lateral Stability Characteristics | 2.10 |
| 2.7 | Aileron Effectiveness Versus Angle of Attack | 2.11 |
| 2.8 | Rudder-Effectiveness Versus Angle of Attack | 2.12 |
| 2.9 | Yawing Moment Coefficient Versus Spin Rate Coefficient | 2.13 |
| 3.1 | 1g Stall Maneuver (Configuration 2, Ailerons Only Entry Rate 1.2 Deg/Sec.) | 3.15 |
| 3.2 | Constant Bank Angle Turn-Stall Maneuver (Configuration 2, Ailerons Only, Entry Rate 1.2 Deg./Sec.) | 3.18 |
| 3.3 | 1g Stall Maneuver (Configuration 2, Aileron/Rudder Entry Rate 2.4 Deg/Sec.) | 3.21 |
| 3.4 | Constant Bank Angle Turn-Stall Maneuver (Configuration 2, Aileron/Rudder, Entry Rate 1.2 Deg/Sec) | 3.24 |
| 3.5 | 1g Stall Maneuver (Configuration 2, Rudder Only Entry Rate 2.4 Deg/Sec.) | 3.27 |
| 3.6 | Constant Bank Angle Turn-Stall Maneuver (Configuration 2, Rudder Only, Entry Rate 1.2 Deg/Sec.) | 3.30 |
| 3.7 | 1g Stall Maneuver (Configuration 2, No Lateral-Directional Control, Entry Rate 1.2 Deg/Sec.) | 3.33 |

LIST OF FIGURES

| Figure No. | Title | Page |
|---|---|---|
| 3.8 | 1g Stall Maneuver (Configuration 2, No Lateral-Directional Control, Entry Rate 2.4 Deg/Sec.) | 3.36 |
| 3.9 | 1g Stall Maneuver (Configuration 2, No Lateral-Directional Control, Entry Rate 5.6 Deg/Sec.) | 3.39 |
| 3.10 | 1g Stall Maneuver (Configuration 2, No Lateral-Directional Control, Entry Rate 10.0 Deg/Sec.) | 3.42 |
| 3.11 | 1g Stall Maneuver (Configuration 2, No Lateral-Directional Control, Entry Rate 15.0 Deg/Sec.) | 3.45 |
| 3.12 | Constant Bank Angle Turn-Stall Maneuver (Configuration 1, Aileron/Rudder, Entry Rate 1.3 Deg/Sec.) | 3.48 |
| 3.13 | Constant Bank Angle Turn-Stall Maneuver (Configuration 1, Aileron/Rudder, Entry Rate 3.2 Deg/Sec.) | 3.51 |
| 3.14 | Constant Bank Angle Turn-Stall Maneuver (Configuration 1, Aileron/Rudder, Entry Rate 10.0 Deg/Sec.) | 3.54 |
| 3.15 | 1g Stall Maneuver (Configuration 3, Ailerons Only, Entry Rate 1.4 Deg/Sec.) | 3.57 |
| 3.16 | 1g Stall Maneuver (Configuration 1, Ailerons Only, Entry Rate 1.4 Deg/Sec.) | 3.60 |
| 3.17 | Constant Bank Angle Turn-Stall Maneuver (Configuration 3, Ailerons Only, Entry Rate 1.2 Deg/Sec.) | 3.63 |
| 3.18 | Constant Bank Angle Turn-Stall Maneuver (Configuration 1, Ailerons Only, Entry Rate 1.3 Deg/Sec.) | 3.66 |
| 3.19 | Recovery From A Constant Bank Angle Turn-Stall (Same as Figure 3.2 except recovery is initiated after departure.) | 3.69 |
| 3.20 | Recovery From A 1g Stall (Same as Figure 3.1 except recovery is initiated after departure.) | 3.72 |
| 3.21 | Recovery From A Constant Bank Angle Turn-Stall (Same as a Figure 3.13 except recovery is initiated after departure.) | 3.75 |

## LIST OF FIGURES (Cont'd)

| Figure No. | Title | Page |
|---|---|---|
| 4.1 | Spin Characteristics (Pro-Spin Controls, Entry At Mach No. 0.6, Alt. 40,000 Ft., Configuration 1) | 4.7 |
| 4.2 | Spin Characteristics (Pro-Spin Controls, Entry At Mach No. 0.6, Alt. 40,000 Ft., Configuration 2) | 4.10 |
| 4.3 | Spin Characteristics (Pro-Spin Controls, Entry At Mach No. 0.6, Alt. 40,000 Ft., Configuration 3) | 4.13 |
| 4.4 | Spin Characteristics (Pro-Spin Controls, Entry At Mach No. 0.6, Alt. 40,000 Ft., Configuration 5 for Basic F-4E, Configuration 3 for slatted F-4E) | 4.16 |
| 4.5 | Spin Characteristics (Spin Entry from a Constant Bank Angle Turn, At Mach No. 0.6, Alt. 20,000 ft., Configuration 1) | 4.19 |
| 5.1 | $C_{n_\beta}$ Dynamic Departure Summary | 5.7 |
| 5.2 | Aileron Alone Divergence Parameter | 5.8 |
| 5.3 | Aileron/Rudder Divergence Parameter ($\delta_r = -K\beta$, $K = 2.0$) | 5.9 |
| 5.4 | Aileron Proportional to Rudder ($\delta_r/\delta_a = K_2$) | 5.10 |
| 5.5 | $\beta$ Plus $\delta$ Axis Stability Indicator Summary (Basic F-4E) | 5.11 |
| 5.6 | $\beta$ Plus $\delta$ Axis Stability Indicator Summary (Slatted F-4E) | 5.12 |

## LIST OF FIGURES (CONT.)

| Figure No. | Title | Page |
|---|---|---|
| A.1 | Variation of Normal Force Coefficient with Angle of Attack (slatted F-4E) | A.7 |
| A.2 | Variation of Axial Force Coefficient with Angle of Attack (slatted F-4E) | A.8 |
| A.3 | Variation of Pitching Moment with Angle of Attack (slatted F-4E) | A.9 |
| A.4 | Variation of Rolling Moment Coefficient with sideslip Angle (slatted F-4E) | A.10 |
| A.5 | Variation of Side Force Coefficient with Sideslip Angle (slatted F-4E) | A.12 |
| A.6 | Variation of Yawing Moment Coefficient with Sideslip Angle (slatted F-4E) | A.14 |
| A.7 | Yawing Moment Asymmetries Versus Angle of Attack (slatted F-4E) | A.16 |
| A.8 | Normal Force Due To Stabilator Deflection Versus Angle of Attack (slatted F-4E) | A.17 |
| A.9 | Axial Force Due To Stabilator Deflection Versus Angle of Attack (slatted F-4E) | A.19 |
| A.10 | Pitching Moment Due To Stabilator Deflection Versus Angle of Attack (slatted F-4E) | A.21 |
| A.11 | Yawing Moment Due To Aileron Deflection Versus Angle of Attack (slatted F-4E) | A.23 |
| A.12 | Rolling Moment Due to Aileron Deflection Versus Angle of Attack (slatted F-4E) | A.25 |
| A.13 | Yawing Moment Due To Rudder Deflection Versus Angle of Attack (slatted F-4E) | A.28 |
| A.14 | Rolling Moment Due to Rudder Deflection Versus Angle of Attack (slatted F-4E) | A.32 |
| A.15 | Side Force Due to Rudder Deflection Versus Angle of Attack (slatted F-4E) | A.33 |

LIST OF FIGURES (Cont'd)

| Figure No. | Title | Page |
|---|---|---|
| A.16 | Summary Of Pitching Moment Coefficient Versus Angle Of Attack (slatted F-4E) | A.34 |
| A.17 | Rolling Moment Due to Rolling Velocity Versus Angle Of Attack (slatted F-4E) | A.35 |
| A.18 | Rolling Moment Due to Yawing Velocity Versus Angle Of Attack (slatted F-4E) | A.36 |
| A.19 | Yawing Moment Due to Rolling Velocity Versus Angle Of Attack (slatted F-4E) | A.37 |
| A.20 | Yawing Moment Due to Yawing Velocity Versus Angle Of Attack (slatted F-4E) | A.38 |
| A.21 | Side Force Due to Rolling Velocity Versus Angle Of Attack (slatted F-4E) | A.39 |
| A.22 | Side Force Due to Yawing Velocity Versus Angle Of Attack (slatted F-4E) | A.40 |
| A.23 | Rolling Moment Due to Rolling Velocity Versus Angle Of Attack (adjustments on slatted F-4E) | A.41 |
| A.24 | Variation of Yawing Moment Coefficient with Spin Coefficient (slatted F-4E) | A.42 |
| A.25 | Variation of Rolling Moment Coefficient with Spin Coefficient (slatted F-4E) | A.44 |
| A.26 | Variation of Side Force Coefficient with Spin Coefficient (slatted F-4E) | A.46 |
| B.1 | Variation of Normal Force Coefficient with Angle of Attack (basic F-4E) | B.7 |
| B.2 | Variation of Axial Force Coefficient with Angle of Attack (basic F-4E) | B.8 |
| B.3 | Variation of Pitching Moment with Angle of Attack (basic F-4E) | B.9 |
| B.4 | Variation of Rolling Coefficient with Sideslip Angle (basic F-4E) | B.10 |
| B.5 | Variation of Side Force Coefficient with Sideslip Angle (basic F-4E) | B.12 |

LIST OF FIGURES (Cont'd)

| Figure No. | Title | Page |
|---|---|---|
| B.6 | Variation of Yawing Moment Coefficient with Sideslip Angle (basic F-4E) | B.14 |
| B.7 | Yawing Moment Asymmetries Versus Angle of Attack (basic F-4E) | B.17 |
| B.8 | Normal Force Due To Stabilator Deflection Versus Angle of Attack (basic F-4E) | B.18 |
| B.9 | Axial Force Due to Stabilator Deflection Versus Angle of Attack (basic F-4E) | B.19 |
| B.10 | Pitching Moment Due to Stabilator Deflection Versus Angle of Attack (basic F-4E) | B.20 |
| B.11 | Yawing Moment Due to Aileron Deflection Versus Angle of Attack (basic F-4E) | B.21 |
| B.12 | Rolling Moment Due to Aileron Deflection Versus Angle of Attack (basic F-4E) | B.23 |
| B.13 | Yawing Moment Due to Rudder Deflection Versus Angle of Attack (basic F-4E) | B.27 |
| B.14 | Rolling Moment Due to Rudder Deflection Versus Angle of Attack (basic F-4E) | B.30 |
| B.15 | Side Force Due to Rudder Deflection Versus Angle of Attack (basic F-4E) | B.31 |
| B.16 | Asymmetric Yawing Moment Coefficient Versus Angle of Attack (basic and slatted F-4E) | B.32 |
| B.17 | Pitching Moment Due to Pitch Velocity Versus Angle of Attack (basic F-4E/slatted F-4E) | B.33 |
| B.18 | Rolling Moment Due to Rolling Velocity Versus Angle of Attack (basic F-4E) | B.34 |
| B.19 | Rolling Moment Due to Yawing Velocity Versus Angle of Attack (basic F-4E) | B.35 |
| B.20 | Yawing Moment Due to Rolling Velocity Versus Angle of Attack (basic F-4E) | B.36 |
| B.21 | Yawing Moment Due to Yawing Velocity Versus Angle of Attack (basic F-4E) | B.37 |

## LIST OF FIGURES (Cont'd)

| Figure No. | Title | Page |
|---|---|---|
| B.22 | Side Force Due to Rolling Velocity Versus Angle of Attack (basic F-4E) | B.38 |
| B.23 | Side Force Due to Yawing Velocity Versus Angle of Attack (basic F-4E) | B.39 |
| B.24 | Variation of Axial Force Coefficient with Spin Coefficient (basic F-4E/slatted F-4E) | B.40 |
| B.25 | Variation of Pitching Moment Coefficient with Spin Coefficient (basic F-4E/slatted F-4E) | B.41 |
| B.26 | Variation of Normal Force Coefficient with Spin Coefficient (basic F-4D/slatted F-4E) | B.43 |
| B.27 | Variation of Yawing Moment Coefficient with Spin Coefficient (basic F-4E) | B.44 |
| B.28 | Variation of Rolling Moment Coefficient with Spin Coefficient (basic F-4E) | B.45 |
| B.29 | Variation of Side Force Coefficient with Spin Coefficient (basic F-4E) | B.46 |
| D.1 | Slope of The Rotary Balance Moment Curves Versus Angle of Attack (basic F-4E) | D.9 |
| D.2 | Slope of The Rotary Balance Moment Curves Versus Angle of Attack (slatted F-4E) | D.10 |
| D.3 | Spin Characteristics (new and old rotary balance data on the basic F-4E) | D.11 |
| D.4 | Yawing Moment Coefficient At a Constant Spin Coefficient (basic F-4E) | D.15 |
| D.5 | Constant Bank Angle Turn-Stall (with and without rotary balance data) | D.16 |

## LIST OF SYMBOLS AND NOMENCLATURE

### Aerodynamic Coefficients

| | |
|---|---|
| $C_x$ | axial-force coefficient $\frac{F_x}{\frac{1}{2}\rho V^2 S}$ |
| $C_y$ | side-force coefficient $\frac{F_y}{\frac{1}{2}\rho V^2 S}$ |
| $C_z$ | normal-force coefficient $\frac{F_z}{\frac{1}{2}\rho V^2 S}$ |
| $C_l$ | rolling-moment coefficient $\frac{M_x}{\frac{1}{2}\rho V^2 Sb}$ |
| $C_m$ | pitching-moment coefficient $\frac{M_y}{\frac{1}{2}\rho V^2 S\bar{c}}$ |
| $C_n$ | yawing-moment coefficient $\frac{M_z}{\frac{1}{2}\rho V^2 Sb}$ |
| $C_{x_{\delta s}}$ | $\left(\frac{\partial C_x}{\partial \delta s}\right)$ |
| $C_{y_{\delta r}}$ | $\left(\frac{\partial C_y}{\partial \delta r}\right)$ |
| $C_{z_{\delta s}}$ | $\left(\frac{\partial C_z}{\partial \delta s}\right)$ |
| $C_{l_{\delta a}}$ | $\left(\frac{\partial C_l}{\partial \delta a}\right)$ |
| $C_{l_{\delta r}}$ | $\left(\frac{\partial C_l}{\partial \delta r}\right)$ |
| $C_{m_{\delta s}}$ | $\left(\frac{\partial C_m}{\partial \delta s}\right)$ |
| $C_{n_{\delta r}}$ | $\left(\frac{\partial C_n}{\partial \delta r}\right)$ |
| $C_{n_{\delta a}}$ | $\left(\frac{\partial C_n}{\partial \delta a}\right)$ |
| $C_{y_r}$ | $\left(\frac{\partial C_y}{\partial \left(\frac{rb}{2V}\right)}\right)$ |
| $C_{y_p}$ | $\left(\frac{\partial C_y}{\partial \left(\frac{pb}{2V}\right)}\right)$ |

# LIST OF SYMBOLS AND NOMENCLATURE

## Aerodynamic Coefficients (Cont'd)

| | |
|---|---|
| $C_{l_r}$ | $\left(\frac{\partial C_l}{\partial \left(\frac{rb}{2V}\right)}\right)$ |
| $C_{l_p}$ | $\left(\frac{\partial C_l}{\partial \left(\frac{pb}{2V}\right)}\right)$ |
| $C_{n_r}$ | $\left(\frac{\partial C_n}{\partial \left(\frac{rb}{2V}\right)}\right)$ |
| $C_{n_p}$ | $\left(\frac{\partial C_n}{\partial \left(\frac{pb}{2V}\right)}\right)$ |
| $C_{y_{\dot{\beta}}}$ | $\left(\frac{\partial C_y}{\partial \left(\frac{\dot{\beta} b}{2V}\right)}\right)$ |
| $C_{l_{\dot{\beta}}}$ | $\left(\frac{\partial C_l}{\partial \left(\frac{\dot{\beta} b}{2V}\right)}\right)$ |
| $C_{m_q}$ | $\left(\frac{\partial C_m}{\partial \left(\frac{qc}{2V}\right)}\right)$ |
| $C_{n_{\dot{\beta}}}$ | $\left(\frac{\partial C_n}{\partial \left(\frac{\dot{\beta} b}{2V}\right)}\right)$ |
| $\Delta C_x$ | change in $C_x$ due to spin rate coefficient, $\frac{\Omega_v b}{2V}$ |
| $\Delta C_y$ | change in $C_y$ due to spin rate coefficient, $\frac{\Omega_v b}{2V}$ |
| $\Delta C_z$ | change in $C_z$ due to spin rate coefficient, $\frac{\Omega_v b}{2V}$ |
| $\Delta C_l$ | change in $C_l$ due to spin rate coefficient, $\frac{\Omega_v b}{2V}$ |
| $\Delta C_m$ | change in $C_m$ due to spin rate coefficient, $\frac{\Omega_v b}{2V}$ |
| $\Delta C_n$ | change in $C_n$ due to spin rate coefficient, $\frac{\Omega_v b}{2V}$ |

## LIST OF SYMBOLS AND NOMENCLATURE (Cont'd)

| Symbol | Description | Units |
|---|---|---|
| b | wing span (38.67 ft.) | ft. |
| $\bar{c}$ | mean aerodynamic chord (16.032 ft.) | ft. |
| c.g. | center of gravity | $\%\bar{c}$ |
| G.W. | gross weight | lb. |
| $F_x$ | force along $X_B$, positive forward (Figure 1.2) | lb. |
| $F_y$ | force along $Y_B$, positive to the right (Figure 1.2) | lb. |
| $F_z$ | force along $A_B$, positive down (Figure 1.2) | lb. |
| $I_x$ | moment of inertia about X body axis | slug-ft$^2$ |
| $I_y$ | moment of inertia about Y body axis | slug-ft$^2$ |
| $I_z$ | moment of inertia about Z body axis | slug-ft$^2$ |
| $I_{xz}$ | product of inertia about X and Z body axes | slug-ft$^2$ |
| $\bar{i}$ | unit vector along $X_B$ positive forward | |
| $\bar{j}$ | unit vector along $Y_B$ positive to the right | |
| $\bar{k}$ | unit vector along $Z_B$ positive down | |
| $M_x$ | moment about $X_B$, positive clockwise looking forward (Figure 1.2) | ft-lb |
| $M_y$ | moment about $Y_B$, positive clockwise looking right (Figure 1.2) | ft-lb |
| $M_z$ | moment about $Z_B$, positive clockwise looking down (Figure 1.2) | ft-lb |
| m | mass of aircraft | slugs |
| P | roll rate, positive right wing down | deg/sec |
| p | roll rate, positive right wind down | rad/sec |
| Q | pitch rate, positive nose up | deg/sec |
| q | pitch rate, positive nose up | rad/sec |
| $q_o$ | dynamic pressure | lb/ft$^2$ |

## LIST OF SYMBOLS AND NOMENCLATURE (Cont'd)

| Symbol | Description | Units |
|---|---|---|
| R | yaw rate, positive nose right | deg/sec |
| r | yaw rate, positive nose right | rad/sec |
| $p_o$, $q_o$, $r_o$ | oscillatory components of p, q and r | rad/sec |
| $p_s$, $q_s$, $r_s$ | steady state components of p, q and r | rad/sec |
| S | wing area (530 $ft^2$) | $ft^2$ |
| T | thrust | lb. |
| t | time | sec. |
| u, v, w | components of V along the $X_B$, $Y_B$, and $Z_B$ Axes, respectively | ft/sec |
| V | total linear velocity | ft/sec |
| $X_B$ | The body axis in the plane of symmetry which is parallel to the fuselage waterline. Positive forward (Figure 1.2) | |
| $Y_B$ | The body axis perpendicular to the plane of symmetry. Positive toward the right wing. (Figure 1.2) | |
| $Z_B$ | The body axis perpendicular to the $X_B$ - $Y_B$ axes. Positive toward the bottom of the aircraft. (Figure 1.2) | |
| $X_E$ | horizontal earth axis which lies in a vertical plane containing the $X_B$ axis at time zero (Figure 1.2) | |
| $Y_E$ | horizontal earth axis perpendicular to the $X_E$ - $Z_E$ plane (Figure 1.2) | |
| $Z_E$ | vertical earth axis pointing downward towards the center of the earth (Figure 1.2) | |
| $X_W$ | Axis in plane of symmetry which is parallel to the wing chord plane (Figure 1.1) | |
| $Y_W$ | Axis perpendicular to the plane of symmetry (Figure 1.1) | |
| $Z_W$ | Axis perpendicular to the $X_W$ - $Y_W$ axes (Figure 1.1) | |
| $X_n$ | distance along $X_B$ from aircraft c.g. to reference point on thrust vector, positive forward of c.g. (Figure 1.3) | ft. |

## LIST OF SYMBOLS AND NOMENCLATURE (Cont'd)

| Symbol | Description | Units |
|---|---|---|
| $Y_n$ | distance along $Y_B$ from aircraft c.g. to reference point on thrust vector, positive to right of c.g. (Figure 1.3) | ft. |
| $Z_n$ | distance along $Z_B$ from aircraft c.g. to reference point on thrust vector, positive down from c.g. (Figure 1.3) | ft. |
| ANU | Aircraft Nose Up | |
| ANR | Aircraft Nose Right | |
| ANL | Aircraft Nose Left | |
| RWD | Right Wing Down | |
| LWD | Left Wing Down | |

## LIST OF SYMBOLS AND NOMENCLATURE (Cont'd)

### Greek Symbols

| Symbol | Description | Units |
|---|---|---|
| $\alpha_W$ | wing angle of attack (Figure 1.1) | deg. |
| $\alpha_b$ | body axis angle of attack ($\alpha_W - 1^\circ$) (Figure 1.1) | deg. |
| $\beta$ | sideslip angle (Figure 1.1) | deg. |
| $\delta_a$ | aileron and spoiler positive when aileron on right wing is deflected down | deg. |
| $\delta_r$ | rudder deflection ~ trailing edge left is positive | deg. |
| $\delta_s$ | stabilator deflection ~ trailing edge down is positive | deg. |
| $\theta$ | Euler angle representing the total angular movement of X body axis from horizontal plane measured in a vertical plane, positive airplane nose up (Figure 1.2) | deg. |
| $\phi$ | Euler angle between Y body axis and horizontal plane measured in the YZ body plane, positive right wing down (Figure 1.2) | deg. |
| $\psi$ | Euler angle representing the horizontal component of total angular deflection of X body axis from reference position in horizontal plane, positive airplane nose right (Figure 1.2) | deg. |
| $\phi_t$ | angle of rotation from the $X_B - Y_B$ plane of a plane parallel to the $X_B$ axis containing the thrust vector, positive $Y_B$ into $Z_B$ (Figure 1.3) | deg. |
| $\lambda_t$ | Angle between thrust vector and a line parallel to the $X_B$ measured in the plane parallel to the $X_B$ axis and containing the thrust vector. Positive when counter-clockwise looking down along axis that was parallel to $Z_B$ before rotation, $\phi_t$ (Figure 1.3) | deg. |
| $\Omega$ | total angular velocity | rad/sec |
| $\Omega_V$ | component of total aircraft angular velocity parallel to velocity vector, positive clockwise looking along velocity vector | rad/sec |
| $\Omega_e$ | engine rotation rate positive clockwise looking forward | rpm, rad/sec |
| $\rho$ | air density | slug/ft$^3$ |

## 1. Introduction

In recent years the F-4 has been operated at the extreme of the maneuvering envelope which requires operating the airplane near stall. As a result an increase in loss of control and departure/spin incidents have occurred. The installation of the two-position leading edge slats, which significantly improves the maneuvering characteristics of the F-4 due to improved lateral-directional stability at high angles of attack, should reduce the number of such incidents.

As a contractual requirement, in retrofiting all existing F-4E aircraft with leading edge slats, an analytical study was to be made of the stall/near stall/spin characteristics of the F-4 airplane. The main objectives of this study were:

1) To define the lateral-directional handling characteristics of the slatted F-4E.
2) To make a recommendation on the need for a stall/near stall/spin flight test program.

To perform this analysis the McDonnell-Douglas Six-Degree-of-Freedom (SDF) digital computer program was utilized. The reference angle of attack and angle of sideslip definitions for this study are presented in Figure 1.1. The Euler angle sequence and sign convention used is presented in Figure 1.2. Likewise, the thrust vector orientation is presented in Figure 1.3.

As previously mentioned the addition of leading edge slats alters the F-4E aerodynamic characteristics at high angles of attack. Therefore, a complete high angle of attack wind tunnel test program was undertaken to obtain both static and dynamic wind tunnel data.

# REFERENCE AXES ANGLE OF ATTACK AND ANGLE OF SIDESLIP DEFINITION

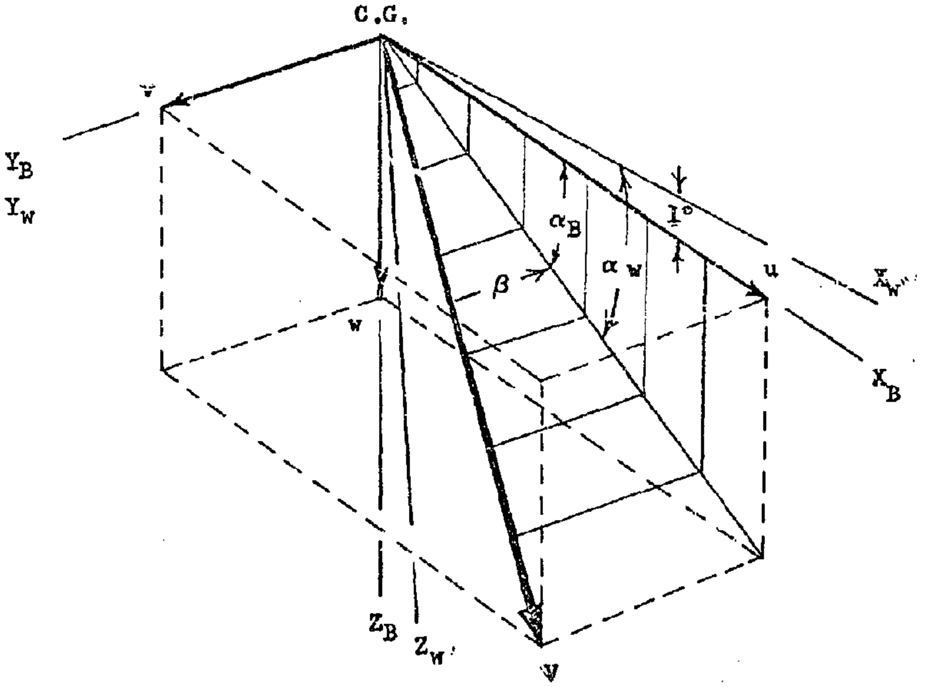

Figure 1.1

EULER ANGLE SEQUENCE
AND SIGN CONVENTION FOR, FORCES, MOMENTS, AND VELOCITIES

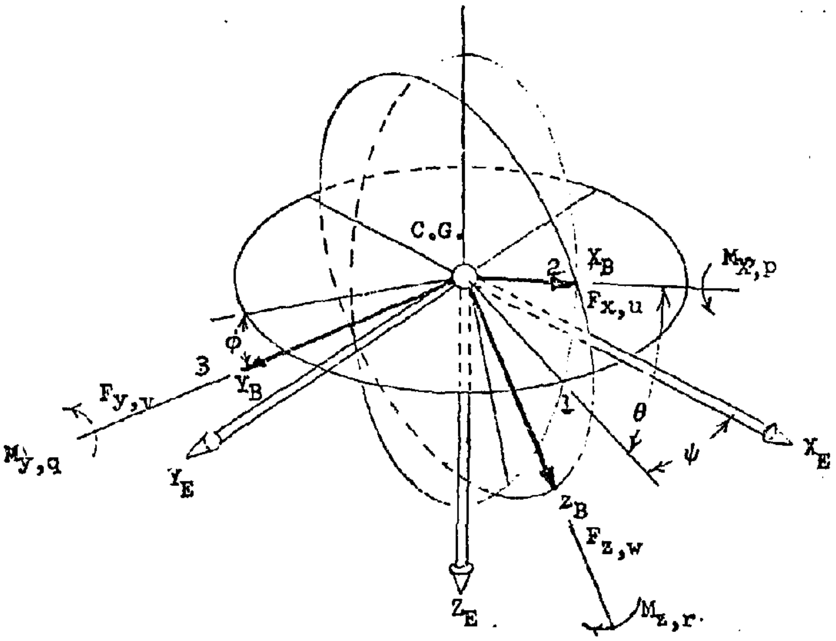

Figure 1.2

# THRUST VECTOR ORIENTATION and SIGN CONVENTION

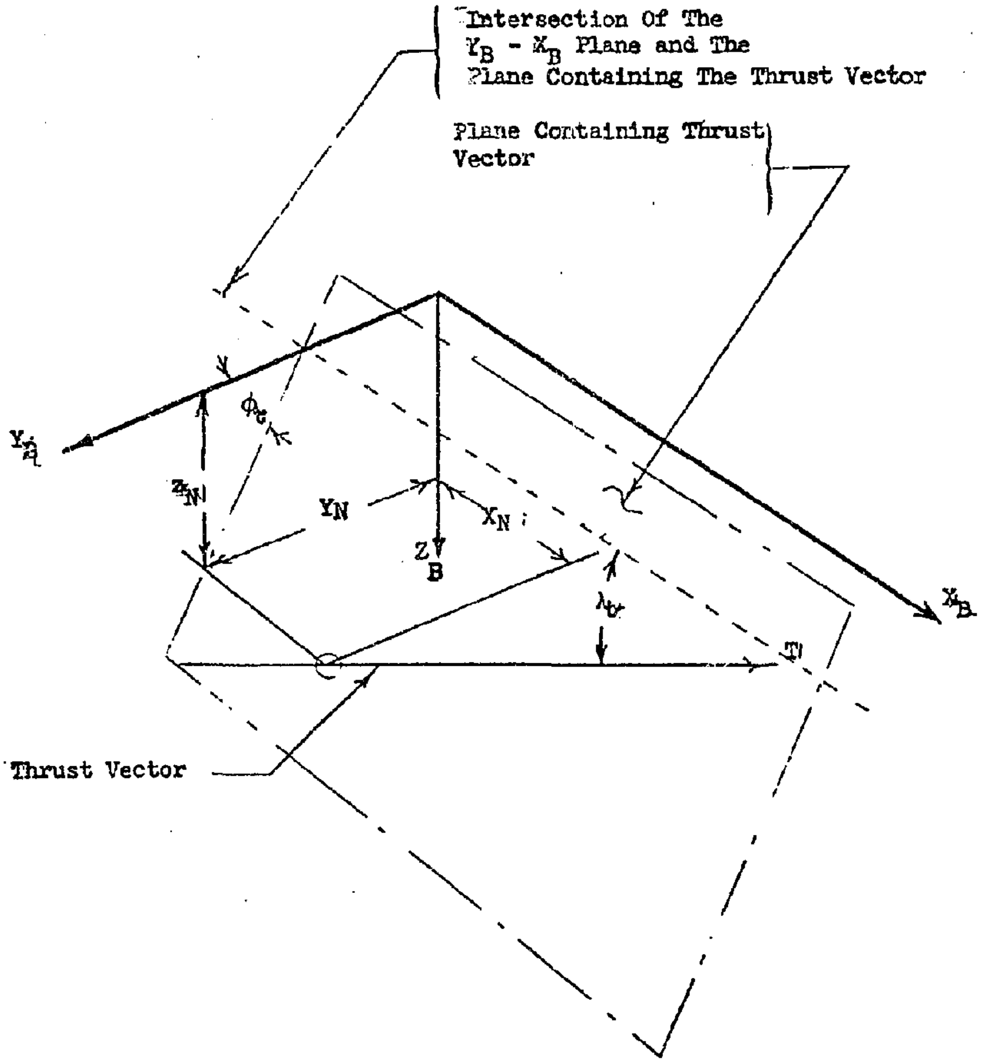
Intersection Of The
$Y_B$ - $X_B$ Plane and The
Plane Containing The Thrust Vector
Plane Containing Thrust Vector
$Y_B$
$X_B$
$Z_B$
$Z_N$
$Y_N$
$X_N$
$\phi_t$
$\lambda_t$
T'
Thrust Vector

Figure 1.3

## 2. Wind Tunnel and Free Flight Model Test Results For The Basic and Slatted F-4E

### 2.1 Wind Tunnel Static and Dynamic Investigation

2.1 Wind Tunnel Static and Dynamic Investigation - At the start of the program studies, a wind tunnel investigation of the F-4 with leading edge slats was conducted using various models.

a) 5% Scale Force & Moment Model
b) 6.67% Scale Force & Moment Model
c) 9.1% Scale Rotary Balance Model
d) 13% Scale Forced Oscillation Model

Some additional new data was obtained on the basic F-4 in the above tests, however, most of the basic F-4 wind tunnel data was obtained during the previous F-4 analytical spin evaluation study effort (Reference 1).

2.1.1 Static Force & Moment Wind Tunnel Results - The slatted F-4E wind tunnel data obtained were used to generate the static force and moment curves used in the analytical study for the slatted F-4E and can be found in Appendix A. A similar set of curves for the basic F-4E can be found in Appendix B. These data, which were obtained from Reference 2, were modified where appropriate to provide a better representation of the airplane.

2.1.1.1 Longitudinal Characteristics - The wind tunnel pitching moment and normal force curves for the slatted and non-slatted configurations are approximately the same above 25° wing angle-of-attack with some improvement in normal force due to slats below 20° wing angle-of-attack (see Figures 2.1 and 2.2). The axial force above 10° angle-of-attack is more positive due to a suction effect caused by the leading edge slats (see Figure 2.3).

Stabilator effectiveness data are obtained for $+7^\circ$ to $0^\circ$ and $0^\circ$ to $-21^\circ$ stabilator settings. Stabilator effectiveness is not affected by the addition of leading edge slats. The $+7^\circ$ stabilator setting is of particular interest for use in recoveries from departures and spins. A comparison of the stabilator power $C_{m_{\delta_S}}$ is shown in Figure 2.4. Above $60^\circ$ angle-of-attack a full forward stick motion ( $\delta_s = +7^\circ$) has little if any effect on increasing the nose down pitching moment over $0^\circ$ stabilator setting.

2.1.1.2 Lateral-Directional Characteristics - The lateral-directional stability characteristics are improved below $40^\circ$ angle of attack due to the addition of leading edge slats. However, above $40^\circ$ angle of attack the characteristics of both configurations are similar. The yawing moment asymmetries noted in Reference 1 on the basic F-4E are approximately the same as those of the slatted F-4E in both magnitude and direction. The directional stability characteristics at $\beta = 0$ are presented in Figure 2.5 for $0^\circ$ and $-21^\circ$ stabilator settings. As can be seen in Figure 2.5 the slatted F-4E directional stability characteristics are improved over those of the basic F-4E.

A comparison of the lateral stability characteristics for both configurations is presented in Figure 2.6. The slatted F-4E maintains a positive lateral stability throughout the angle of attack range while the basic F-4E has almost no lateral stability in the $20^\circ$ to $40^\circ$ angle-of-attack range.

The addition of the leading edge slats increased both the aileron and the rudder effectiveness in the 20° angle-of-attack region. The adverse yaw due to aileron deflection ($C_{n_{\delta_a}}$) is reduced up to a wing angle of attack of 30° due to the slats. These lateral-directional control comparisons are presented in Figures 2.7 and 2.8.

2.1.2 Dynamic Wind Tunnel Test Results - The data obtained from the forced oscillation and rotary balance tests were used in generating dynamic derivatives for the anlytical study for the slatted F-4E. These dynamic derivatives are presented in Appendix A. A similar set of curves for the basic F-4E can be found in Appendix B.

The most important of these test results is the yawing moment coefficient versus rotation rate which was obtained from the rotary balance tests. The leading edge slats adversely effect the yawing moment due to rotation rate in the 36° to 91° angle-of-attack range as shown in Figure 2.9. In general, the propelling $C_n$ which is apparent on the basic F-4E is higher in magnitude due to the addition of leading edge slats.

2.2 Free Flight Model Results - Free flight tests were made with a 13% scale model F-4E with and without slats. The tests were conducted in the NASA LRC 30 by 60 foot tunnel which included steady flight at high angles of attack and 1g stalls. The same model was also dropped from a helicopter. The results of these tests were used as a guide in this analytical study of the stall/near stall/spin regions.

2.2.1 Free Flight Tests Results - The results from the 13% scale free flight model wind tunnel test are found in Reference 3. The basic F-4E model was flown in a 1g stall from 27° to 28° wing angle of attack before the model diverged in yaw. The slatted F-4E was flown to 33° wing angle of attack before it diverged in yaw. It was noted that the use of the ailerons alone to control the lateral aircraft motions would cause both configurations to diverge at a much lower angle of attack.

2.2.2 Helicopter Drop Model Results - Helicopter drops of a 13% scale model of the F-4E were made by NASA LRC to investigate the stall spin characteristics. Both the basic F-4E and the slatted F-4E were tested. The spin characteristics of the two aircraft are similar. However, the only spin modes obtained occurred at a very low angle of attack (40° to 50°) in all cases. Both configurations recovered when pro-spin controls were neutralized.

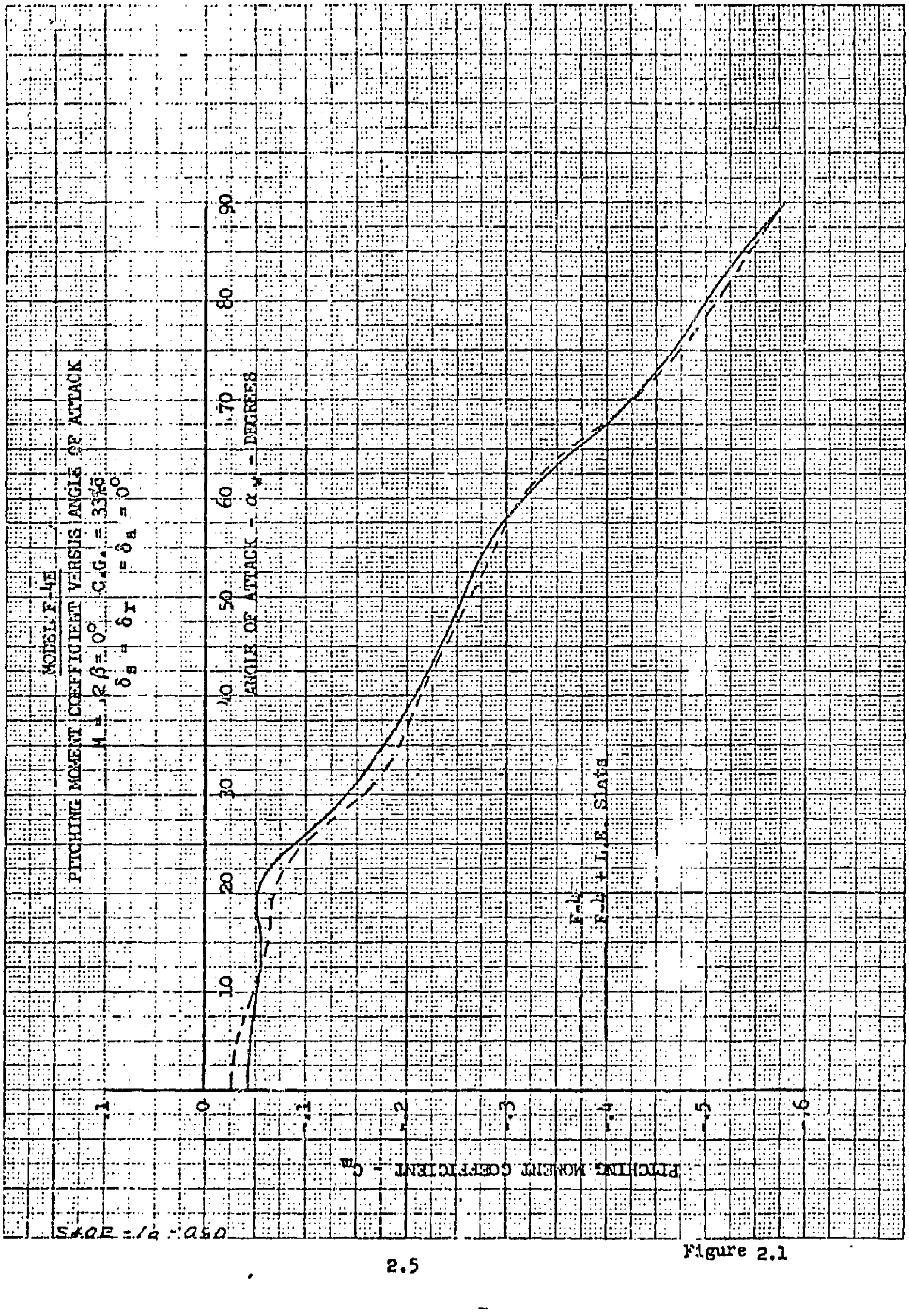
MODEL F-4E
PITCHING MOMENT COEFFICIENT VERSUS ANGLE OF ATTACK
M = .2 β = 0° C.G. = 33%c̄
δs = δr = δa = 0°
ANGLE OF ATTACK - α - DEGREES
10
20
30
40
50
60
70
80
90
PITCHING MOMENT COEFFICIENT - Cm
.1
0
-.1
-.2
-.3
-.4
-.5
-.6
F-4
F-4 + L.E. Slats

Figure 2.1

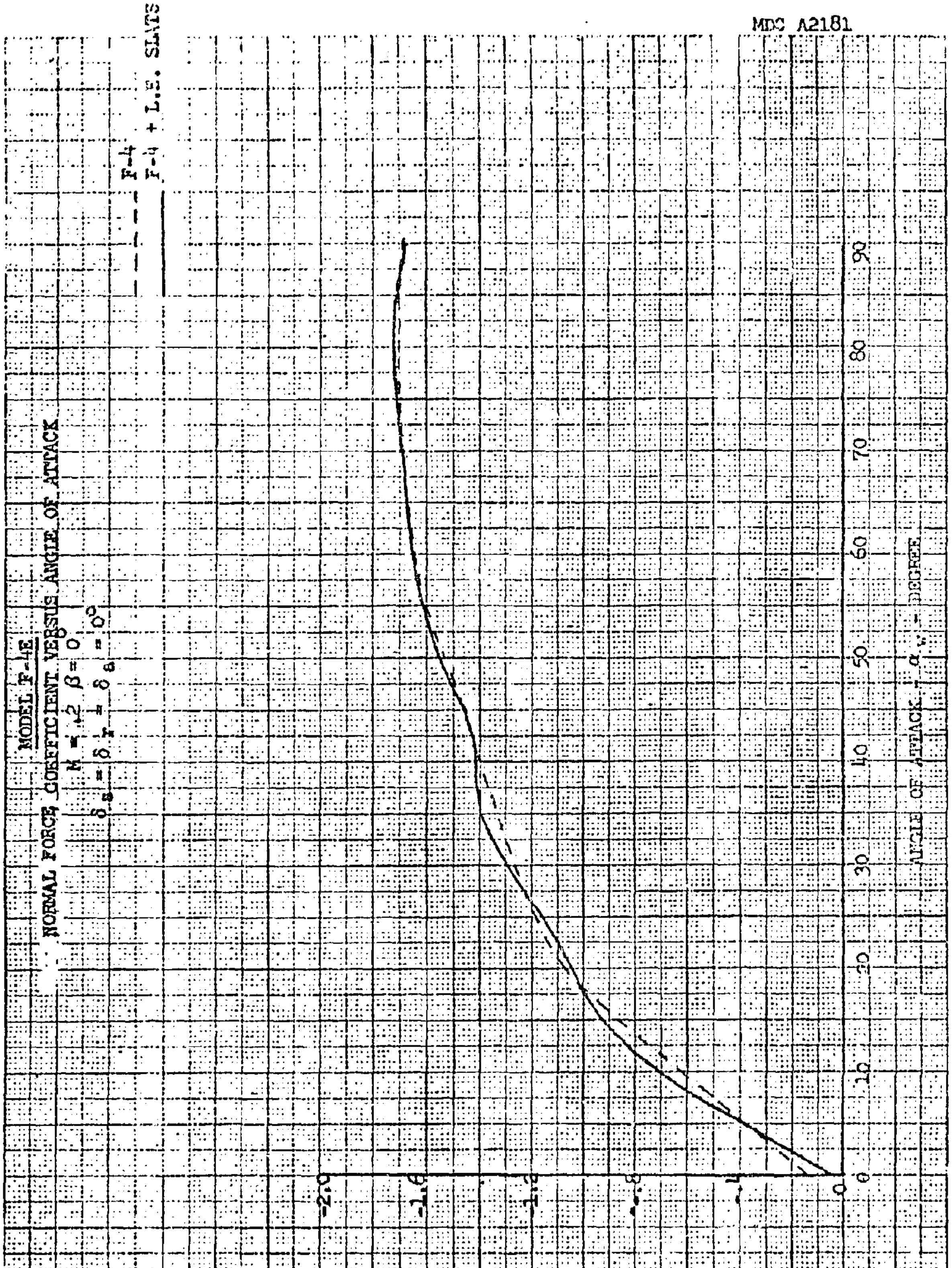
MODEL F-4E
NORMAL FORCE COEFFICIENT VERSUS ANGLE OF ATTACK
M = .2 β = 0°
δa = δr = δe = 0°
F-4
F-4 + L.E. SLATS
0
-.4
-.8
-1.2
-1.6
-2.0
NORMAL FORCE COEFFICIENT - $C_N$
0
10
20
30
40
50
60
70
80
90
ANGLE OF ATTACK - $\alpha_w$ - DEGREE
5402-Va-060

Figure 2.2

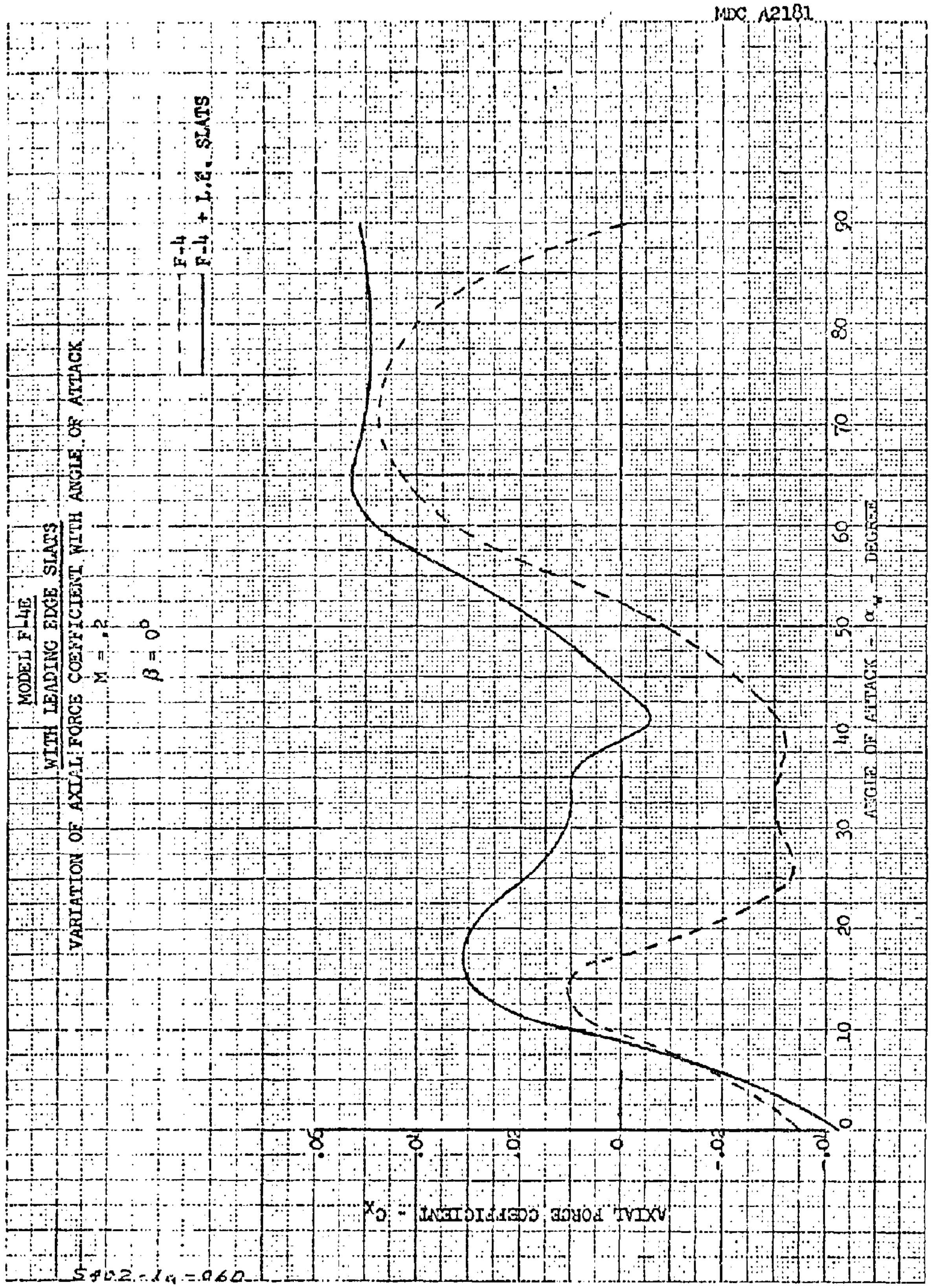

S402-1a-060

Figure 2.3

NATIONAL TRACING PAPER
INDIANAPOLIS INDIANA

UN [illegible]
LITHO IN U.S.A.

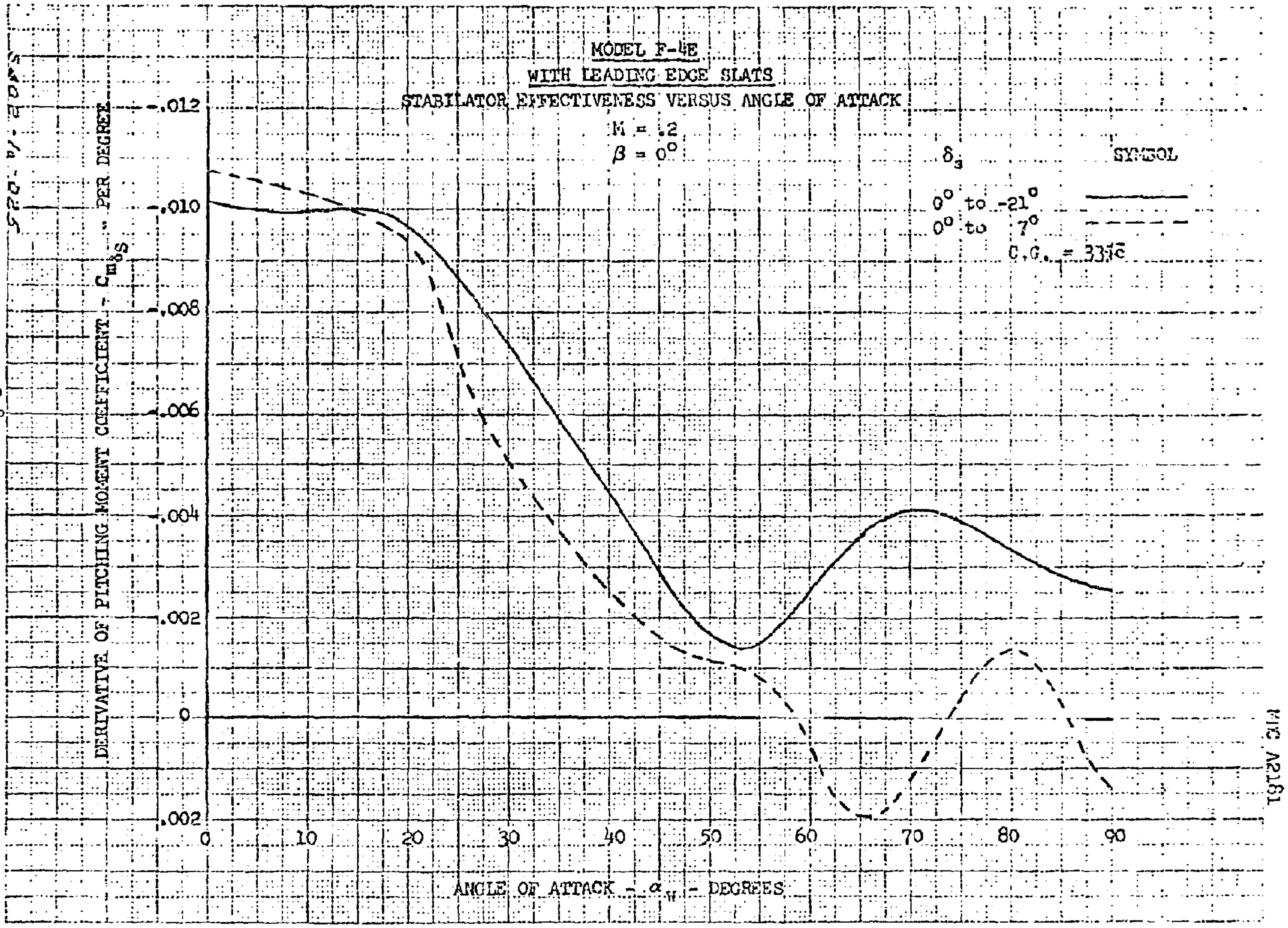
MODEL F-4E
WITH LEADING EDGE SLATS
STABILATOR EFFECTIVENESS VERSUS ANGLE OF ATTACK
$M = .2$
$\beta = 0^\circ$

Figure 2.4

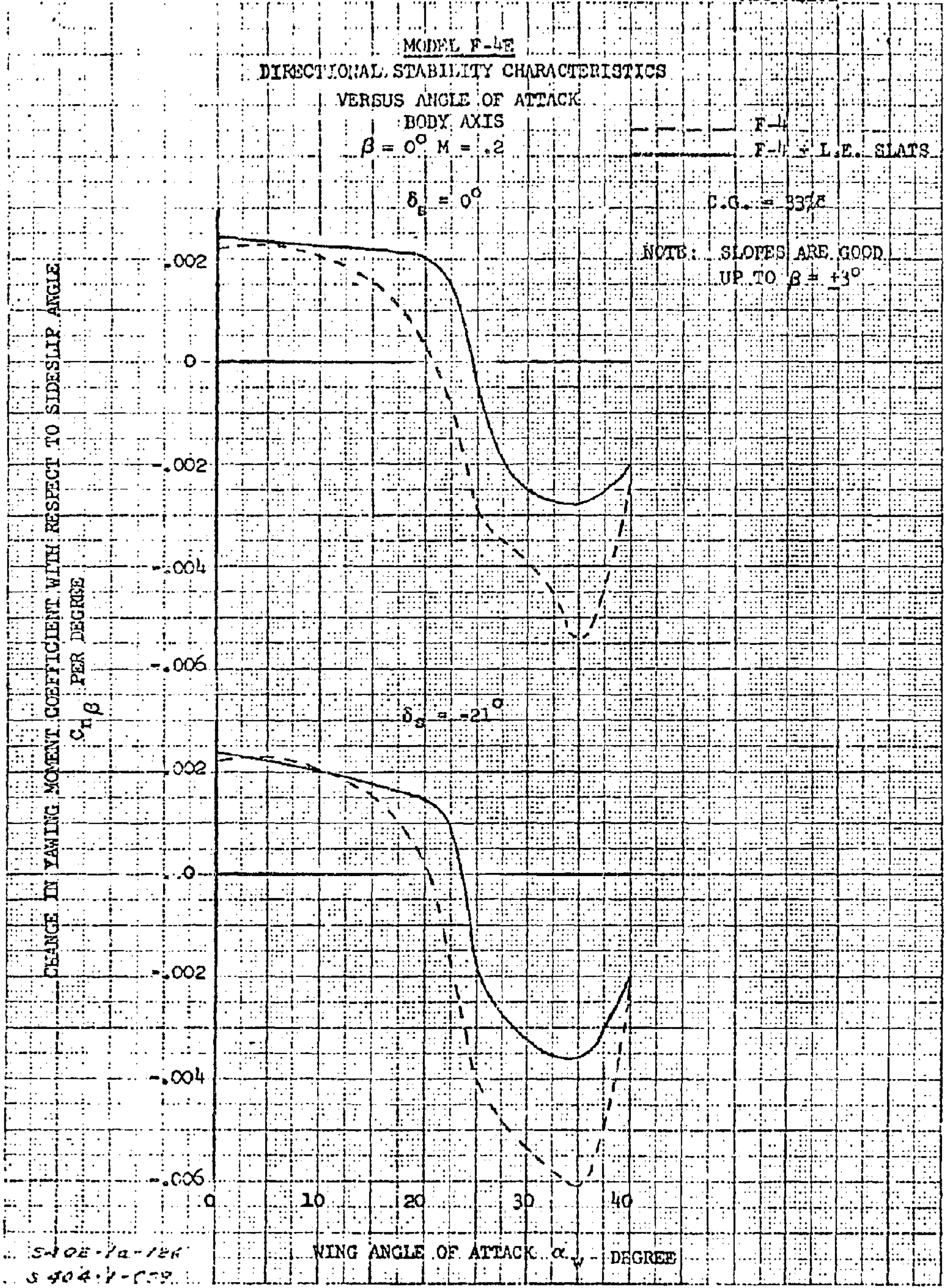
MODEL F-4E
DIRECTIONAL STABILITY CHARACTERISTICS
VERSUS ANGLE OF ATTACK
BODY AXIS
$\beta = 0^\circ$ M = .2
F-4
F-4 + L.E. SLATS
$\delta_s = 0^\circ$
C.G. = 33%c
NOTE: SLOPES ARE GOOD
UP TO $\beta = \pm 3^\circ$
$\delta_s = -21^\circ$
.002
0
-.002
-.004
-.006
.002
0
-.002
-.004
-.006
0
10
20
30
40
CHANGE IN YAWING MOMENT COEFFICIENT WITH RESPECT TO SIDESLIP ANGLE
$C_{n_\beta}$ PER DEGREE
WING ANGLE OF ATTACK $\alpha_w$ - DEGREE
S-402-7a-12K
S 404-7-C72

Figure 2.5

## MODEL F-4E
## LATERAL STABILITY CHARACTERISTICS VERSUS ANGLE OF ATTACK

BODY AXIS

$\beta = 0^\circ$ M = .2

NOTE: SLOPES ARE GOOD UP TO $\beta = \pm 3^\circ$

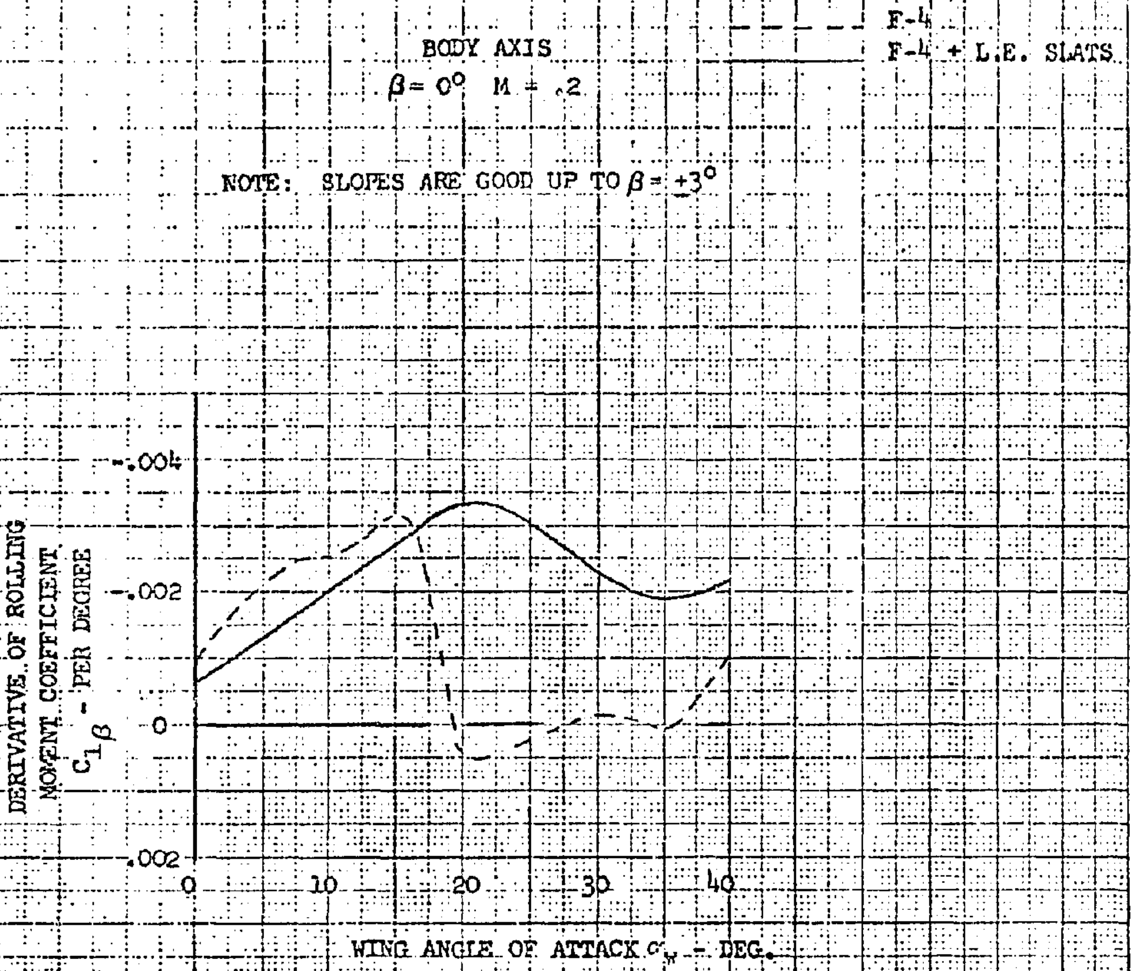

5402-10-126
5402-1-008

NATIONAL TRACING PAPER INDIANAPOLIS, INDIANA
UN 220 ... LITHO IN U.S.A.

Figure 2.6

MODEL F-4E

AILERON EFFECTIVENESS VERSUS
ANGLE OF ATTACK

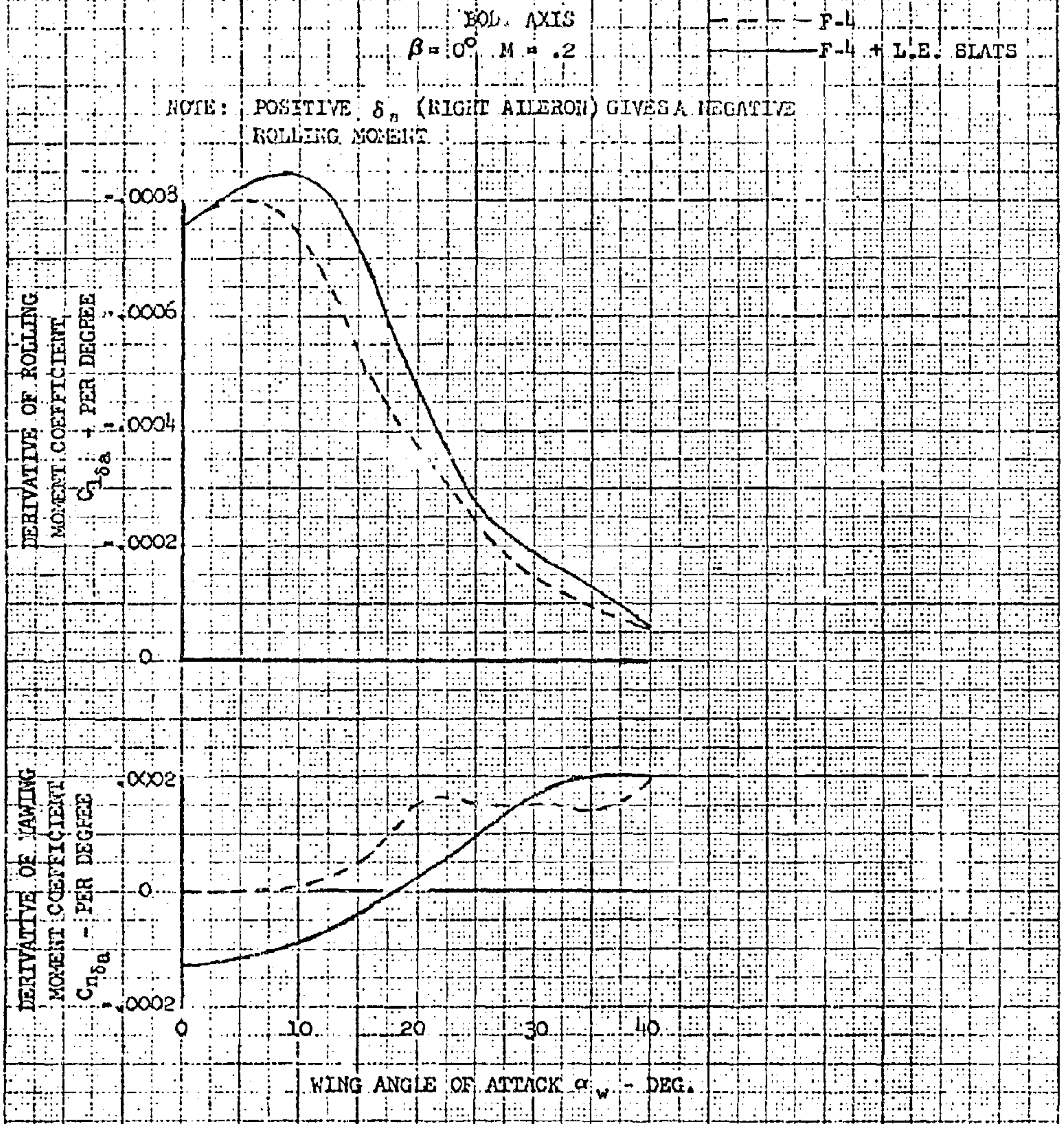

S4.02-1a-078, 076

UN 23RIDGN 10X10 TO CM.
LITHO IN U.S.A.

NATIONAL TRACING PAPER
INDIANAPOLIS, INDIANA

Figure 2.7

MODEL F-4E

RUDDER EFFECTIVENESS VERSUS ANGLE OF ATTACK

BODY AXIS

$\beta = 0^\circ \quad M = .2$

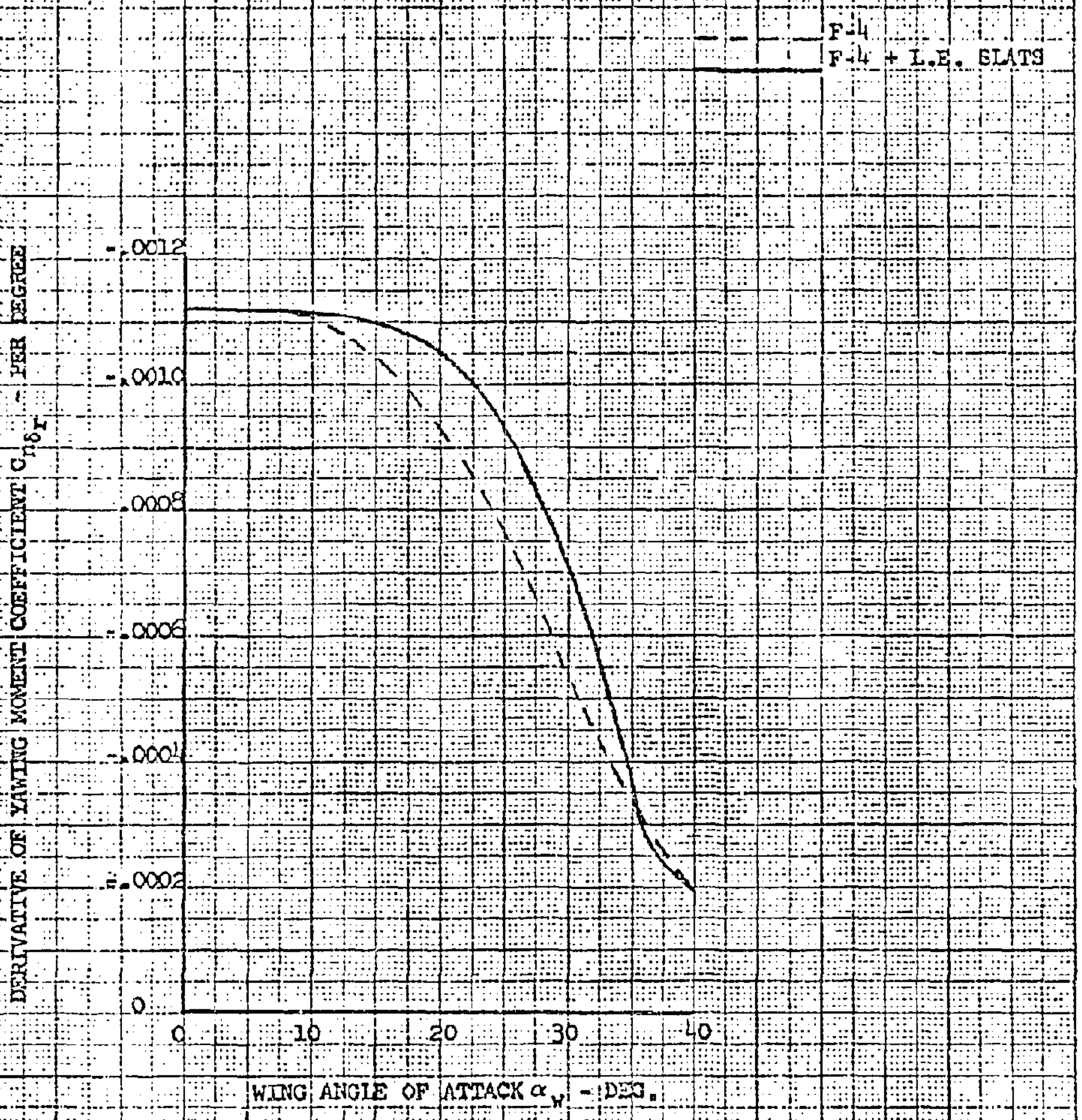

5-402-(a-10)

Figure 2.8

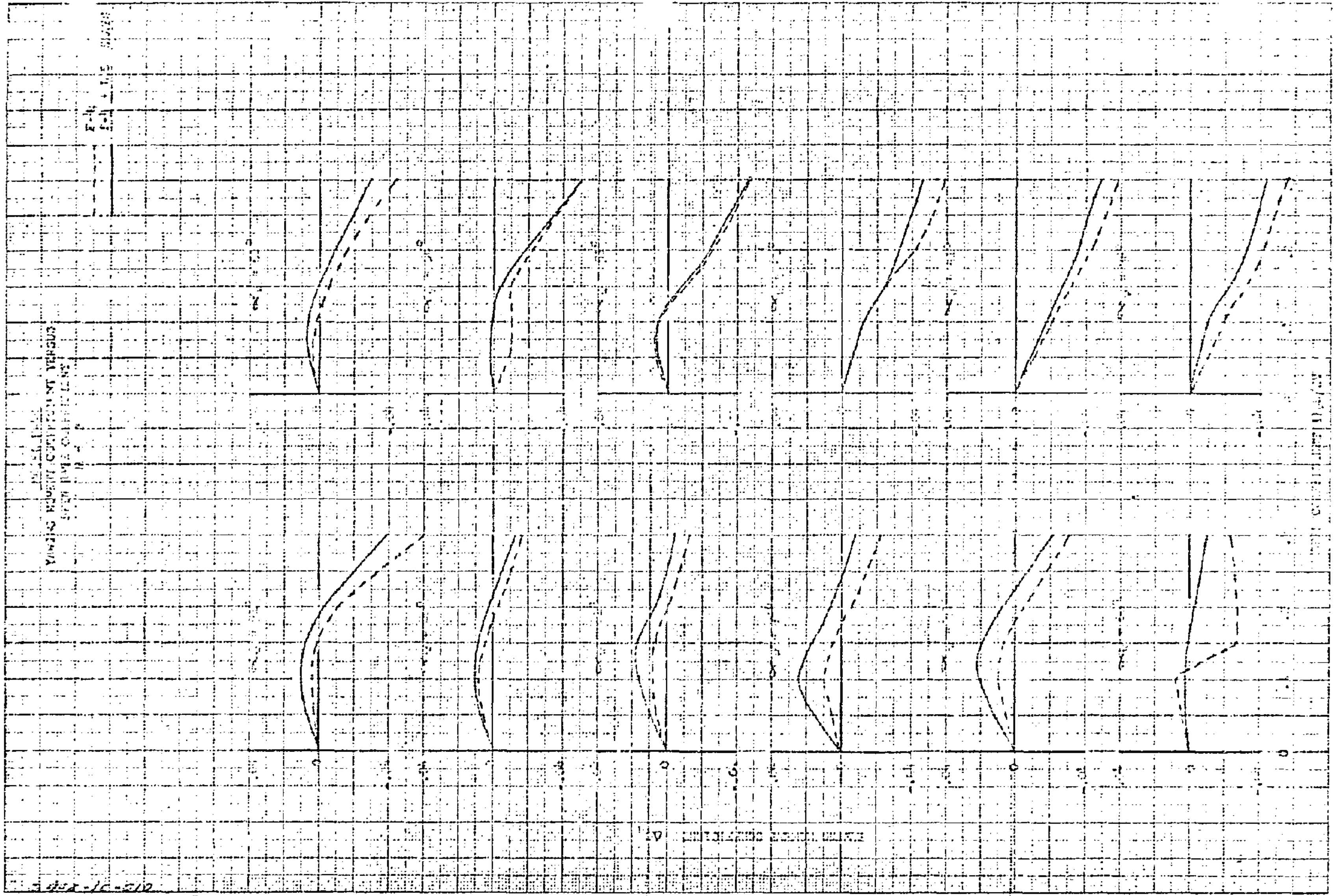

Figure 3.5

## 3. Stall/Near Stall/Departure Characteristics

The purpose of this section is to show the results of the stall/departure analysis on the slatted F-4E aircraft and to show the changes in departure characteristics between the slatted and non-slatted configurations. A six-degree-of-freedom computer program which is described in Appendix C is used to calculate the stall time histories. The aerodynamic data used in this program is presented in Appendix A for the slatted F-4E and Appendix B for the non-slatted F-4E. The production slatted F-4E weights and inertias are used when computing the stall/departure characteristics with both the slatted and non-slatted aerodynamic data. Comparisons of the departure characteristics due to aerodynamic changes are made for various lateral-directional control techniques, aircraft c.g. location and stall entry rates. Two types of maneuvers are used, an idle-power 1g stall and a maximum power constant bank angle turn-stall. Recoveries after departure are also analyzed.

The principle criteria used in the comparison of stall characteristics are angle of attack at departure and the angular accelerations ($\dot{p}$ and $\dot{r}$) at departure. The aerodynamic differences between the slatted F-4E and the basic F-4E cause differences in departure characteristics. Angle of attack for departure of the basic F-4E was selected as the angle of attack at which sideslip angle diverges since it usually departs first in yaw. Roll rate or yaw rate divergence is used to select the departure angle of attack of the slatted F-4E since it usually departs first in roll.

The 1g stalls are started at an initial Mach of .35 and at an altitude of 18000 ft., The constant bank angle turns are initiated at .6 Mach number at an altitude of 20000 ft.. The angle of attack is increased by inputting into the computer program increasing values of aircraft-nose-up stabilator as a function of time up to the control limit ( $\delta_s = -21^{\circ}$). A yaw gust was input below stall in the 1g stalls to excite the roll-yaw motion. However the yaw gust input was not used in the constant bank angle turn because out-of-trim rolling and yawing moments are already presented in this type of maneuver.

Aileron and rudder controls are used for lateral-directionally controlling the aircraft in the stall maneuver. The aileron is used to control bank angle by using a linear gain times the amount of difference between the actual bank angle and the desired bank angle,

$$\delta_a = -A(\phi_{desired} - \phi_{actual})$$

where A is a constant gain (A = 1 or 2).

The rudder, when used with the aileron, controls sideslip angle as follows;

$$\delta_r = -R\beta$$

where R is a constant gain (R = 1 or 2).

When the rudder control is used alone it controls bank angle by inducing a small sideslip angle which creates a rolling moment due to $C_{l_\beta}$. The sideslip angle is also limited by the rudder to $\pm 2^{\circ}$.

$$\delta_r = -R_1(\phi_{desired} - \phi_{actual})$$

where $R_1$ is a constant gain ($R_1$ = 1 or 2)

The aircraft weight and inertia configurations used in this analysis are presented in Table 1. The SDF stall time histories which are presented in this section of the report are summarized in Table 2.

3.1 Effects of Flight Maneuver On Departures - The angle of attack for departure between the slatted and basic F-4E for 1g stall and constant bank

## TABLE 1

## AIRCRAFT WEIGHTS AND INERTIAS

| Configuration No. | Weight (LB) | C.G. % MAC | $I_x$ SLUG-FT$^2$ | $I_y$ SLUG-FT$^2$ | $I_z$ SLUG-FT$^2$ | $I_{xz}$ SLUG-FT$^2$ |
|---|---|---|---|---|---|---|
| 1 (1) | 46500 | 31.5 | 31000 | 165500 | 188500 | 6300 |
| 2 (1) | 42262 | 29.0 | 28292 | 155948 | 176839 | 4628 |
| 3 (1) | 37000 | 27.0 | 25000 | 149000 | 168000 | 3700 |
| 4 (2) | 36950 | 31.7 | 22600 | 163000 | 182000 | 5450 |
| 5 (3) | 36422 | 27.0 | 22900 | 149000 | 166400 | 3500 |

NOTES: (1) Production Slatted F-4E Aircraft
(2) F-4E Flight Test Stall/Spin Aircraft
(3) Production F-4E Aircraft

## TABLE 2

### STALL TIME HISTORY SUMMARY

1g Stalls, .35 Mach No. , Alt. - 18000 Ft.

| Figure No. | Configuration No. | Aircraft | Entry Rate $\dot{\alpha}$ - Deg/Sec | Lateral/Directional Controls $\delta_{a_{max}}$ | $\delta_{r_{max}}$ |
|---|---|---|---|---|---|
| 3.1 | 2 | F-4E/F-4E + SLATS | 1.2 | ±30° | — |
| 3.3 | " | " " | 2.4 | ±30° | ±20.5° |
| 3.5 | " | " " | 2.4 | — | ±20.5° |
| 3.7 | " | " " | 1.2 | — | — |
| 3.8 | " | " " | 2.4 | — | — |
| 3.9 | " | " " | 5.6 | — | — |
| 3.10 | " | " " | 10.0 | — | — |
| 3.11 | " | " " | 15.0 | — | — |
| 3.15 | 3 | " " | 1.4 | ±30° | — |
| 3.16 | 1 | " " | 1.4 | ±30° | — |
| 3.20(1) | 2 | " " | 1.2 | ±30° | — |

NOTE: (1) Recovery after Departure

## TABLE 2 (CONT.)

### Constant Bank Angle Turn-Stalls, .6 Mach No., Alt. - 20000 Ft.

| Figure No. | Configuration No. | Aircraft | Entry Rate $\dot{\alpha}$ - Deg/Sec | Lateral/Directional Controls $\delta_{a_{max}}$ | $\delta_{r_{max}}$ |
|---|---|---|---|---|---|
| 3.2 | 2 | F-4E/F-4E + SLATS | 1.2 | ±30° | — |
| 3.4 | 2 | " " | 1.2 | ±10° | ±20.5° |
| 3.6 | 2 | " " | 1.2 | — | ±30° |
| 3.12 | 1 | " " | 1.3 | ±6° | ±20.5° |
| 3.13 | 1 | " " | 3.2 | ±6° | ±20.5° |
| 3.14 | 1 | " " | 10.0 | ±6° | ±20.5° |
| 3.17 | 3 | " " | 1.2 | ±30° | — |
| 3.18 | 1 | " " | 1.3 | ±30° | — |
| 3.19(1) | 2 | " " | 1.2 | ±30° | — |
| 3.21(1) | 2 | " " | 1.2 | ±30° | — |

NOTE: (1) Recovery after Departure

angle turn-stalls are summarized in Table 3 and the time histories are presented in Figure 3.1 through 3.6. The slatted F-4E departs at a higher angle of attack than the basic F-4E when maneuvering with either ailerons only or aileron and rudder control. The slatted F-4E does not depart when using the rudder only for lateral-directional control (see Figure 3.5 and 3.6). The departure angle of attack is lower in the constant bank angle turn for both the slatted and the basic F-4E at a given aileron or aileron/ rudder control combination. Examination of Figures 3.1 through 3.6 show the angular roll and yaw accelerations are much higher for the basic F-4E at departure than the slatted F-4E for either flight maneuver. The basic F-4E also experiences a rapid increase in angle of attack after departure because of inertia coupling effects caused by the high roll and yaw rates at departure.

3.2 Effect of Rate of Entry On Departure - The angles of attack at departure for the slatted and basic F-4E at various entry rates are presented in Table 4. The corresponding time histories are presented in Figures 3.7 through 3.14. The slatted F-4E does not depart even at the highest entry rate in the 1g stall maneuver while the basic F-4E departs at all of the entry rates. The slatted F-4E departs at an angle of attack well above the basic F-4E in the constant bank angle turn (see Figures 3.12, 3.13, and 3.14). Increasing the entry rate ($\dot{\alpha}$) of the basic F-4E results in increasing angle of attack for departure. However increasing the entry rate ($\dot{\alpha}$) on the slatted F-4E results in no increase in angle of attack for departure since departure occurs at some finite time after the maximum stabilized angle of attack as determined by aircraft-nose-up stabilator.

## TABLE 3

### EFFECT OF 1g STALL AND CONSTANT BANK ANGLE TURN ON DEPARTURE
Configuration No.2

| Figure No. | Maneuver | Entry Rate $\dot{\alpha}$ - Deg/Sec | Lateral-Directional Controls | Departure Angle of Attack Basic F-4E $\alpha_B$ ($\alpha_{c/p}$)(1) | Departure Angle of Attack Slatted F-4E $\alpha_B$ ($\alpha_{c/p}$)(1) |
|---|---|---|---|---|---|
| 3.1 | 1g Stall | 1.2 | Ailerons Only | 22° (28 units) | 27° (33 units) |
| 3.2 | Constant Bank Angle Turn | 1.2 | Ailerons Only | 18° (24 units) | 21° (27 units) |
| 3.3 | 1g Stall | 2.4 | Aileron/Rudder | 24° (30 units) | 30° (37 units) |
| 3.4 | Constant Bank Angle Turn | 1.2 | Aileron/Rudder(2) | 20° (26 units) | 25°-30°(31-37 units) |
| 3.5 | 1g Stall | 2.4 | Rudder Only | 26° (32 units) | No Departure |
| 3.6 | Constant Bank Angle Turn | 1.2 | Rudder Only | 20° (26 units) | No Departure |

NOTE: (1) $\alpha_{c/p} = 3.98 + 1.09\alpha_B \sim$ UNITS (MACH NO. 0.6)

(2) Aileron Deflection Limited to ±10°

## TABLE 4

## EFFECT OF RATE OF ENTRY ON DEPARTURE

| Figure No. | Maneuver | Config. No. | Entry Rate $\dot{\alpha}$ - Deg/Sec | Lateral-Directional Controls | Departure Angle of Attack<br>Basic F-4E<br>$\alpha_B$ ($\alpha_{c/p}$)(1) | <br>Slatted F-4E<br>$\alpha_B$ ($\alpha_{c/p}$)(1) |
|---|---|---|---|---|---|---|
| 3.7 | 1g Stall | 2 | 1.2 | None | $19^\circ$ (25 units) | No Departure |
| 3.8 | 1g Stall | 2 | 2.4 | None | $19^\circ$ (25 units) | No Departure |
| 3.9 | 1g Stall | 2 | 5.6 | None | $20^\circ$ (26 units) | No Departure |
| 3.10 | 1g Stall | 2 | 10.0 | None | $29^\circ$ (36 units) | No Departure |
| 3.11 | 1g Stall | 2 | 15.0 | None | $34^\circ$ (41 units) | No Departure |
| 3.12 | Constant Bank Angle Turn | 1 | 1.3 | Aileron/Rudder(2) | $22^\circ$ (28 units) | $32.5^\circ$ (39 units) |
| 3.13 | Constant Bank Angle Turn | 1 | 3.2 | Aileron/Rudder | $21^\circ$-$24^\circ$(27-30 units) | $32.5^\circ$ (39 units) |
| 3.14 | Constant Bank Angle Turn | 1 | 10.0 | Aileron/Rudder | $25^\circ$ (31 units) | $32.5^\circ$ (39 units) |

NOTE: (1) $\alpha_{c/p} = 3.98 + 1.09\,\alpha_B \sim$ UNITS (MACH NO. 0.6)

(2) Aileron Deflection Limited to $\pm 6^\circ$

As the rate of entry increases for both aircraft the amplitude of the lateral-directional oscillations increases, and at departure there is higher roll and yaw accelerations. However, above moderately high entry rates ($\dot{\alpha} = 5$ to 10 deg/sec) the amplitude of the lateral-directional oscillations no longer increases or may even decrease slightly (see Figures 3.7 through 3.14). The roll and yaw accelerations at departure also no longer increase with increasing entry rate. While these trends are the same for both aircraft the basic F-4E has much higher roll and yaw accelerations at departure than the slatted F-4E (see Figures 3.7 through 3.14). In addition, the amplitude of lateral-directional oscillations are much higher for the basic F-4E than the slatted F-4E.

3.3 Effect of Aircraft Weight, C.G., and Inertia On Departure - The departure angles of attack of the slatted and basic F-4E for various weight, c.g. and inertia configurations are presented in Table 5 (see Figures 3.1, 3.2, 3.15, 3.16, 3.17, and 3.18 for corresponding time histories). The differences in departure characteristics due to aircraft c.g. and weight changes are in general very minor. There isn't any consistent trend between c.g. and the angle of attack at departure for either the 1g stall or the constant bank angle turn maneuvers. There is an apparent increase in the roll rate at departure as the c.g. was varied from forward to aft in the 1g stalls. However, there isn't any trend with roll rate in the constant bank angle turns.

3.4 Effect of Lateral-Directional Control Inputs On Departure - The departure angles of attack for both aircraft using various aileron and rudder control techniques to maintain controlled flight are summaried in

TABLE 5

EFFECT OF AIRCRAFT WEIGHT, C.G., AND INERTIAS ON DEPARTURE.

| Figure No. | Maneuver | Config. No. | Entry Rate $\dot{\alpha}$ - Deg/Sec | Lateral-Directional Controls | Departure Angle of Attack Basic F-4E $\alpha_B$ ($\alpha_{c/p}$) (1) | Departure Angle of Attack Slatted F-4E $\alpha_B$ ($\alpha_{c/p}$) (1) |
|---|---|---|---|---|---|---|
| 3.15 | 1g Stall | $3(27\%\bar{c})$ | 1.4 | Ailerons Only | $21^\circ$ (27 units) | $26^\circ$ (32 units) |
| 3.1 | 1g Stall | $2(29\%\bar{c})$ | 1.2 | Ailerons Only | $22^\circ$ (28 units) | $27^\circ$ (33 units) |
| 3.16 | 1g Stall | $1(31.5\%\bar{c})$ | 1.4 | Ailerons Only | $20^\circ$-$22^\circ$(26-28 units) | $25^\circ$-$27^\circ$(29-33 units) |
| 3.17 | Constant Bank Angle Turn | $3(27\%\bar{c})$ | 1.2 | Ailerons Only | $18^\circ$ (24 units) | $21^\circ$-$22^\circ$(27-28 units) |
| 3.2 | Constant Bank Angle Turn | $2(29\%\bar{c})$ | 1.2 | Ailerons Only | $18^\circ$ (24 units) | $21^\circ$(27 units) |
| 3.18 | Constant Bank Angle Turn | $1(31.5\%\bar{c})$ | 1.3 | Ailerons Only | $18^\circ$ (24 units) | $22^\circ$-$23^\circ$(28-29 units) |

NOTE: (1) $\alpha_{c/p} = 3.98 + 1.09\,\alpha_B$ ~ UNITS (MACH NO. 0.6)

Table 6 (see Figures 3.1, 3.2, 3.3 3.4, 3.5, 3.6, 3.7, and 3.12 for corresponding time histories). The slatted F-4E departs at higher angles of attack and has lower roll and yaw accelerations at departure than the basic F-4E regardless of what lateral control device was used. However, the aileron and rudder can either improve or degrade the angle of attack at departure depending on the magnitude of the aileron deflection used in the maneuver (see Table 6).

The basic F-4E departs at $19^{\circ}$ (25 units) angle of attack in the 1g stall maneuver with no lateral-directional controls while the slatted F-4E does not depart (see Figure 3.7). This improvement in departure characteristics is due to the increase in both lateral and directional stability for the slatted F-4E.

The use of the rudder alone to control the aircraft lateral-directionally in the stall results in no departure for the slatted F-4E in both the 1g stall and the constant bank angle turn-stall. The rudder is used to control bank angle by inducing a sideslip angle which creates a rolling moment due to $C_{l_\beta}$. This method is very effective for the slatted F-4E because the dihedral effect is strong throughout the angle of attack range. The basic F-4E did show some improvement in angle of attack at departure over the no controls case in the 1g stall (see Figure 3.5).

The results of the aileron and rudder together to control the aircraft lateral-directionally in the stall are presented in Table 6 and show that departure occurs when the ailerons are used in conjunction with the rudder. The ailerons are limited to small deflections (6-10 degrees). The departure

## TABLE 6

## EFFECT OF LATERAL-DIRECTIONAL CONTROL INPUTS ON DEPARTURE

| Figure No. | Maneuver | Config. No. | Entry Rate $\dot{\alpha}$ - Deg/Sec | Lateral-Directional Controls | Departure Angle of Attack Basic F-4E $\alpha_B$ ($\alpha_{c/p}$) (1) | Departure Angle of Attack Slatted F-4E $\alpha_B$ ($\alpha_{c/p}$) (1) |
|---|---|---|---|---|---|---|
| 3.7 | 1g Stall | 2 | 1.2 | None | 19° (25 units) | No Departure |
| 3.5 | 1g Stall | 2 | 2.4 | Rudder Only | 26° (32 units) | No Departure |
| 3.3 | 1g Stall | 2 | 2.4 | Aileron/Rudder | 24° (30 units) | 30° (37 units) |
| 3.1 | 1g Stall | 2 | 1.2 | Ailerons Only | 22° (28 units) | 27° (33 units) |
| 3.6 | Constant Bank Angle Turn | 2 | 1.2 | Rudder Only | 20° (26 units) | No Departure |
| 3.12 (2) | Constant Bank Angle Turn | 1 | 1.3 | Aileron/Rudder (2) | 22° (28 units) | 32.5° (39 units) |
| 3.4 | Constant Bank Angle Turn | 2 | 1.2 | Aileron/Rudder (3) | 20° (26 units) | 25°-30°(31-27 units) |
| 3.2 | Constant Bank Angle Turn | 2 | 1.2 | Ailerons Only | 18° (24 units) | 21° (27 units) |

NOTE: (1) $\alpha_{c/p} = 3.98 + 1.09\,\alpha_B \sim$ UNITS (MACH NO. 0.6)

(2) Aileron Deflection Limited to ±6°

(3) Aileron Deflection Limited to ±10°

angle of attack is high and the roll and yaw accelerations are small for the slatted F-4E. The departure angle of attack (Figure 3.12) corresponds to the maximum attainable angle of attack using full aircraft-nose-up stabilator control. The basic F-4E shows a slight reduction in angle of attack at departure when the aileron and rudder controls are used in comparison to only rudder control.

The ailerons used alone to control the aircraft laterally is the least effective of all the aileron and rudder control combinations. Departure angles of attack are the lowest and the angular accelerations at departure are the highest. While it is clear that even with the addition of slats the use of ailerons alone greatly restricts the angle of attack capabilities, however, the slatted F-4E still departs from 1° to 5° angle of attack higher than the basic F-4E with lower magnitudes in roll and yaw accelerations at departure (see Figures 3.1 and 3.2). This is due to the reduction in adverse yaw from the aileron and the increase in static lateral and directional stability of the slatted F-4E.

3.5 Recovery From Departures - Recoveries after departure were attempted on both the 1g stall and the constant bank angle turn maneuvers. The recovery method used for these calculations is full aircraft-nose-down stabilator with aileron and rudder neutralized. This is the same procedure as recommend in the basic F-4E flight manual (Reference 4). The time histories showing the basic F-4E and the slatted F-4E recovery characteristics are presented in Figures 3.19, 3.20, and 3.21. Both aircraft recover in all three cases, but the slatted F-4E is more responsive in the recovery than the basic F-4E. There is a tendency for the basic F-4E to have a rapid increase in angle of attack just after departure, thereby requiring a longer time to reduce the angle of attack below stall compared to the slatted F-4E. The reduction of roll rates and yaw rates takes a longer time on the basic F-4E than the slatted F-4E (see Figure 3.19 through 3.21). The flight manual recovery technique was quite successful on the slatted F-4E and it is considered to be the optimum recovery method.

3.6 Flight Test Qualitative Results - In the flight test evaluation of the slatted F-4 conducted by McDonnell Douglas Corporation a large number of stalls were made both in 1g and accelerated flight. The results of this test program revealed a tremendous improvement in lateral-directional handling characteristics over the basic F-4E. During wings level stalls the angle of attack values approached 35° and above before a rolling departure would occur. In most cases departures were not experienced. At these high angles of attack pitch control was positive, and angle of attack was easily reduced by forward stick movement. Recovery was positive using forward stick and neutral aileron and rudder. Departures from accelerated windup turn stalls occurred in the 32° to 40° angle of attack range, and tended to be more gentle than the basic F-4E and are primarily in roll rather than yaw. Recovery was again positive in all cases using forward stick and neutral aileron and rudder.

The analytical calculations for the near stall flight conditions indicate the same change in departure characteristics due to the slats as was indicated by the flight test results.

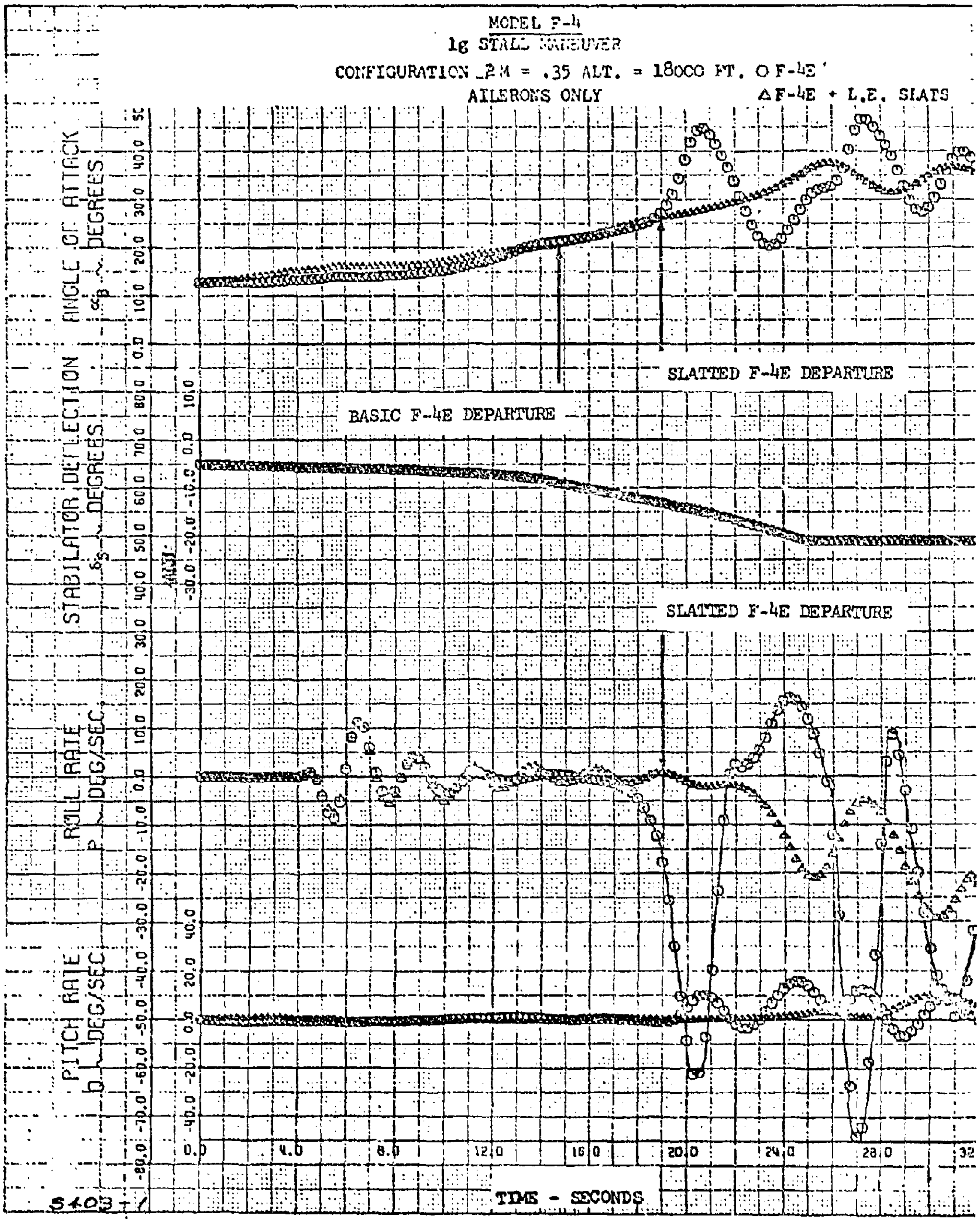
MODEL F-4
1g STALL MANEUVER
CONFIGURATION 2 M = .35 ALT. = 18000 FT. ○ F-4E
AILERONS ONLY
△ F-4E + L.E. SLATS
ANGLE OF ATTACK
$\alpha_B$ ~ DEGREES
0.0
10.0
20.0
30.0
40.0
50
STABILATOR DEFLECTION
$\delta_S$ ~ DEGREES
10.0
0.0
-10.0
-20.0
-30.0
ROLL RATE
P ~ DEG/SEC
80.0
70.0
60.0
50.0
40.0
30.0
20.0
10.0
0.0
-10.0
-20.0
-30.0
-40.0
-50.0
-60.0
-70.0
-80.0
PITCH RATE
Q ~ DEG/SEC
40.0
20.0
0.0
-20.0
-40.0
SLATTED F-4E DEPARTURE
BASIC F-4E DEPARTURE
SLATTED F-4E DEPARTURE
0.0
4.0
8.0
12.0
16.0
20.0
24.0
28.0
32
TIME - SECONDS
5403-1

Figure 3.1

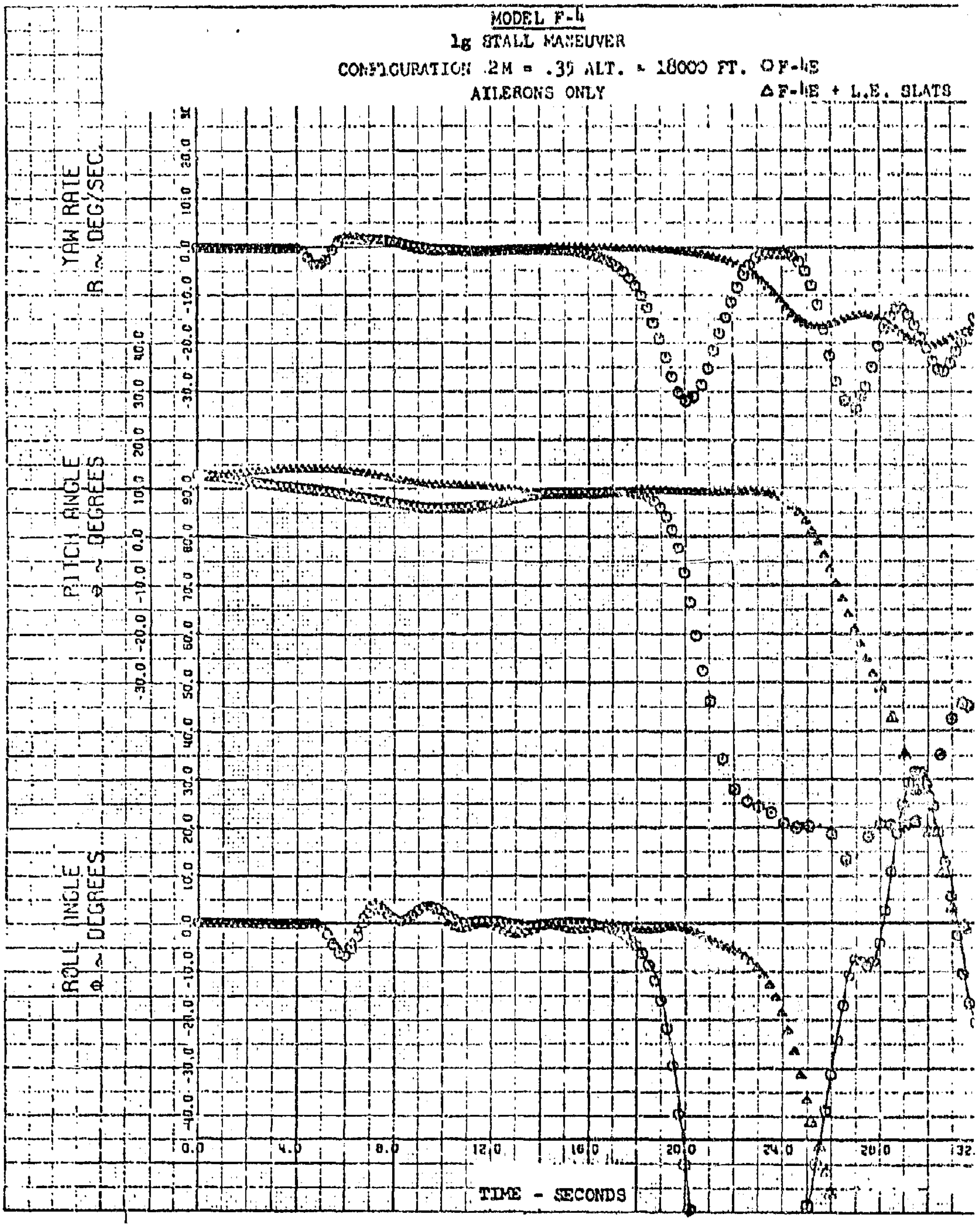

Figure 3.1 Con't

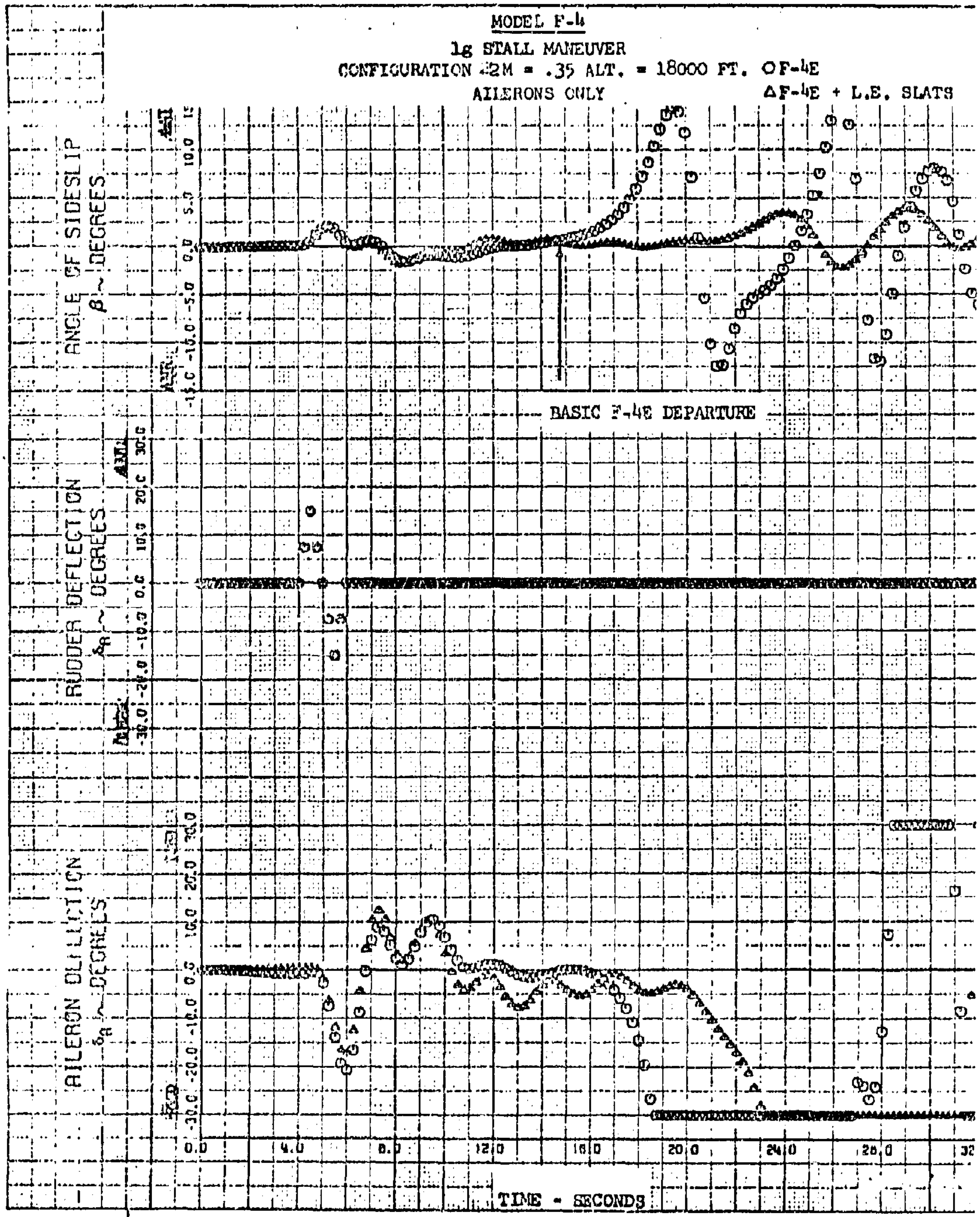

Figure 3.1 Con't

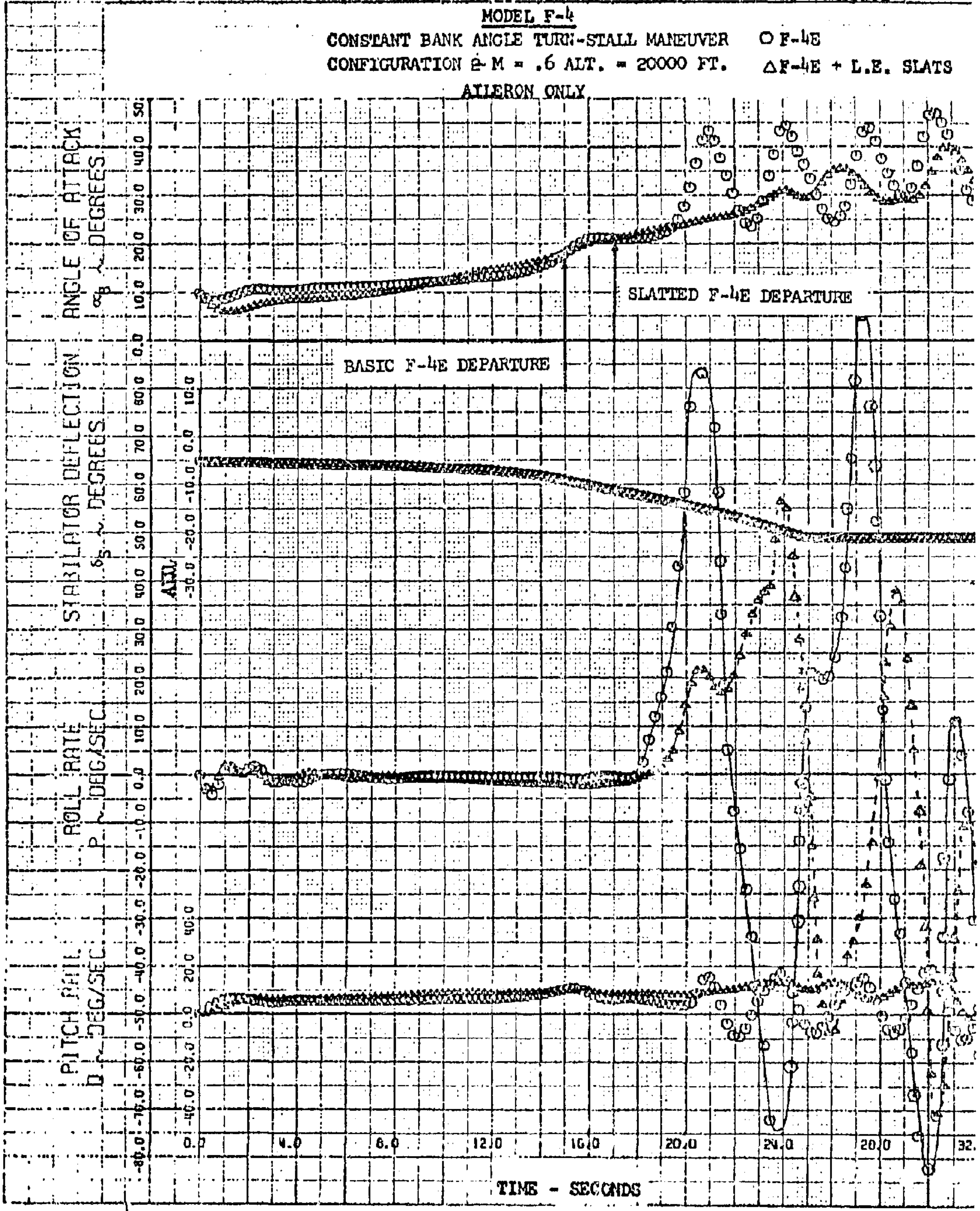

MODEL F-4

CONSTANT BANK ANGLE TURN-STALL MANEUVER
CONFIGURATION 2 M = .6 ALT. = 20000 FT.
AILERON ONLY

Figure 3.2

MODEL F-4

CONSTANT BANK ANGLE TURN-STALL MANEUVER ○ F-4E
CONFIGURATION 2 M = .6 ALT. = 20000 FT. △ F-4E + L.E. SLATS
AILERON ONLY

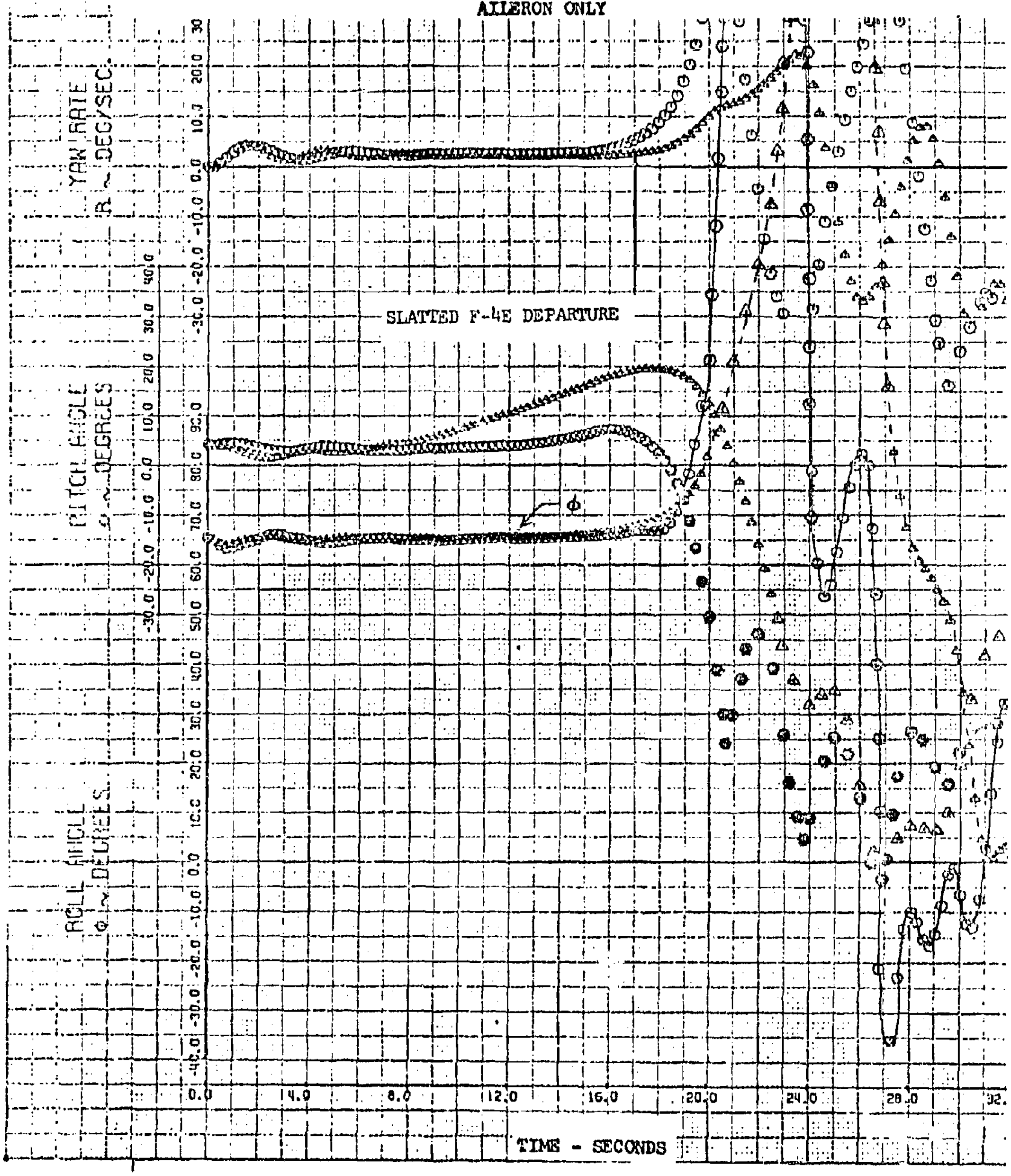

Figure 3.2 Con't

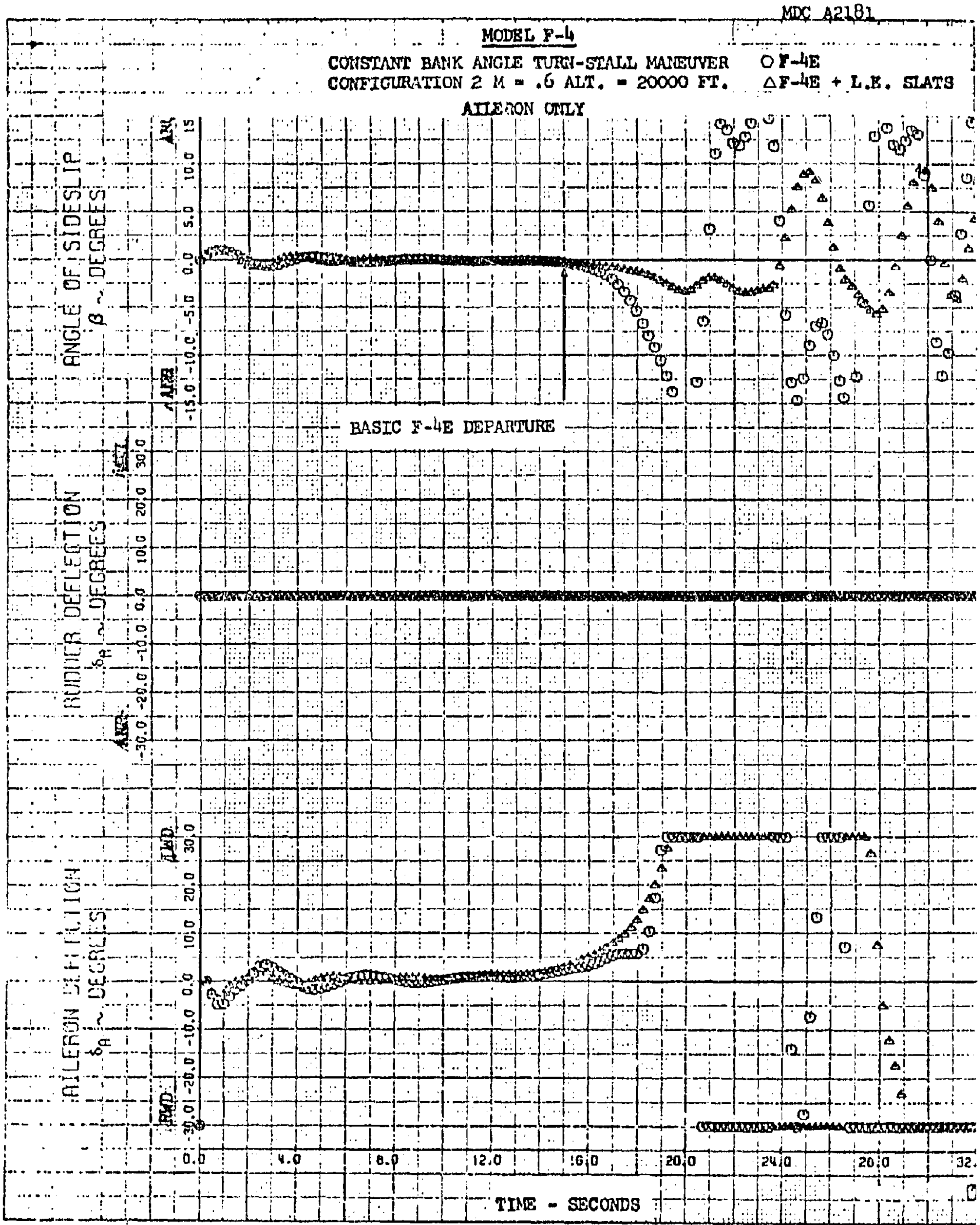

MODEL F-4

CONSTANT BANK ANGLE TURN-STALL MANEUVER
CONFIGURATION 2 M = .6 ALT. = 20000 FT.
AILERON ONLY

○ F-4E
△ F-4E + L.E. SLATS

BASIC F-4E DEPARTURE

Figure 3.2 Con't

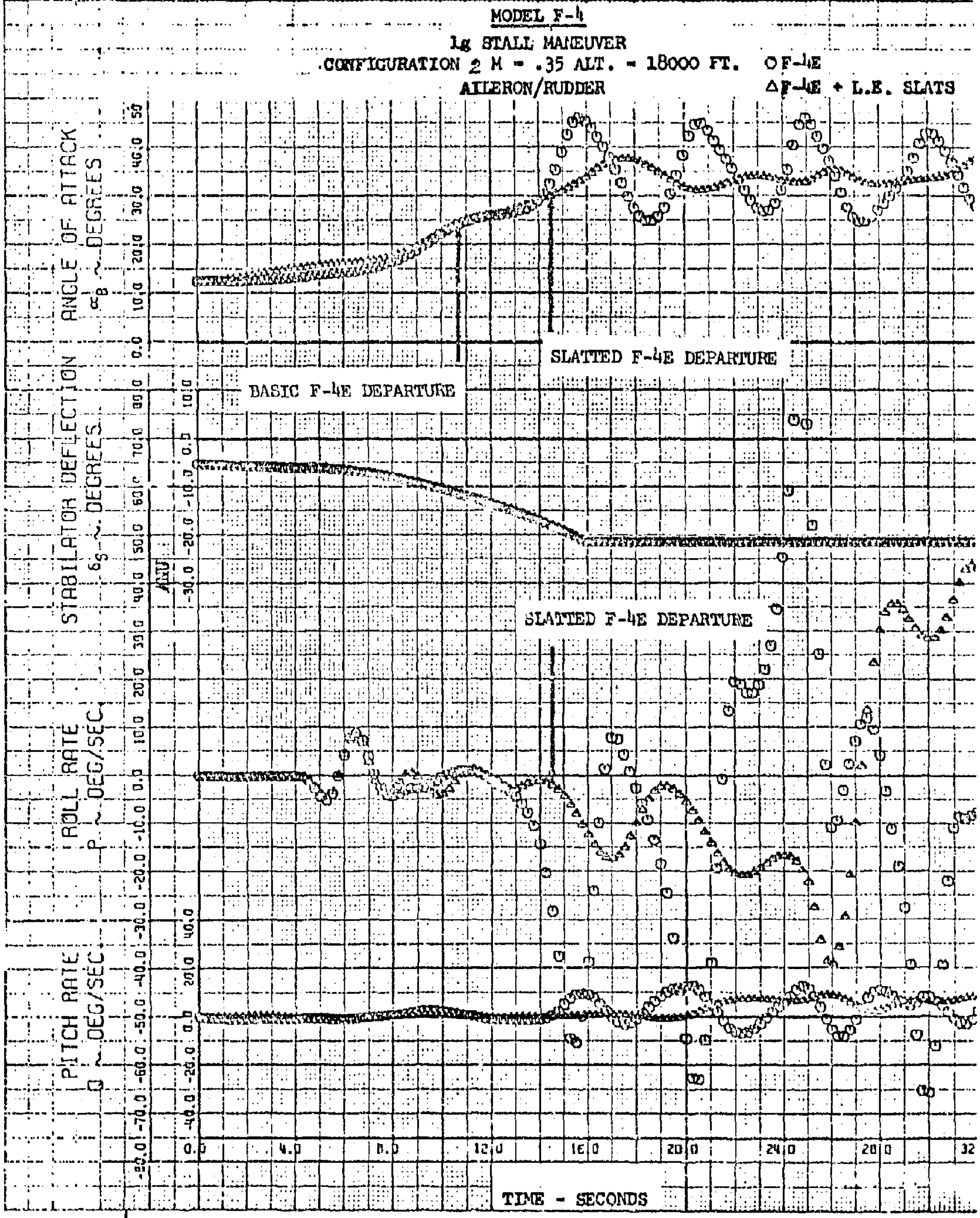

**MODEL F-4**

1g STALL MANEUVER

CONFIGURATION 2 M = .35 ALT. = 18000 FT.

AILERON/RUDDER

○ F-4E

△ F-4E + L.E. SLATS

Figure 3.3

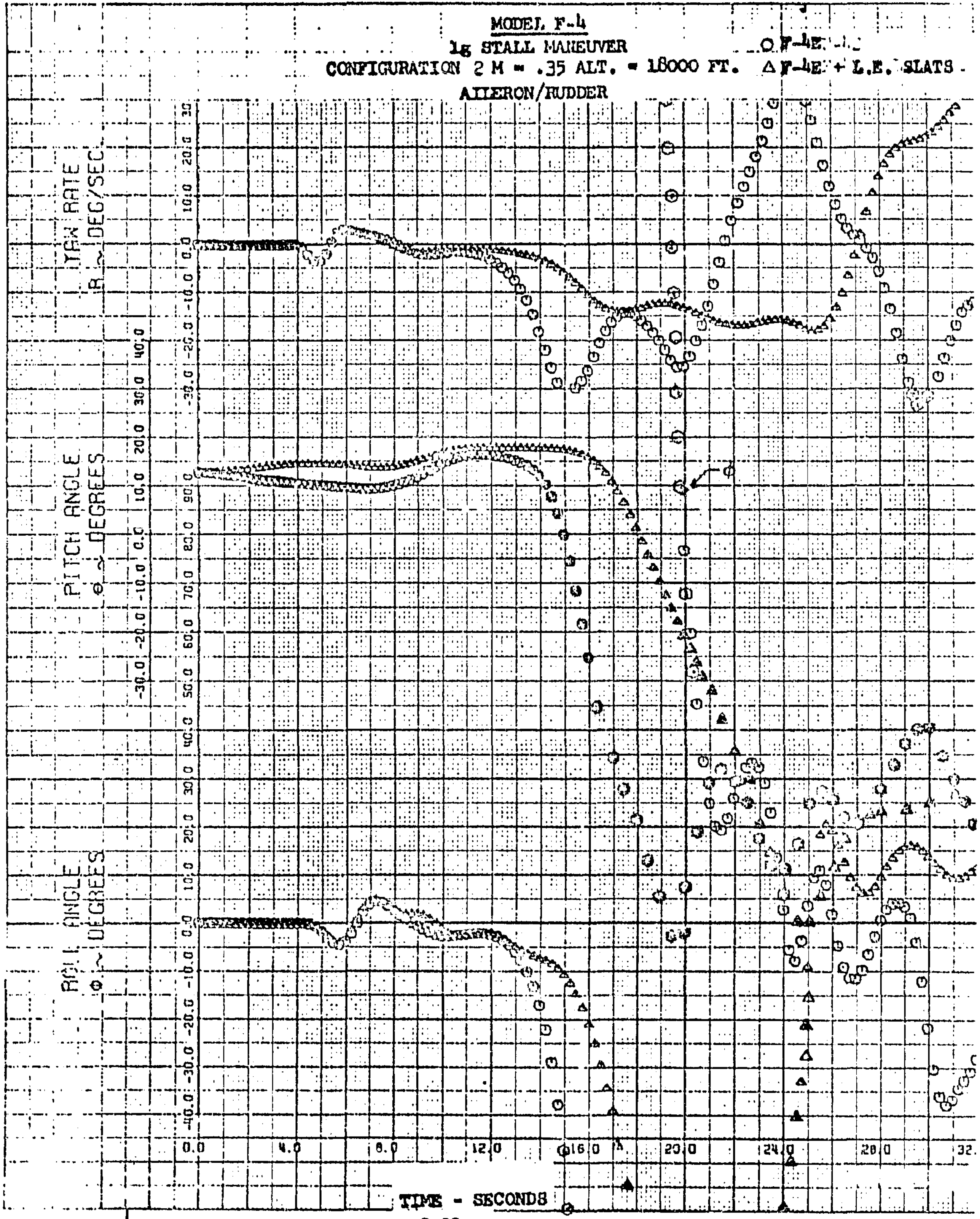

MODEL F-4

1g STALL MANEUVER

CONFIGURATION 2 M = .35 ALT. = 18000 FT.

○ F-4E

△ F-4E + L.E. SLATS

AILERON/RUDDER

Figure 3.3

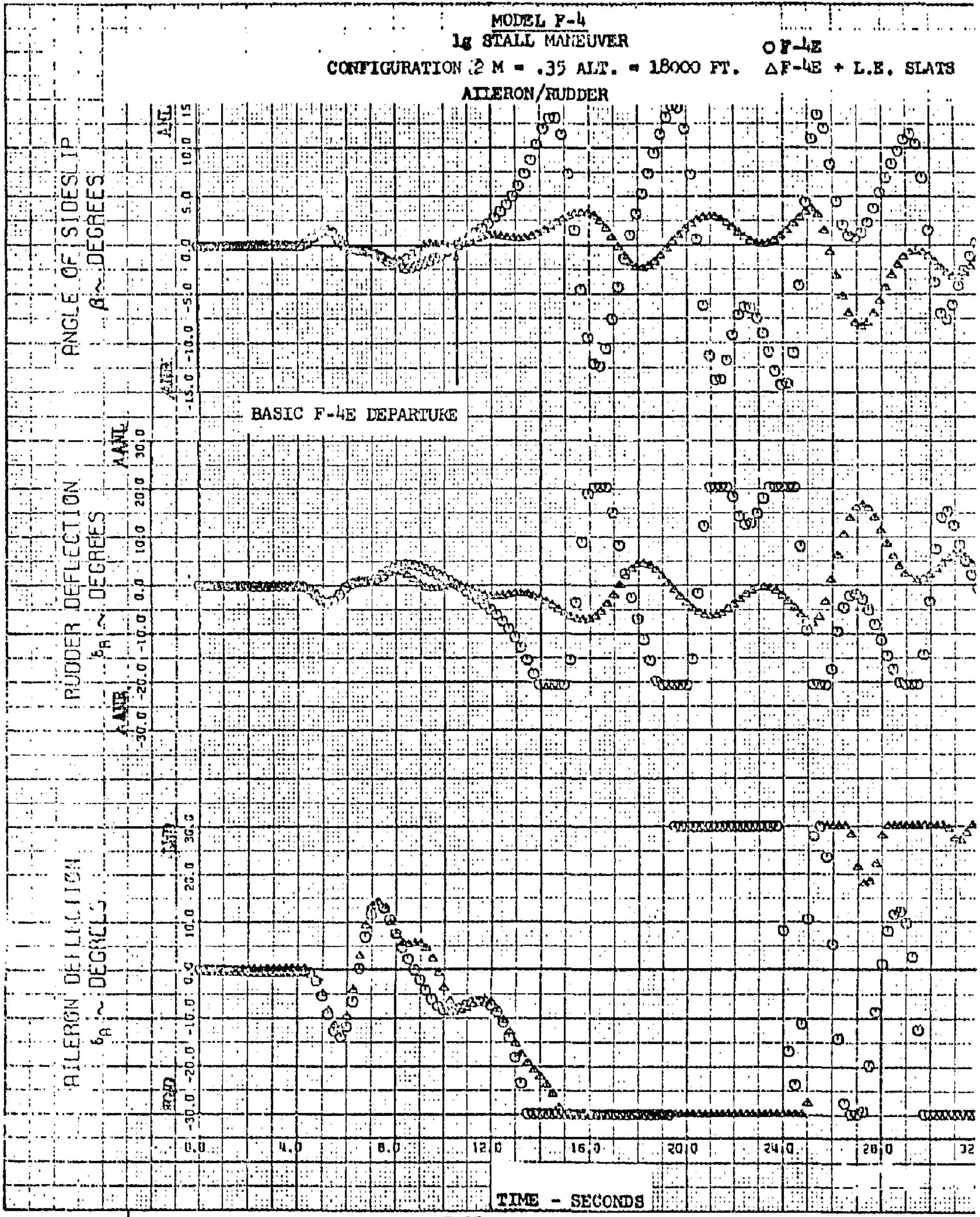

Figure 3.3 Con't

MODEL F-4

CONSTANT BANK ANGLE TURN-STALL MANEUVER ○ F-4E
CONFIGURATION 2 M = .6 ALT. = 20000 FT. △ F-4E + L.E. SLATS
AILERON/RUDDER

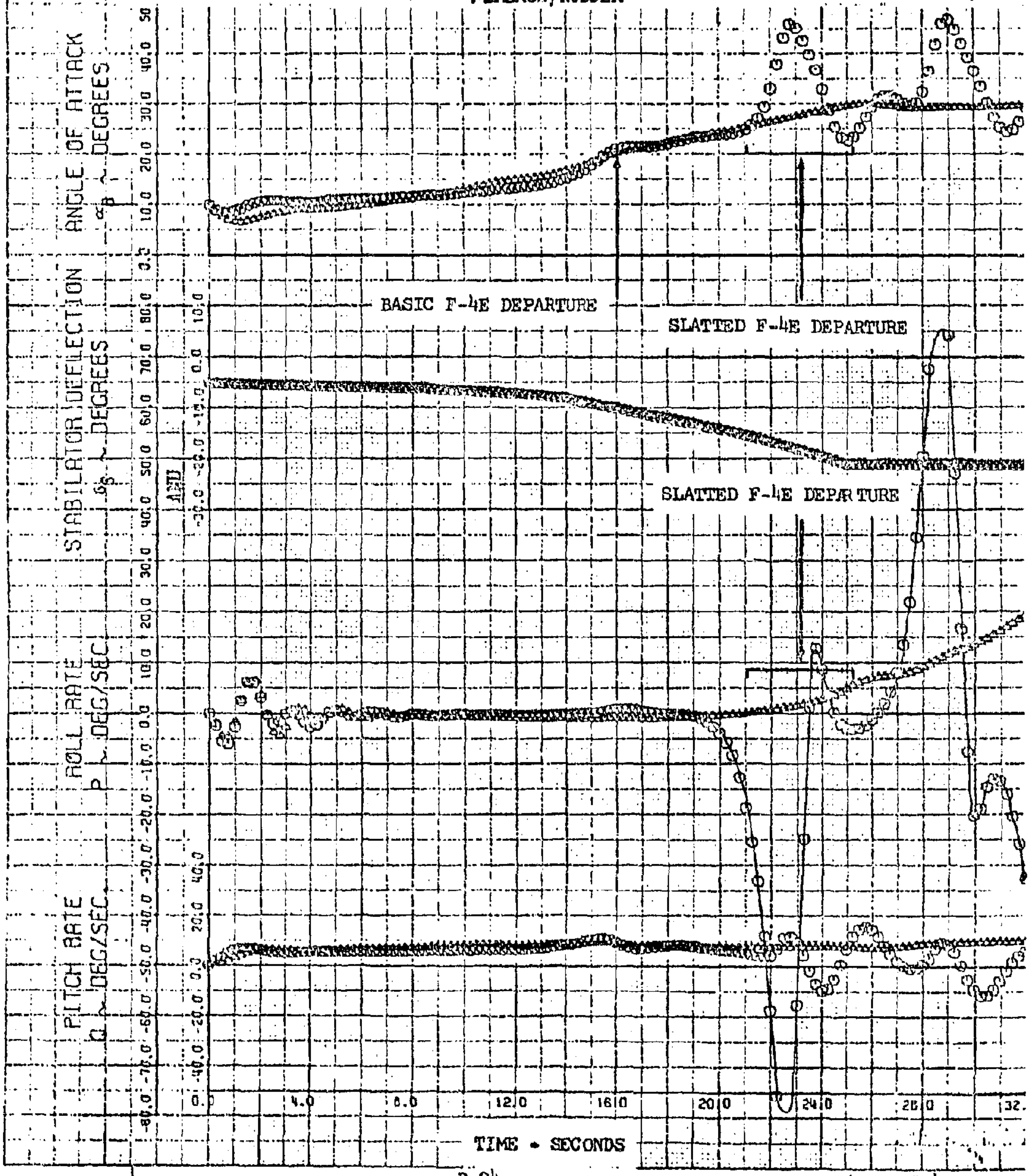

Figure 3.4

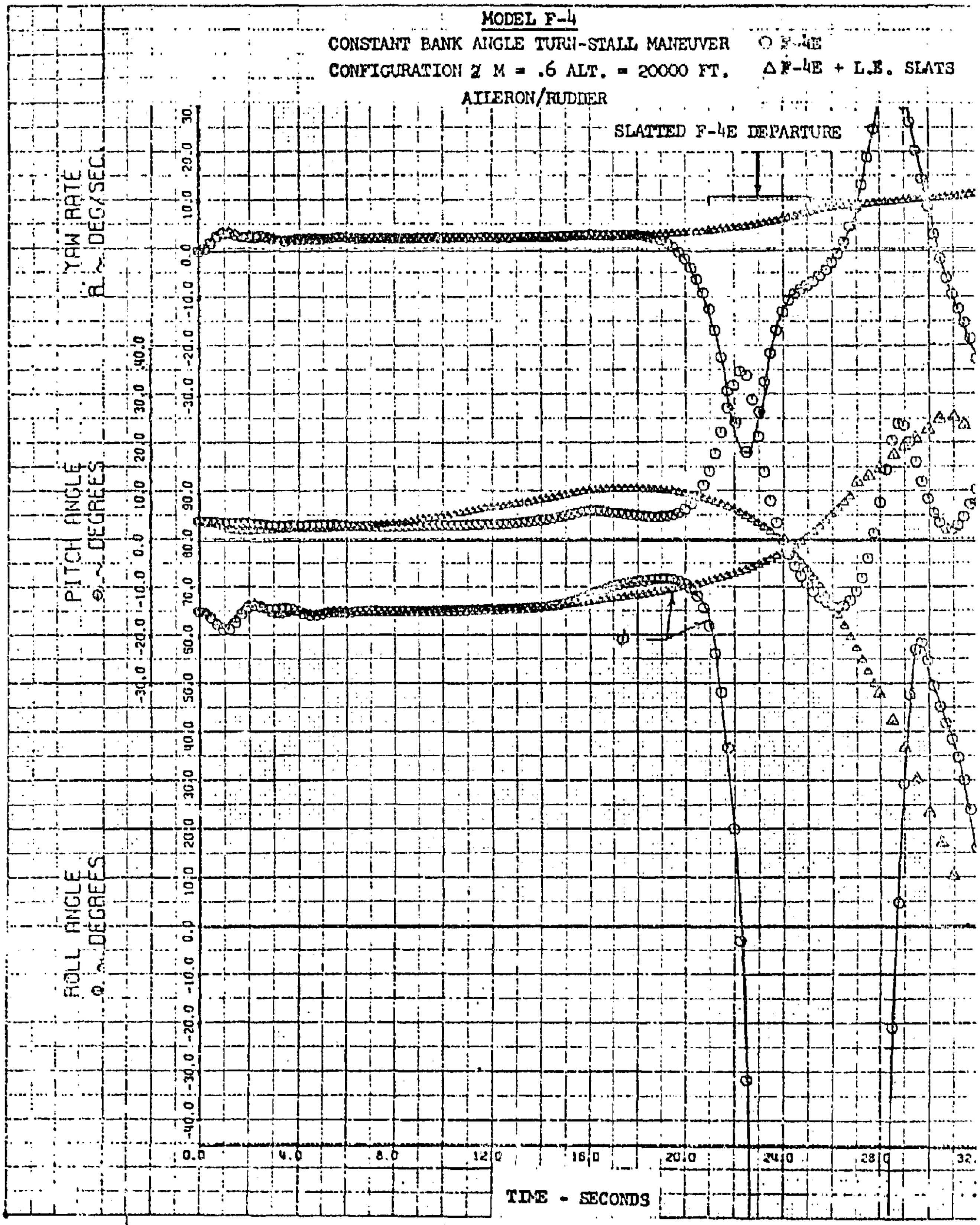

MODEL F-4

CONSTANT BANK ANGLE TURN-STALL MANEUVER

CONFIGURATION 2 M = .6 ALT. = 20000 FT.

AILERON/RUDDER

Figure 3.4 Con't

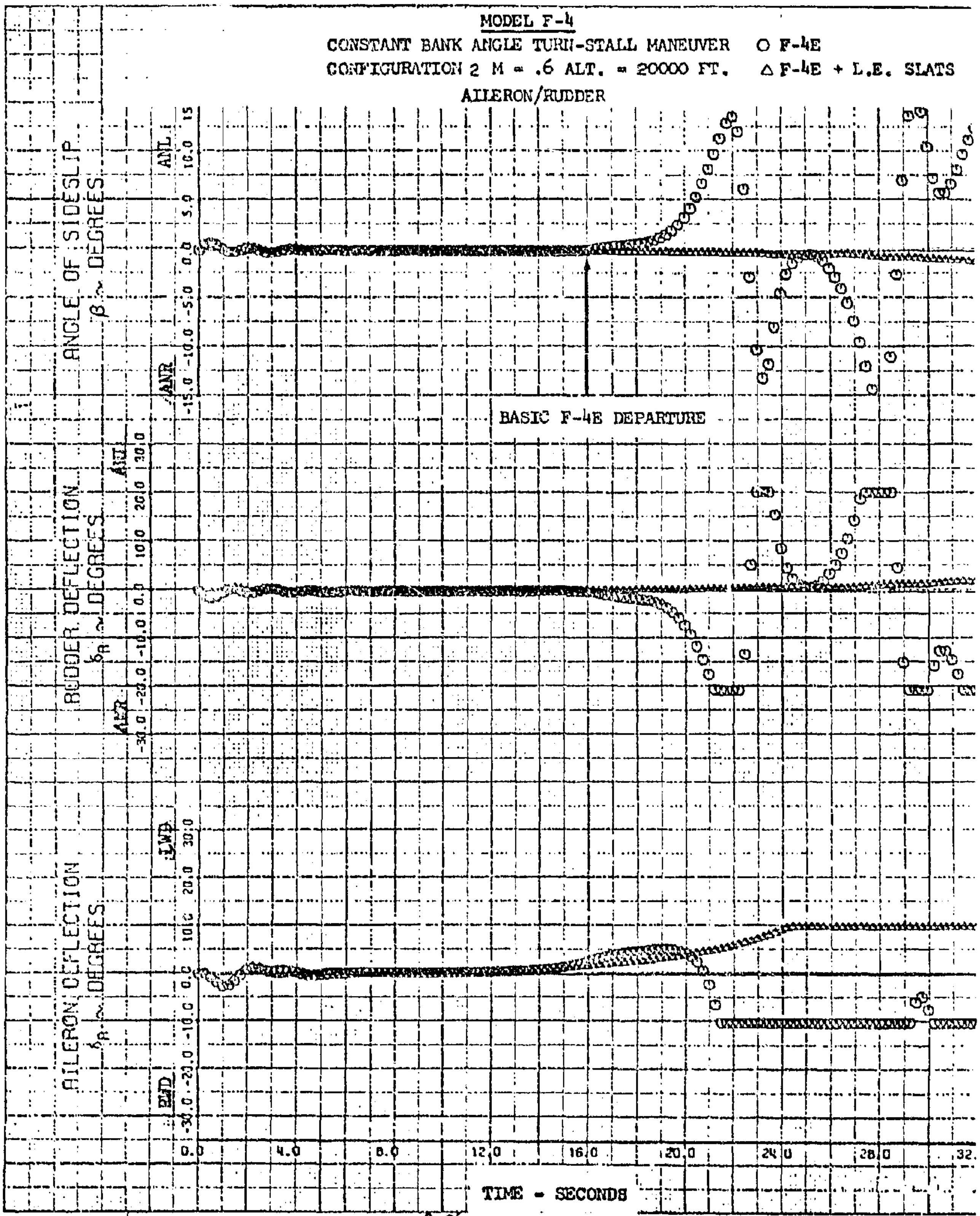

Figure 3.4 Con't

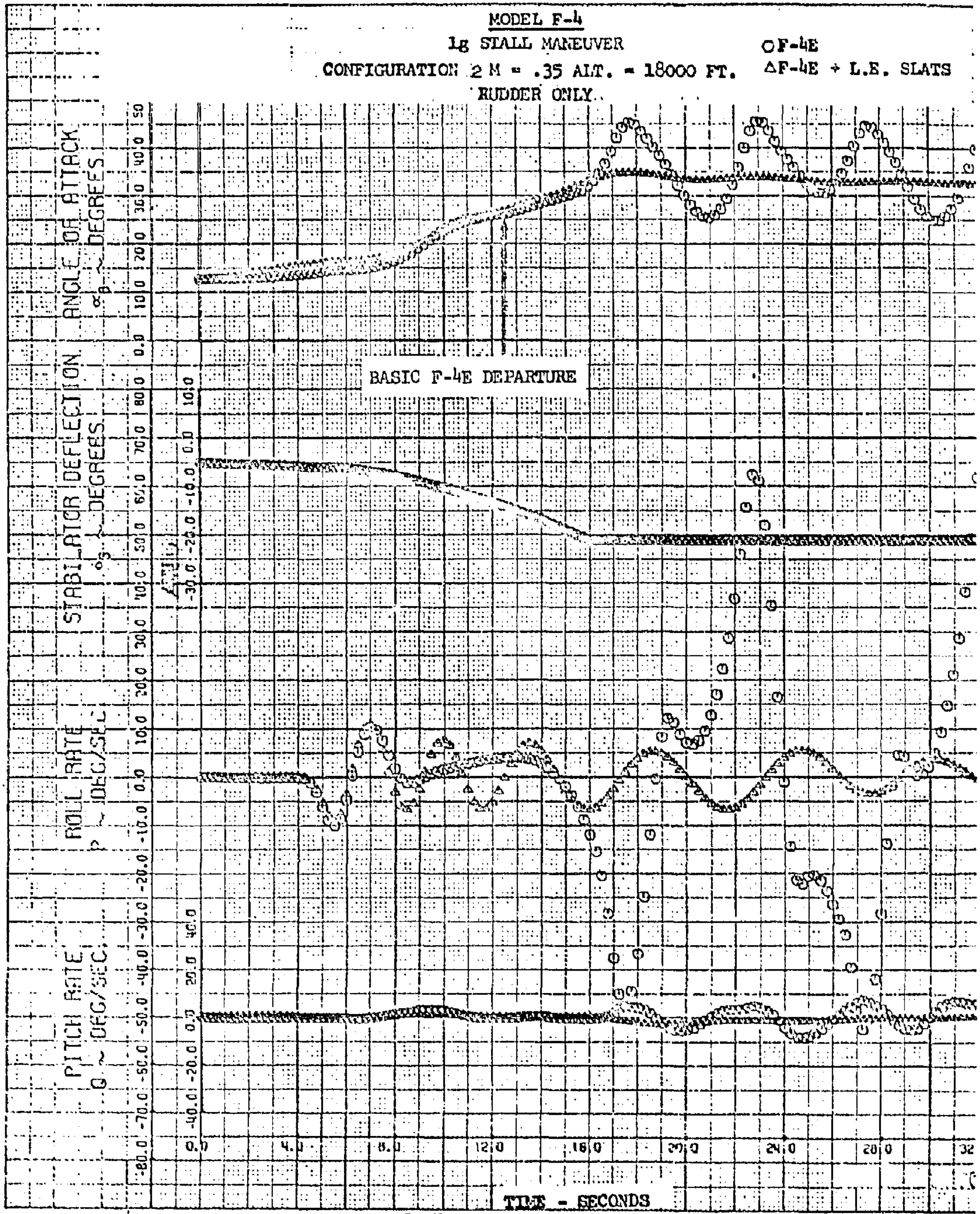
MODEL F-4
1g STALL MANEUVER
CONFIGURATION 2 M = .35 ALT. = 18000 FT.
RUDDER ONLY
○F-4E
ΔF-4E + L.E. SLATS
ANGLE OF ATTACK
α_B ~ DEGREES
0.0
10.0
20.0
30.0
40.0
50
BASIC F-4E DEPARTURE
STABILATOR DEFLECTION
δ_S ~ DEGREES
10.0
0.0
-10.0
-20.0
-30.0
ROLL RATE
P ~ DEG/SEC
80.0
70.0
60.0
50.0
40.0
30.0
20.0
10.0
0.0
-10.0
-20.0
-30.0
-40.0
-50.0
-60.0
-70.0
-80.0
PITCH RATE
Q ~ DEG/SEC
40.0
20.0
0.0
-20.0
-40.0
0.0
4.0
8.0
12.0
16.0
20.0
24.0
28.0
32
TIME - SECONDS

Figure 3.5

MODEL F-4

1g STALL MANEUVER

CONFIGURATION 2 M = .35 ALT. = 18000 FT.

RUDDER ONLY

○ F-4E

△ F-4E + L.E. SLATS

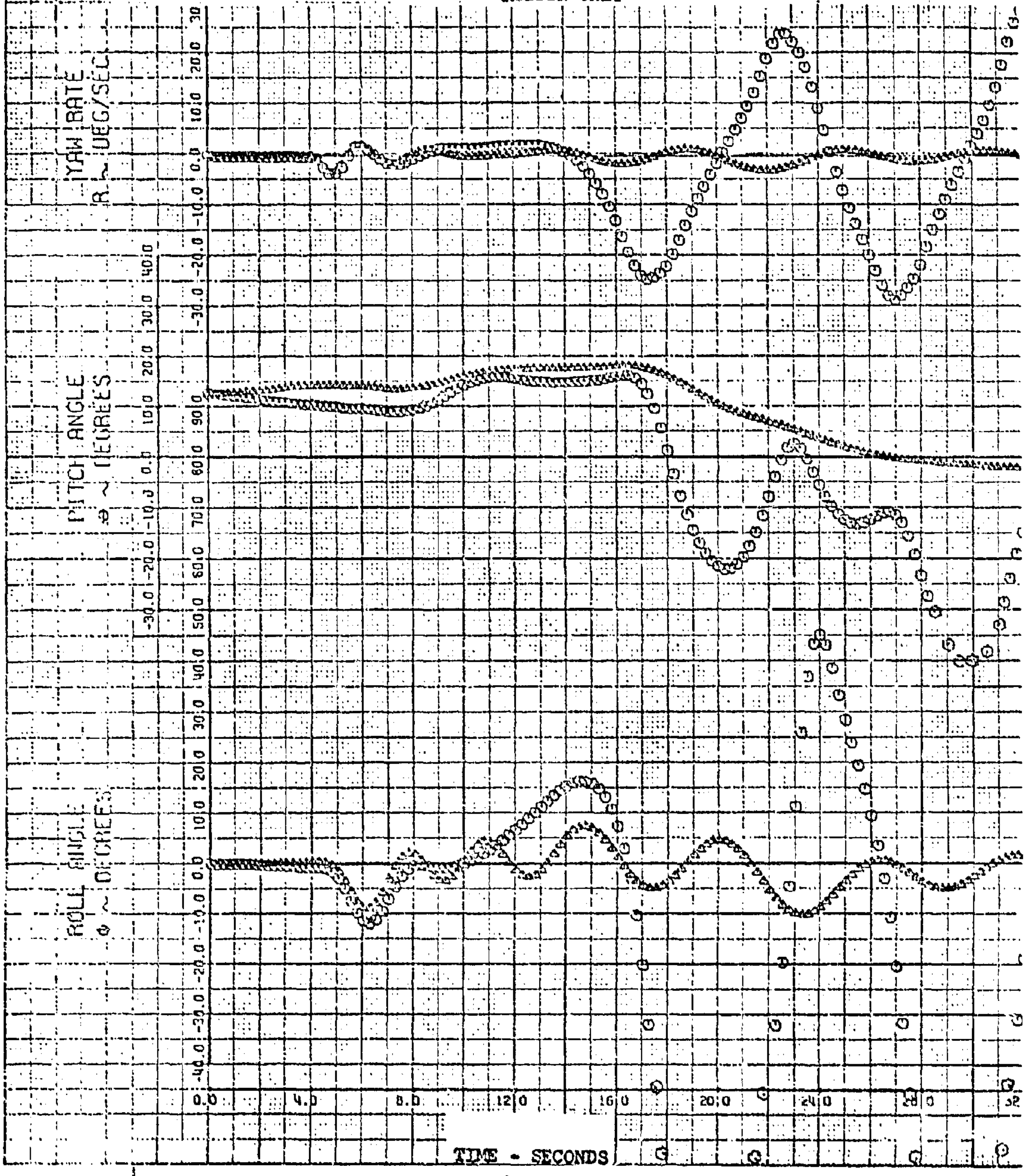

Figure 3.5 Con't

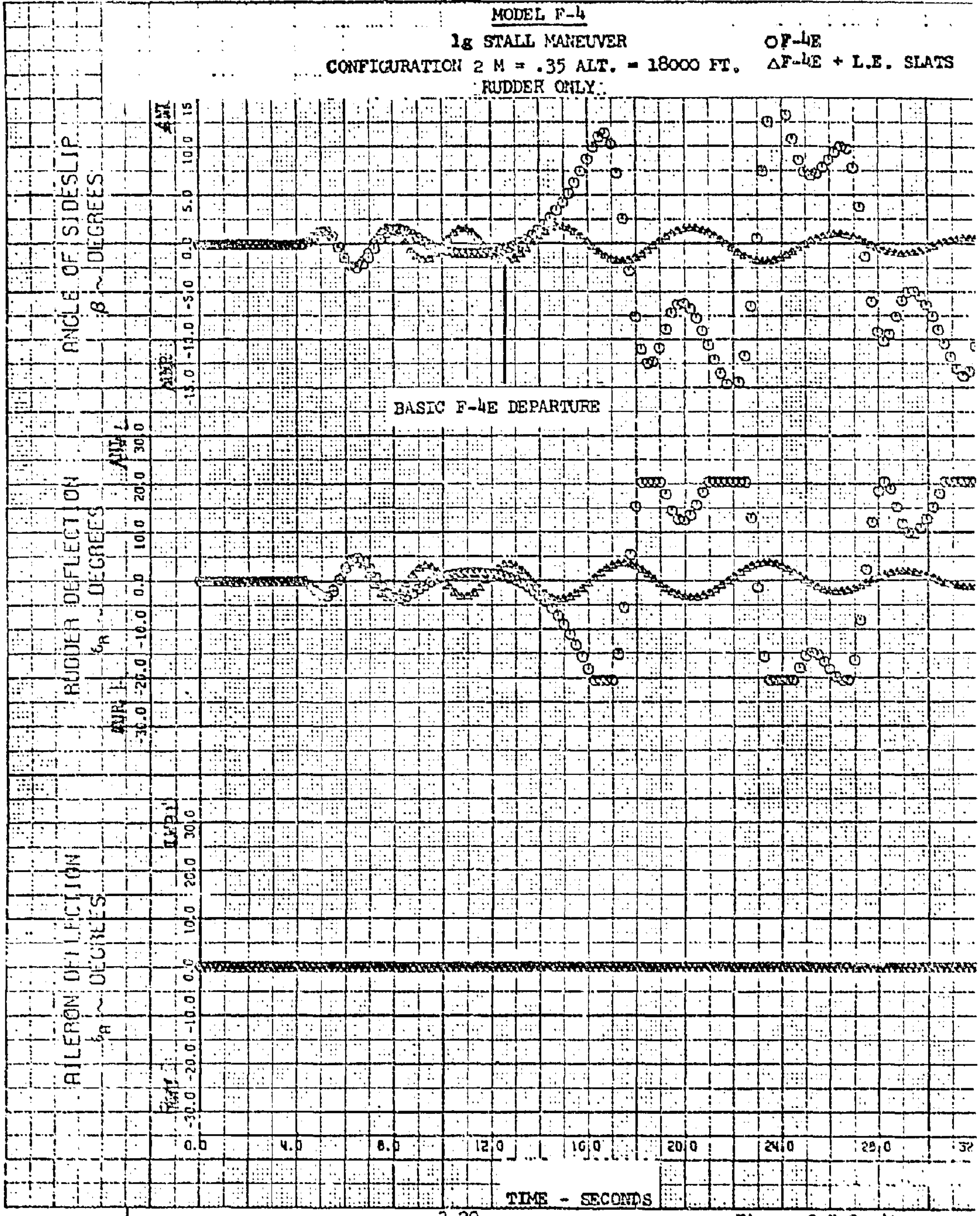

MODEL F-4

1g STALL MANEUVER

CONFIGURATION 2 M = .35 ALT. = 18000 FT.

RUDDER ONLY

○F-4E

△F-4E + L.E. SLATS

Figure 3.5 Con't

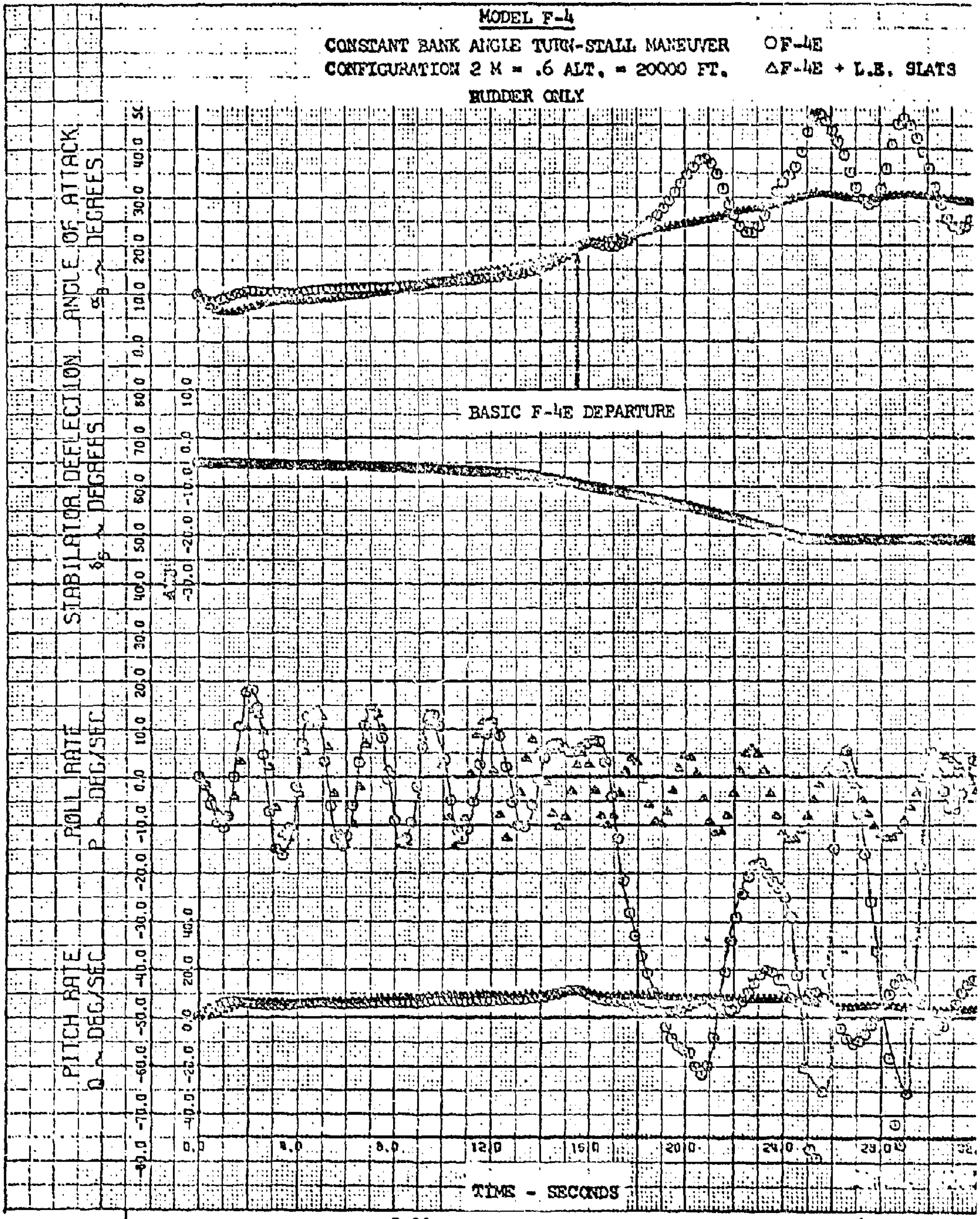
MODEL F-4
CONSTANT BANK ANGLE TURN-STALL MANEUVER
CONFIGURATION 2 M = .6 ALT. = 20000 FT.
RUDDER ONLY
○F-4E
△F-4E + L.E. SLATS
ANGLE OF ATTACK
α_B ~ DEGREES
STABILATOR DEFLECTION
δ_S ~ DEGREES
ROLL RATE
P ~ DEG/SEC
PITCH RATE
Q ~ DEG/SEC
-80.0
-70.0
-60.0
-50.0
-40.0
-30.0
-20.0
-10.0
0.0
10.0
20.0
30.0
40.0
50.0
60.0
70.0
80.0
0.0
10.0
20.0
30.0
40.0
50
-30.0
-20.0
-10.0
0.0
10.0
-40.0
-20.0
0.0
20.0
40.0
BASIC F-4E DEPARTURE
0.0
4.0
8.0
12.0
16.0
20.0
24.0
28.0
32.
TIME - SECONDS

Figure 3.6

**MODEL F-4**

CONSTANT BANK ANGLE TURN-STALL MANEUVER
CONFIGURATION 2 M = .6 ALT. = 20000 FT.
RUDDER ONLY

○ F-4E
Δ F-4E + L.E. SLATS

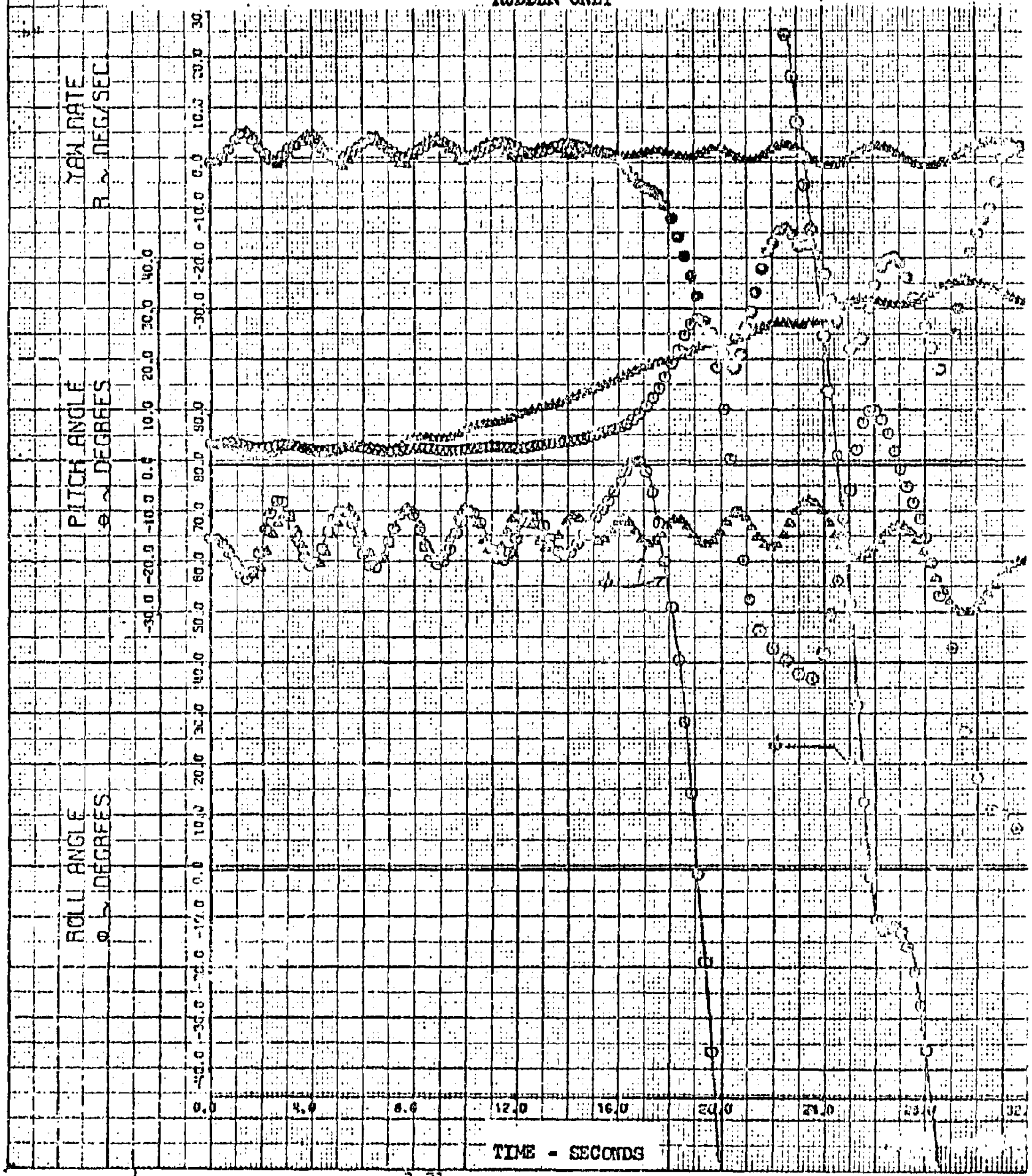

Figure 3.6 Con't

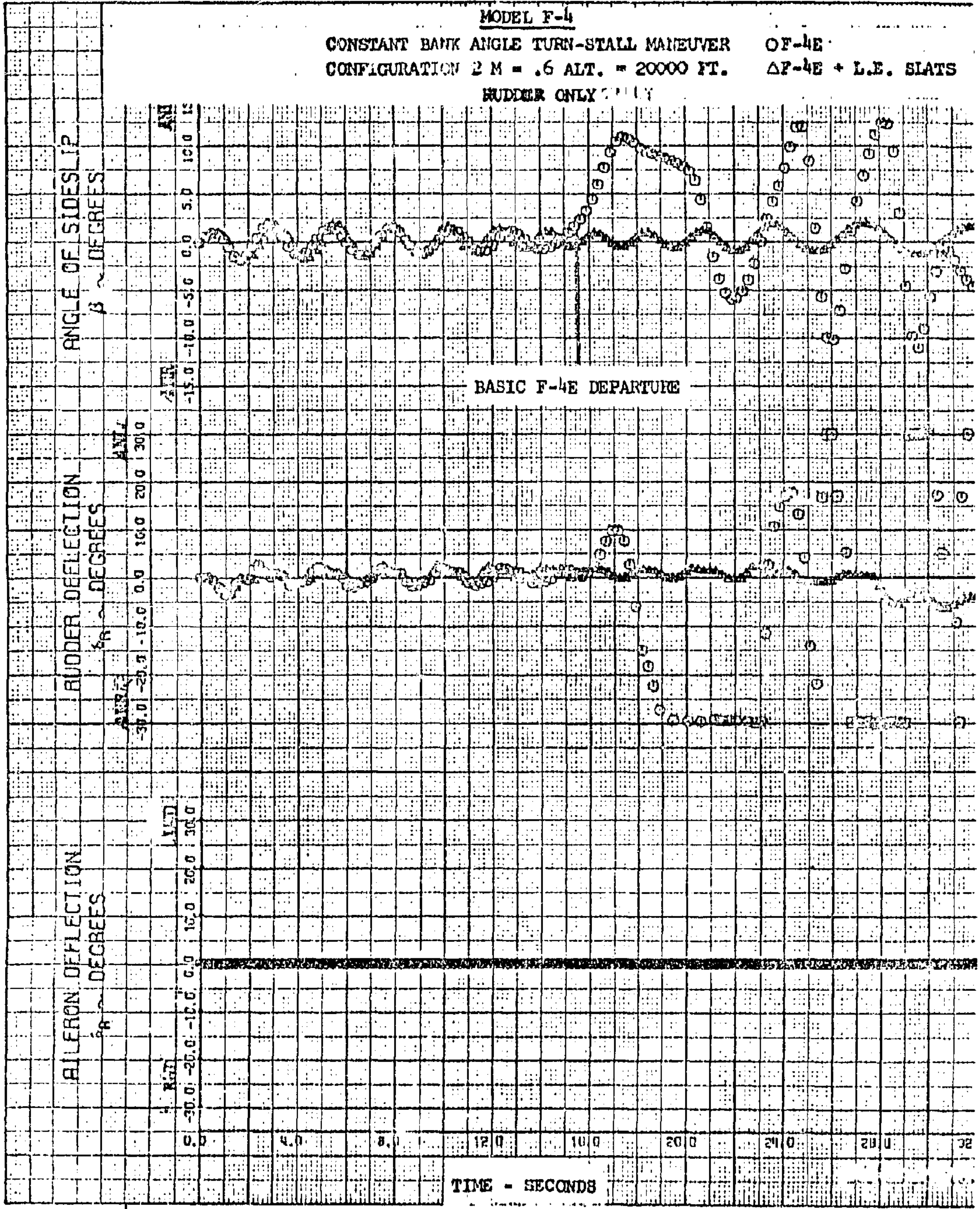

Figure 3.6 Con't

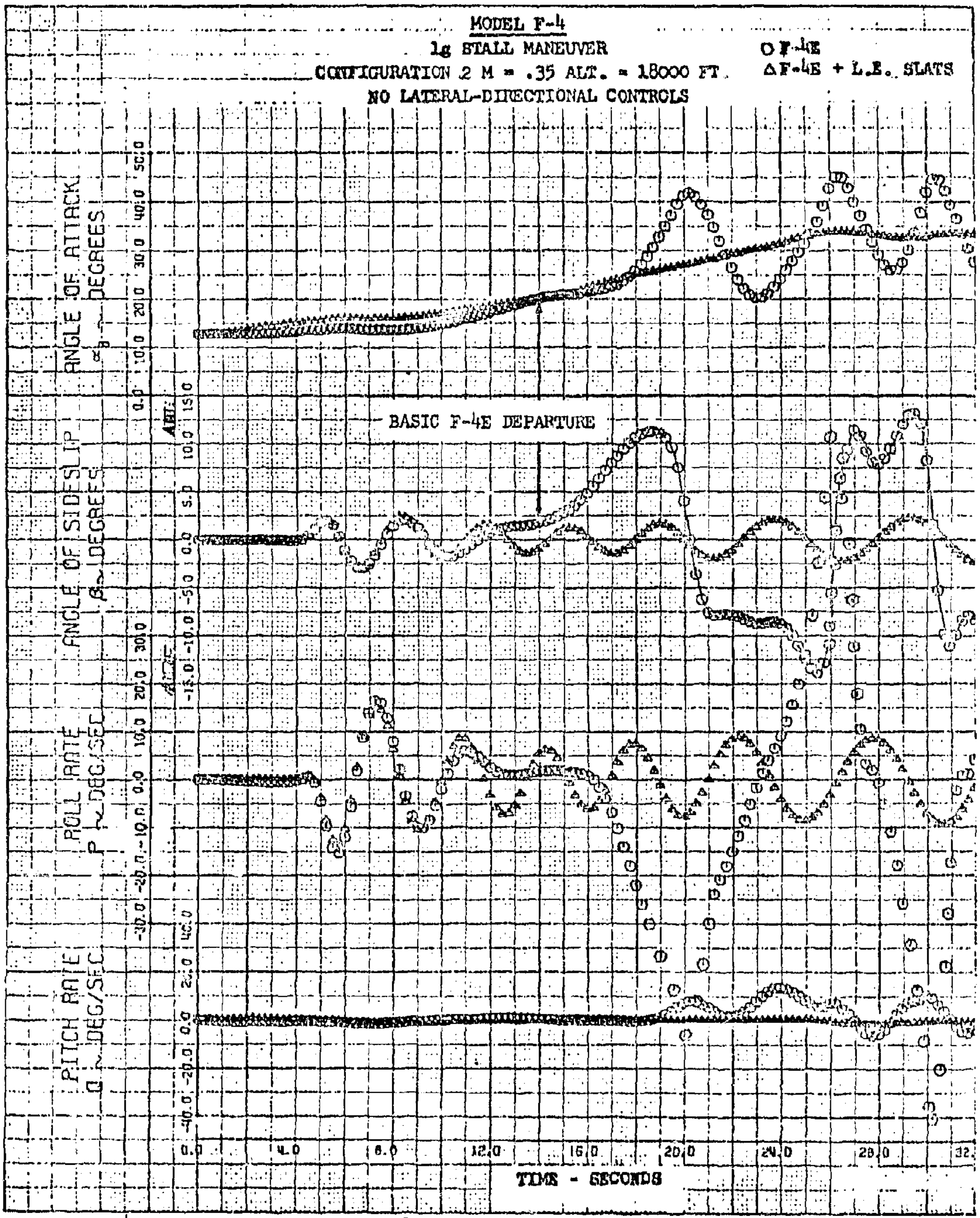
MODEL F-4
1g STALL MANEUVER
CONFIGURATION 2 M = .35 ALT. = 18000 FT.
NO LATERAL-DIRECTIONAL CONTROLS
○ F-4E
△ F-4E + L.E. SLATS
ANGLE OF ATTACK
α ~ DEGREES
0.0
10.0
20.0
30.0
40.0
50.0
BASIC F-4E DEPARTURE
ANGLE OF SIDESLIP
β ~ DEGREES
15.0
10.0
5.0
0.0
-5.0
-10.0
-15.0
ROLL RATE
P ~ DEG/SEC
30.0
20.0
10.0
0.0
-10.0
-20.0
-30.0
PITCH RATE
Q ~ DEG/SEC
40.0
20.0
0.0
-20.0
-40.0
0.0
4.0
8.0
12.0
16.0
20.0
24.0
28.0
32.
TIME - SECONDS

Figure 3.7

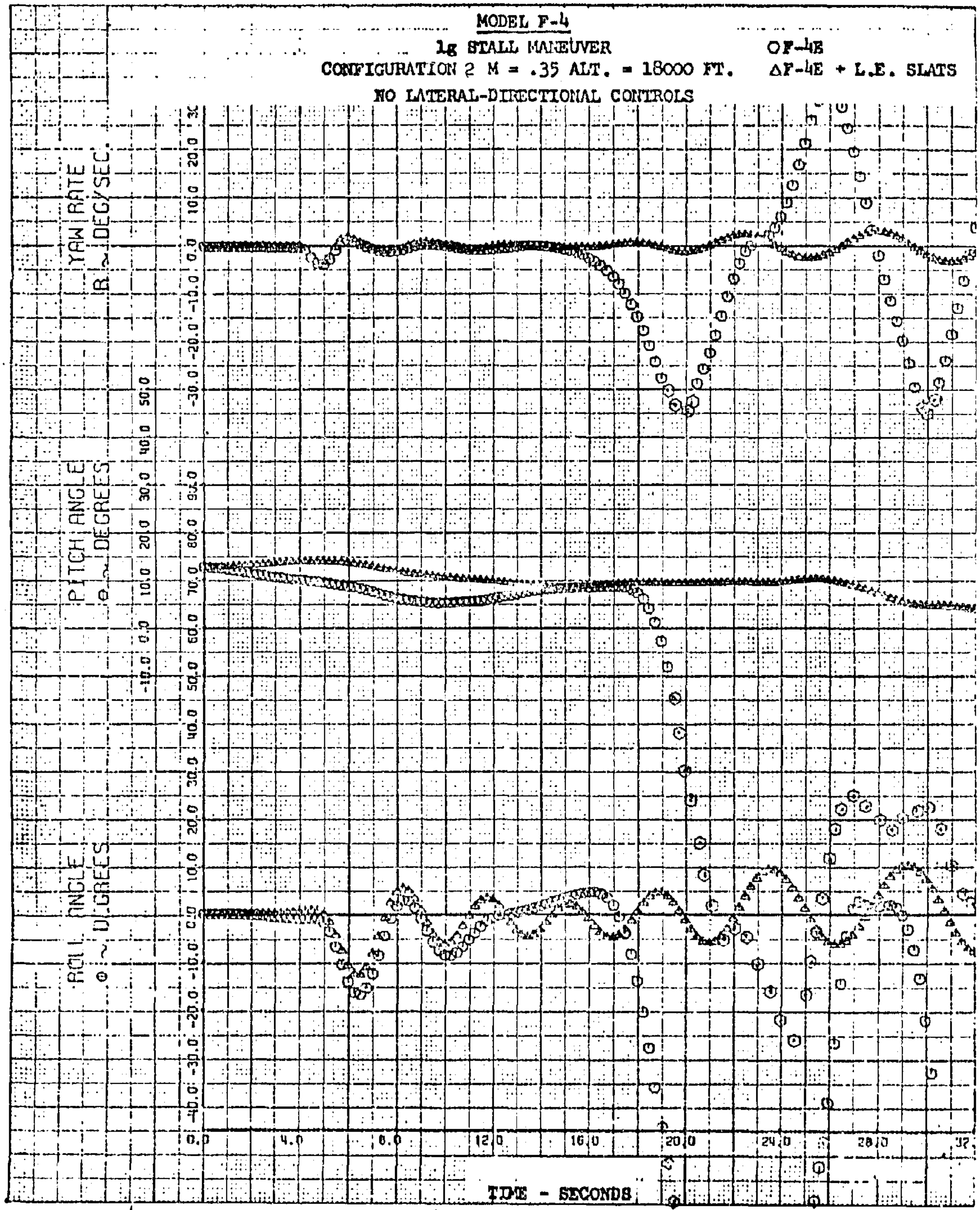

MODEL F-4

1g STALL MANEUVER

CONFIGURATION 2 M = .35 ALT. = 18000 FT.

NO LATERAL-DIRECTIONAL CONTROLS

○ F-4E

△ F-4E + L.E. SLATS

Figure 3.7 Con't

**MODEL F-4**

1g STALL MANEUVER

CONFIGURATION 2 M = .35 ALT. = 18000 FT.

NO LATERAL-DIRECTIONAL CONTROLS

○ F-4E

△ F-4E + L.E. SLATS

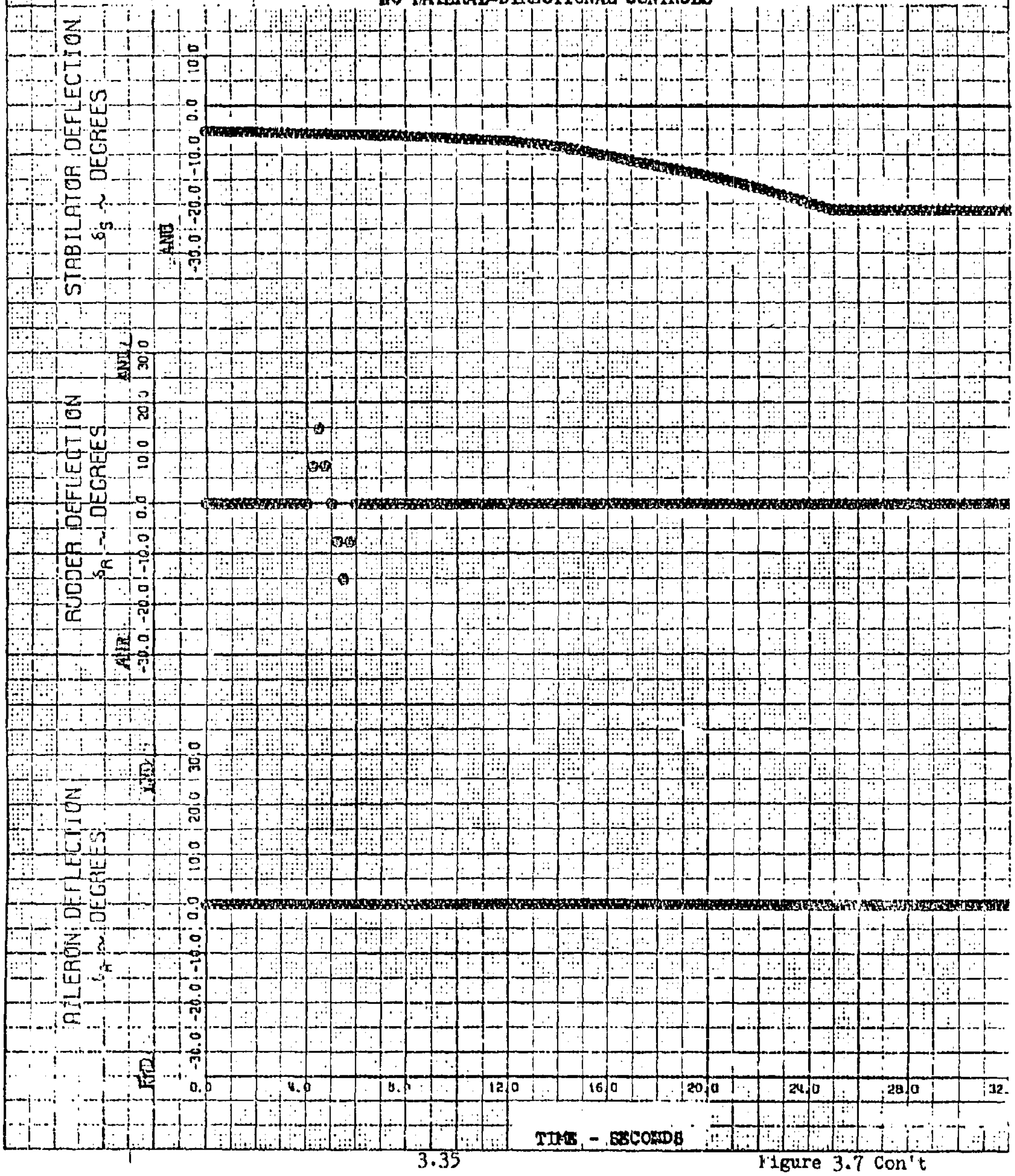

Figure 3.7 Con't

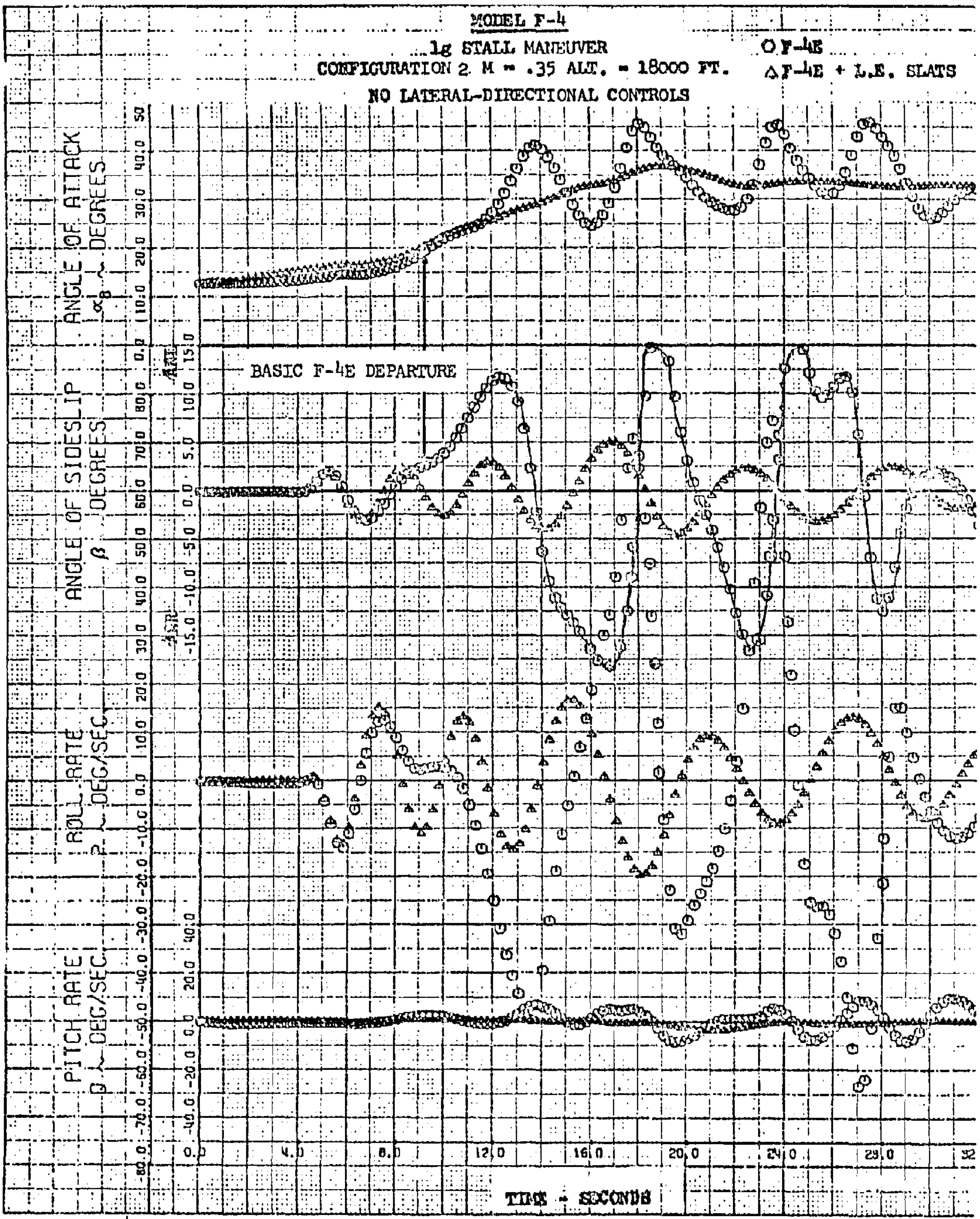
MODEL F-4
1g STALL MANEUVER
CONFIGURATION 2 M = .35 ALT. = 18000 FT.
NO LATERAL-DIRECTIONAL CONTROLS
○ F-4E
△ F-4E + L.E. SLATS
BASIC F-4E DEPARTURE

Figure 3.8

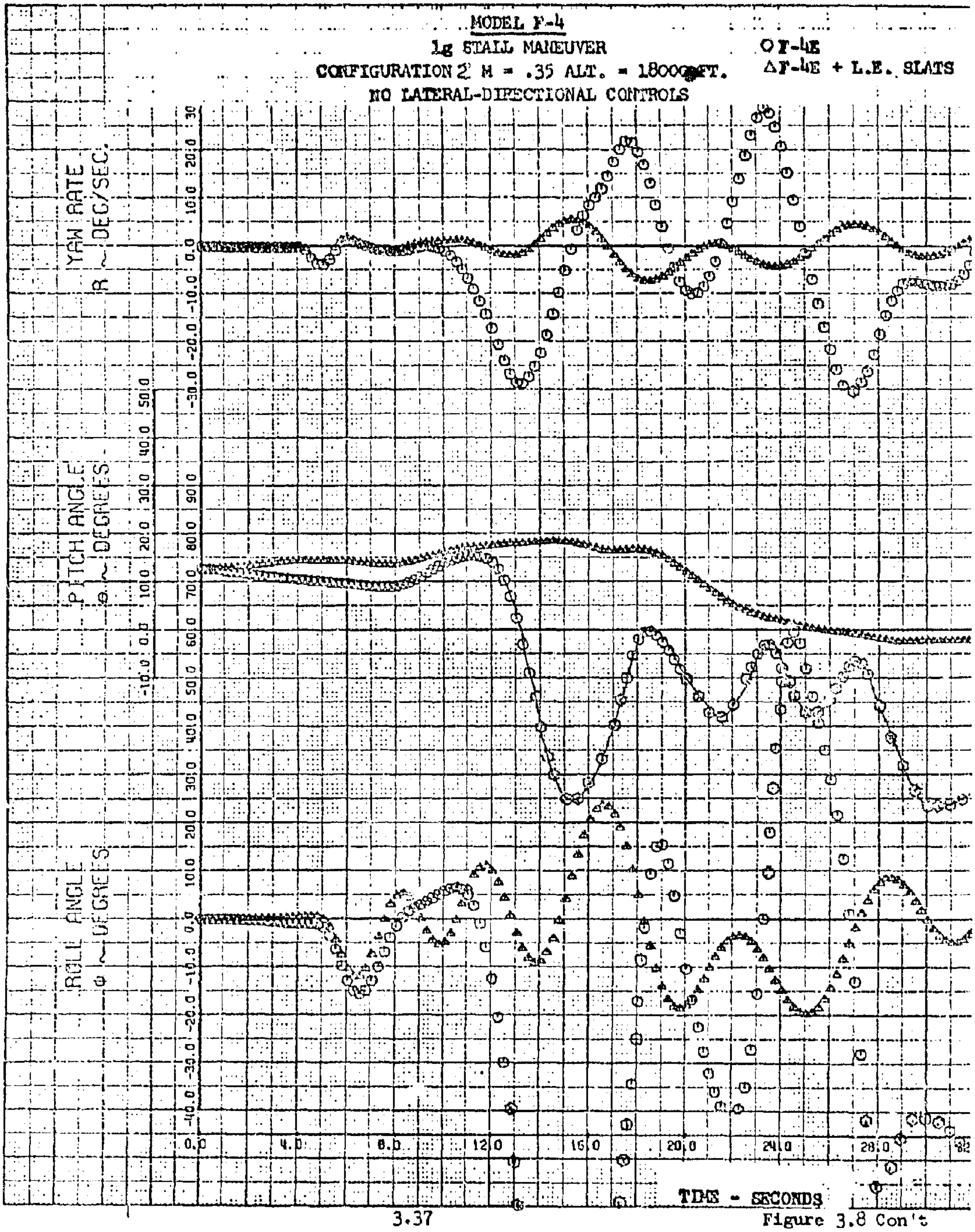

Figure 3.8 Con't

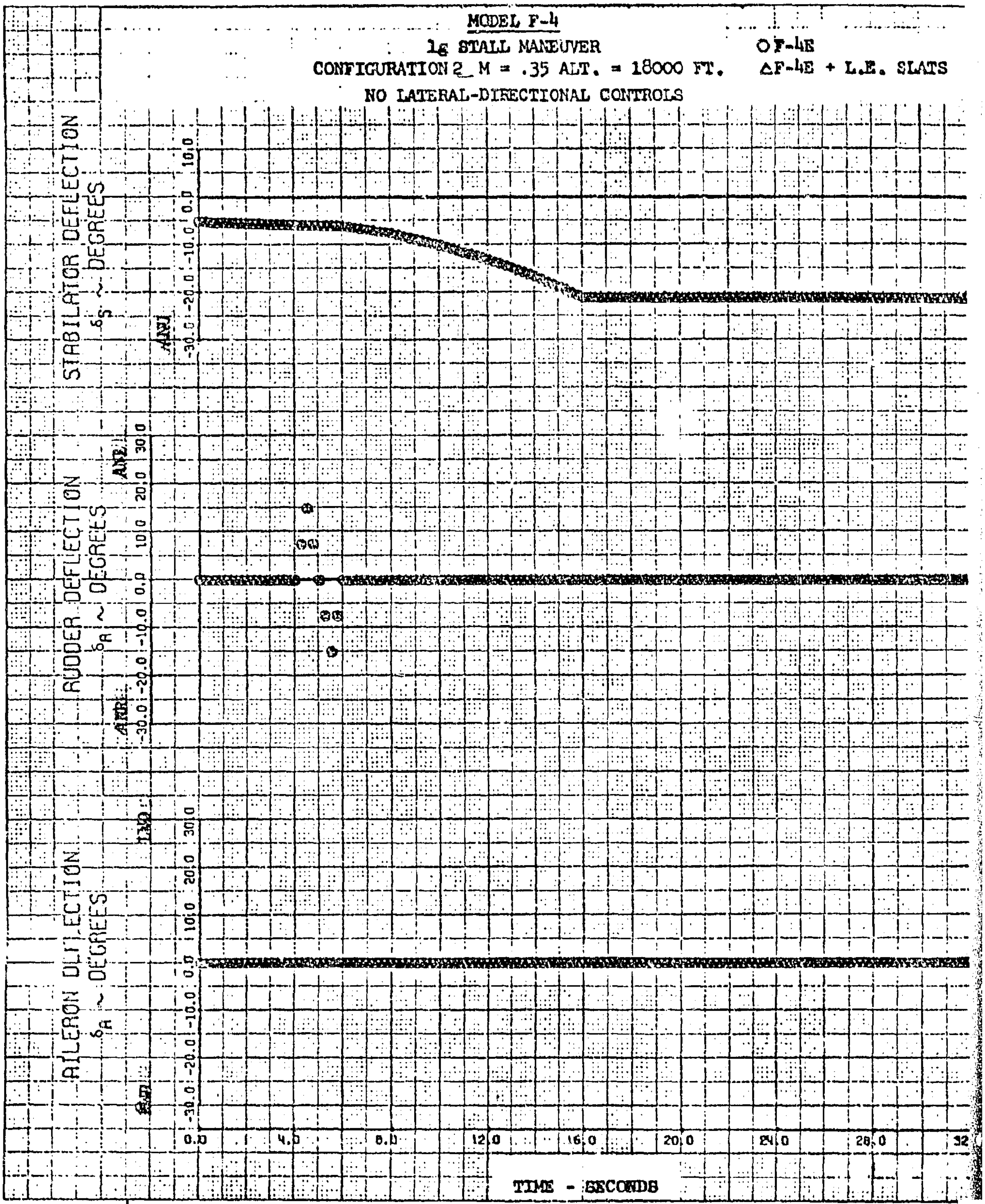

MODEL F-4

1g STALL MANEUVER

CONFIGURATION 2 M = .35 ALT. = 18000 FT.

NO LATERAL-DIRECTIONAL CONTROLS

○ F-4E

△ F-4E + L.E. SLATS

Figure 3.8 Con't

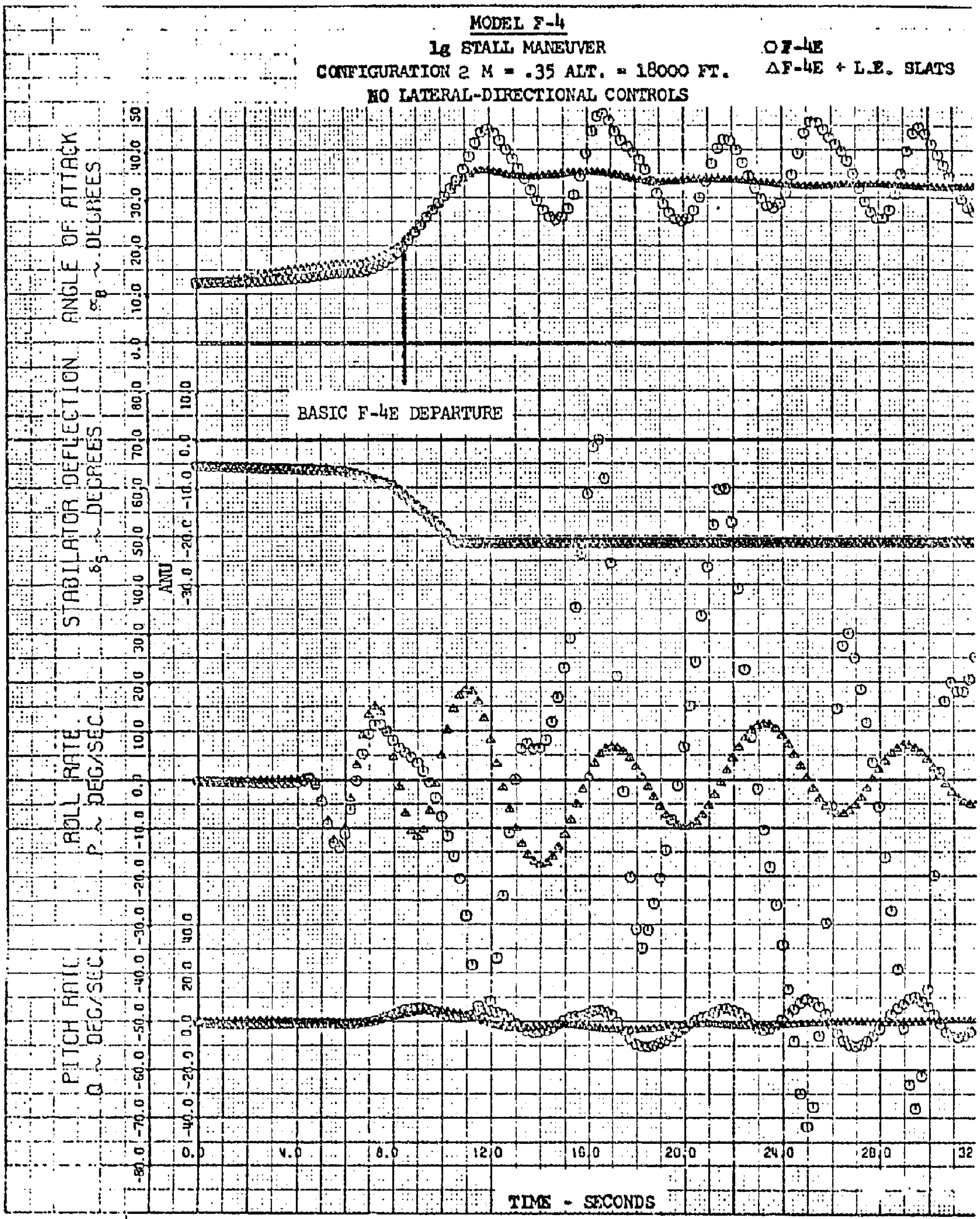
MODEL F-4
1g STALL MANEUVER
CONFIGURATION 2 M = .35 ALT. = 18000 FT.
NO LATERAL-DIRECTIONAL CONTROLS
○ F-4E
△ F-4E + L.E. SLATS
ANGLE OF ATTACK
α_B ~ DEGREES
STABILATOR DEFLECTION
δ_S ~ DEGREES
ROLL RATE
P ~ DEG/SEC
PITCH RATE
Q ~ DEG/SEC
ANU
BASIC F-4E DEPARTURE
-80.0
-70.0
-60.0
-50.0
-40.0
-30.0
-20.0
-10.0
0.0
10.0
20.0
30.0
40.0
50.0
60.0
70.0
80.0
40.0
-20.0
0.0
20.0
40.0
-30.0
-20.0
-10.0
0.0
10.0
0.0
4.0
8.0
12.0
16.0
20.0
24.0
28.0
32
TIME - SECONDS

Figure 3.9

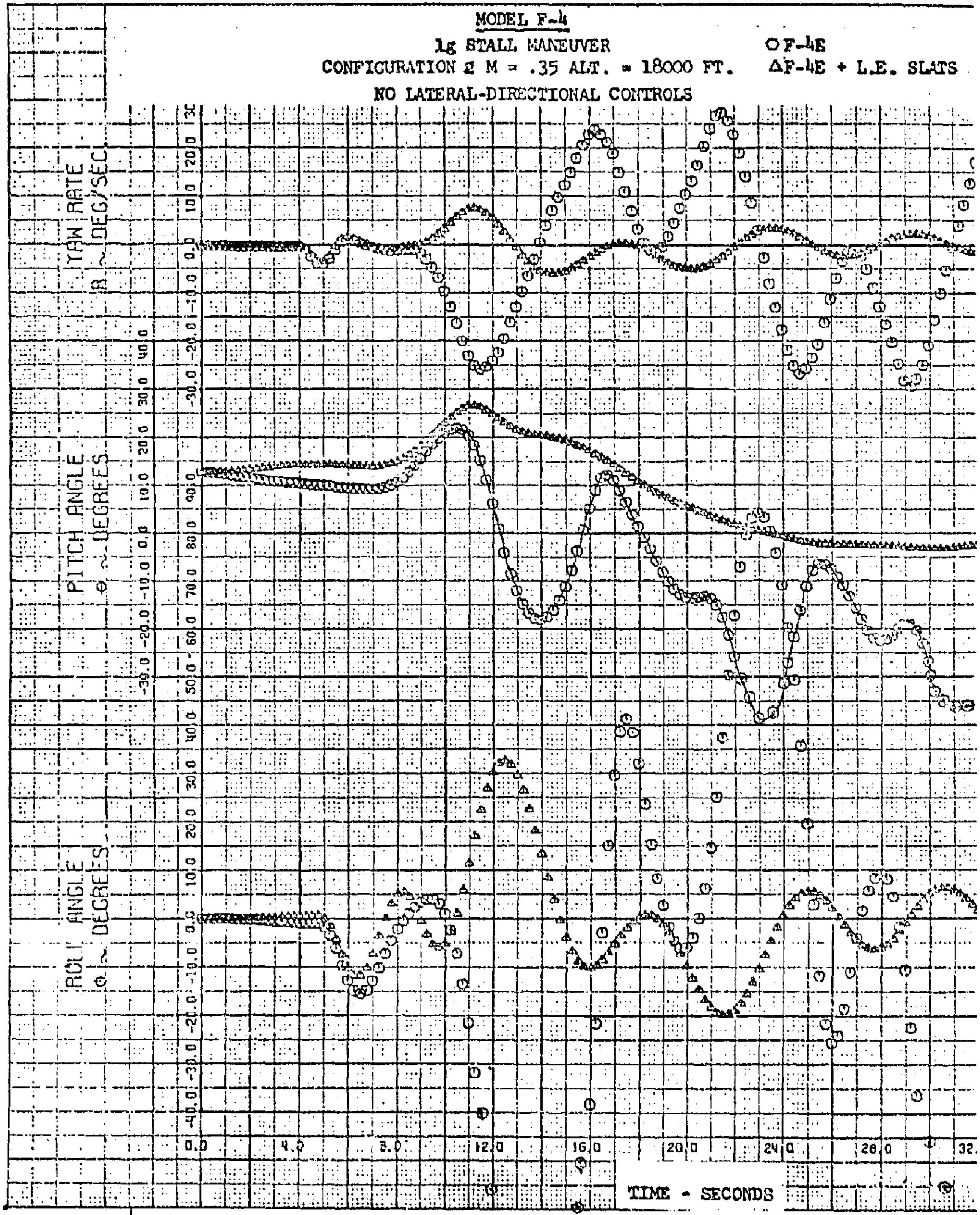

MODEL F-4

1g STALL MANEUVER

CONFIGURATION 2 M = .35 ALT. = 18000 FT.

NO LATERAL-DIRECTIONAL CONTROLS

Figure 3.9 Con't

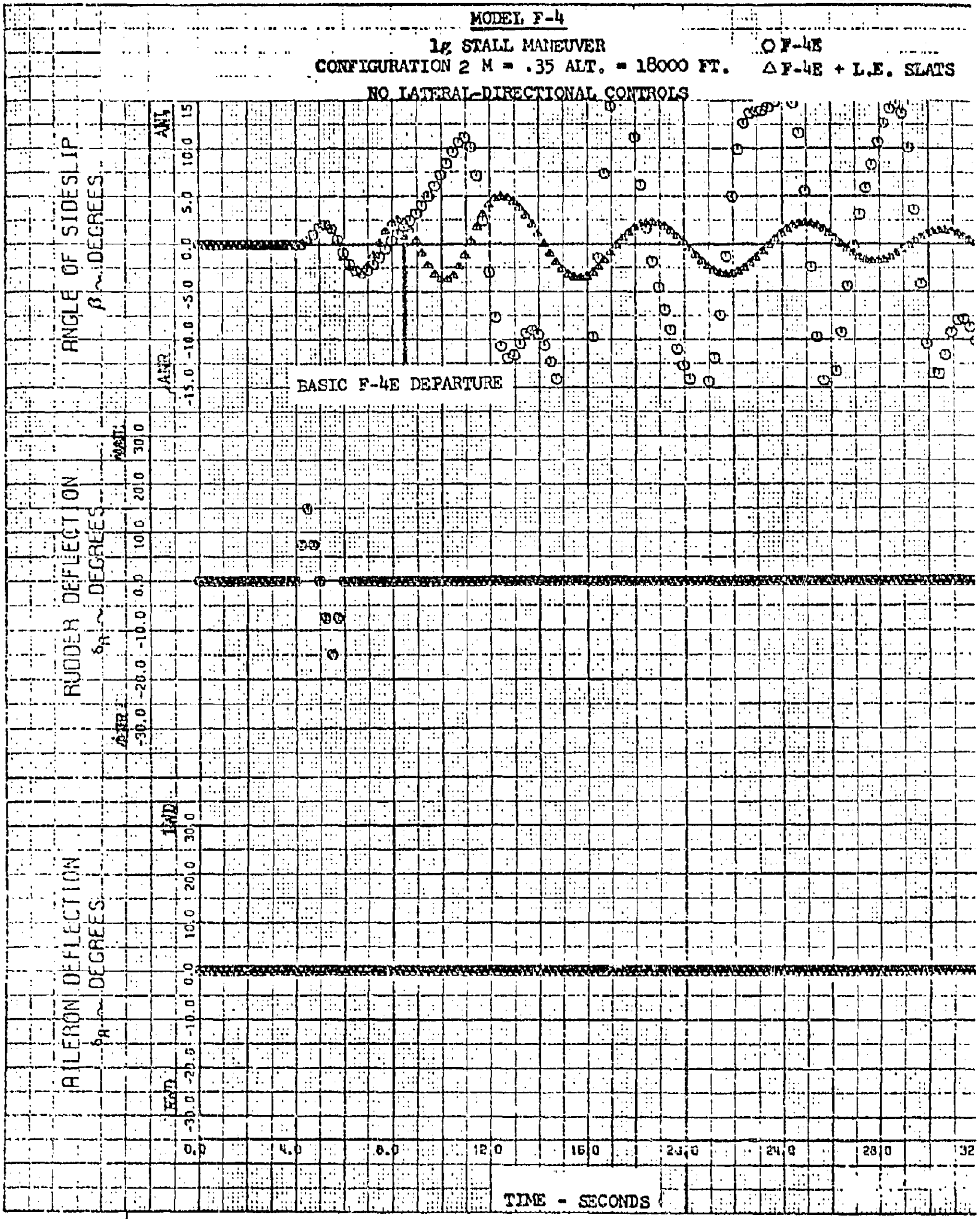

Figure 3.9 Con't

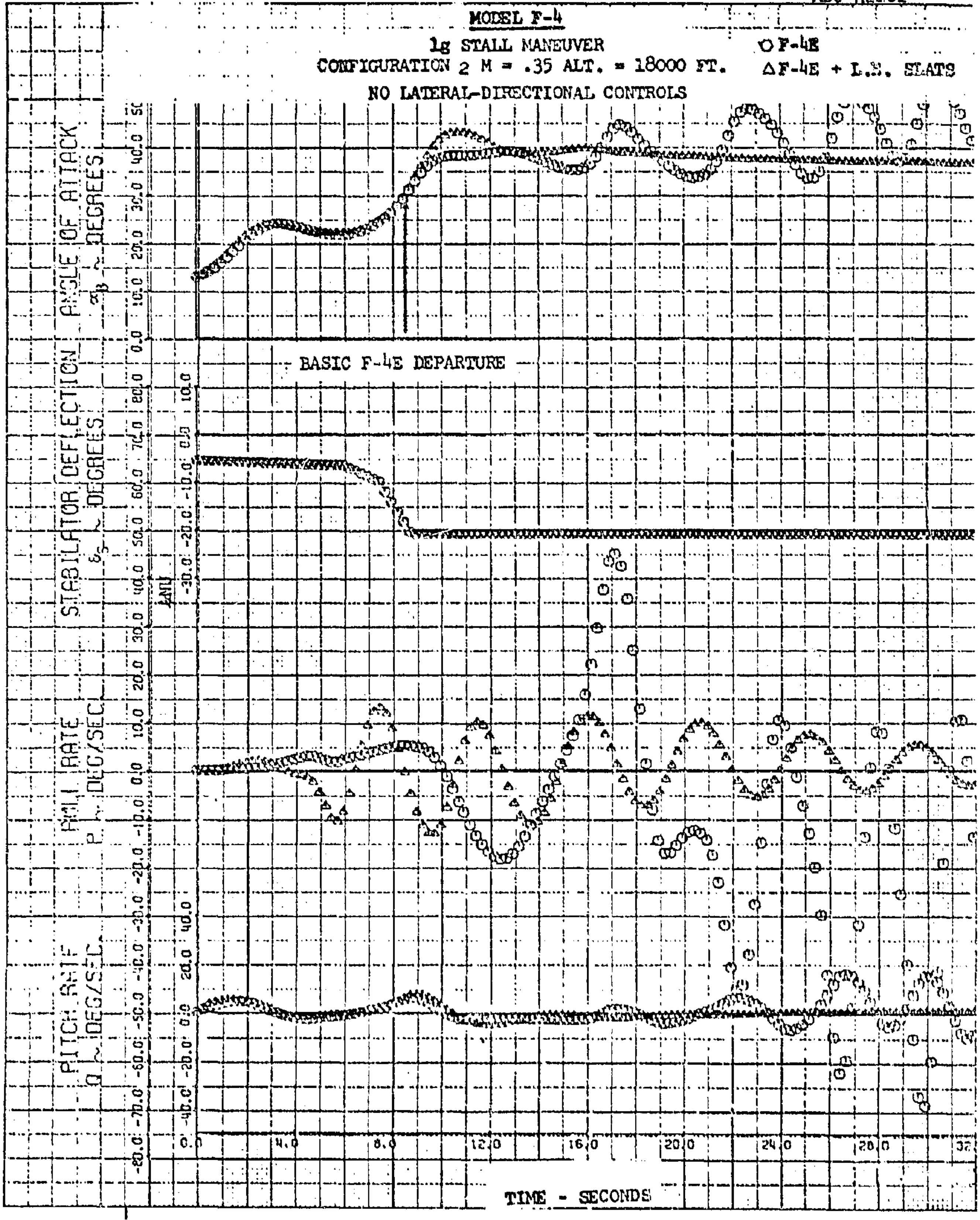

**MODEL F-4**

1g STALL MANEUVER
CONFIGURATION 2 M = .35 ALT. = 18000 FT.
NO LATERAL-DIRECTIONAL CONTROLS

Figure 3.10

MODEL F-4

1g STALL MANEUVER

CONFIGURATION 2 M = .35 ALT. = 18000 FT.

NO LATERAL-DIRECTIONAL CONTROLS

○ F-4E

△ F-4E + L.E. SLATS

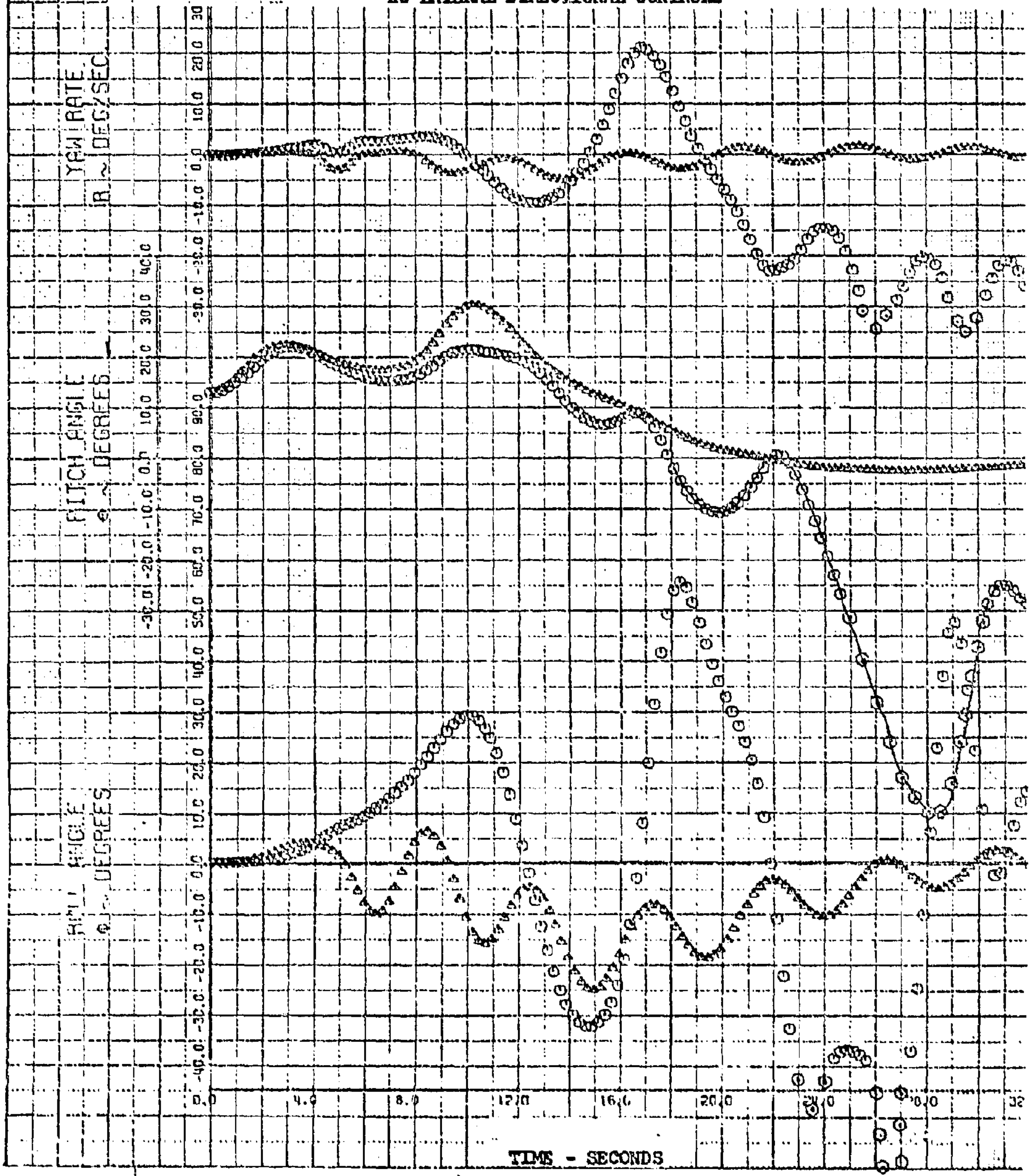

Figure 3.10 Con't

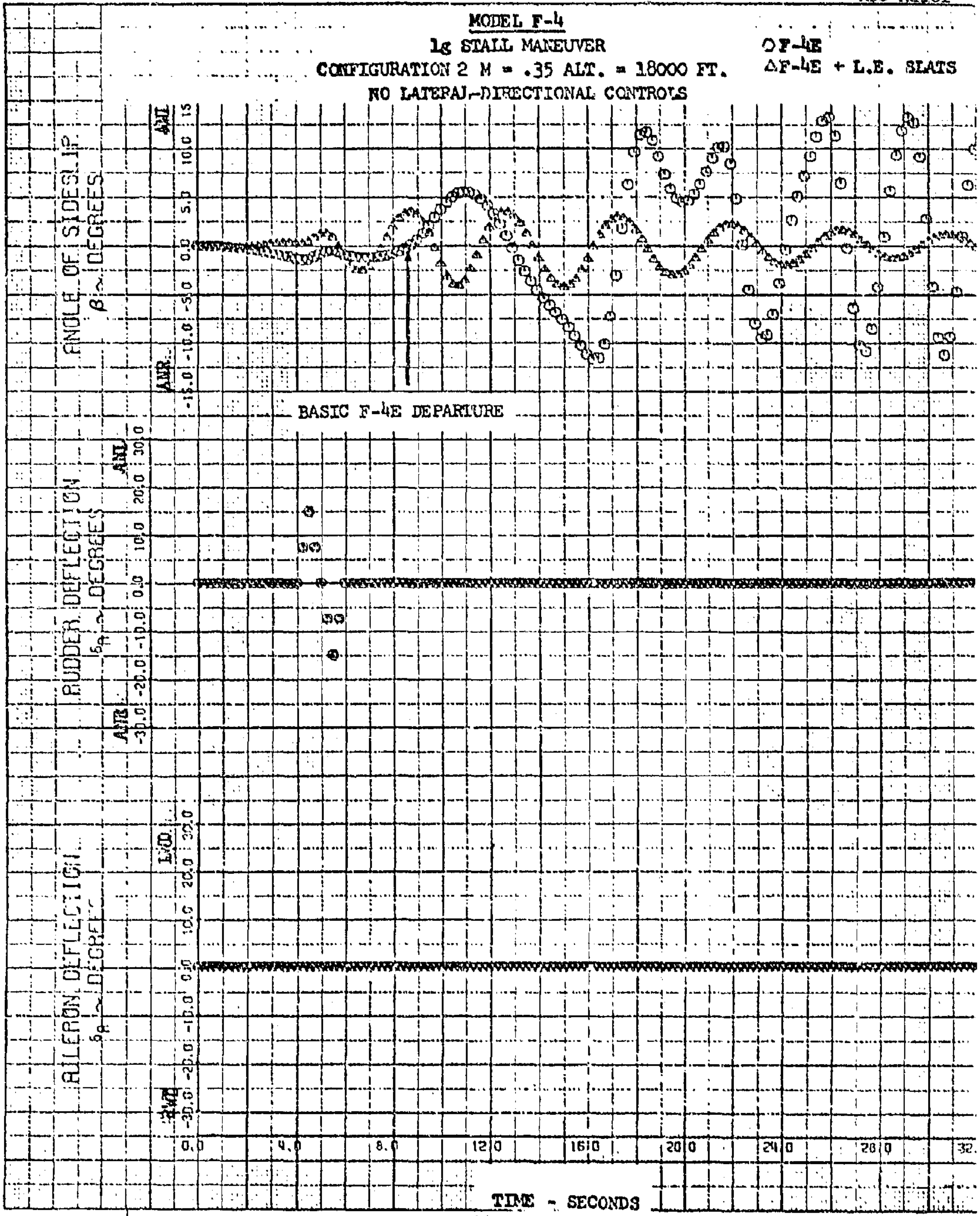

**MODEL F-4**

1g STALL MANEUVER

CONFIGURATION 2 M = .35 ALT. = 18000 FT.

NO LATERAL-DIRECTIONAL CONTROLS

○ F-4E

△ F-4E + L.E. SLATS

Figure 3.10 Con't

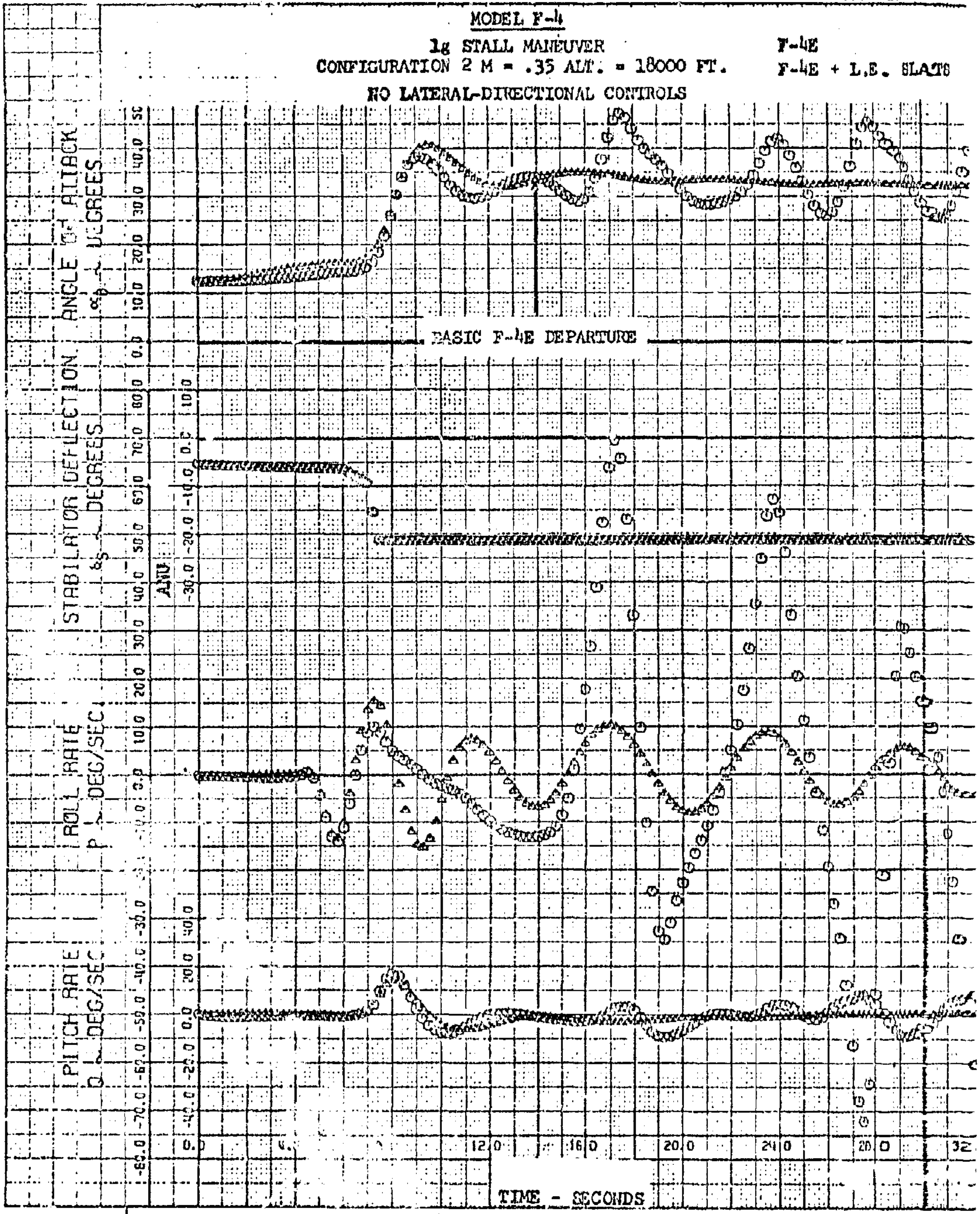

MODEL F-4

1g STALL MANEUVER

CONFIGURATION 2 M = .35 ALT. = 18000 FT.

NO LATERAL-DIRECTIONAL CONTROLS

F-4E

F-4E + L.E. SLATS

Figure 3.11

MODEL F-4

1g STALL MANEUVER

CONFIGURATION 2 M = .35 ALT. = 18000 FT.

NO LATERAL-DIRECTIONAL CONTROLS

F-4E

F-4E + L.E. SLATS

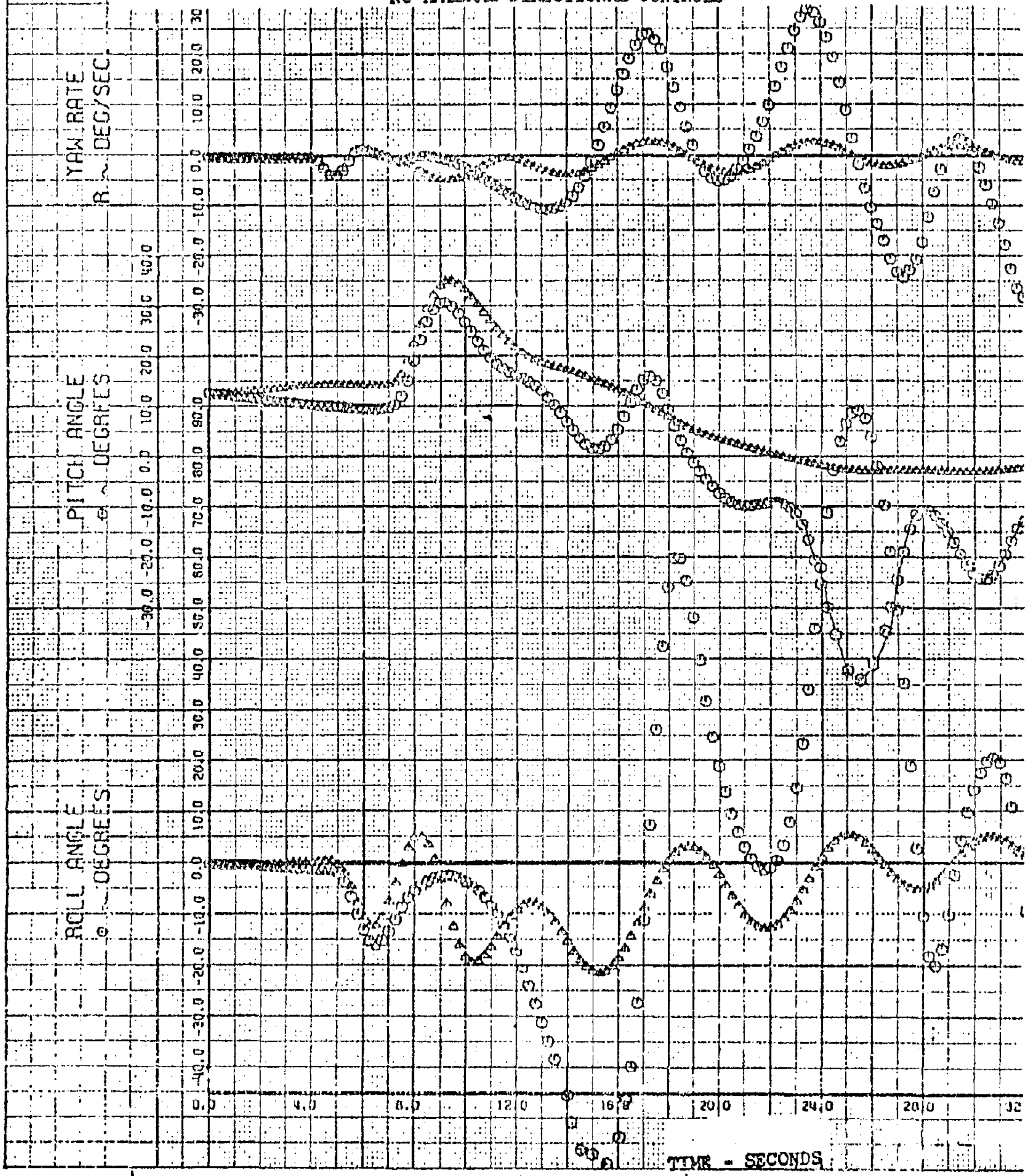

Figure 3.1[illegible] Con't

MODEL F-4

1g STALL MANEUVER

CONFIGURATION 2 M = .35 ALT. = 18000 FT.

NO LATERAL-DIRECTIONAL CONTROLS

F-4E

F-4E + L.E. SLATS

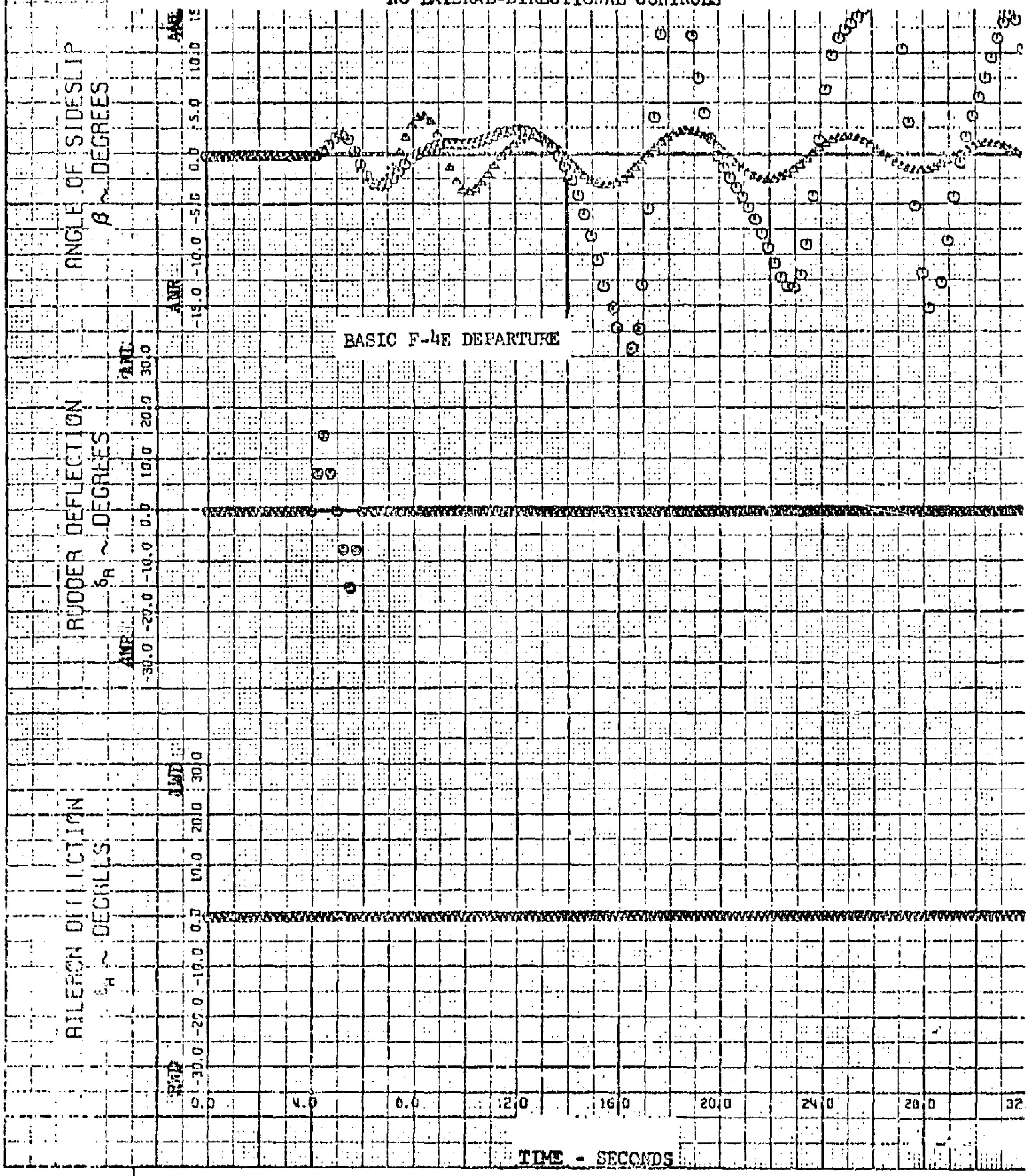

Figure 3.11 Con't

## MODEL F-4

CONSTANT BANK ANGLE TURN-STALL MANEUVER
CONFIGURATION 1 M = .6 ALT. = 20000 FT.
AILERON/RUDDER

○ F-4E
△ F-4E + L.E. SLATS

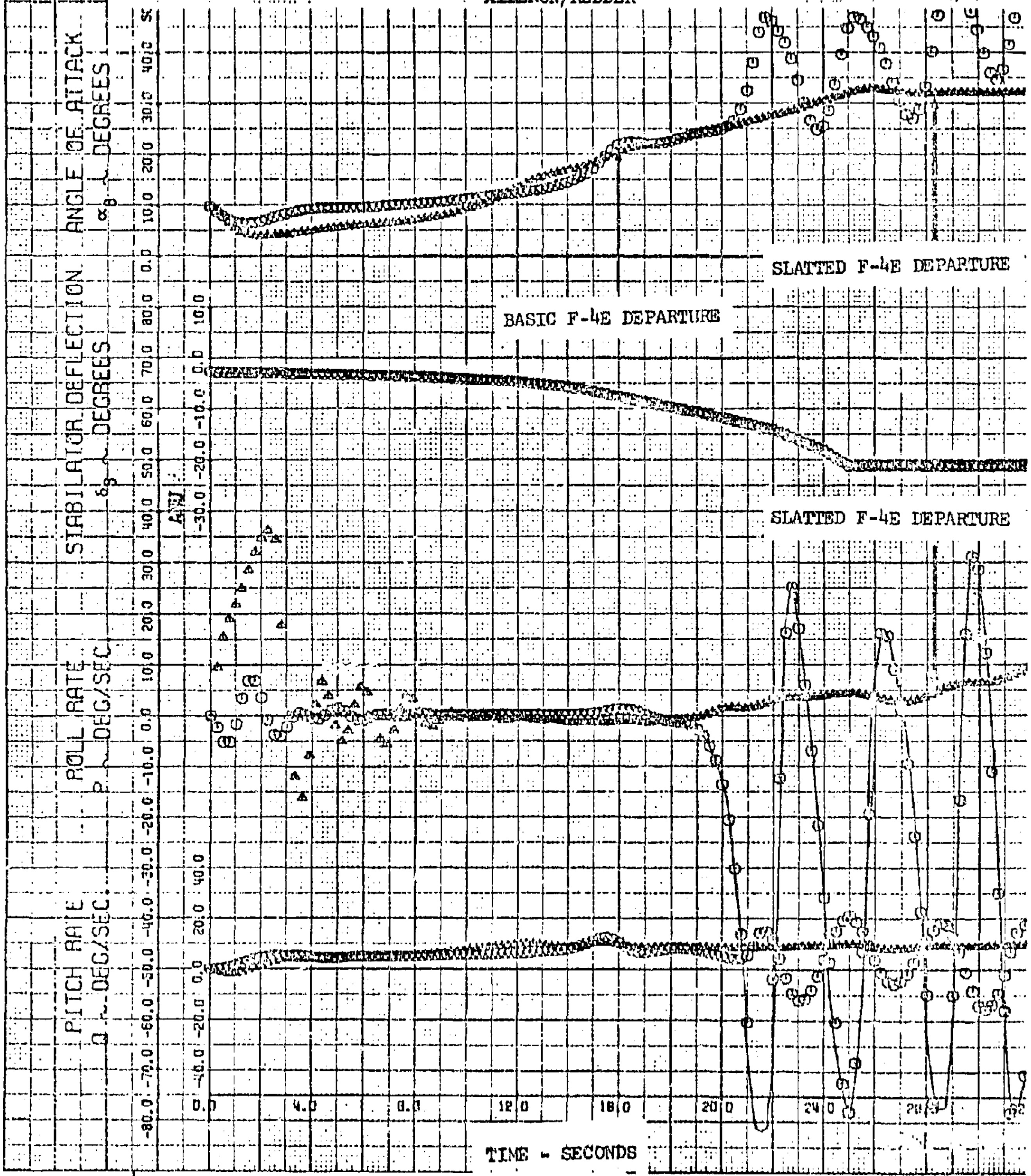

Figure 3.12

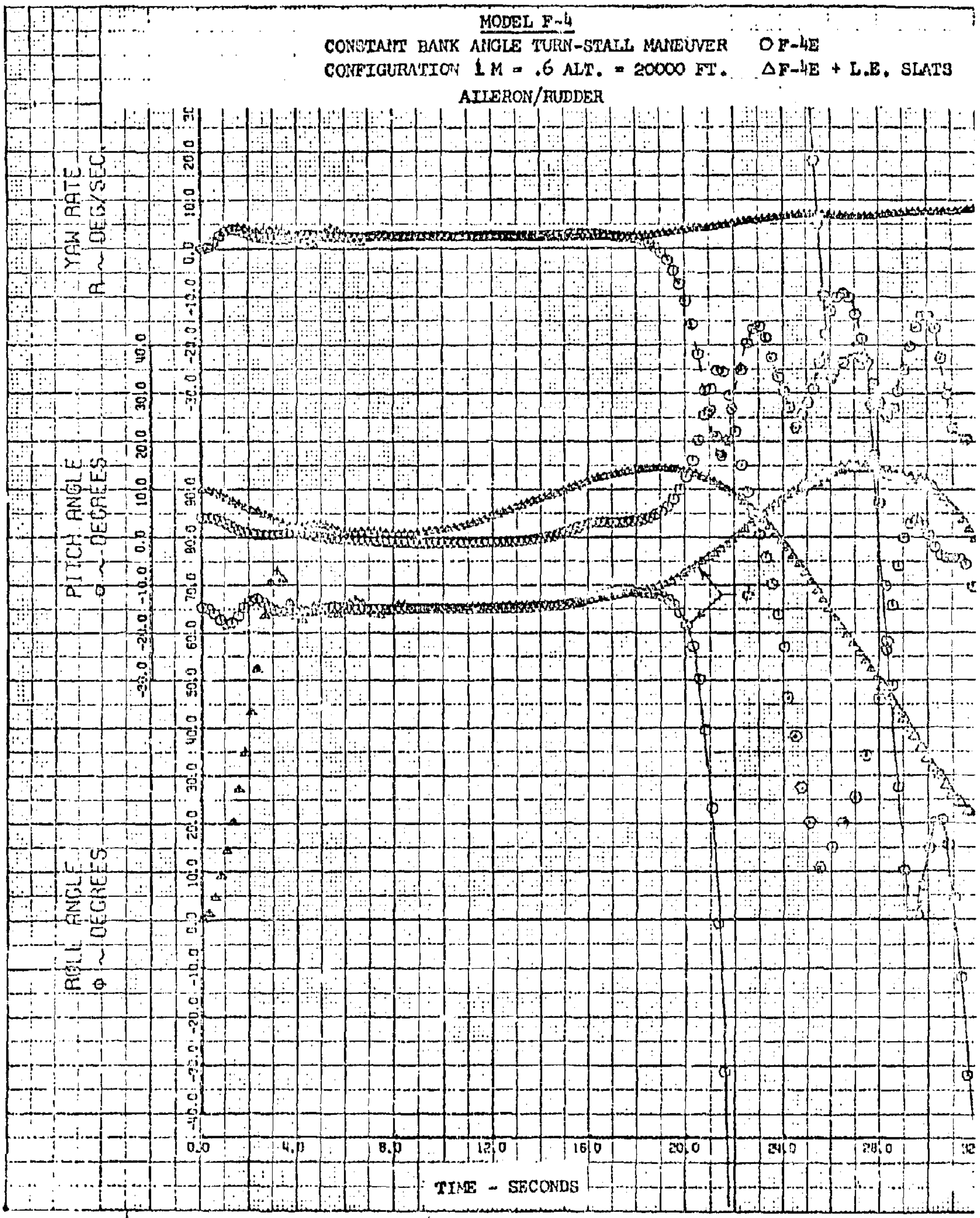

MODEL F-4

CONSTANT BANK ANGLE TURN-STALL MANEUVER ○ F-4E

CONFIGURATION 1 M = .6 ALT. = 20000 FT. △ F-4E + L.E. SLATS

AILERON/RUDDER

Figure 3.12 Con't

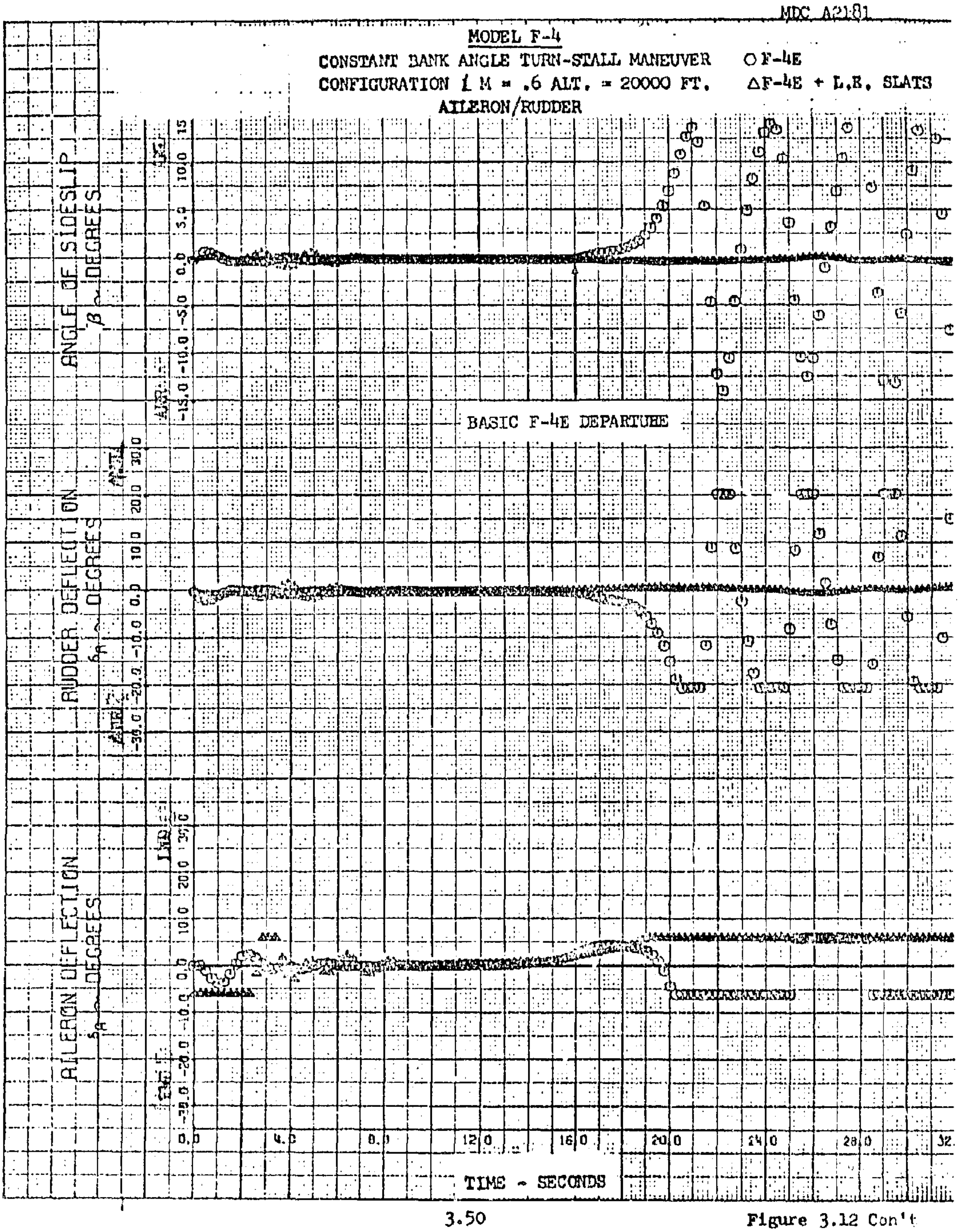

MODEL F-4

CONSTANT BANK ANGLE TURN-STALL MANEUVER ○ F-4E

CONFIGURATION 1 M = .6 ALT. = 20000 FT. △ F-4E + L.E. SLATS

AILERON/RUDDER

Figure 3.12 Con't

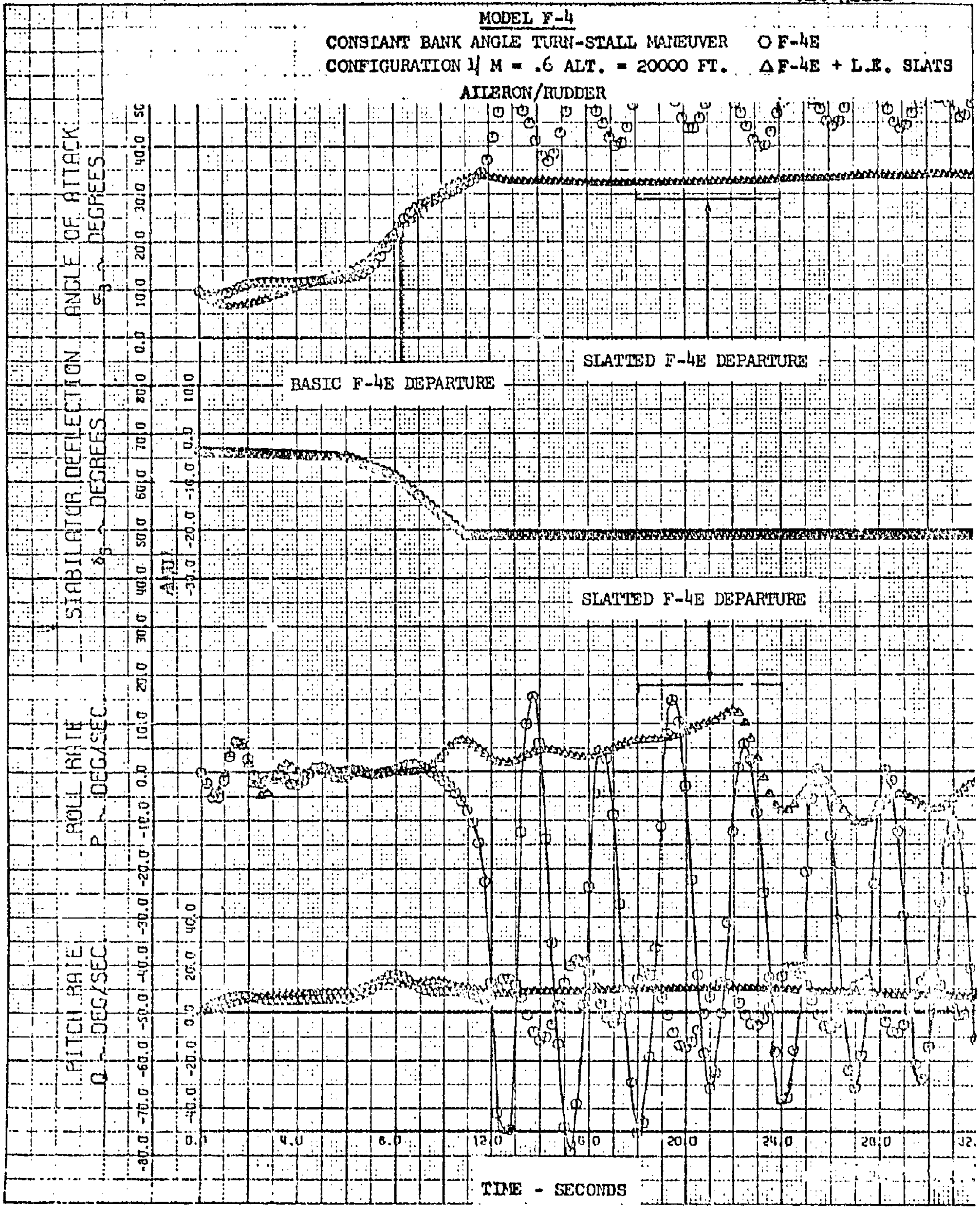
MODEL F-4
CONSTANT BANK ANGLE TURN-STALL MANEUVER
CONFIGURATION 1 M = .6 ALT. = 20000 FT.
AILERON/RUDDER
○ F-4E
△ F-4E + L.E. SLATS
ANGLE OF ATTACK α ~ DEGREES
STABILATOR DEFLECTION δs ~ DEGREES
ROLL RATE P ~ DEG/SEC
PITCH RATE Q ~ DEG/SEC
BASIC F-4E DEPARTURE
SLATTED F-4E DEPARTURE
SLATTED F-4E DEPARTURE
-80.0
-70.0
-60.0
-50.0
-40.0
-30.0
-20.0
-10.0
0.0
10.0
20.0
30.0
40.0
50
60.0
70.0
80.0
-40.0
-20.0
0.0
20.0
40.0
-30.0
-20.0
-10.0
0.0
10.0
0.0
4.0
8.0
12.0
16.0
20.0
24.0
28.0
32.
TIME - SECONDS

Figure 3.13

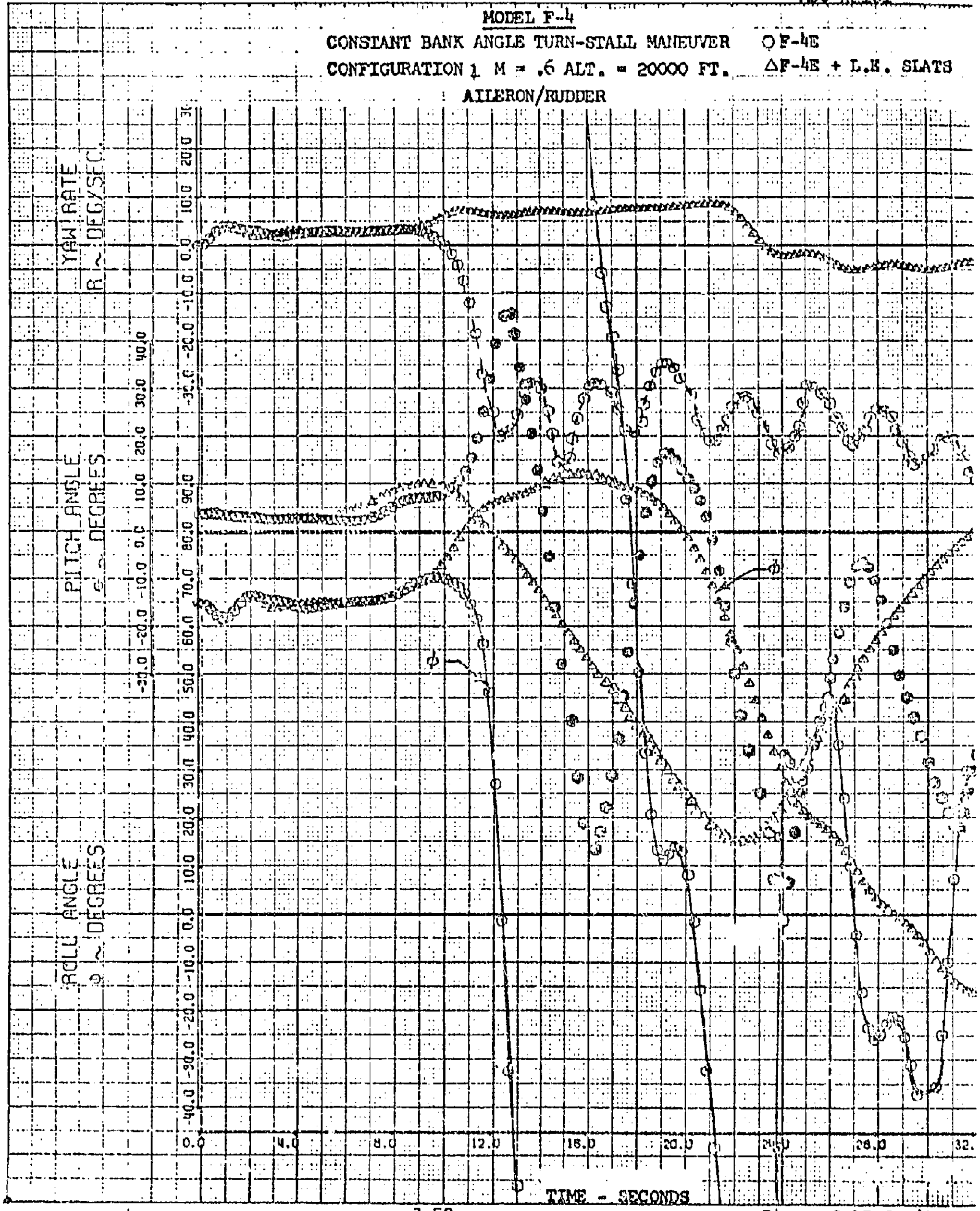

Figure 3.13 Con't

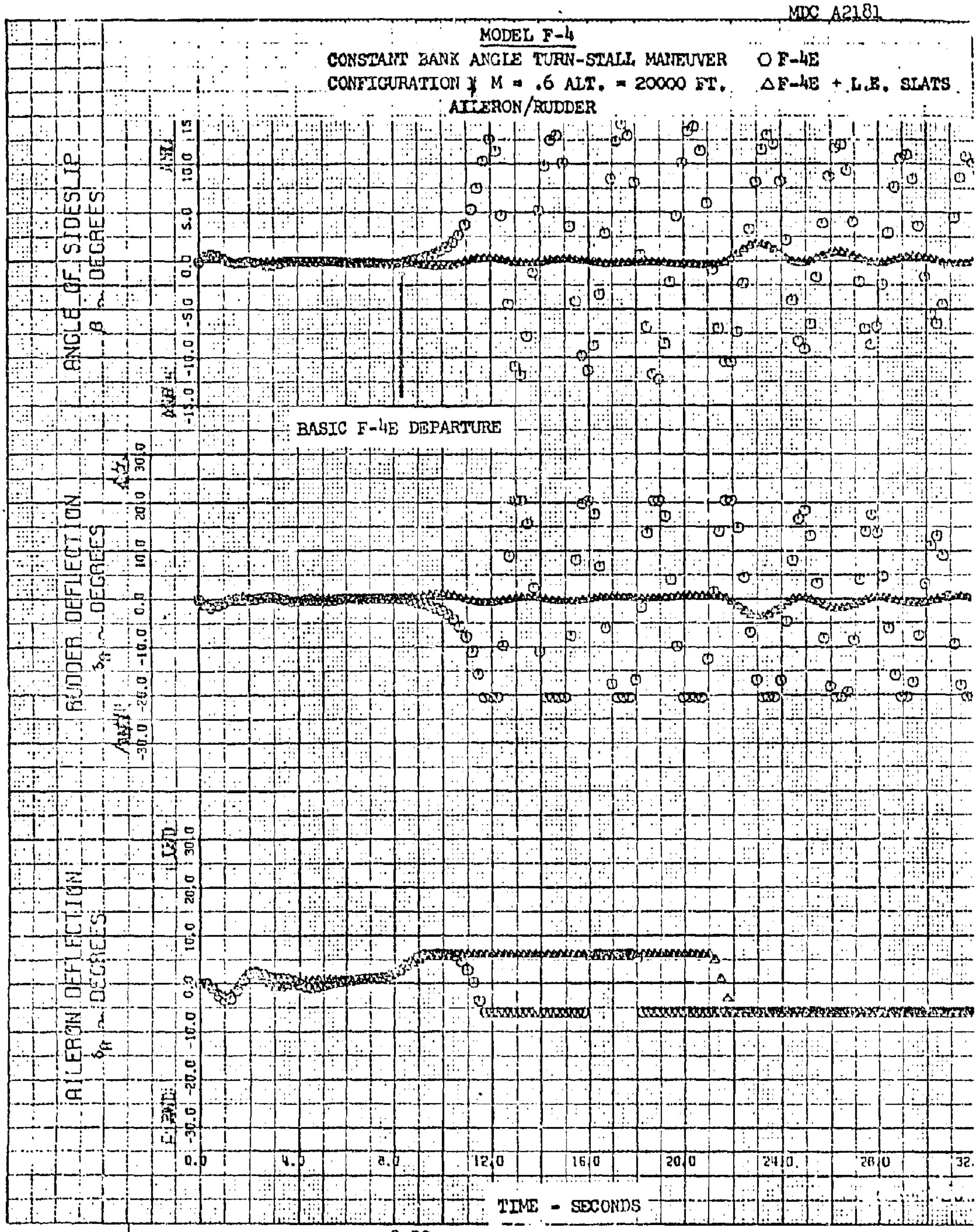

MODEL F-4

CONSTANT BANK ANGLE TURN-STALL MANEUVER ○ F-4E

CONFIGURATION I M = .6 ALT. = 20000 FT. △ F-4E + L.E. SLATS

AILERON/RUDDER

Figure 3.13 Con't

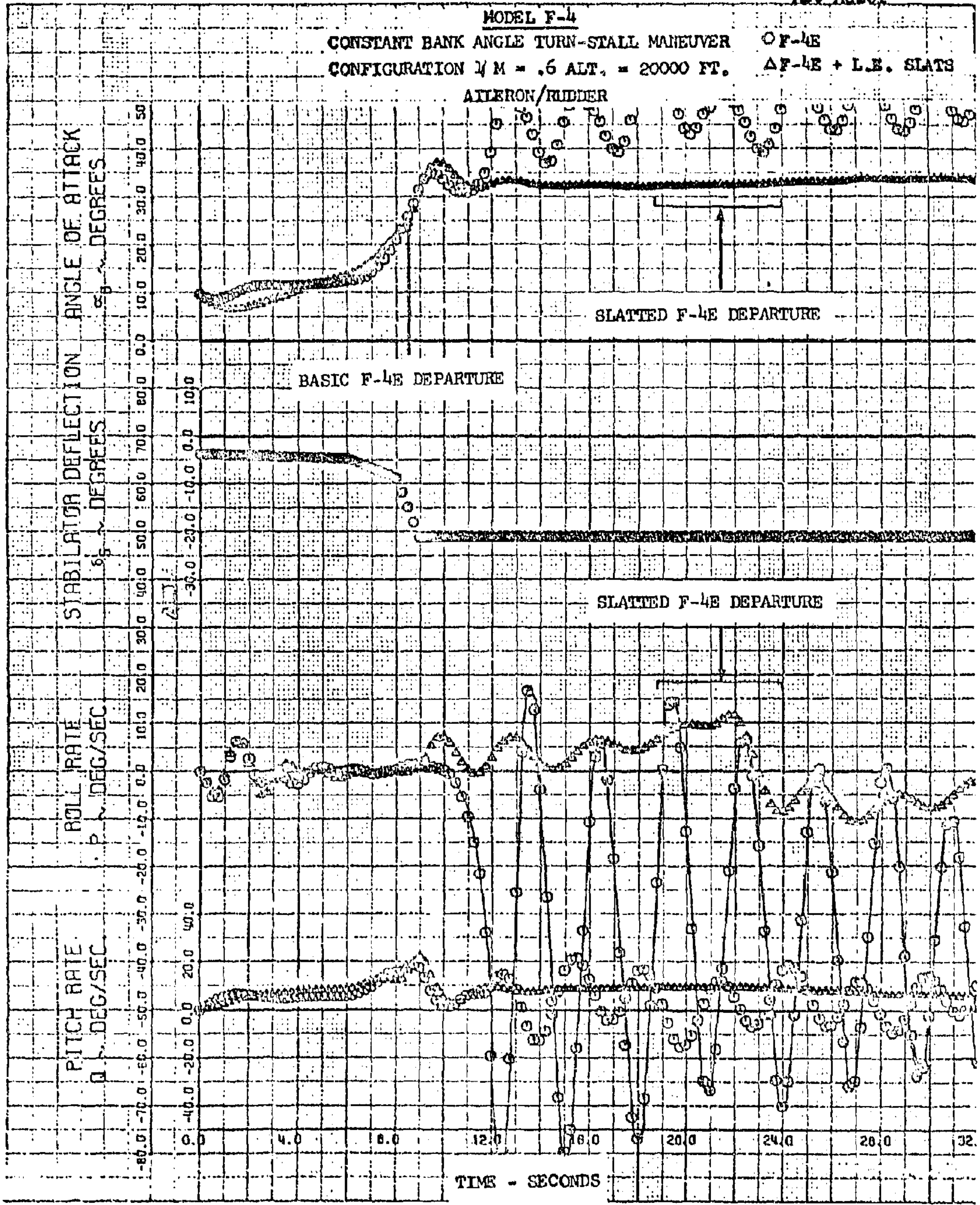
MODEL F-4
CONSTANT BANK ANGLE TURN-STALL MANEUVER
CONFIGURATION 1/ M = .6 ALT. = 20000 FT.
AILERON/RUDDER
○ F-4E
△ F-4E + L.E. SLATS
ANGLE OF ATTACK
α_B ~ DEGREES
STABILATOR DEFLECTION
δ_S ~ DEGREES
ROLL RATE
P ~ DEG/SEC
PITCH RATE
Q ~ DEG/SEC
SLATTED F-4E DEPARTURE
BASIC F-4E DEPARTURE
SLATTED F-4E DEPARTURE
0.0
10.0
20.0
30.0
40.0
50
80.0
70.0
60.0
50.0
40.0
30.0
20.0
10.0
0.0
-10.0
-20.0
-30.0
-40.0
-50.0
-60.0
-70.0
-80.0
10.0
0.0
-10.0
-20.0
-30.0
40.0
20.0
0.0
-20.0
-40.0
0.0
4.0
8.0
12.0
16.0
20.0
24.0
28.0
32.
TIME - SECONDS

Figure 3.14

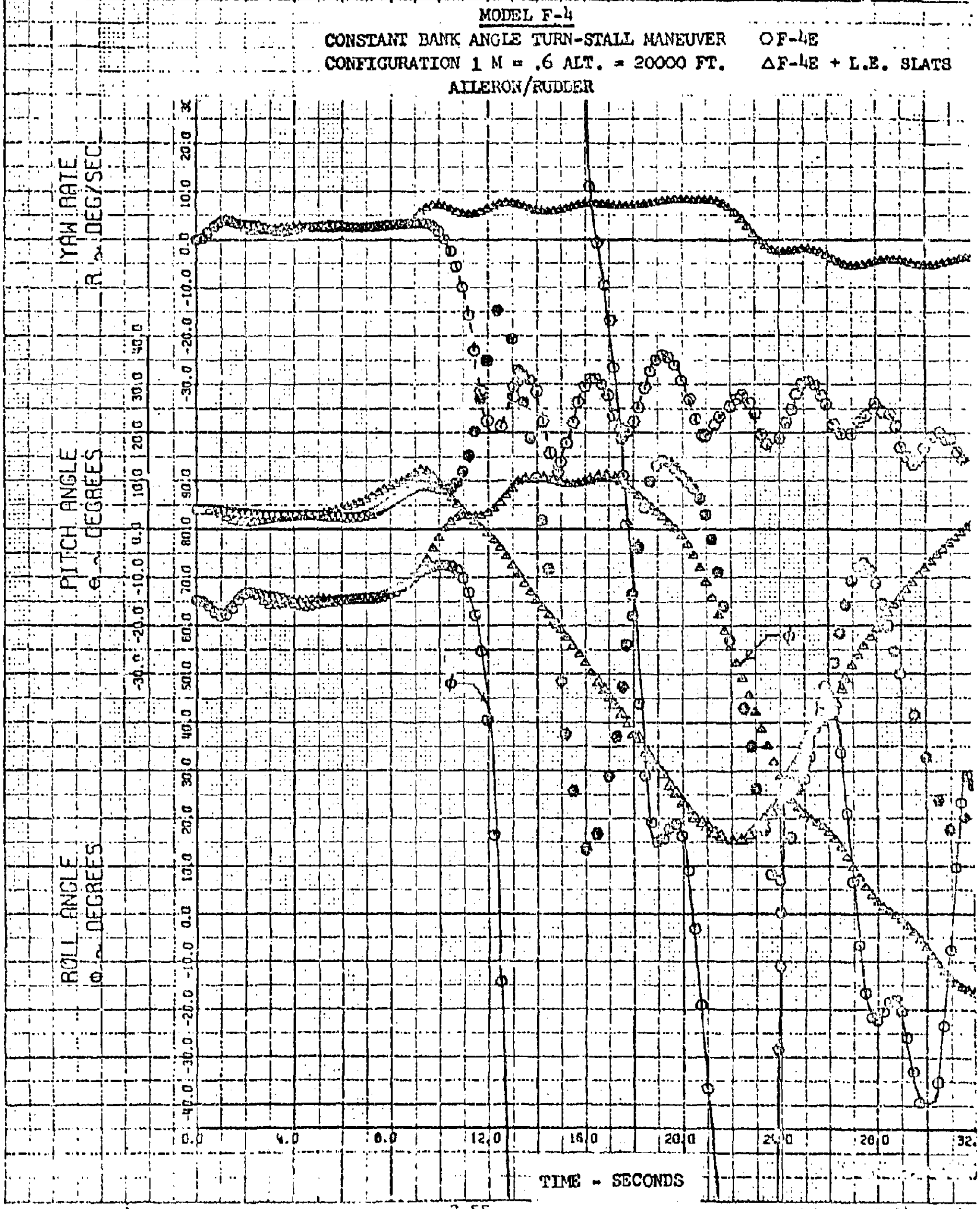

Figure 3.14 Con't

MODEL F-4

CONSTANT BANK ANGLE TURN-STALL MANEUVER
CONFIGURATION 1 M = .6 ALT. = 20000 FT.
AILERON/RUDDER

○F-4E
ΔF-4E + L.E. SLATS

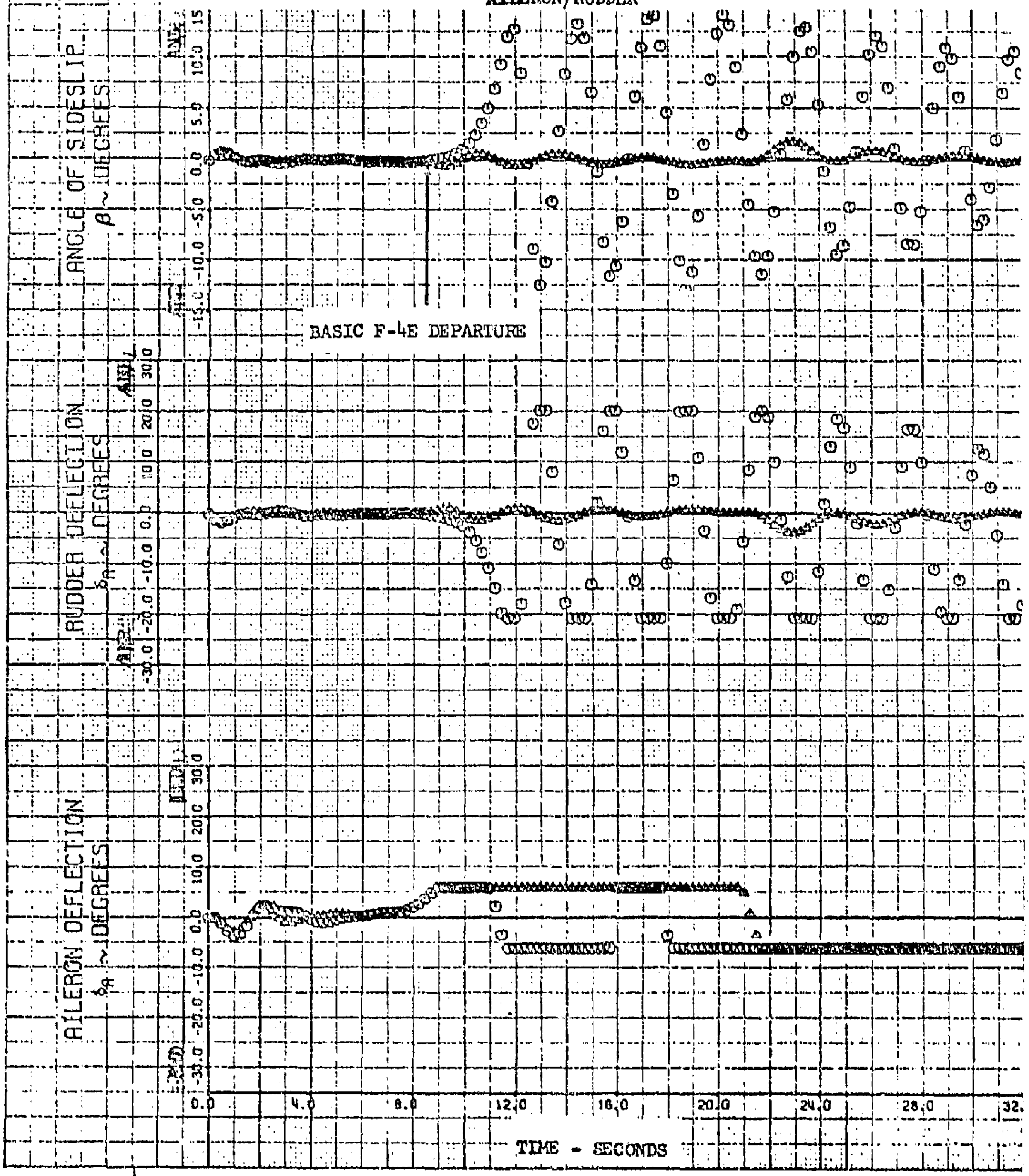

Figure 3.14 Con't

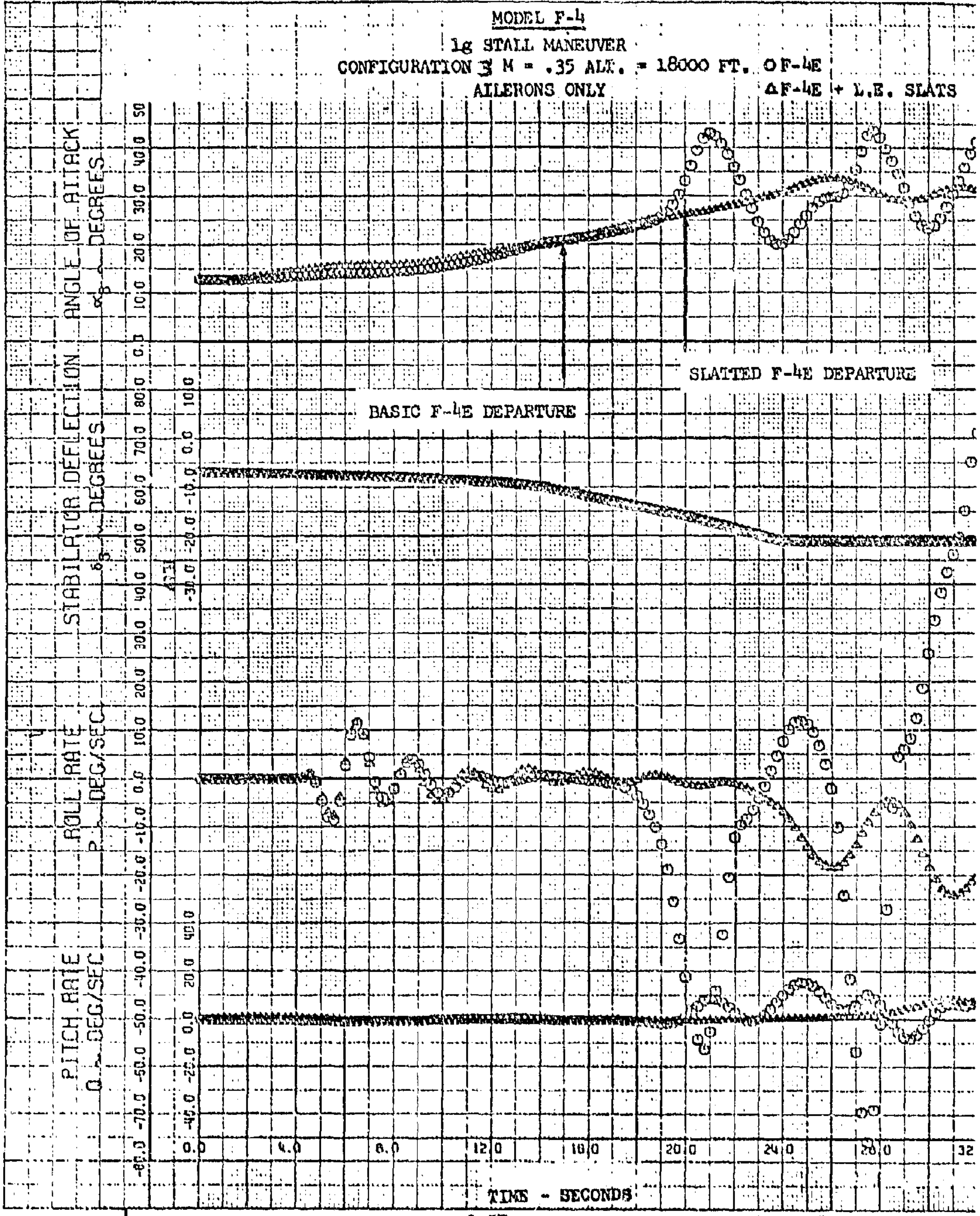
MODEL F-4
1g STALL MANEUVER
CONFIGURATION 3 M = .35 ALT. = 18000 FT.
AILERONS ONLY
○ F-4E
△ F-4E + L.E. SLATS
ANGLE OF ATTACK
$\alpha_B$ ~ DEGREES
STABILATOR DEFLECTION
$\delta_S$ ~ DEGREES
ROLL RATE
P ~ DEG/SEC
PITCH RATE
Q ~ DEG/SEC
0.0
10.0
20.0
30.0
40.0
50
-30.0
-20.0
-10.0
0.0
10.0
-80.0
-70.0
-60.0
-50.0
-40.0
-30.0
-20.0
-10.0
0.0
10.0
20.0
30.0
40.0
50.0
60.0
70.0
80.0
-40.0
-20.0
0.0
20.0
40.0
SLATTED F-4E DEPARTURE
BASIC F-4E DEPARTURE
0.0
4.0
8.0
12.0
16.0
20.0
24.0
28.0
32
TIME - SECONDS

Figure 3.15

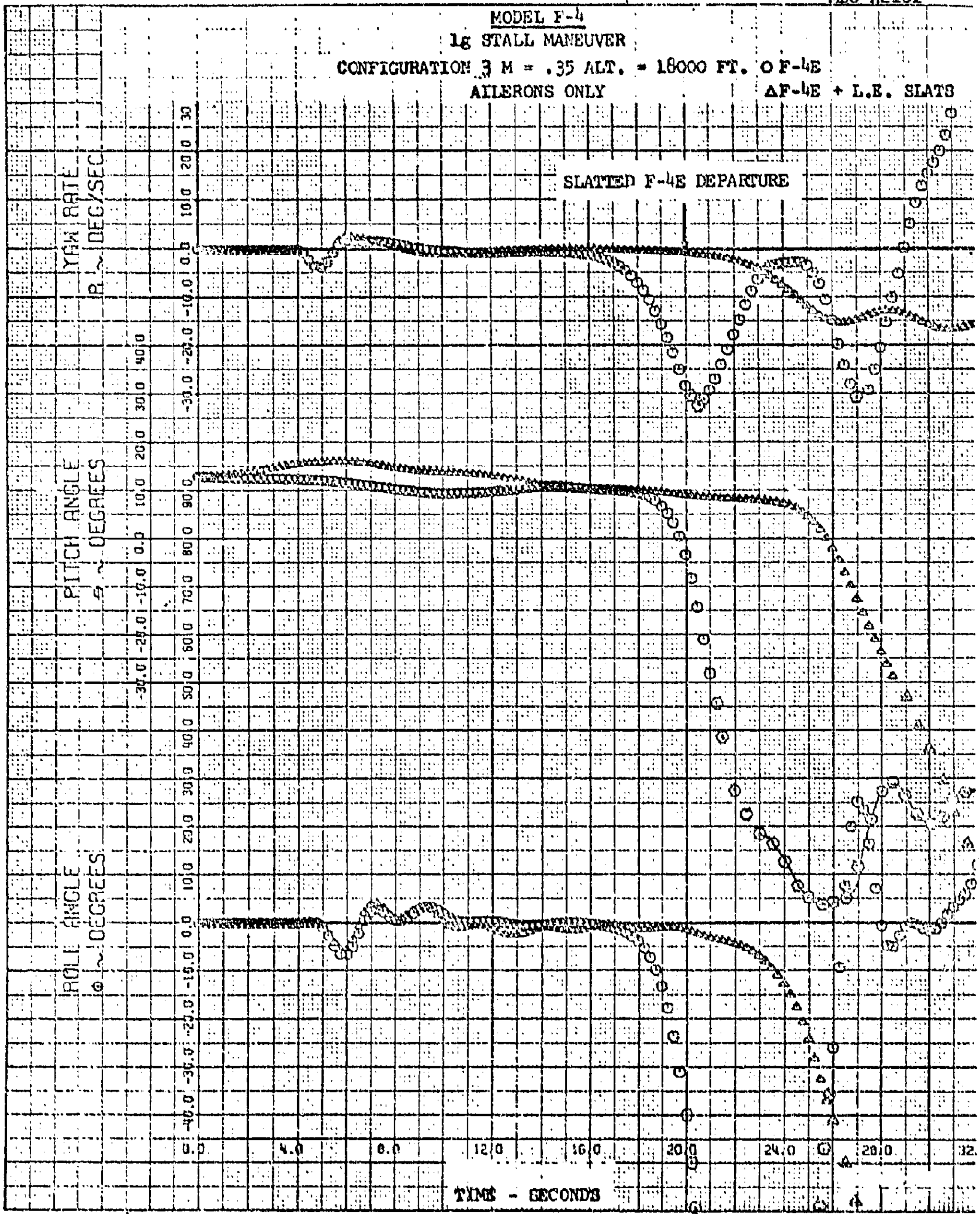

Figure 3.15 Con't

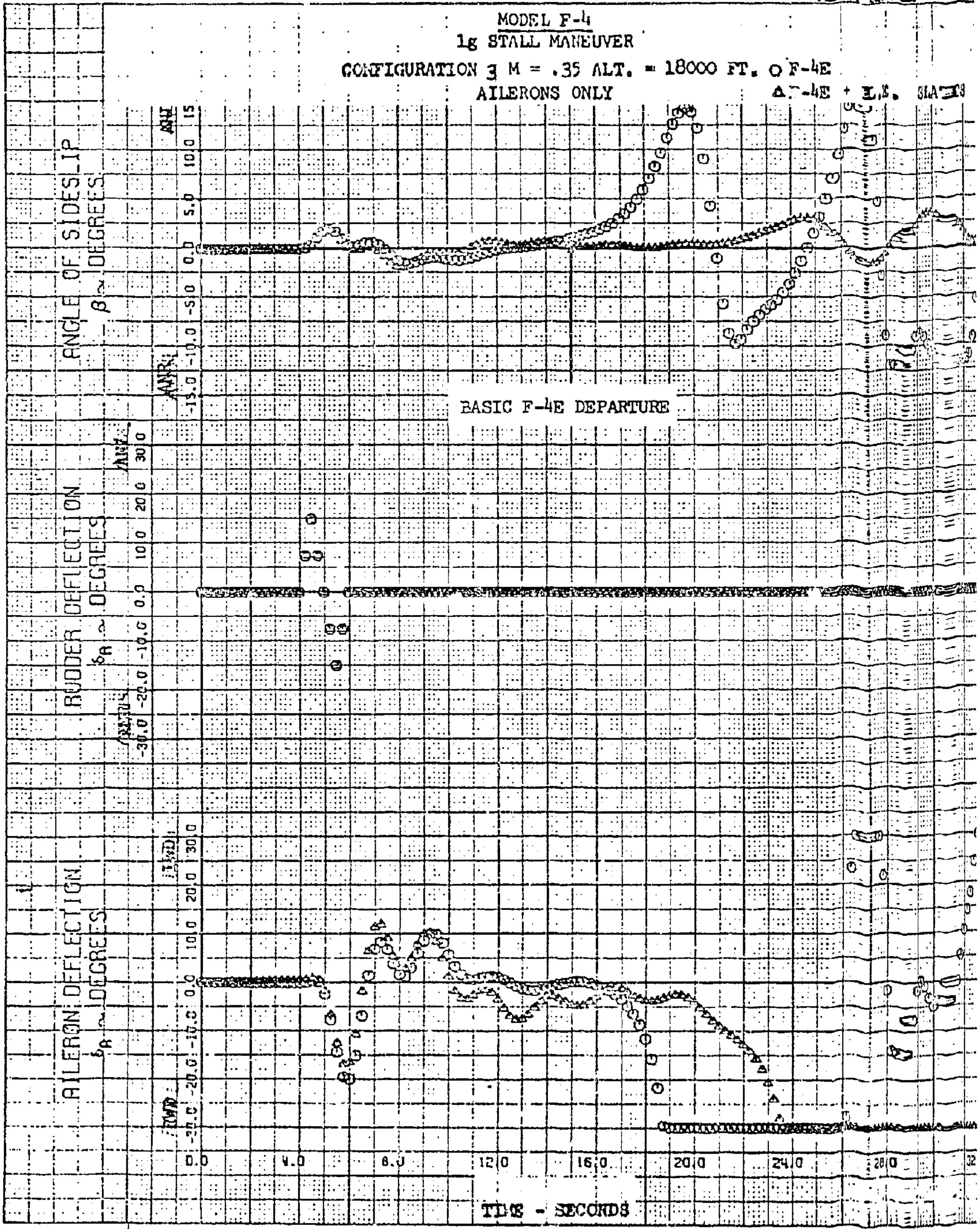

Figure 3.15 Con't

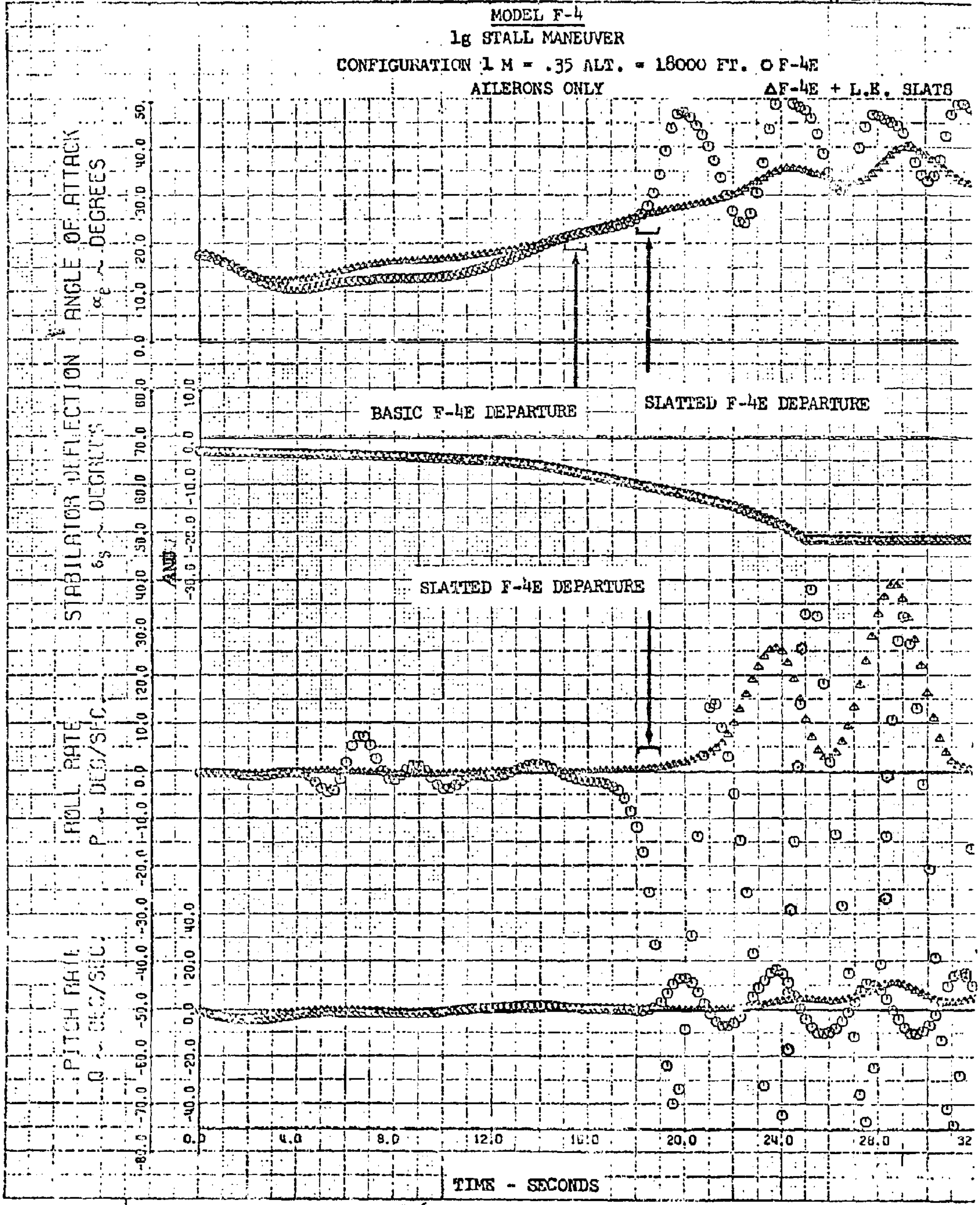
MODEL F-4
1g STALL MANEUVER
CONFIGURATION 1 M = .35 ALT. = 18000 FT. ○ F-4E
AILERONS ONLY △ F-4E + L.E. SLATS
ANGLE OF ATTACK
$\alpha_c$ ~ DEGREES
0.0
10.0
20.0
30.0
40.0
50.
BASIC F-4E DEPARTURE
SLATTED F-4E DEPARTURE
STABILATOR DEFLECTION
$\delta_S$ ~ DEGREES
10.0
0.0
-10.0
-20.0
-30.0
AND
SLATTED F-4E DEPARTURE
ROLL RATE
P ~ DEG/SEC
80.0
70.0
60.0
50.0
40.0
30.0
20.0
10.0
0.0
-10.0
-20.0
-30.0
-40.0
-50.0
-60.0
-70.0
-80.0
PITCH RATE
Q ~ DEG/SEC
40.0
20.0
0.0
-20.0
-40.0
0.0
4.0
8.0
12.0
16.0
20.0
24.0
28.0
32
TIME - SECONDS

Figure 3.16

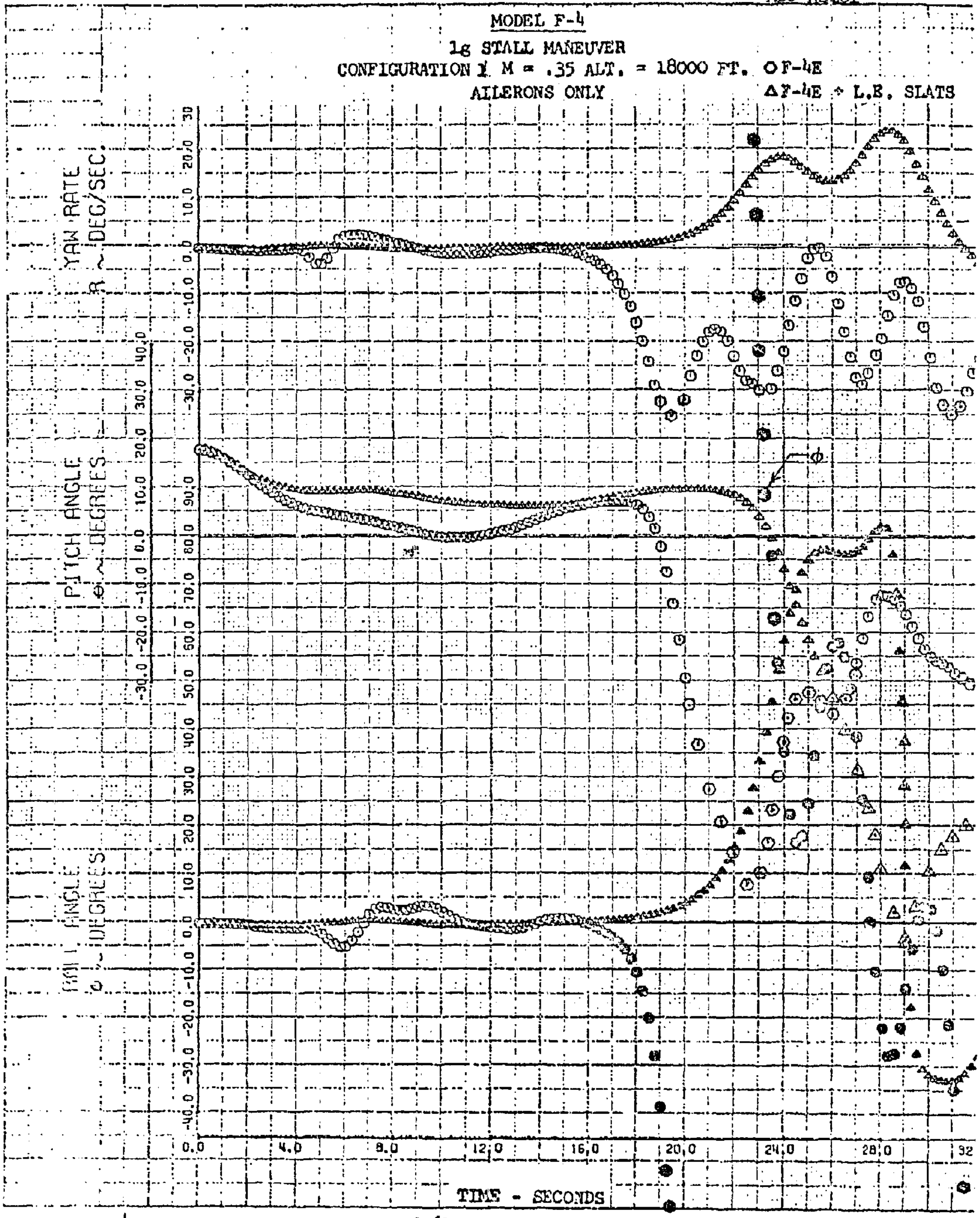

MODEL F-4

1g STALL MANEUVER

CONFIGURATION 1 M = .35 ALT. = 18000 FT.

AILERONS ONLY

Figure 3.16 Con't

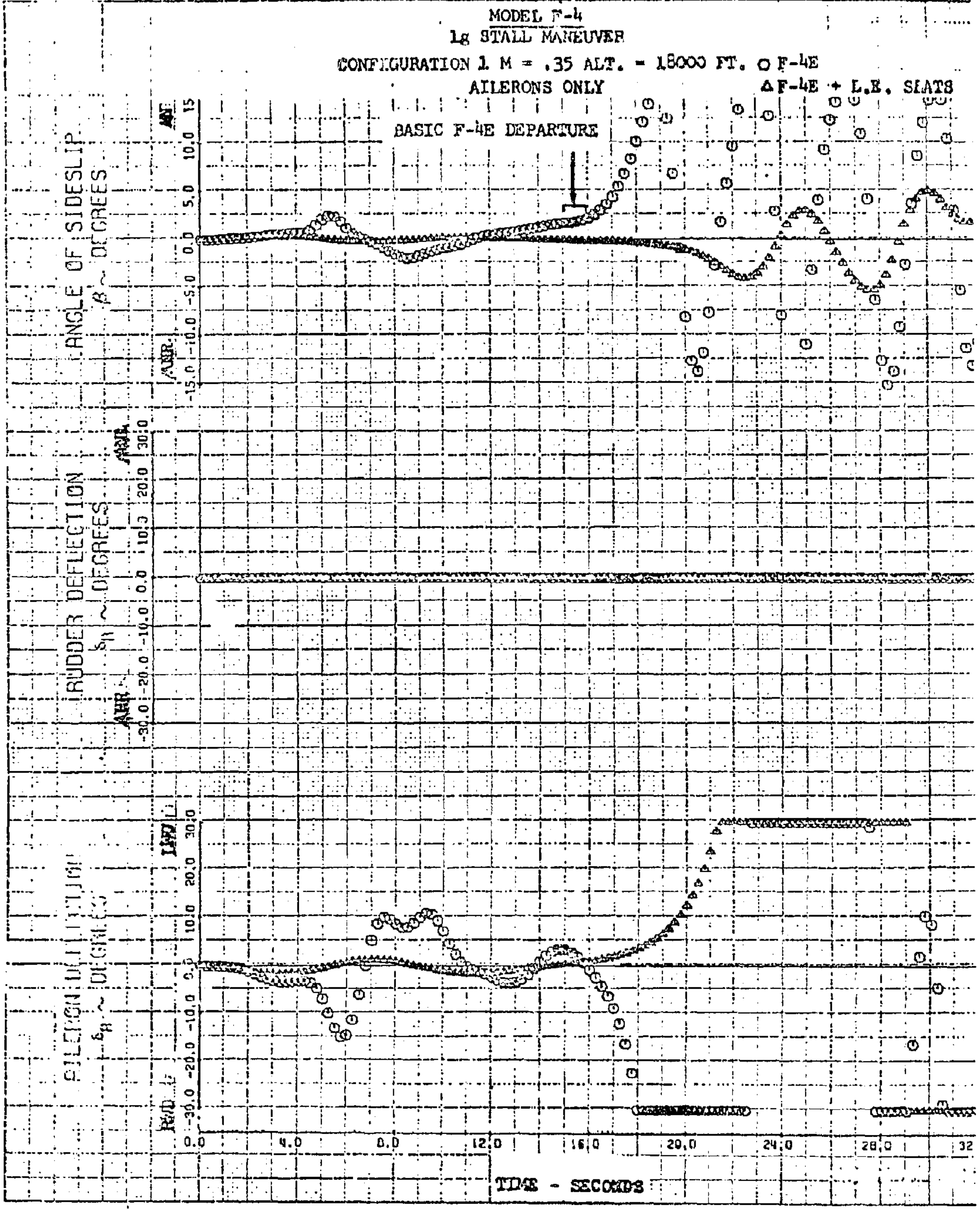

Figure 3.16 Con't

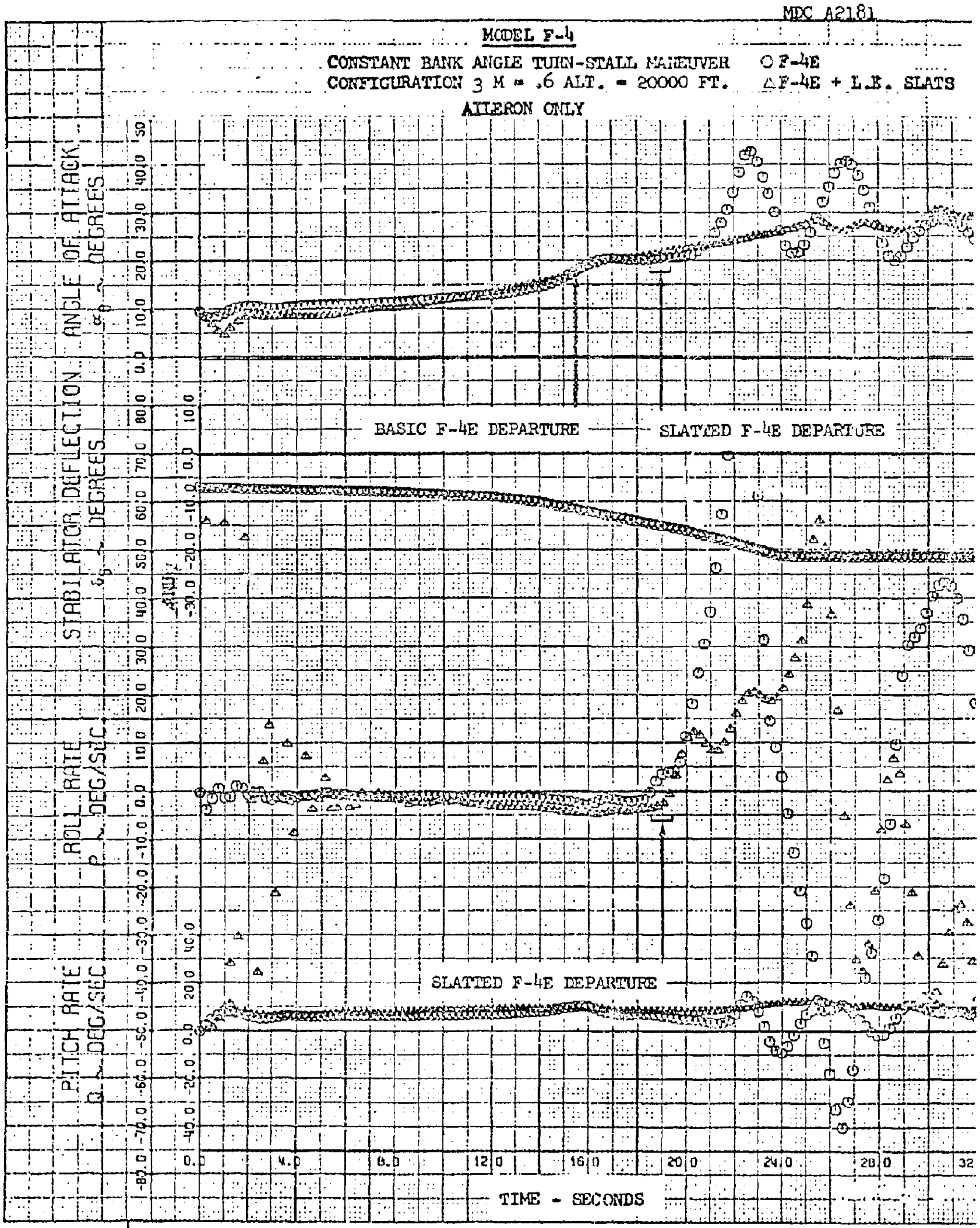
MODEL F-4
CONSTANT BANK ANGLE TURN-STALL MANEUVER
○ F-4E
CONFIGURATION 3 M = .6 ALT. = 20000 FT.
△ F-4E + L.E. SLATS
AILERON ONLY
ANGLE OF ATTACK $\alpha_B$ ~ DEGREES
STABILATOR DEFLECTION $\delta_S$ ~ DEGREES
ROLL RATE P ~ DEG/SEC
PITCH RATE Q ~ DEG/SEC
BASIC F-4E DEPARTURE
SLATTED F-4E DEPARTURE
SLATTED F-4E DEPARTURE
0.0
10.0
20.0
30.0
40.0
50
-80.0
-70.0
-60.0
-50.0
-40.0
-30.0
-20.0
-10.0
0.0
10.0
20.0
30.0
40.0
50.0
60.0
70.0
80.0
-40.0
-20.0
0.0
20.0
40.0
-30.0
-20.0
-10.0
0.0
10.0
0.0
4.0
8.0
12.0
16.0
20.0
24.0
28.0
32
TIME - SECONDS

Figure 3.17

MODEL F-4

CONSTANT BANK ANGLE TURN-STALL MANEUVER
CONFIGURATION 3 M = .6 ALT. = 20000 FT.
AILERON ONLY

○ F-4E
△ F-4E + L.E. SLATS

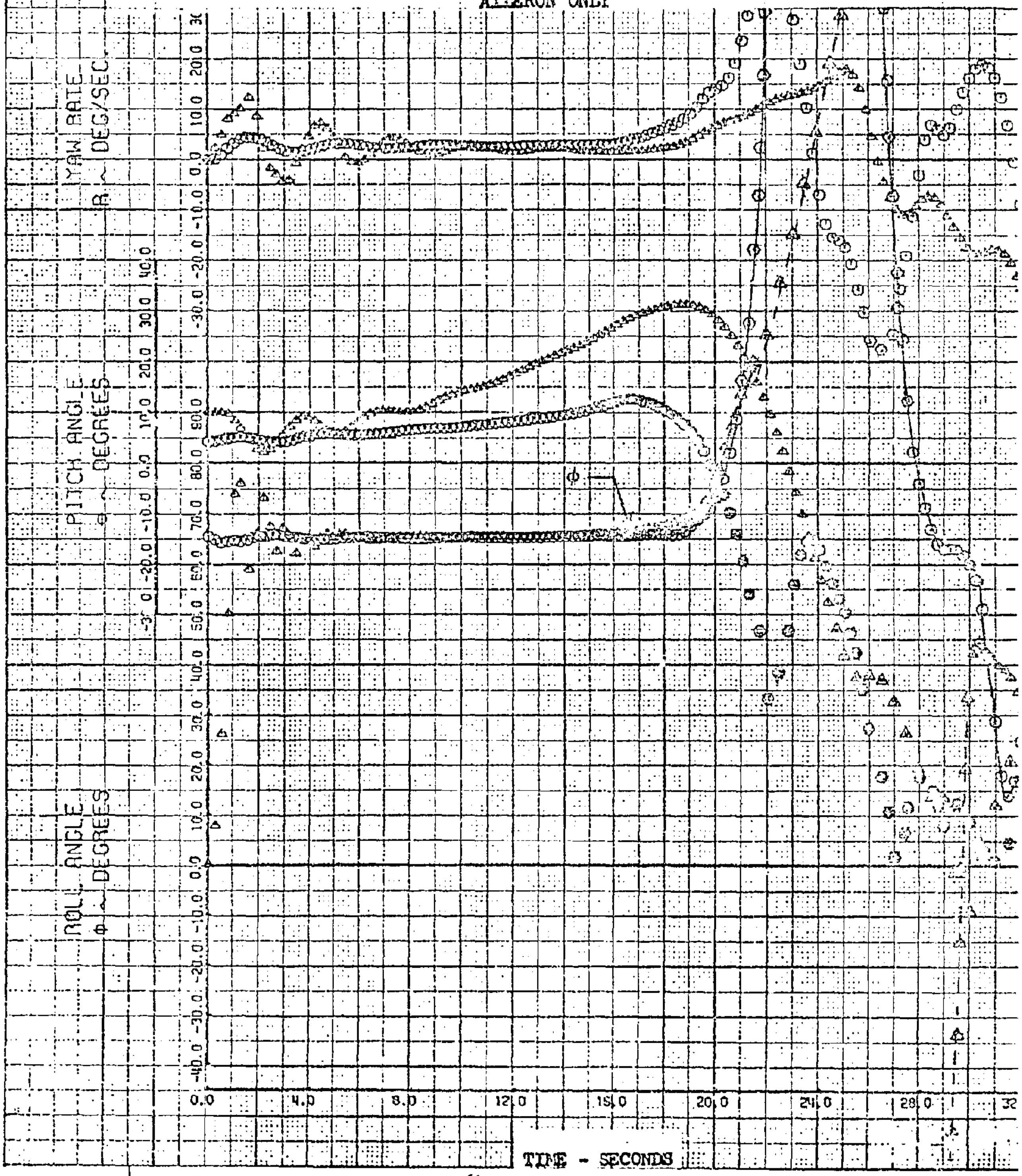

Figure 3.17 Con't

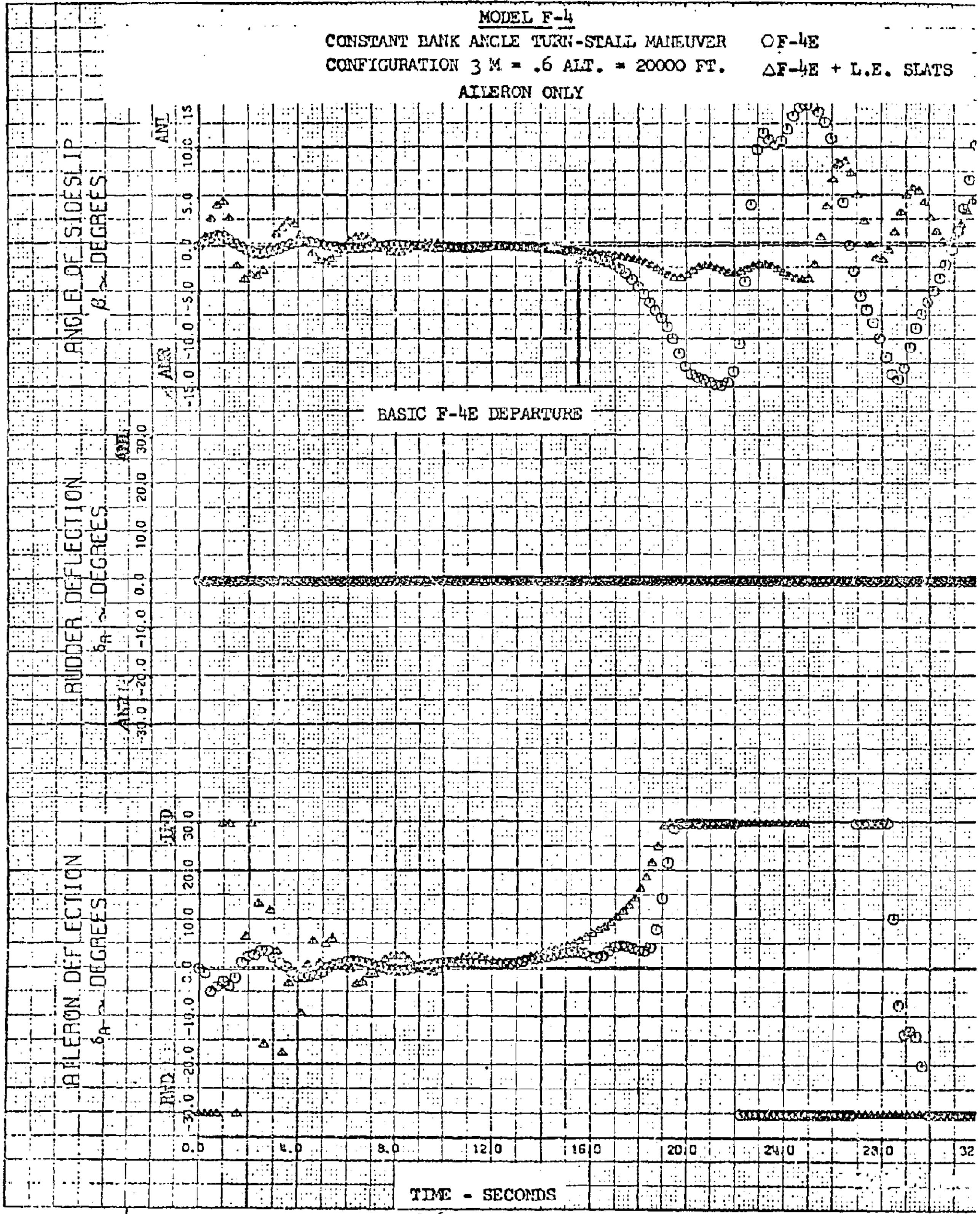

MODEL F-4

CONSTANT BANK ANGLE TURN-STALL MANEUVER
CONFIGURATION 3 M = .6 ALT. = 20000 FT.
AILERON ONLY

Figure 3.17 Con't

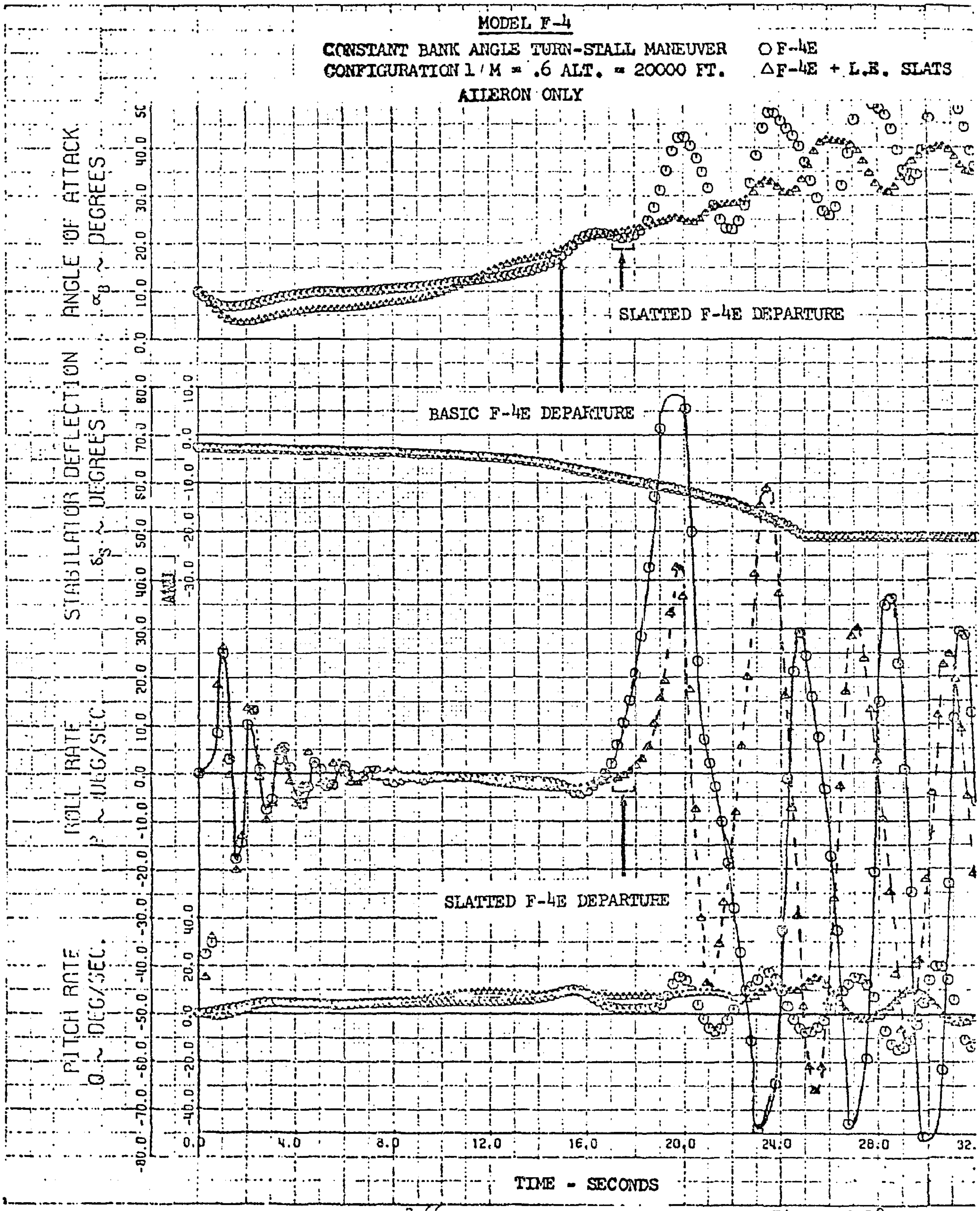

MODEL F-4
CONSTANT BANK ANGLE TURN-STALL MANEUVER
CONFIGURATION 1 / M = .6 ALT. = 20000 FT.
AILERON ONLY

Figure 3.18

MODEL F-4

CONSTANT BANK ANGLE TURN-STALL MANEUVER

CONFIGURATION 1, M = .6 ALT. = 20000 FT.

AILERON ONLY

○ F-4E

△ F-4E + L.E. SLATS

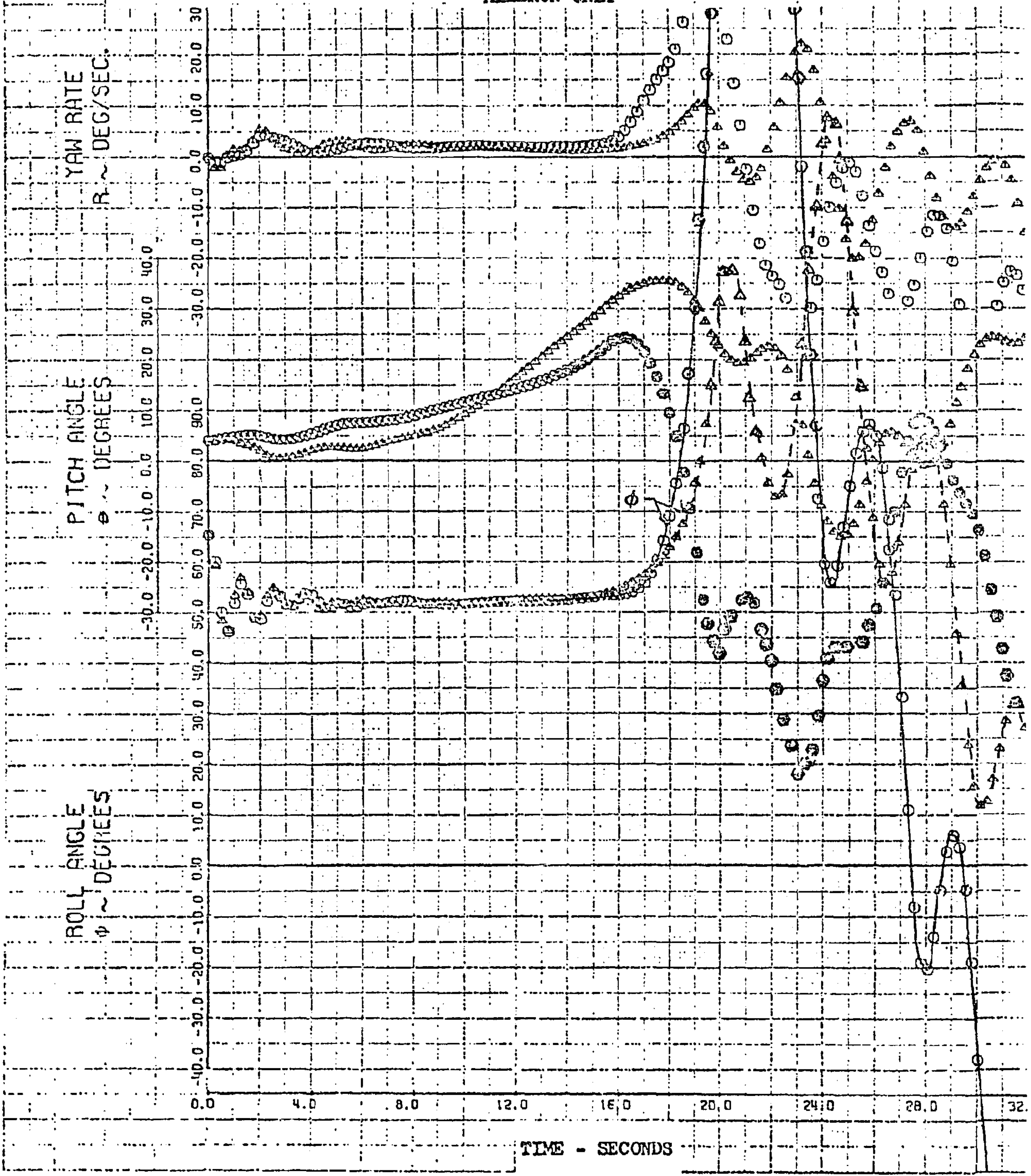

Figure 3.18 Con't

**MODEL F-4**

CONSTANT BANK ANGLE TURN-STALL MANEUVER ○ F-4E
CONFIGURATION 11 M = .6 ALT. = 20000 FT. △ F-4E + L.E. SLATS

AILERON ONLY

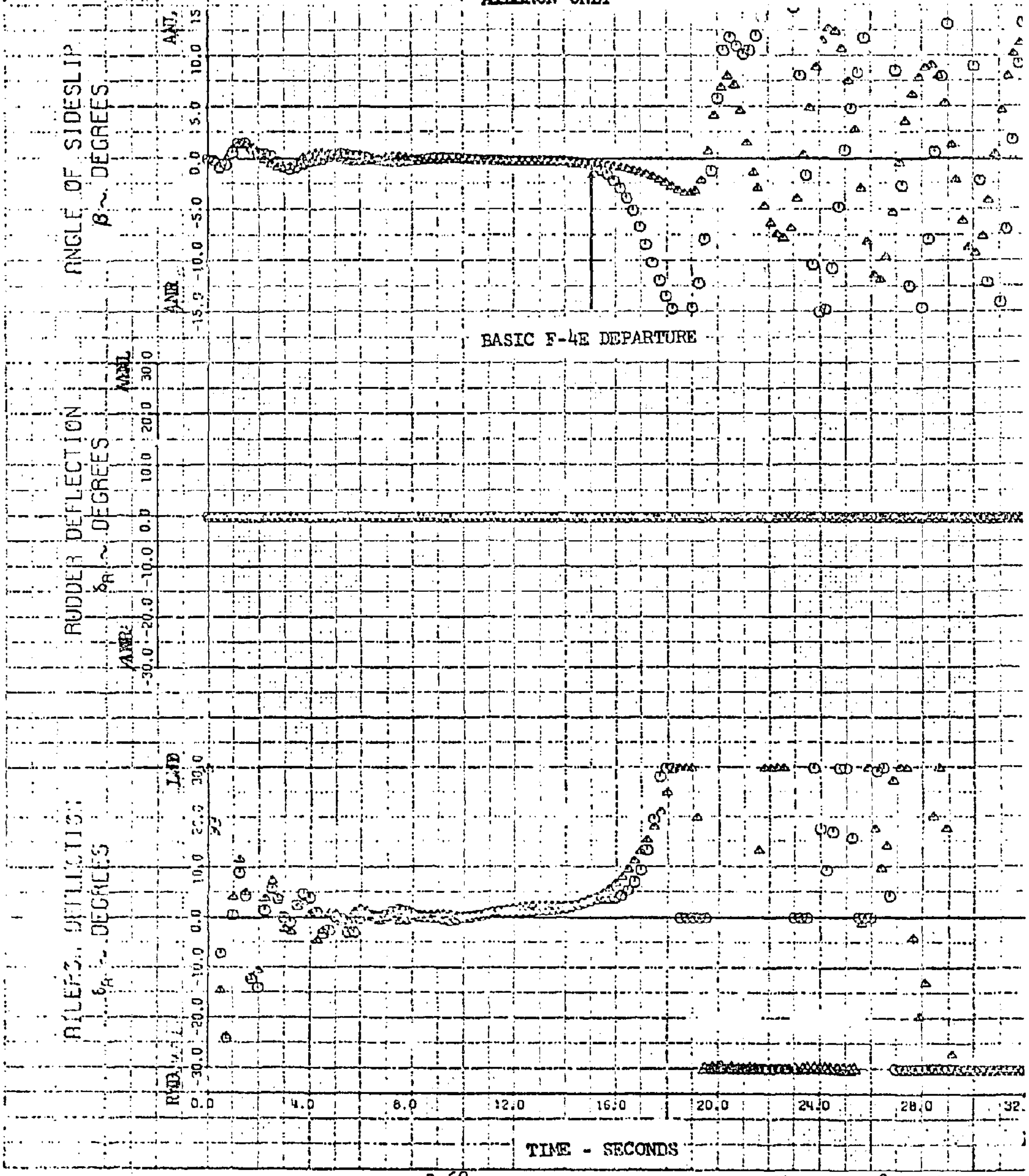

Figure 3.18 Con't

MODEL F-4

RECOVERY FROM A CONSTANT BANK ANGLE TURN-STALL
CONFIGURATION 2 M = .6 ALT. = 20000 FT.

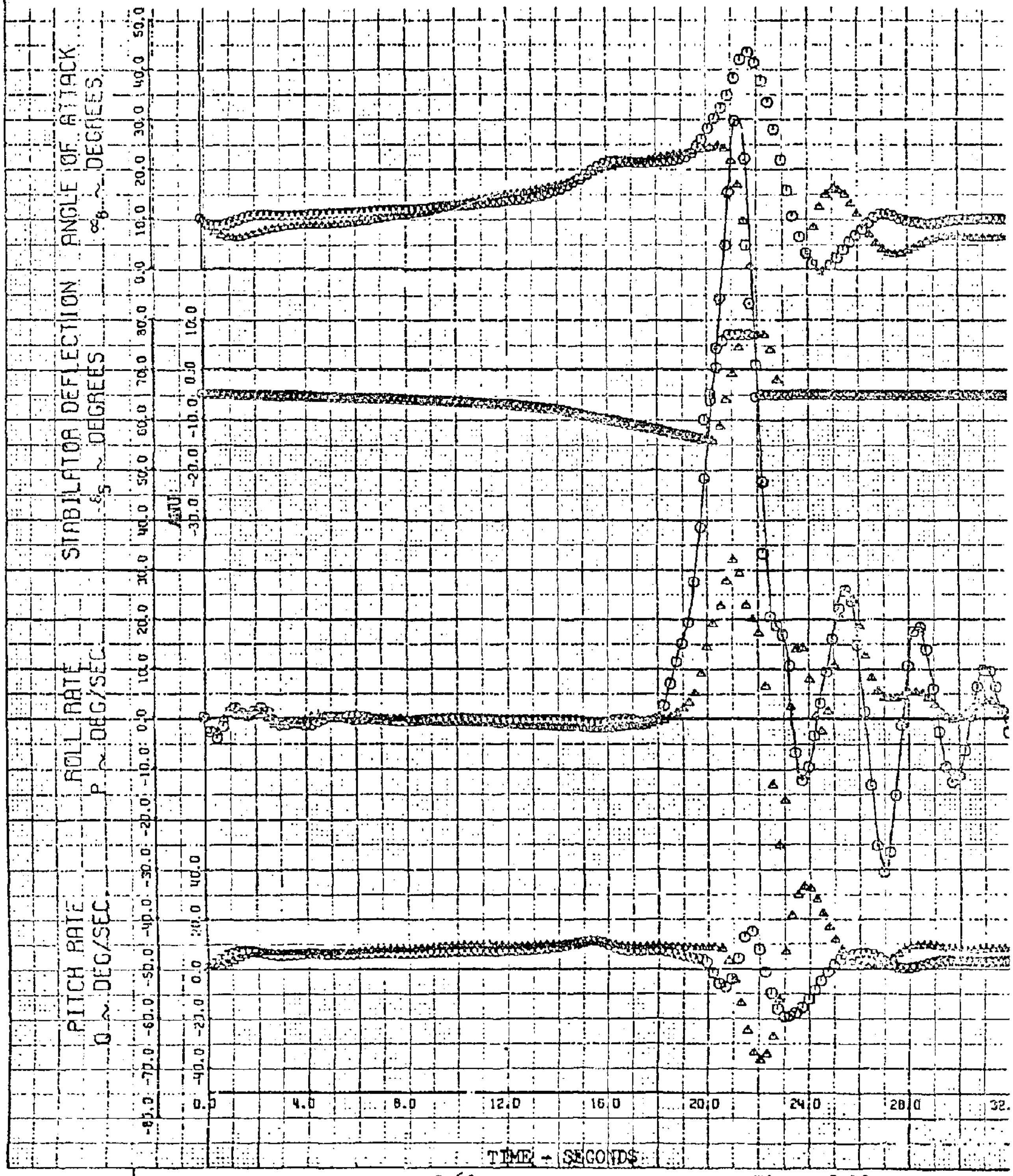

Figure 3.19

MODEL F-4

RECOVERY FROM A CONSTANT BANK ANGLE TURN-STALL
CONFIGURATION 2 M = .6 ALT. = 20000 FT.

○ F-4E
△ F-4E + L.E. SLATS

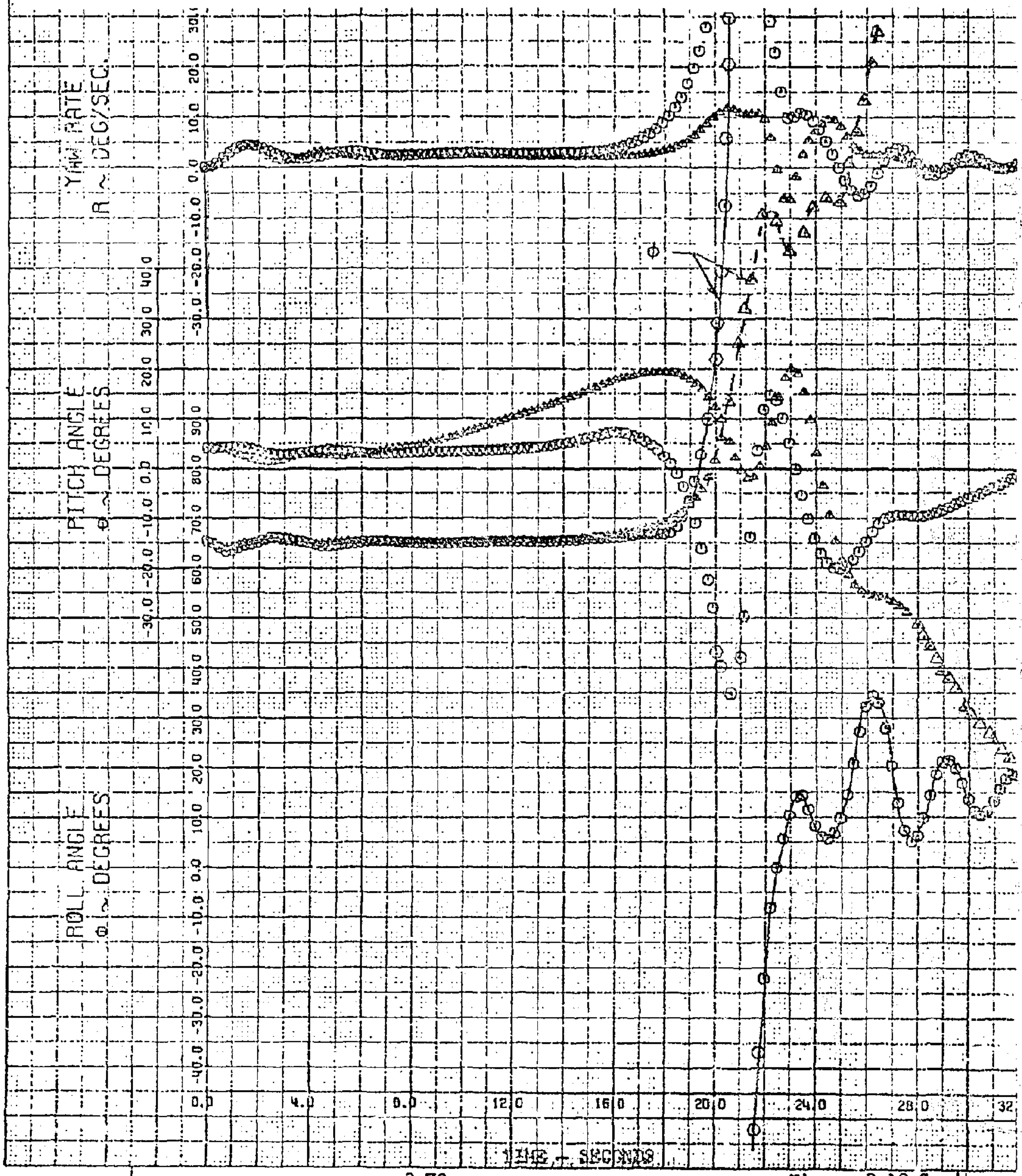

Figure 3.19 Con't

MODEL F-4

RECOVERY FROM A CONSTANT BANK ANGLE TURN-STALL

CONFIGURATION 2 M = .6 ALT. = 20000 FT.

○ F-4E

△ F-4E + L.E. SLATS

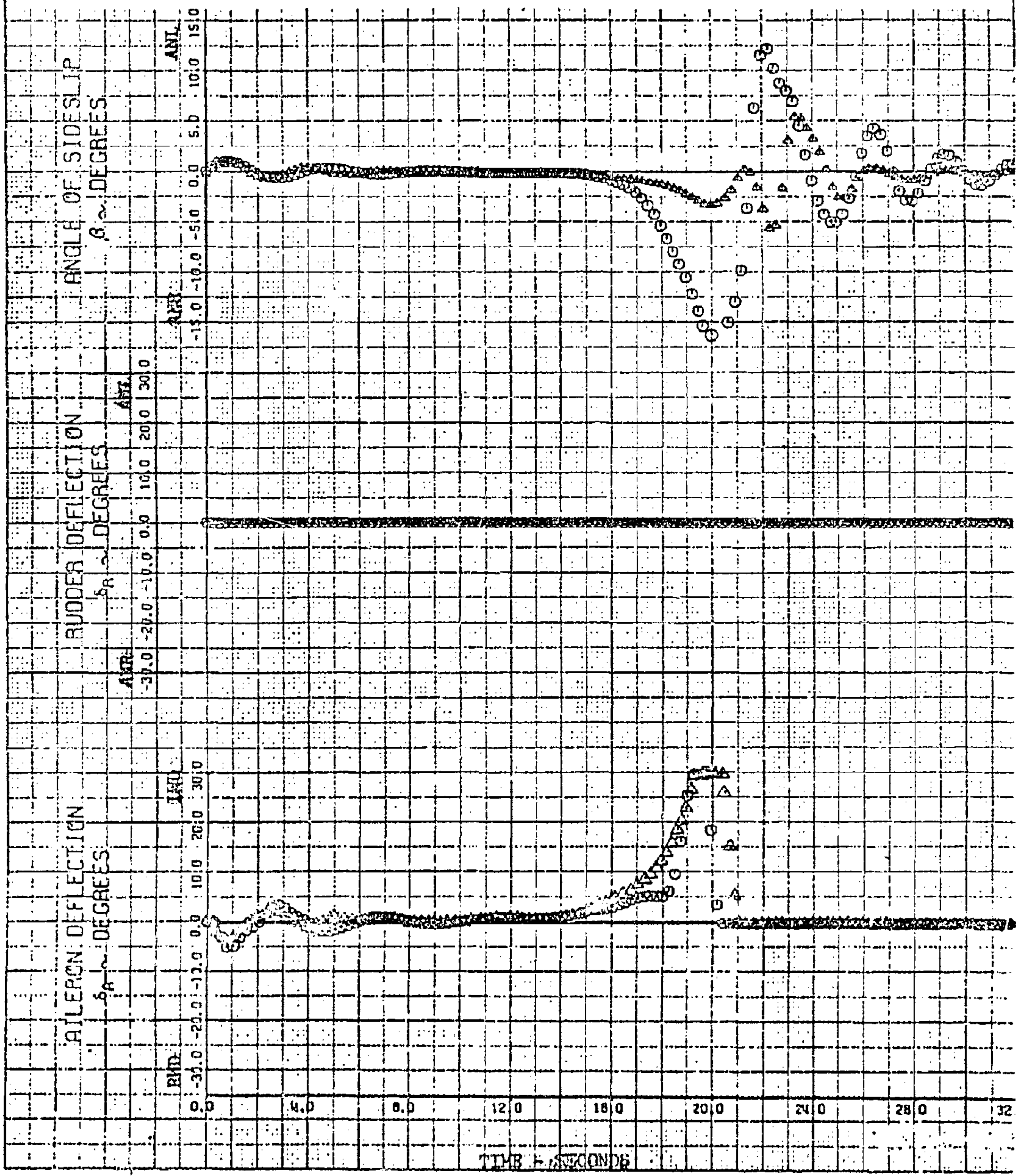

Figure 3.19 Con't

MODEL F-4
RECOVERY FROM A 1g STALL
CONFIGURATION 2 M = .35 ALT. = 18000 FT.

○ F-4E
△ F-4E + L.E. SLATS

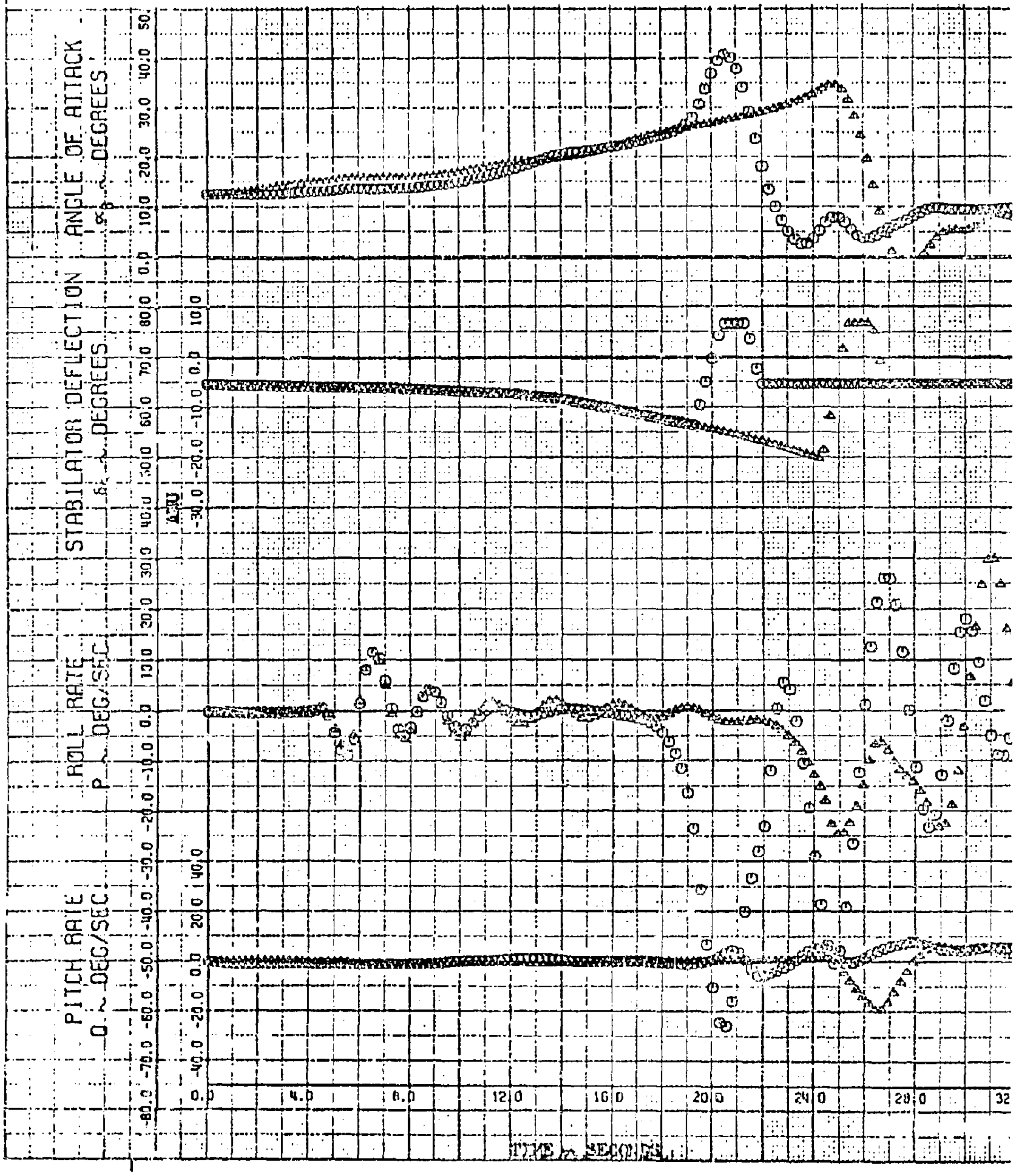

Figure 3.20

MODEL F-4
RECOVERY FROM A 1g STALL
CONFIGURATION 2 M = .35 ALT. = 18000 FT.

○ F-4E
△ F-4E + L.E. SLATS

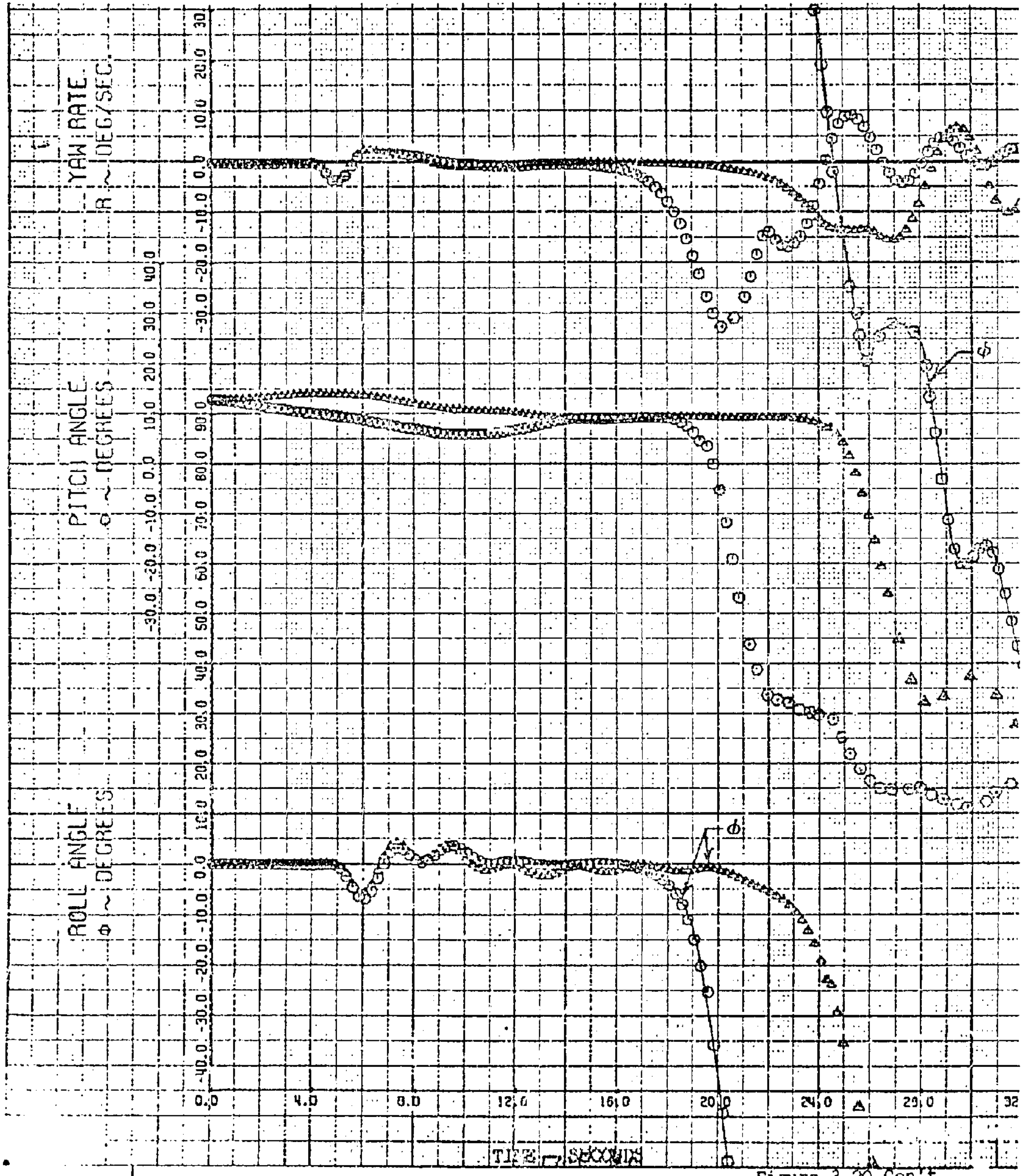

Figure 3.20 Con't

MODEL F-4

RECOVERY FROM A 1g STALL

CONFIGURATION 2 M = .35 ALT. = 18000 FT.

○ F-4E

△ F-4E + L.E. SLATS

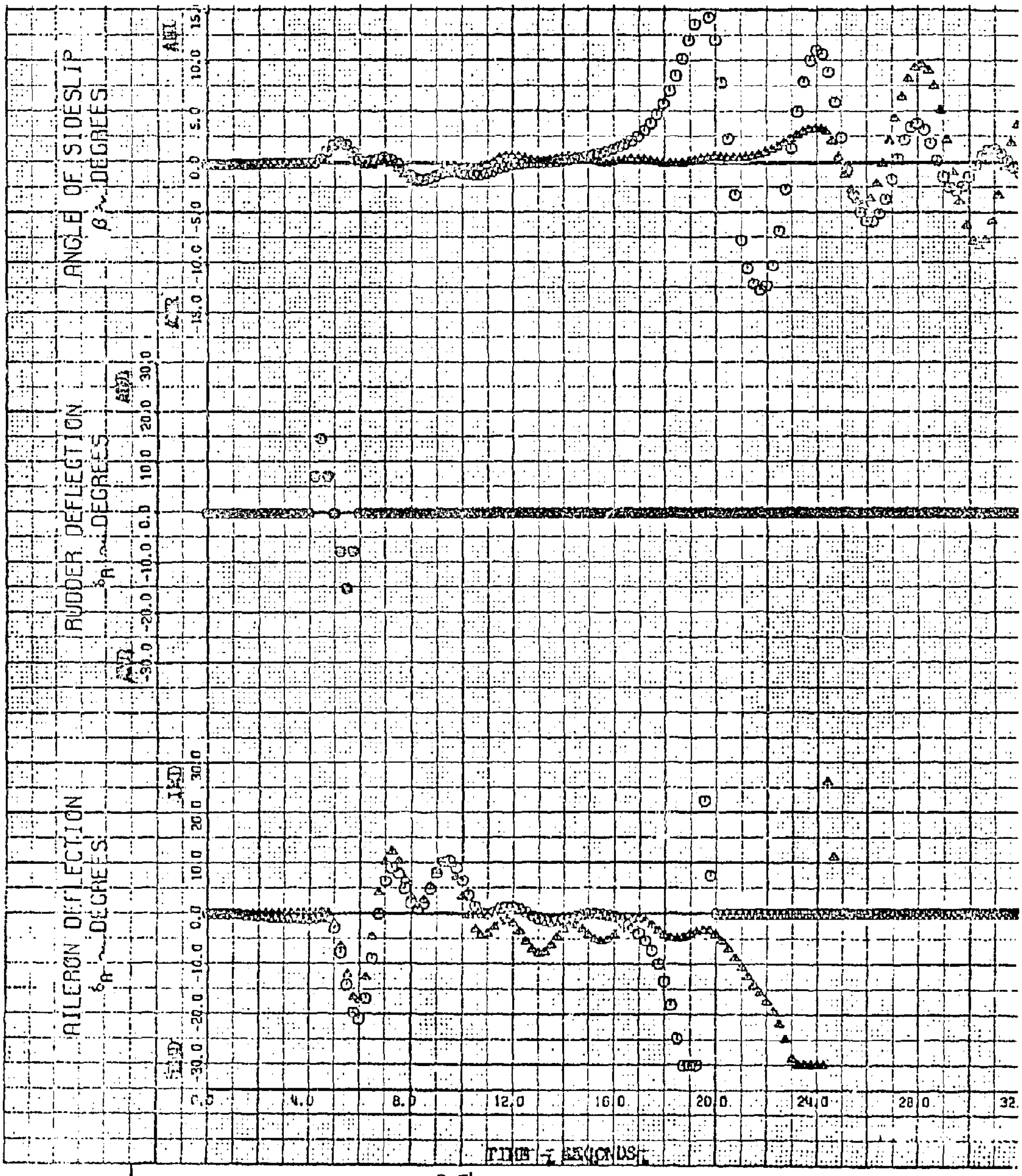

Figure 3.20 Con't

MODEL F-4

RECOVERY FROM A CONSTANT BANK ANGLE TURN-STALL

CONFIGURATION 1 M = .6 ALT. = 20000 FT.

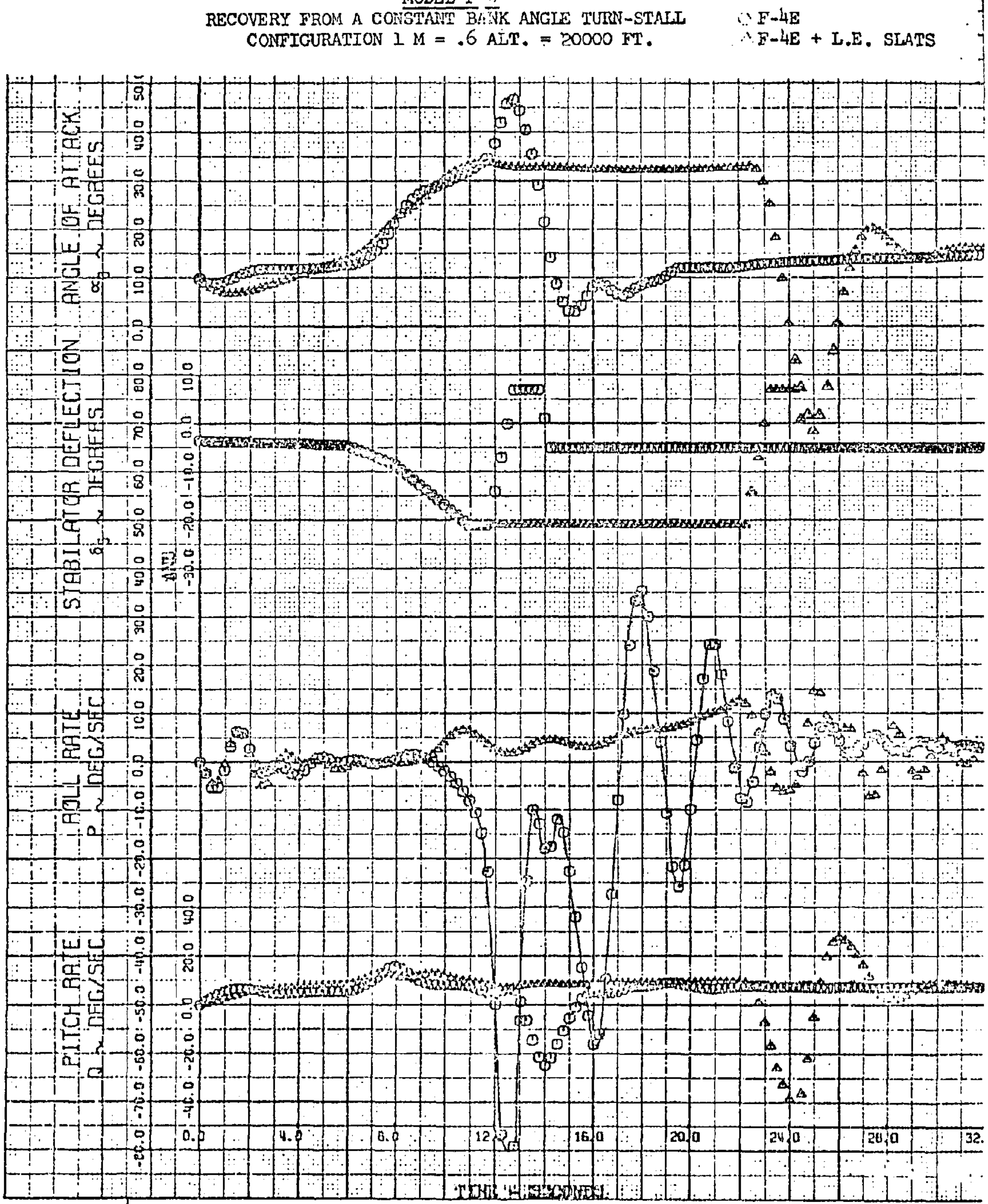

Figure 3.21

MODEL F-4
RECOVERY FROM A CONSTANT BANK ANGLE TURN-STALL
CONFIGURATION 1 M = .6 ALT. = 20000FT.

○ F-4E
△ F-4E + L.E. SLATS

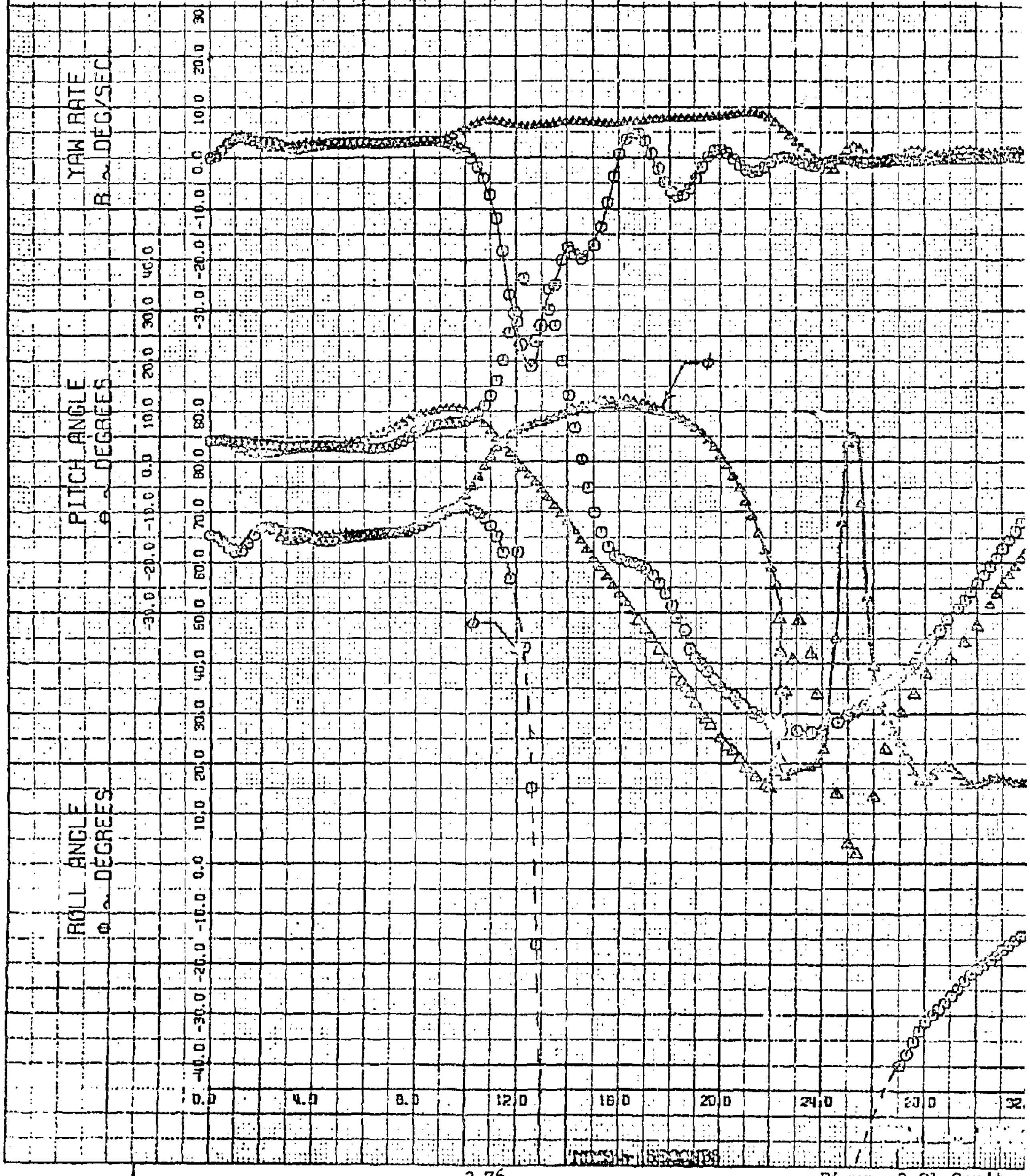

Figure 3.21 Con't

MODEL F-4

RECOVERY FROM A CONSTANT BANK ANGLE TURN-STALL

CONFIGURATION 1 M = .6 ALT. ≈ 20000 FT.

○ F-4E

△ F-4E + L.E. SLATS

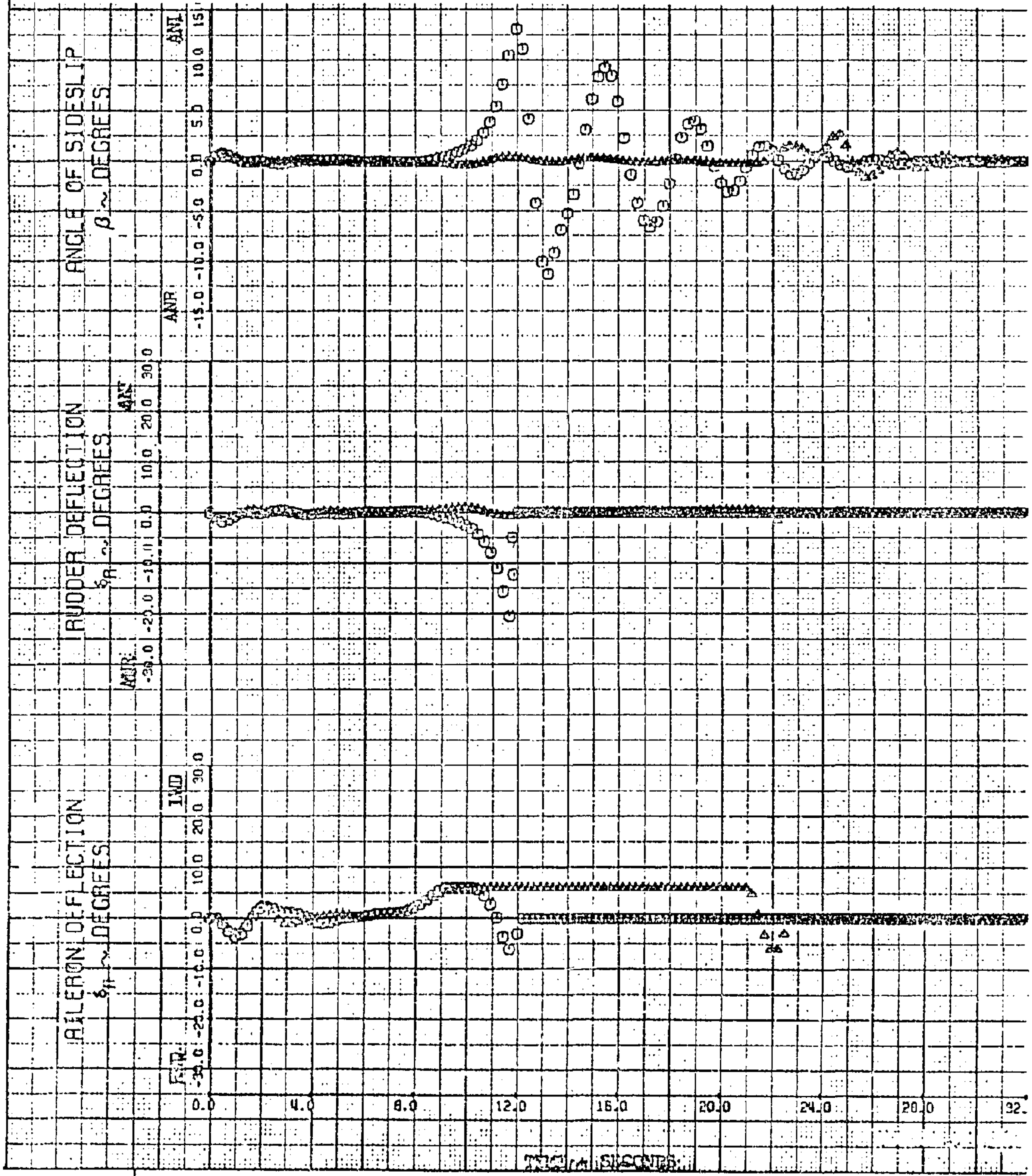

Figure 3.21 Con't

## 4. Spin Characteristics

The purpose of this section is to show the results of this analysis and compare the basic and slatted F-4E's spin entry, spin, and spin recovery charcteristics at various c.g.-gross weight configurations. The six-degree-of-freedom computer program which is described in Appendix C is used to calculate the time histories. The aerodynamic inputs used by the computer are presented in Appendix A for the slatted F-4E and Appendix B for the basic F-4E. The analytical technique used for evaluating the spin characteristics is to start at initial 1g trim conditions of .6 Mach number at 40,000 feet. A rapid full aircraft-nose-up stabilator is input along with full right-wing-down aileron and full aircraft-nose-left rudder. These control inputs are held for 39 seconds after which recovery controls are implemented. Recovery is accomplished with full aircraft nose down stabilator, full aileron with the spin (right-wing-up) and rudder neutralized. The aerodynamic yawing moment asymmetries, which are present in the wind tunnel data above 40° angle of attack for both the slatted and basic F-4E (Appendix A and B), have been applied in the same direction (aircraft-nose-left) as the engine gyroscopic effects so as to obtain the most critical pro spin condition. Therefore all the spins evaluated in this analysis are to the left. The weight and c.g. configurations used are presented in Table I (see Section 3.0). A spin time history summary is presented in Table 7.

The spin entry characteristics are compared on the basis of the rate at which angle of attack and rotation rate ($\Omega$) increases with time. In the fully developed spin, the angle of attack and rotation rate ($\Omega$) are used in comparing spin mode characteristics between the slatted and basic F-4E. Recovery from a spin is compared on the basis of the rate at which angle of attack and rotation rate ($\Omega$) decreases with time.

4.1 Spin Entry and Spin Characteristics - The spin mode characteristics of the slatted F-4E is presented in Table 8. The spin time histories are

## TABLE 7

## SPIN TIME HISTORY SUMMARY

Spins, Entry At .6 Mach No., Alt. - 40000 Ft.

| Figure No. | Configuration No. | Aircraft | Entry Rate $\dot{\alpha}$ - Deg/Sec | Entry Controls $\delta_s$ | $\delta_a$ | $\delta_r$ |
|---|---|---|---|---|---|---|
| D.3 (1) | 4 | F-4E | 20. | $-21^{\circ}$ | $-30^{\circ}$ | $30^{\circ}$ |
| 4.1 (1) | 1 | F-4E/F-4E + SLATS | 20. | $-21^{\circ}$ | $-30^{\circ}$ | $30^{\circ}$ |
| 4.2 (1) | 2 | " " | 20. | $-21^{\circ}$ | $-30^{\circ}$ | $30^{\circ}$ |
| 4.3 (1) | 3 | " " | 20. | $-21^{\circ}$ | $-30^{\circ}$ | $30^{\circ}$ |
| 4.4 (1) | 5/3 | " " | 20. | $-21^{\circ}$ | $-30^{\circ}$ | $30^{\circ}$ |
| 4.5 (2) | 1 | " " | 1.5 | $-21^{\circ}$ | $\pm 30^{\circ}$ | — |

NOTE: (1) Denotes wings level entry with recovery controls applied at 39 seconds.
(2) Denotes constant bank angle turn entry with aileron used to hold a given bank angle. Entry conditions were at .6 Mach No. Alt. = 20,000 Ft.

## TABLE 8
## SPIN CHARACTERISTICS SUMMARY

| Figure No. | Config. No. | Initial Entry Rate $\dot{\alpha}$ - Deg/Sec. | Aircraft Aerodynamics | Spin Mode $\alpha_B$ - Deg. | Spin Mode $\Omega$- Deg/Sec | Results of Applying Recovery Control |
|---|---|---|---|---|---|---|
| 4.1 | 1(31.5%$\bar{c}$)(1) | 22 | Slatted F-4E | 81 | 130 | No Recovery |
| | 1(31.5%$\bar{c}$)(1) | 19 | Basic F-4E | 77 | 110 | No Recovery |
| 4.2 | 2(29%$\bar{c}$)(1) | 21 | Slatted F-4E | 81 | 130 | No Recovery |
| | 2(29%$\bar{c}$)(1) | 20 | Basic F-4E | 76 | 115 | No Recovery |
| 4.3 | 3(27%$\bar{c}$)(1) | 22 | Slatted F-4E | 81 | 130 | No Recovery |
| | 3(27%$\bar{c}$)(1) | 20 | Basic F-4E | 45-63 | 50-125 | Recovery Occurred |
| 4.4 | 3(27%$\bar{c}$)(1) | 20 | Slatted F-4E | 81 | 130 | No Recovery |
| | 5(27%$\bar{c}$)(2) | 20 | Basic F-4E | 76 | 115 | No Recovery |
| 4.5 | 1(31.5%$\bar{c}$)(1) | 1.5 | Slatted F-4E | 35-41 | 20-80 | ——— |
| | 1(31.5%$\bar{c}$)(1) | 2.0 | Basic F-4E | 77 | 95 (3) | ——— |

NOTE: (1) Production Slatted F-4E Weight, C.G., and Inertias

(2) Production Basic F-4E Weight, C.G., and Inertias

(3) Rotation Rate at 60 seconds.

presented in Figures 4.1 through 4.5. The effect of aerodynamic differences (with and without leading edge slats) on the spin entry and spin characteristics are compared at the slatted F-4E's weight and c.g. conditions (Configurations 1, 2, and 3).

The spin times histories (with and without leading edge slats) for Configuration 1 (C.G. = 31.5%$\bar{c}$) are presented in Figure 4.1. The data without slats, has slightly higher entry rates ($\dot{\alpha}$ and $\dot{\Omega}$) than with slats up to time equal 16 seconds. However, after 16 seconds the rotation rate increases with time faster on the slatted F-4E. The developed spin mode of both cases is considered to be a flat spin with the slatted F-4E having both a higher spin angle of attack as well as higher rotation rate than the non-slatted F-4E.

The spin time histories for Configuration 2 (C.G. = 29%$\bar{c}$) are presented in Figure 4.2. The entry rates ($\dot{\alpha}$ and $\dot{\Omega}$) are about the same up to 20 seconds, with and without slats. After 20 seconds the slatted F-4E increases in rotation rate faster with time than the non-slatted F-4E. The flat spin mode characteristics with and without slats are about the same as Configuration 1.

For Configuration 3 (C.G. = 27%$\bar{c}$, Figure 4.3), the spin entry $\dot{\alpha}$ and $\dot{\Omega}$ are about the same for either the slatted or non-slatted configuration. However after 16 seconds the slatted F-4E continues to enter a flat spin ($\alpha_B = 81^\circ$, $\Omega = 130$ deg/sec) but the non-slatted F-4E remains in a steep oscillatory spin ($\alpha_B = 45^\circ$ to $63^\circ$, $\Omega = 50$ to $125$ deg/sec). The aerodynamic comparison between the slatted and non-slatted F-4E indicates that initial spin entry characteristics ($\dot{\alpha}$ and $\dot{\Omega}$) are about the same, but after 16 to 20 seconds the slatted F-4E has a greater tendency to enter the flat spin than the basic F-4E.

A spin time history comparison using the aerodynamic as well as inertia of the slatted F-4E (Configuration 3) and the basic F-4E (Configuration 5) is presented in Figure 4.4. While the inertias and gross weights of the two aircraft are slightly different (see Table 1) the c.g. of both configurations is 27%$\bar{c}$. The spin entry rates ($\dot{\alpha}$ and $\dot{\Omega}$ ) of both aircraft are about the same up 16 seconds. After 16 seconds the slatted F-4E progresses much faster into a flat spin mode than the basic F-4E. However, unlike the previous case where the basic F-4E went into a steep oscillatory spin, this time the basic F-4E went into a flat spin at the forward c.g. (27%$\bar{c}$). The slatted F-4E has a slightly higher angle of attack and rotation rate than the basic F-4E in the flat spin. The primary reason for the slightly higher angle of attack and rotation rates in the flat spin modes of the slatted F-4E is due to the higher values of propelling $C_n$ (see Section 2.1.2).

The four spin cases that were previously discussed were deliberately forced into a spin by means of very rapid control inputs. It should be pointed out that the initial angle of attack entry rates ( $\dot{\alpha}$ ) resulting from the rapid stabilator inputs were about 20 degrees per second. This is much higher than one would normally experience in flight. With this high entry rate the aircraft quickly accelerates through the angle of attack range ($20^\circ$ to $40^\circ$) where the leading edge slats improve the lateral-directional handling characteristics. An additional case was run (see Figure 4.5) to demonstrate a more normal spin entry from a constant bank angle turn using Configuration 1 for both aircraft. In this case no attempt is made to spin the aircraft and the ailerons are used only to maintain a 65° bank angle. After departure the basic F-4E progresses into a high angle of attack flat spin while the slatted F-4E remains in a low angle of attack (35°-41°), highly oscillatory spin which is easily recoverable.

4.2 Spin Recovery Characteristics - Anti-spin controls were applied in Figures 4.1 thru 4.4 at 39 seconds. The recovery method of full aircraft nose down stabilator, aileron with, and rudder at neutral is the same as recommended in the F-4E flight manual. No other recovery method was tried since control effectiveness of both the slatted and the basic F-4E in this region ($\alpha_B = 70^\circ$-$90^\circ$) is the same. The results show that regardless of the configuration if the aircraft goes into a flat spin ($\alpha_B = 74^\circ$ to $84^\circ$), recovery is not possible with the use of existing aircraft control surfaces. As demonstrated by the recovery from a steep oscillatory spin (see Figure 4.3), either aircraft recovers from any type of spin other than a high angle of attack flat spin.

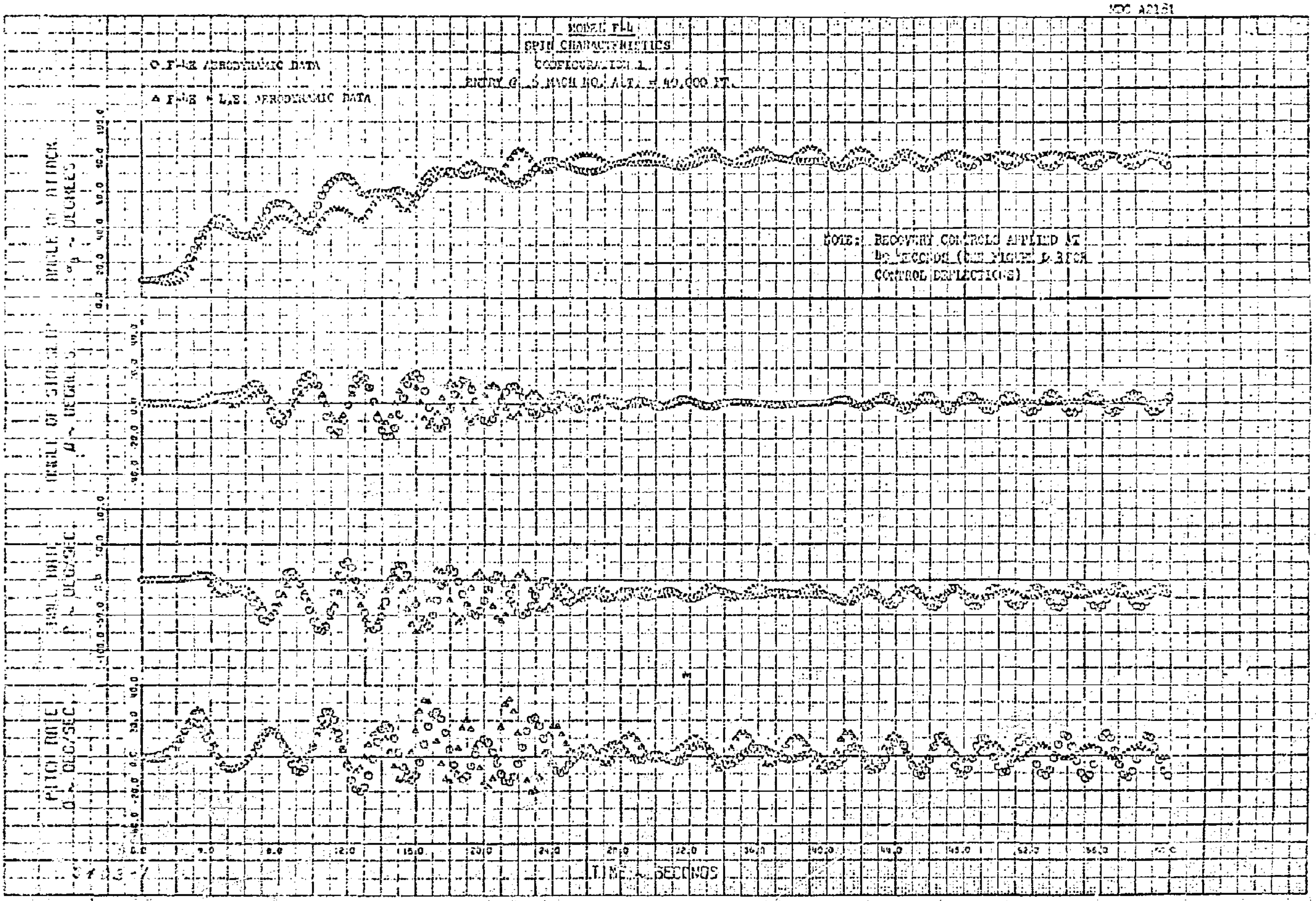
MODEL F-4
SPIN CHARACTERISTICS
CONFIGURATION 1
ENTRY @ .5 MACH NO.; ALT. = 40,000 FT.
○ F-4E AERODYNAMIC DATA
△ F-4E + L.E. AERODYNAMIC DATA
NOTE: RECOVERY CONTROLS APPLIED AT 
40 SECONDS (CHUTE FIGHT & PITCH
CONTROL DEFLECTIONS)
ANGLE OF ATTACK
$\alpha_F$ ~ DEGREES
0.0
20.0
40.0
60.0
80.0
100.0
ANGLE OF SIDESLIP
$\beta$ ~ DEGREES
-40.0
-20.0
0.0
20.0
40.0
ROLL RATE
P ~ DEG/SEC
-100.0
-50.0
0.0
50.0
100.0
PITCH RATE
Q ~ DEG/SEC
-40.0
-20.0
0.0
20.0
40.0
0.0
4.0
8.0
12.0
16.0
20.0
24.0
28.0
32.0
36.0
40.0
44.0
48.0
52.0
56.0
60.0
TIME ~ SECONDS
3183-7

Figure 4.1

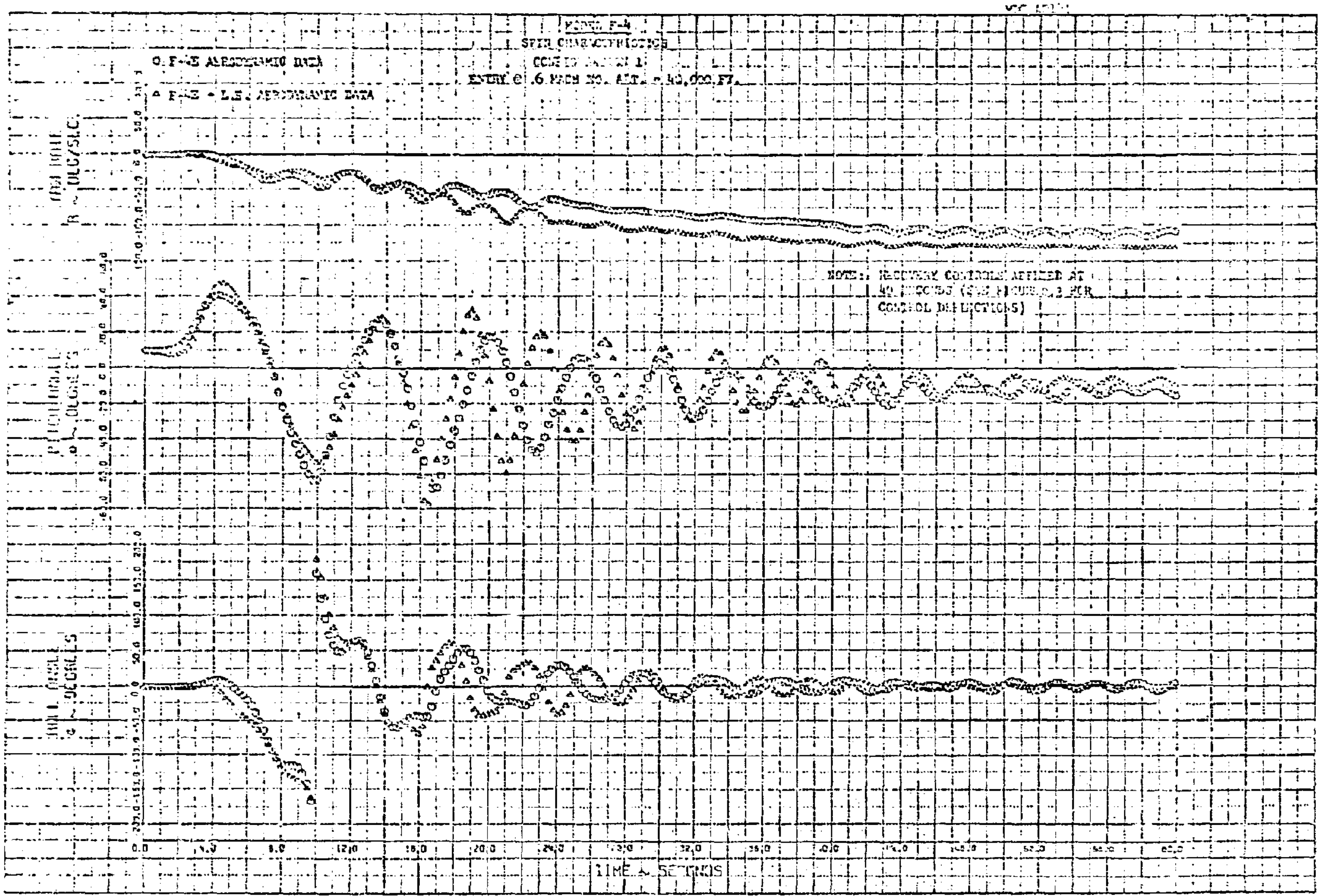

FIGURE F-4

SPIN CHARACTERISTICS

CONFIGURATION 1

ENTRY @ .6 MACH NO. ALT. = 40,000 FT.

NOTE: RECOVERY CONTROLS APPLIED AT 40 SECONDS (SEE FIGURE F-3 FOR CONTROL DEFLECTIONS)

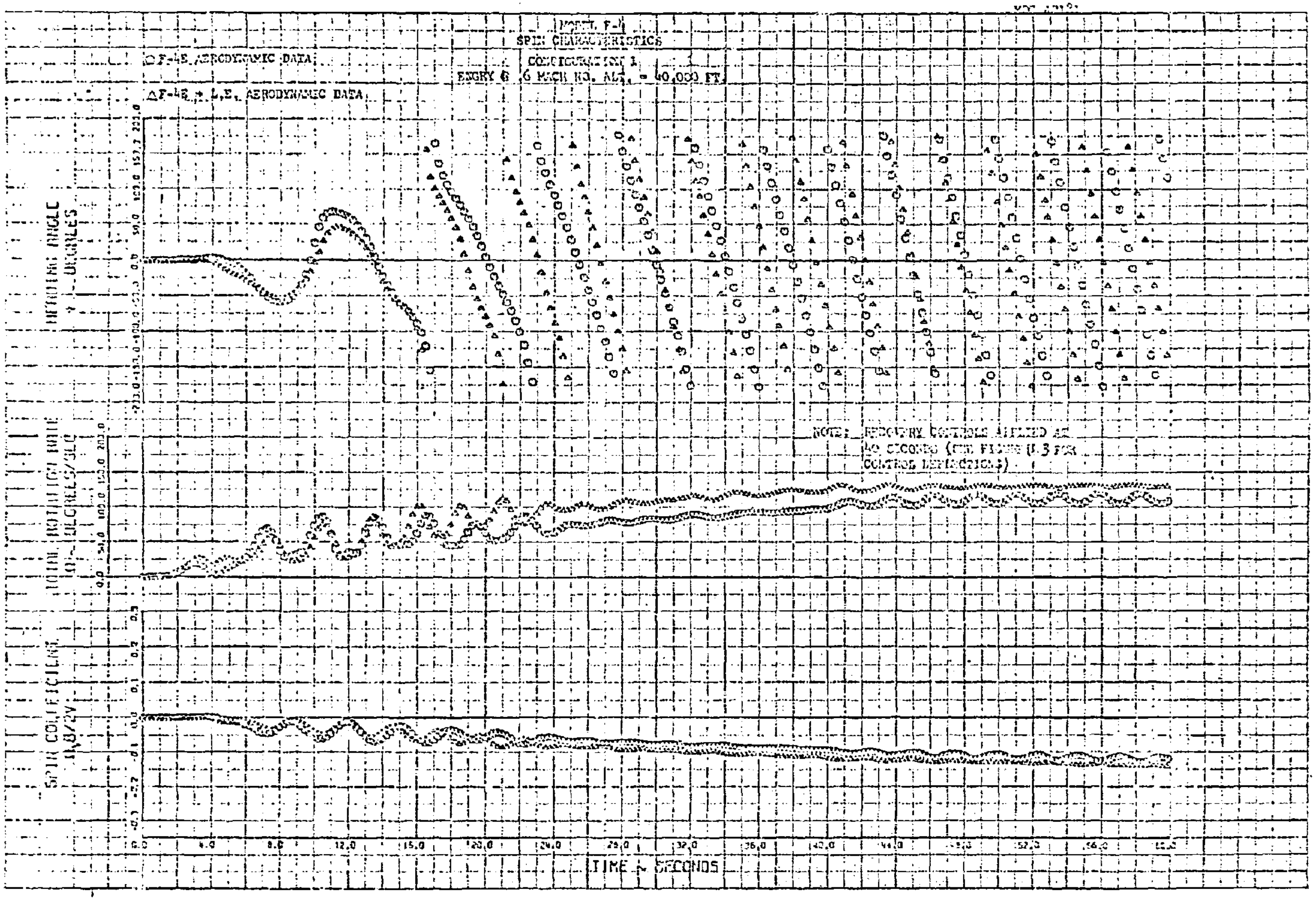
MODEL F-4
SPIN CHARACTERISTICS
CONFIGURATION 1
ENTRY @ .6 MACH NO. ALT. = 40,000 FT.
○ F-4E AERODYNAMIC DATA
△ F-4E + L.E. AERODYNAMIC DATA
HEADING ANGLE ψ ~ DEGREES
TOTAL ROTATION RATE Ω ~ DEGREES/SEC
SPIN COEFFICIENT ΩB/2V
NOTE: RECOVERY CONTROLS APPLIED AT 40 SECONDS (SEE FIGURE 4.3 FOR CONTROL DEFLECTIONS)
TIME ~ SECONDS
0.0
4.0
8.0
12.0
16.0
20.0
24.0
28.0
32.0
36.0
40.0
44.0
48.0
52.0
56.0
60.0

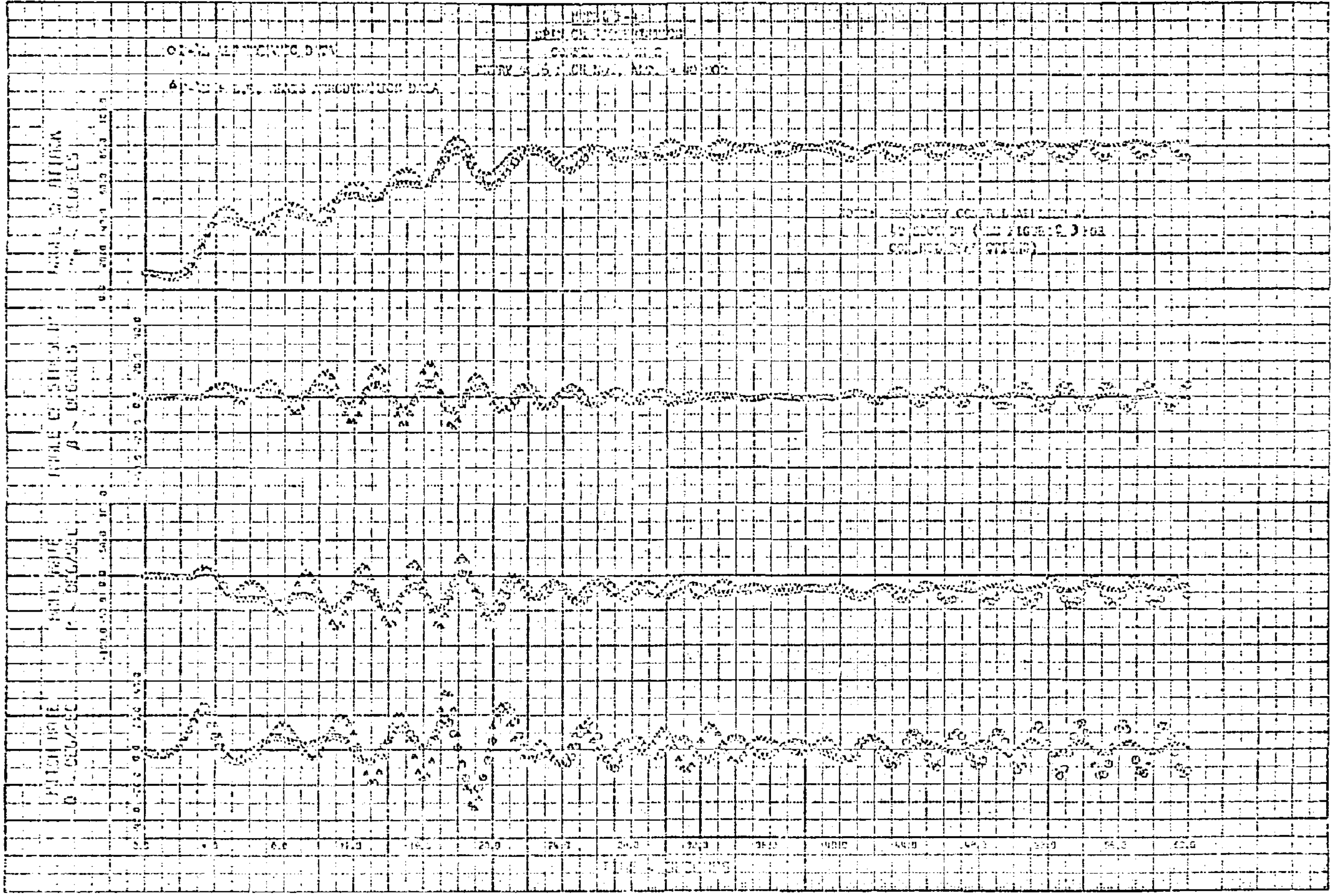ANGLE OF ATTACK
α ~ DEGREES
ANGLE OF SIDESLIP
β ~ DEGREES
ROLL RATE
p ~ DEG/SEC
PITCH RATE
θ ~ DEG/SEC
TIME ~ SECONDS
0.0
4.0
8.0
12.0
16.0
20.0
24.0
28.0
32.0
36.0
40.0
44.0
48.0
52.0
56.0
60.0

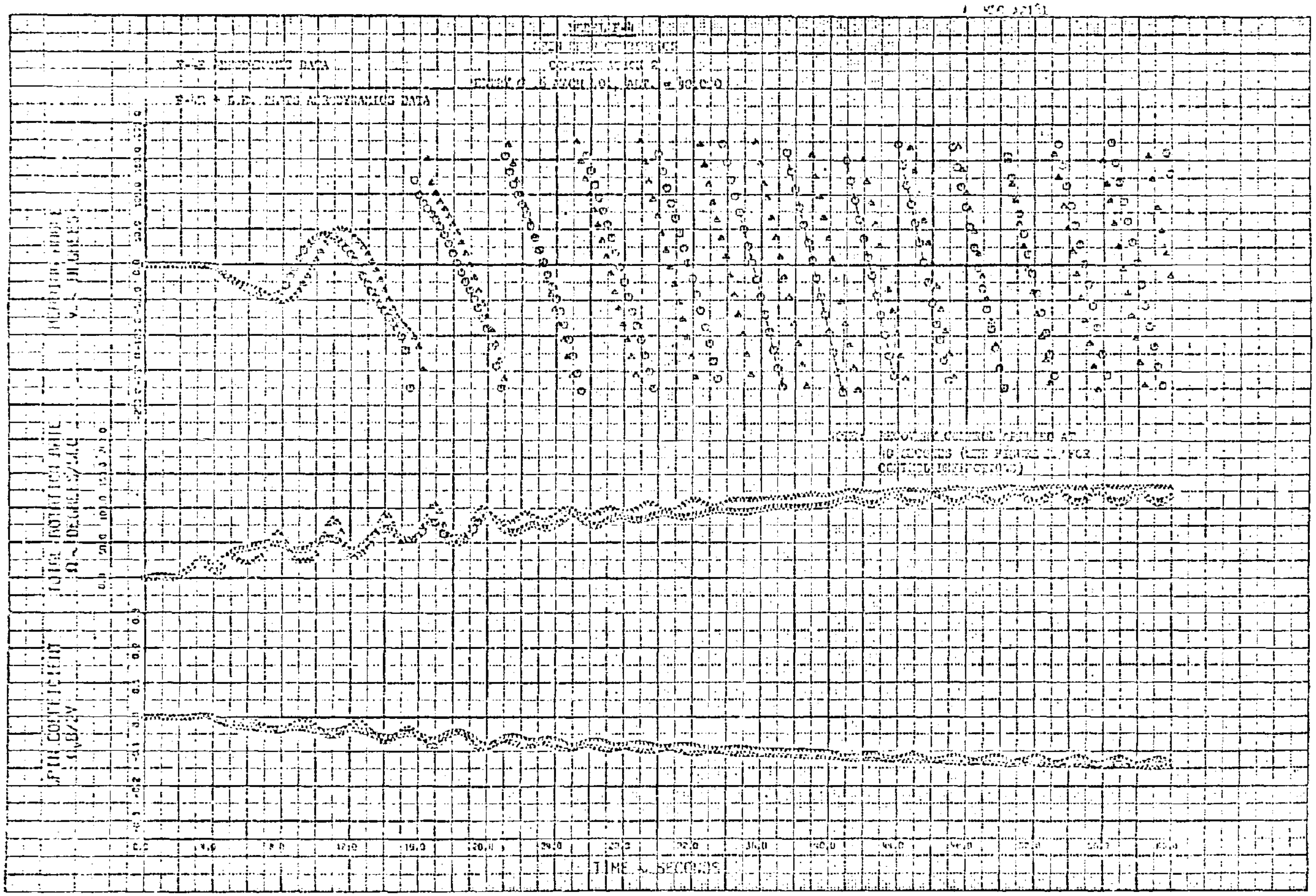

Figure 4.2 Con't

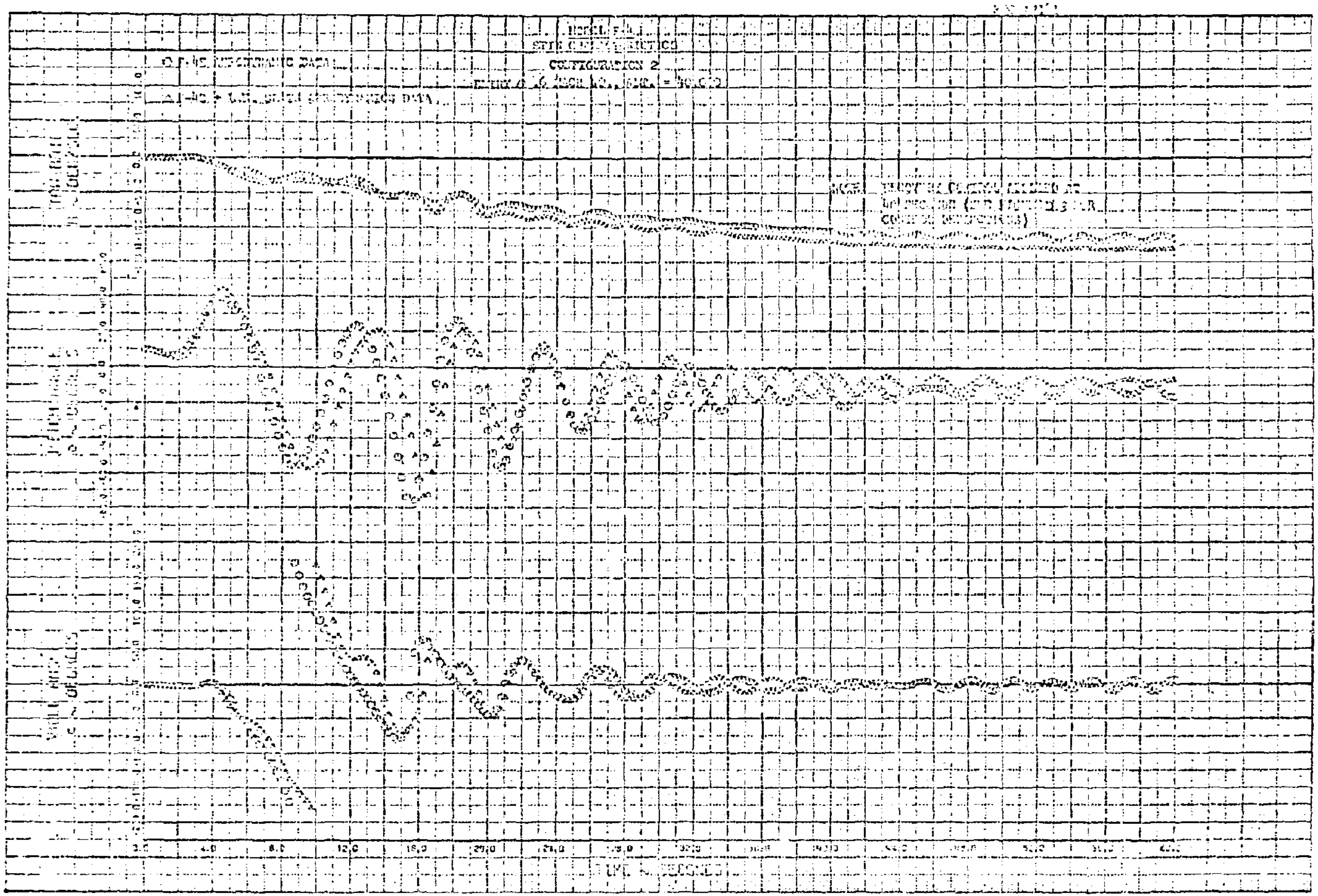

Figure 4.7 Cont'd

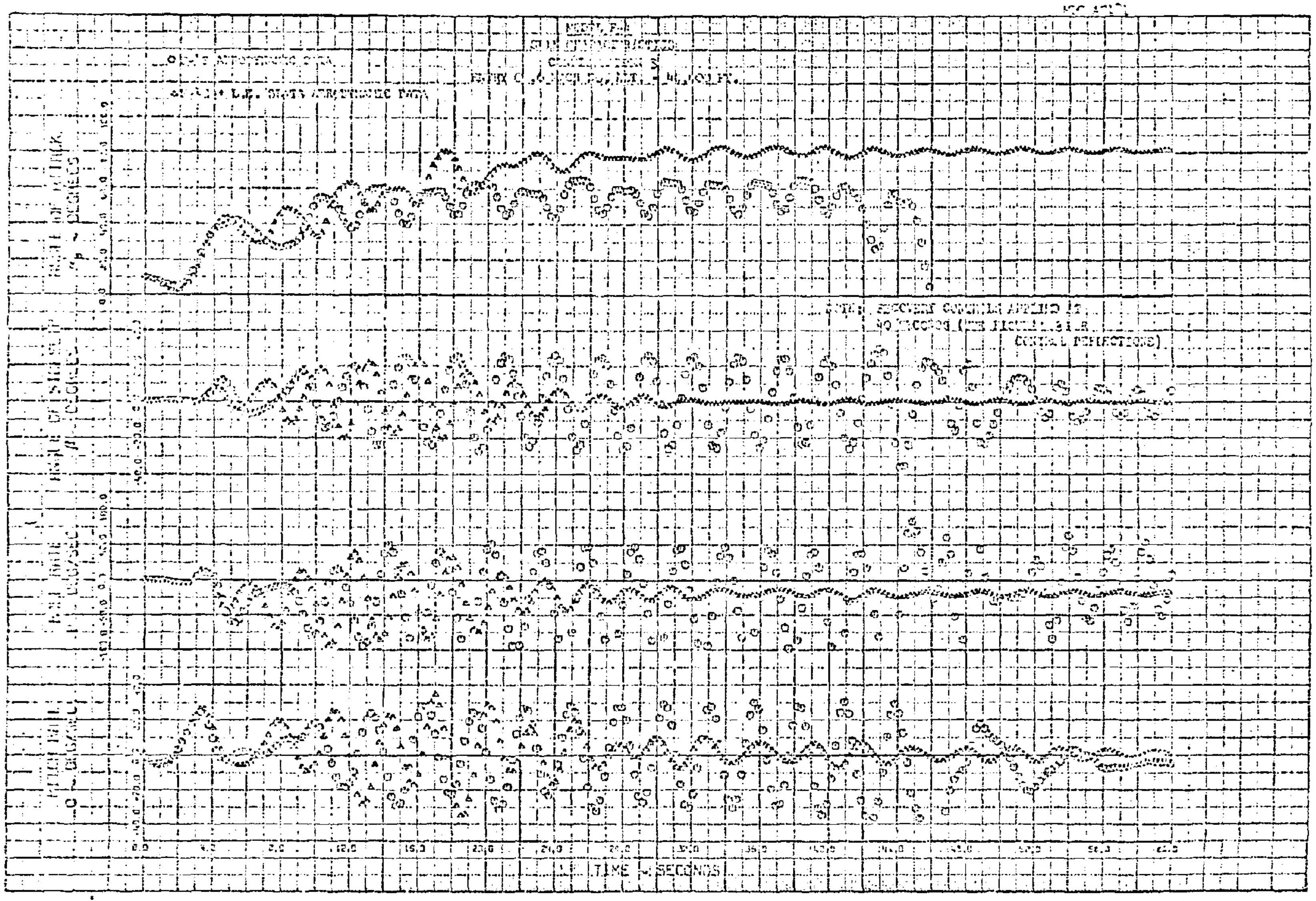

ANGLE OF ATTACK
α ~ DEGREES
ANGLE OF SIDESLIP
β ~ DEGREES
ROLL RATE
P ~ DEG/SEC
PITCH RATE
Q ~ DEG/SEC
TIME ~ SECONDS
0.0
4.0
8.0
12.0
16.0
20.0
24.0
28.0
32.0
36.0
40.0
44.0
48.0
52.0
56.0
60.0
SPIN CHARACTERISTICS
CONFIGURATION S
NOTE: RECOVERY CONTROLS APPLIED AT
L.E. SLATS AERODYNAMIC DATA
CONTROL DEFLECTIONS)

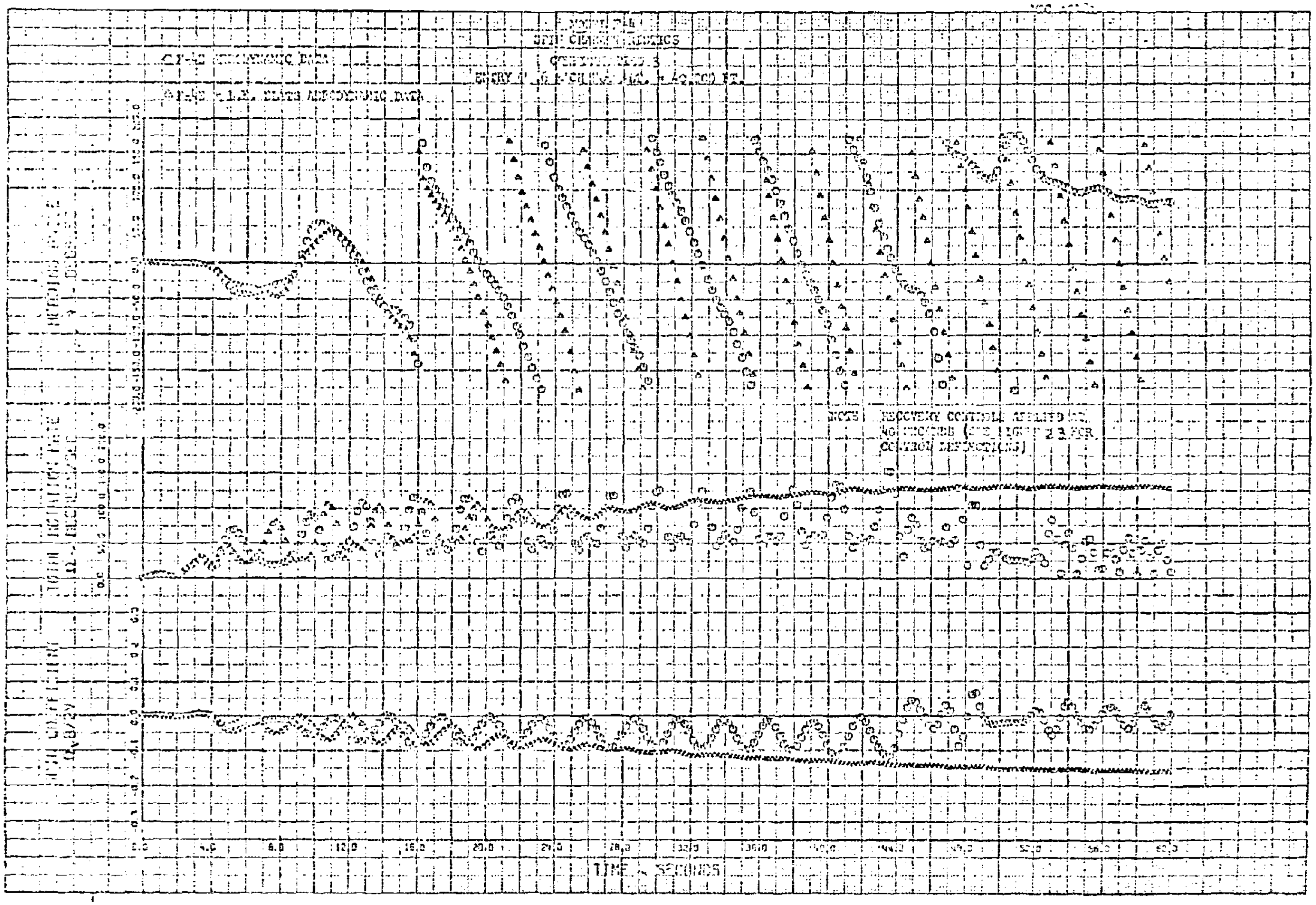
SPIN CHARACTERISTICS
ENTRY ... 40,000 FT.
NOTE: RECOVERY CONTROLS APPLIED ... (SEE FIGURE 2.3 FOR CONTROL DEFLECTIONS)
HEADING ANGLE ~ DEGREES
TOTAL ROTATION RATE ~ DEG/SEC
SPIN COEFFICIENT Ωb/2V
0.0
4.0
8.0
12.0
16.0
20.0
24.0
28.0
32.0
36.0
40.0
44.0
48.0
52.0
56.0
60.0
TIME ~ SECONDS

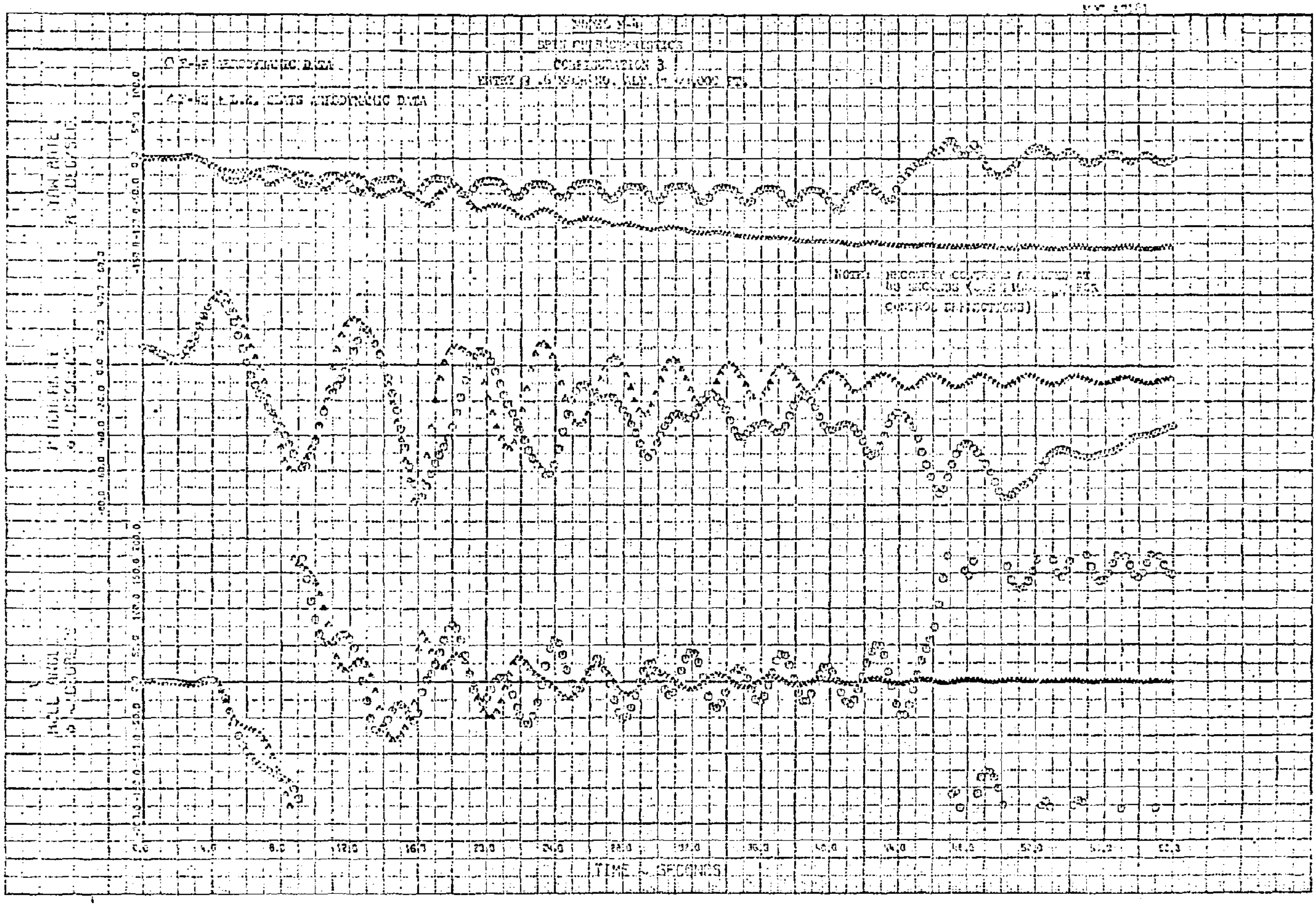
SPIN CHARACTERISTICS
CONFIGURATION 3
○ F-4E AERODYNAMIC DATA
△ F-4E L.E. SLATS AERODYNAMIC DATA
NOTE: RECOVERY CONTROLS APPLIED AT 40 SECONDS
CONTROL DEFLECTIONS)
YAW RATE
DEG/SEC
PITCH ANGLE
DEGREES
ROLL ANGLE
DEGREES
0.0
4.0
8.0
12.0
16.0
20.0
24.0
28.0
32.0
36.0
40.0
44.0
48.0
52.0
56.0
60.0
TIME ~ SECONDS

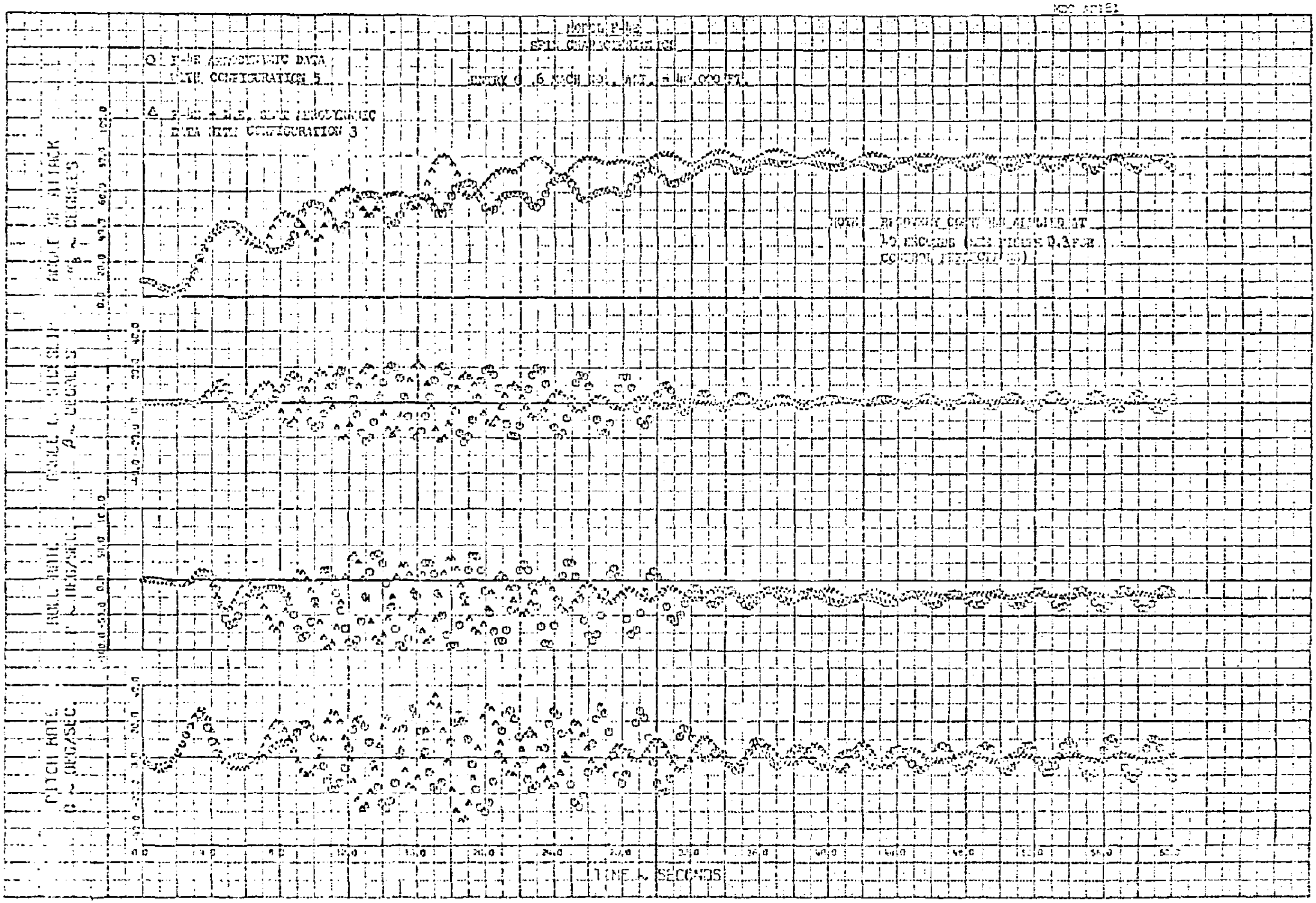
MODEL F-4E
SPIN CHARACTERISTICS
ENTRY @ .6 MACH NO., ALT. = 40,000 FT.
○ F-4E AERODYNAMIC DATA WITH CONFIGURATION 5
△ F-4E + L.E. SLAT AERODYNAMIC DATA WITH CONFIGURATION 3
NOTE: RECOVERY CONTROLS APPLIED AT 15 SECONDS (SEE FIGURE D.3 FOR CONTROL POSITIONS)
ANGLE OF ATTACK
α_B ~ DEGREES
0.0
20.0
40.0
60.0
80.0
100.0
ANGLE OF SIDESLIP
β ~ DEGREES
-40.0
-20.0
0.0
20.0
40.0
ROLL RATE
P ~ DEG/SEC
-100.0
-50.0
0.0
50.0
100.0
PITCH RATE
Q ~ DEG/SEC
-40.0
-20.0
0.0
20.0
40.0
0.0
4.0
8.0
12.0
16.0
20.0
24.0
28.0
32.0
36.0
40.0
44.0
48.0
52.0
56.0
60.0
TIME ~ SECONDS

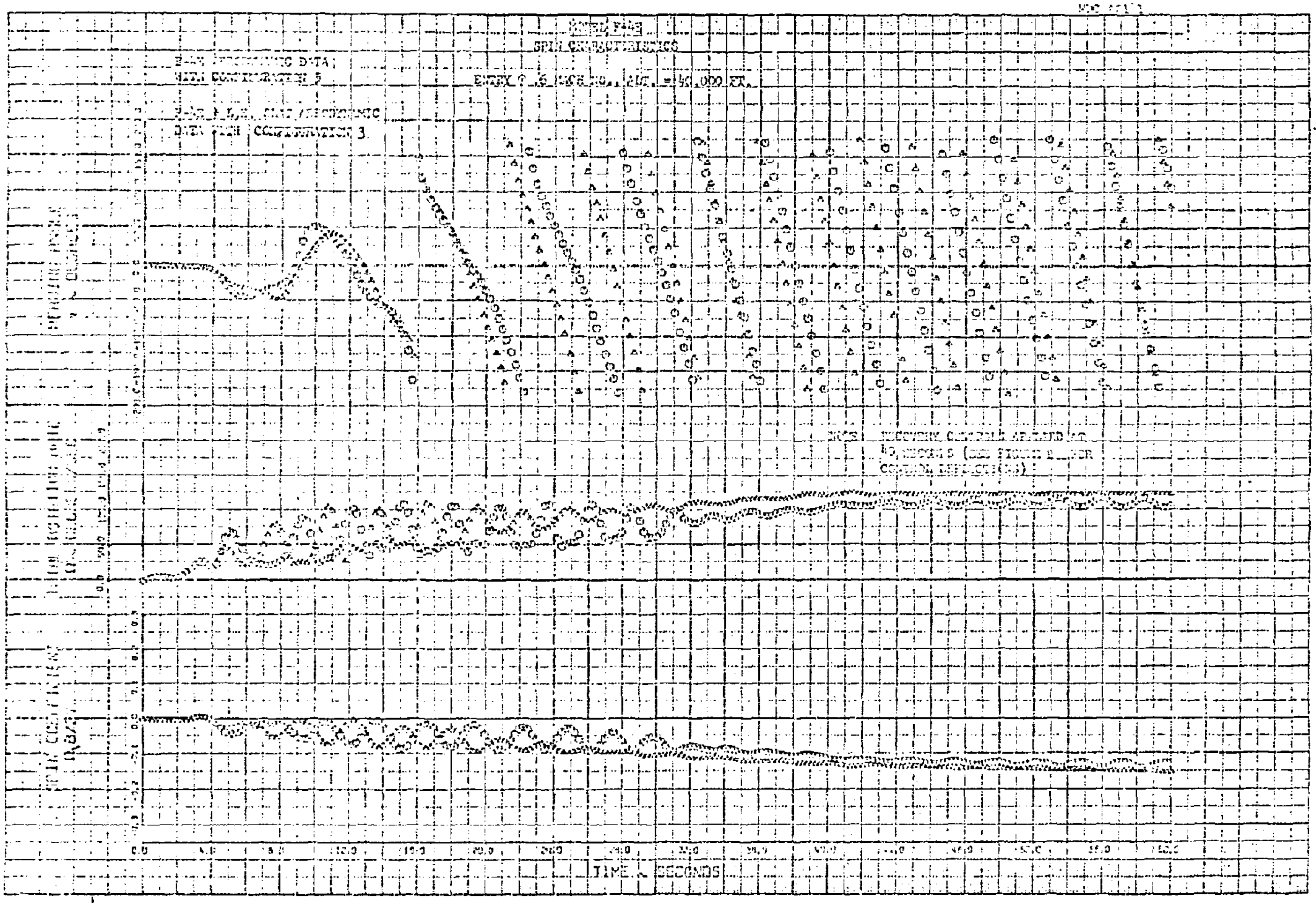
SPIN CHARACTERISTICS
DATA WITH CONFIGURATION 3
ENTRY @ .6 MACH NO., ALT. = 40,000 FT.
0.0
5.0
10.0
15.0
20.0
25.0
30.0
35.0
40.0
45.0
50.0
55.0
60.0
TIME ~ SECONDS

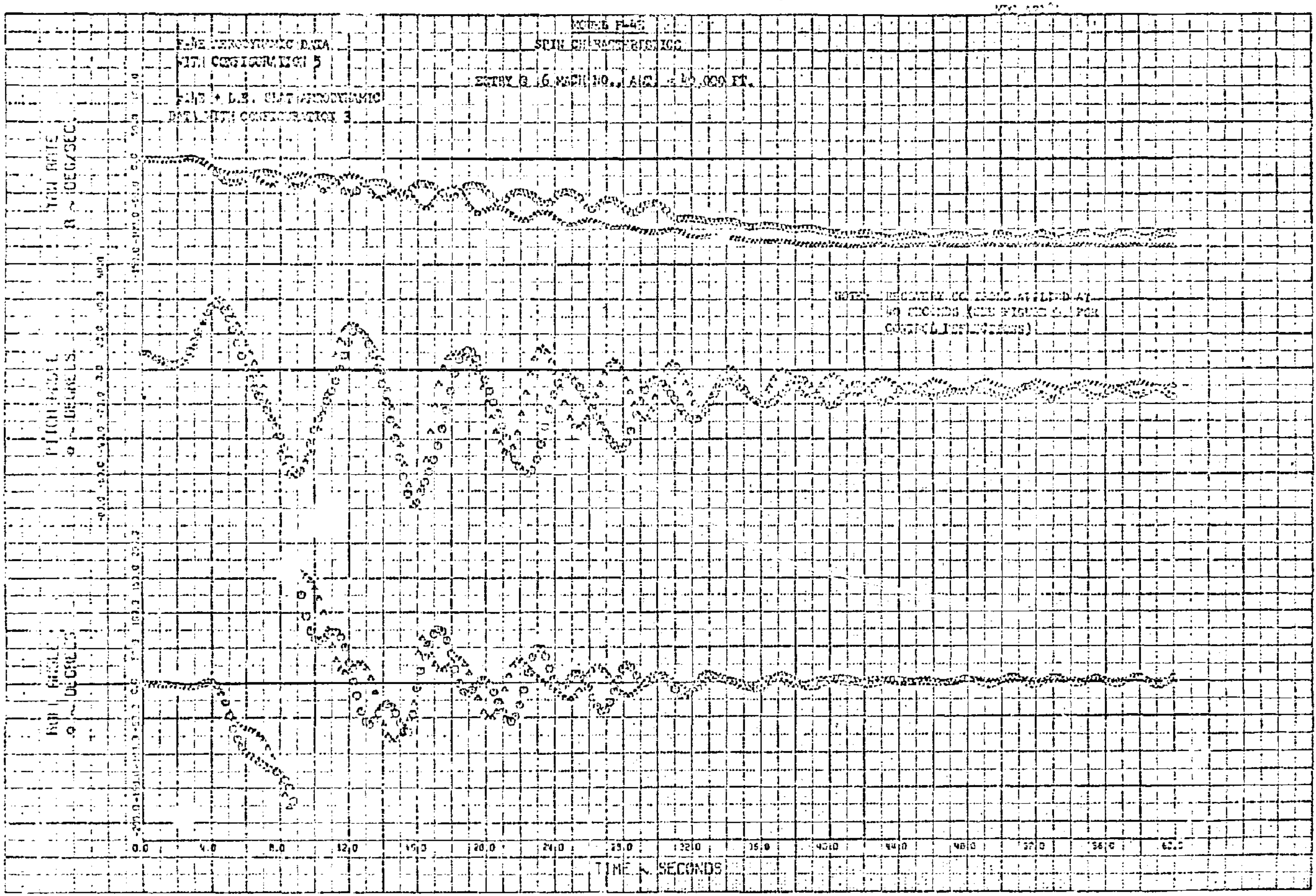ROUND FLAT
SPIN CHARACTERISTICS
ENTRY @ .6 MACH NO., ALT. = 45,000 FT.
FLAT AERODYNAMIC DATA
WITH CONFIGURATION 5
FLAT + L.E. SLAT AERODYNAMIC
DATA WITH CONFIGURATION 3
YAW RATE
R ~ DEG/SEC.
PITCH ANGLE
θ ~ DEGREES
ROLL ANGLE
φ ~ DEGREES
NOTE: RECOVERY CONTROLS APPLIED AT
40 SECONDS (SEE FIGURE 4 FOR
CONTROL DEFLECTIONS)
-200.0
-150.0
-100.0
-50.0
0.0
50.0
100.0
150.0
200.0
0.0
4.0
8.0
12.0
16.0
20.0
24.0
28.0
32.0
36.0
40.0
44.0
48.0
52.0
56.0
60.0
TIME ~ SECONDS

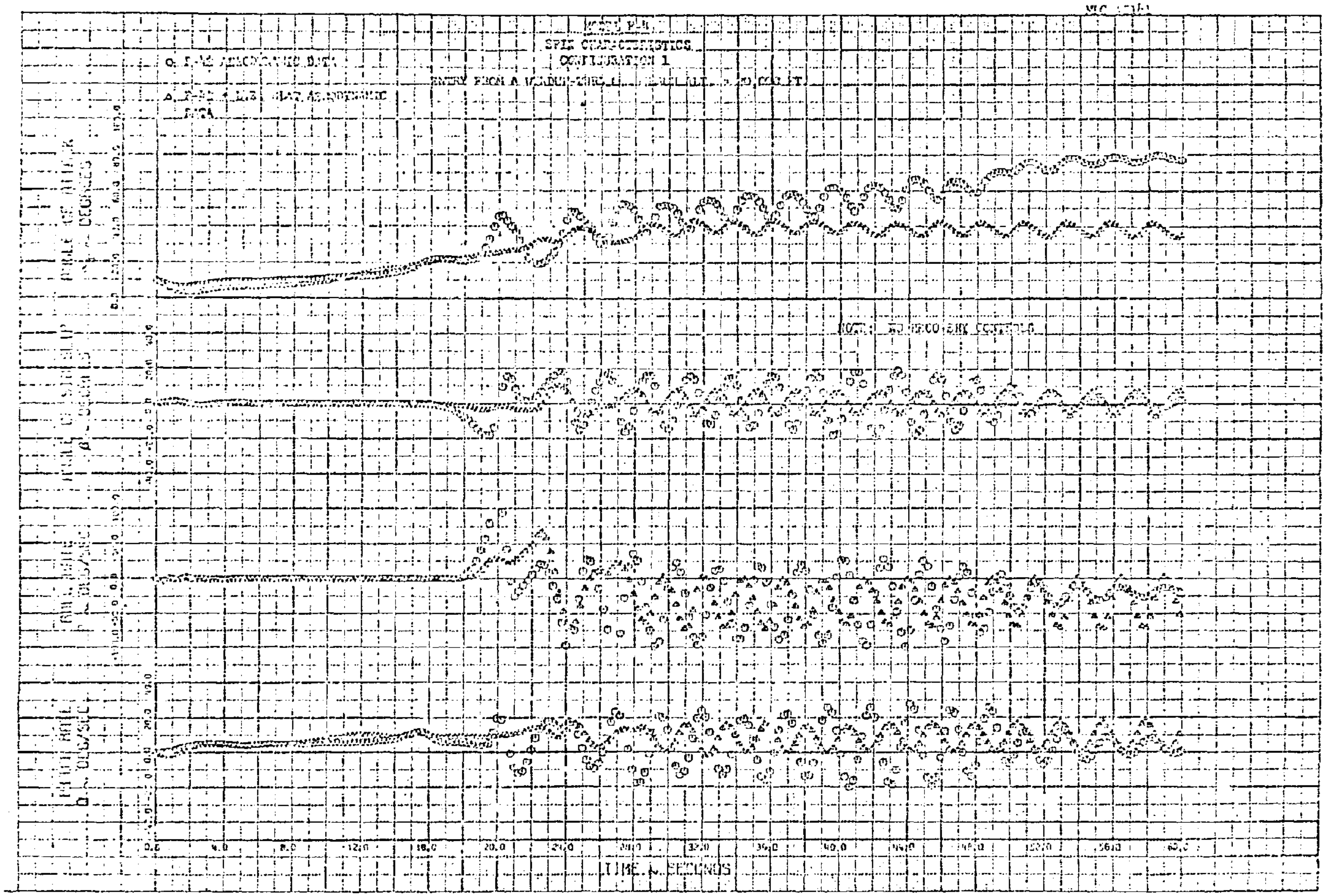
SPIN CHARACTERISTICS
CONFIGURATION 1
○ F-14 AERODYNAMIC DATA
△ F-14 + LEX AERODYNAMIC DATA
NOTE: NO RECOVERY CONTROLS
ANGLE OF ATTACK α ~ DEGREES
ANGLE OF SIDESLIP β ~ DEGREES
ROLL RATE p ~ DEG/SEC
PITCH RATE q ~ DEG/SEC
0.0
4.0
8.0
12.0
16.0
20.0
24.0
28.0
32.0
36.0
40.0
44.0
48.0
52.0
56.0
60.0
TIME ~ SECONDS

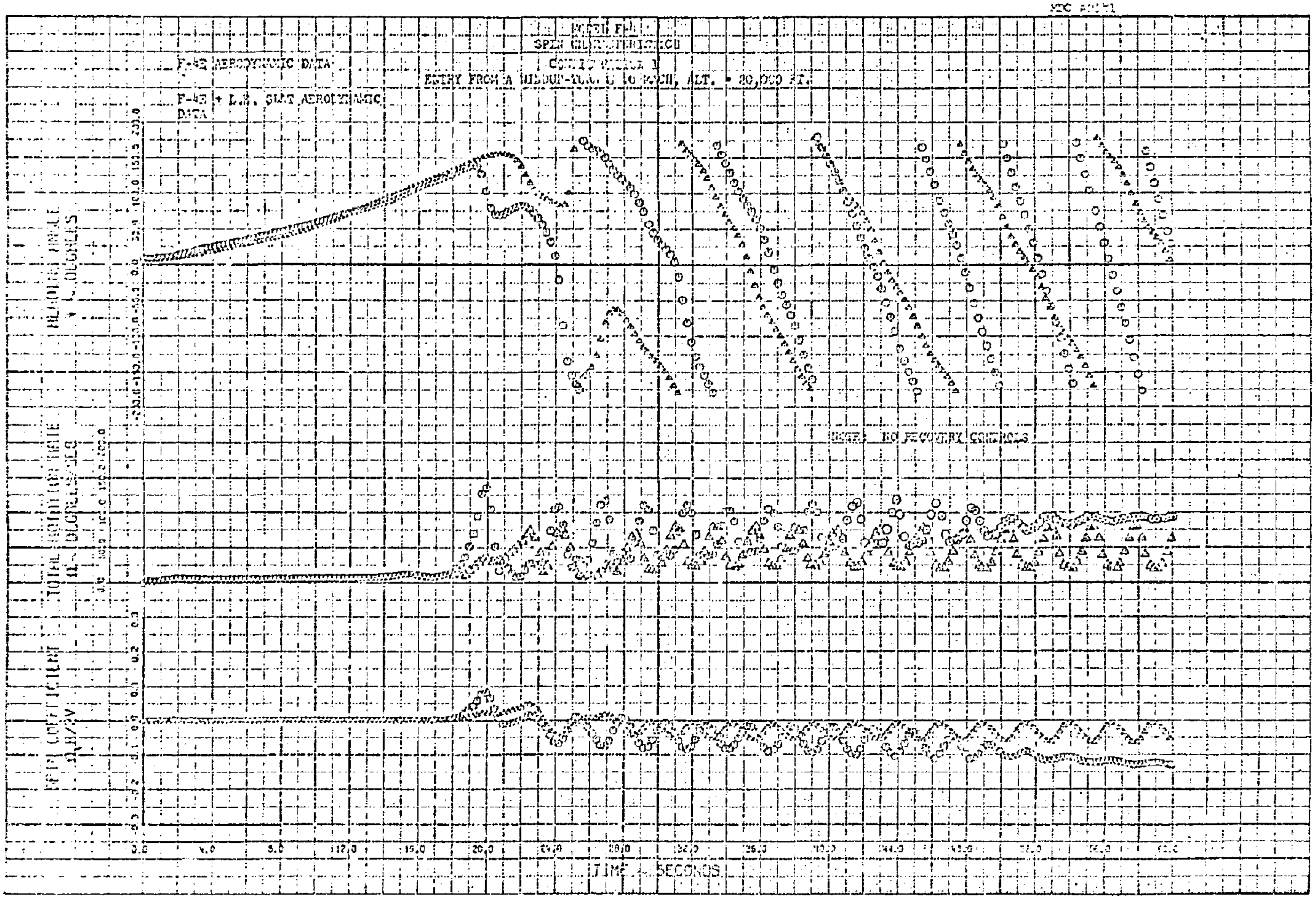

Figure 4.7 (Cont'd)

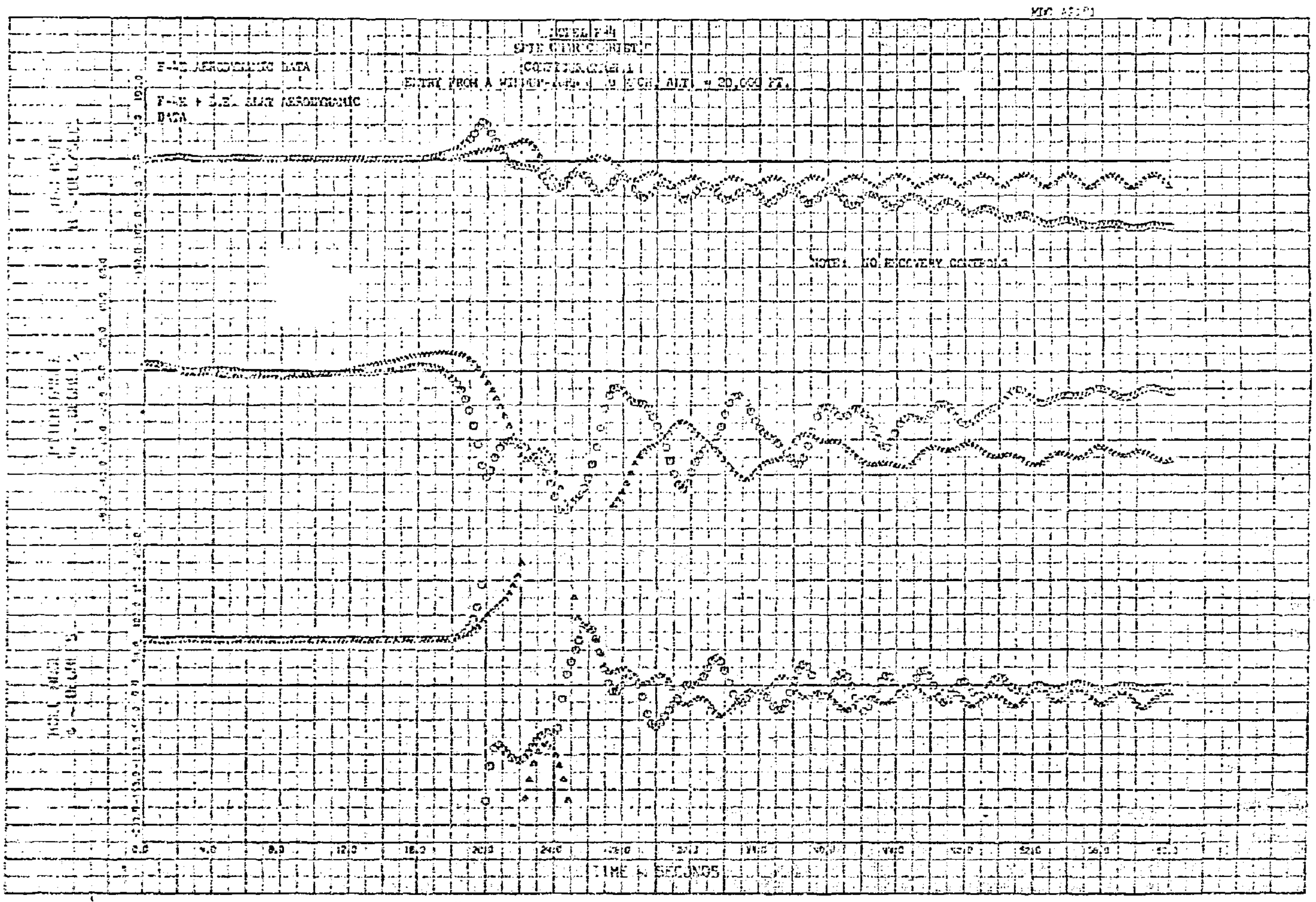

Figure 3.5 Cont'd

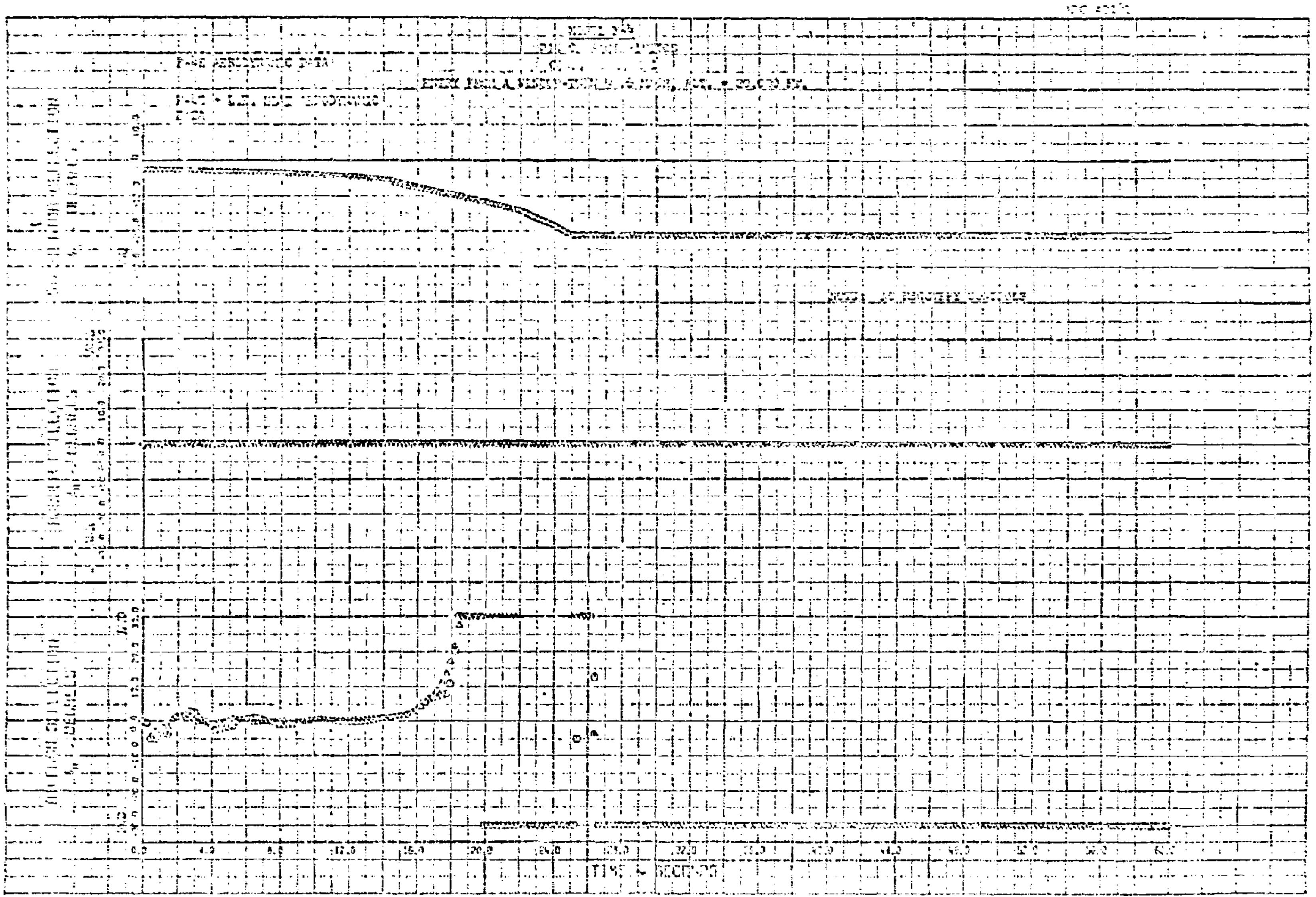
F-86 AERODYNAMIC DATA
F-86 + L.E. SLAT
TIME ~ SECONDS
0.0
4.0
8.0
12.0
16.0
20.0
24.0
28.0
32.0
36.0
40.0
44.0
48.0
52.0
56.0
60.0

## 5. Departure Prediction Techniques

Several methods have been used in the past to predict the angle of attack at which an airplane becomes lateraly-directionally unstable thereby indicating the departure point of the aircraft. It is the intent of this section of compare several departure criteria with the results from Section 3.0 (see Tables 3, 4, 5, and 6). These divergence criteria were calculated using the same aerodynamic data as used for Section 3.0.

5.1 Directional Divergence Parameter "Dynamic $C_{n_\beta}$" - The parameter "dynamic $C_{n_\beta}$" is a static derivative which includes the principle contributing terms to the undamped natural frequency of the dutch roll mode. This parameter indicates directional stability with zero lateral-directional control deflections. The expression as described in Reference (5) is:

$$C_{n_\beta \, DYN} = \left[ C_{n_\beta} - (I_z/I_x) \, C_{l_\beta} \tan\alpha \right] \cos\alpha > 0$$

The results using this parameter to predict departure are summarized in Figure 5.1 for both configurations. The slatted F-4E has a positive "dynamic $C_{n_\beta}$" through out the angle of attack range and no departures resulted during the SDF investigation. The basic F-4E "dynamic $C_{n_\beta}$" goes to zero between 18° to 20° angle of attack. Departure occurred between 19° to 20° angle of attack during the computer investigation. This directional divergence parameter predicted lateral-directional controls-fixed departure as long as the entry rates ($\dot{\alpha}$) are low (1 to 5 degs/sec.). Generally high entry rates (5 deg/sec and above) resulted in much higher departure angles of attack during the computer investigation than was the predicted by $C_{n_\beta \, DYN}$ values.

5.2 Lateral Control Divergence Parameter - A further look at the lateral-directional equations of motion in terms of bank angle response to aileron deflection yields another criterion. This criteria should be satisfied when the aileron and rudder controls are used to maintain a given bank angle. These expressions as described in Reference (5) are as follows:

Aileron Alone:

$$C_{n_\beta} - C_{l_\beta}\frac{C_{n_{\delta_a}}}{C_{l_{\delta_a}}} > 0 \qquad \text{Equation (1)}$$

Aileron plus rudder proportional to sideslip:

$$\delta_r = -K_1\beta$$

$$C_{n_\beta} - C_{l_\beta}\frac{C_{n_{\delta_a}}}{C_{l_{\delta_a}}} + K_1\left[\frac{C_{n_{\delta_a}}}{C_{l_{\delta_a}}} C_{l_{\delta_r}} - C_{n_{\delta_r}}\right] > 0 \qquad \text{Equation (2)}$$

Likewise an extension of Equation 1 for the use of proportional controls is represented by the following:

Aileron proportional to rudder: $\delta_r = K_2\delta_a$

$$C_{n_\beta} - C_{l_\beta}\left[\frac{C_{n_{\delta_a}} + K_2 C_{n_{\delta_r}}}{C_{l_{\delta_a}} + K_2 C_{l_{\delta_r}}}\right] > 0 \qquad \text{Equation (3)}$$

All three equations are evaluated by comparing their calculated departure angles of attack with those obtained from the computer time histories of Section 3.0. As stated previously only the lower entry rates ($\dot{\alpha}$ = 1 to 5 deg/sec) were used in these comparisons. It is felt that the departure angle of attack is affected very little by these lower entry rates.

5.2.1 Aileron Alone Divergence Parameter - The predicted angle of attack at departure for the aileron alone criterion (Equation 1) is compared with the computer time history results (Figure 3.1, 3.2, 3.15, 3.16, 3.17 and 3.18) on Figure 5.2. This criterion predicted the basic F-4E departures within $1^\circ$ to $2^\circ$ angle of attack. This was not the case for the slatted F-4E where the criterion is unsatisfactory in predicting the departure angle attack.

5.2.2 Aileron/Rudder Divergence Parameter - The aileron/rudder criterion is calculated using $K_1$ equal to 2. This is the same gain that is used for rudder proportional to sideslip in the computer results from Section 3.0. This divergence criterion is calculated for both the basic and slatted F-4E and the results are shown in Figure 5.3. There is again good agreement between the SDF computer results and the departure criterion for the basic F-4E, however the agreement is unsatisfactory for the slatted F-4E. This criterion predicts departure well below the actual departure angle of the slatted computer results. It is suspected that had $K_1$ been 10 or larger there would have been much better agreement with SDF results for the slatted F-4E, but the basic F-4E correlation would have been unsatisfactory. The aileron/rudder divergence parameter is not very reliable in particular when strong dihedral effect is present as in the case of the slatted F-4E.

5.2.3 Aileron Proportional to Rudder Divergence Criteria - Equation 3 is an empirical expansion of Equation 1 in Section 5.2 where both rudder and aileron are consider to have a proportional relationship. Thus $K_2$ is expressed as:

$$\delta_r = K_2 \delta_a$$

The aileron and rudder are not directly proportional to each other in the time histories computed in Section 3.0. The aileron is used to control bank angle and the rudder is used to control angle of sideslip. Therefore $K_2$ is determined by the aileron and rudder deflections at the point of departure (computer results, Figures 3.3, 3.4 and 3.12). These values for $K_2$ are used to evaluate the aileron proportional to rudder divergence criterion (Equation 3).

The results of this departure criterion are summarized in Figure 5.4. This criterion is unsatisfactory in predicting the angle of attack for departure particularly for the slatted F-4E.

5.3 $\beta$ Plus $\delta$ Axis Stability Indicator - A new method of determining the point of lateral-directional divergence has been developed by MCAIR and is presented in detail in Reference 5 along with comparative free flight results. Because of the newness of this method a very brief derivation and explanation is appropriate.

First we will consider the aircraft's instanteous response to sideslip angle about the X and Z body axes system.

$$\frac{\partial \ddot{\psi}}{\partial \beta} = \frac{C_{n_\beta} q s b}{I_z}$$

$$\frac{\partial \ddot{\phi}}{\partial \beta} = \frac{C_{l_\beta} q s b}{I_x}$$

These vectors are shown in their positive sense in the diagram below.

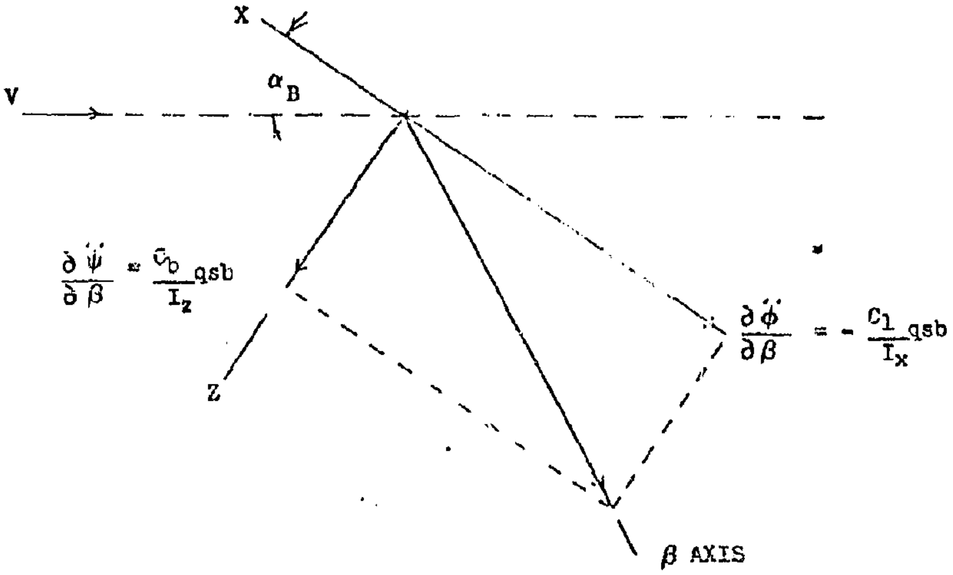
X
V
$\alpha_B$
$\frac{\partial \ddot{\psi}}{\partial \beta} = \frac{C_b}{I_z} qsb$
Z
$\frac{\partial \ddot{\phi}}{\partial \beta} = - \frac{C_l}{I_x} qsb$
$\beta$ AXIS

The vector sum is called the $\beta$ axis. As long as the $\beta$ axis is in the two lower quadrants the aircraft is stable and no divergence is predicted. If the $\beta$ axis should lie in the upper two quadrants or above the horizontal line the aircraft is unstable. The first point of instability or divergence is when the $\beta$ axis vector lies along the horizontal or along the velocity vector.

In the same manner as before we will consider the instantaneous response to either a lateral or a directional control input or a combination of the two. These responses are again with respect to the x and z body axes system.

$$\frac{\partial \ddot{\phi}}{\partial \delta} = \left[\frac{C_{l_{\delta a}} \delta a + C_{l_{\delta r}} \delta r}{I_x \, (\delta_a + \delta_r)}\right] qSb = \frac{C_{l_\delta}}{I_x} qSb$$

$$\frac{\partial \ddot{\psi}}{\partial \delta} = \left[\frac{C_{n_{\delta a}} \delta a + C_{n_{\delta r}} \delta r}{I_z \, (\delta_a + \delta r)}\right] qSb = \frac{C_{n\delta}}{I_z} qSb$$

where $\delta = \delta a + \delta r$

These vectors are shown in their positive sense in the diagram below.

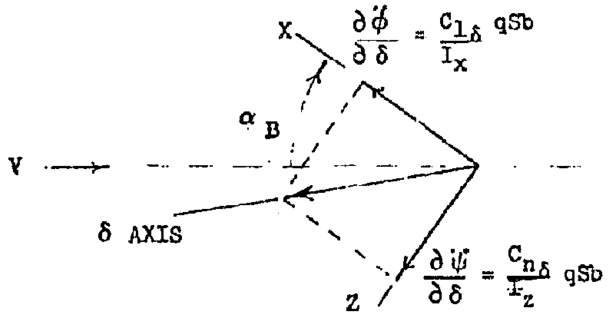
X
$\frac{\partial \ddot{\phi}}{\partial \delta} = \frac{C_{l_\delta}}{I_x} qSb$
$\alpha_B$
V
δ AXIS
Z
$\frac{\partial \ddot{\psi}}{\partial \delta} = \frac{C_{n\delta}}{I_z} qSb$

The vector sum is called the $\delta$ axis.

When using aileron or rudder control this criteria must consider both the $\beta$ and the $\delta$ axis vectors as described in the diagram on the next page.

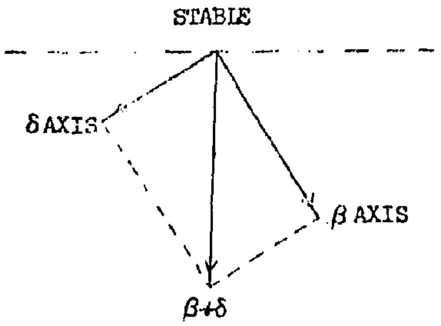

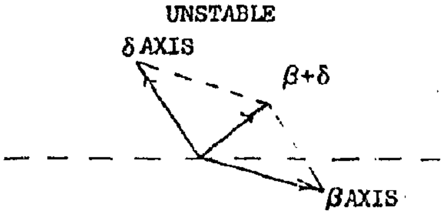

This method can be applied to any control combination case or with no lateral-directional controls at all.

Summaries of predicted versus actual SDF computer divergencies are presented on Figure 5.5 and 5.6. Four combinations of control inputs were looked at along with the no control input cases. The rudder and aileron deflections at the angle of attack for departure (computer results) were used in this criterion just as in Section 5.2.3. For cases of rudder control alone as described in Section 3.0, the rudder controls bank angle by producing small sideslip angles and utilizes the dihedral effect to roll the aircraft. The $\beta$ and $\delta$ axis method in general predicts the point of divergence reasonably well. This method is very versatile since it is good for all possible combinations of aileron and rudder, aileron alone, rudder alone, and no lateral-directional controls.

MODEL F-4E

$C_{n\beta}$ DYNAMIC DEPARTURE SUMMARY

WINGS LEVEL 1g STALL ENTRY WITH NO LATERAL-DIRECTIONAL CONTROLS

C.G. = 33%c̄ M = .35 ALT. = 18000 FT.

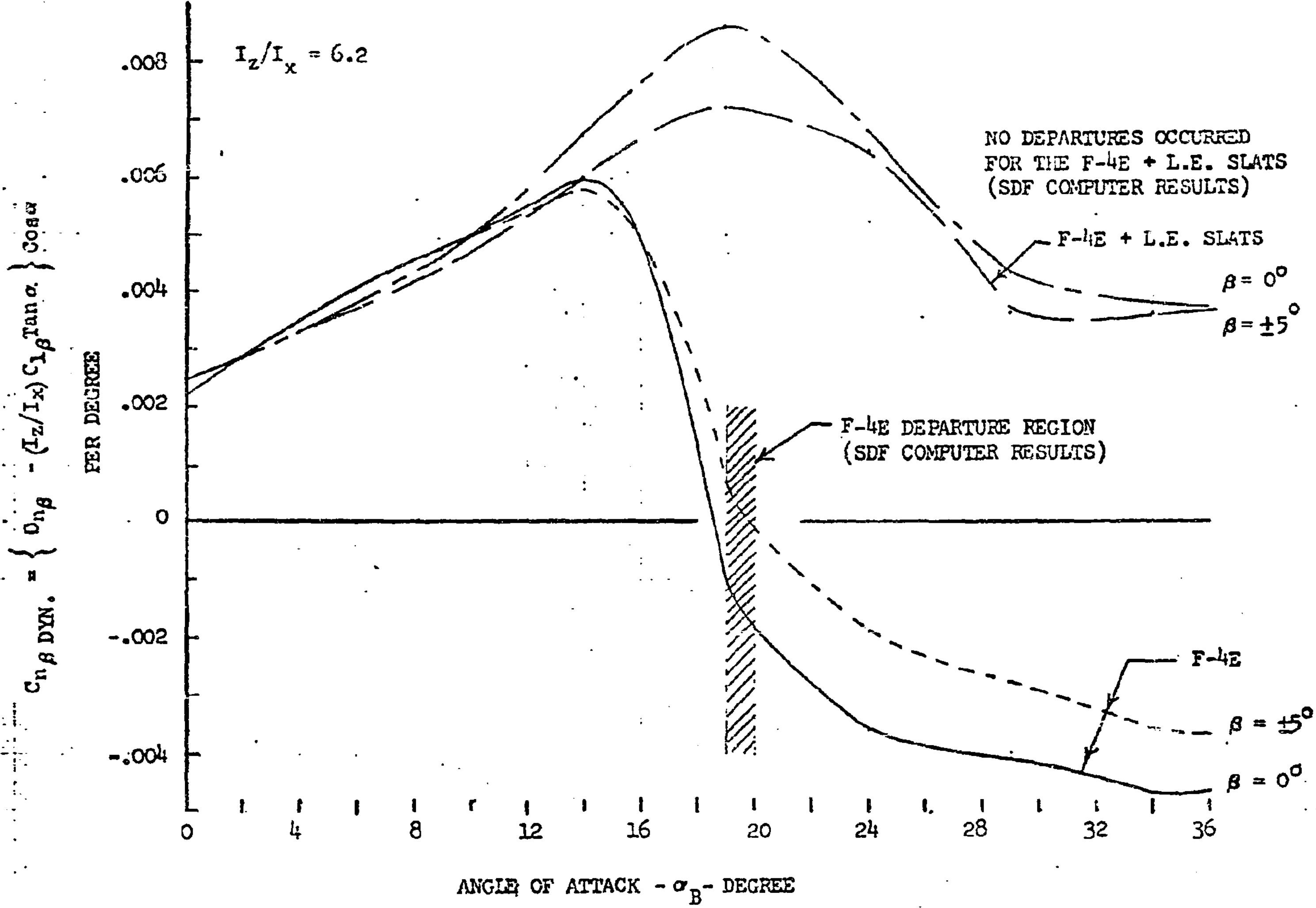

Figure 5.1

5404-1-036

## MODEL F-4E
## AILERON ALONE DIVERGENCE PARAMETER

$$C_{n_\beta} - C_{l_\beta}\left(\frac{C_{n_{\delta_a}}}{C_{l_{\delta_a}}}\right) > 0$$

| Symbol | Figure | Maneuver | $\dot{\alpha}$ (Deg/Sec) |
|---|---|---|---|
| ○ | 3.1 | 1g Stall | 1.2 |
| □ | 3.2 | Turn | 1.2 |
| ◇ | 3.15 | 1g Stall | 1.3 |
| △ | 3.16 | 1g Stall | 1.3 |
| ◊ | 3.17 | Turn | 1.2 |
| ◁ | 3.18 | Turn | 1.5 |

NOTE: Open Symbols denote basic F-4E and solid symbols denote slatted F-4E.

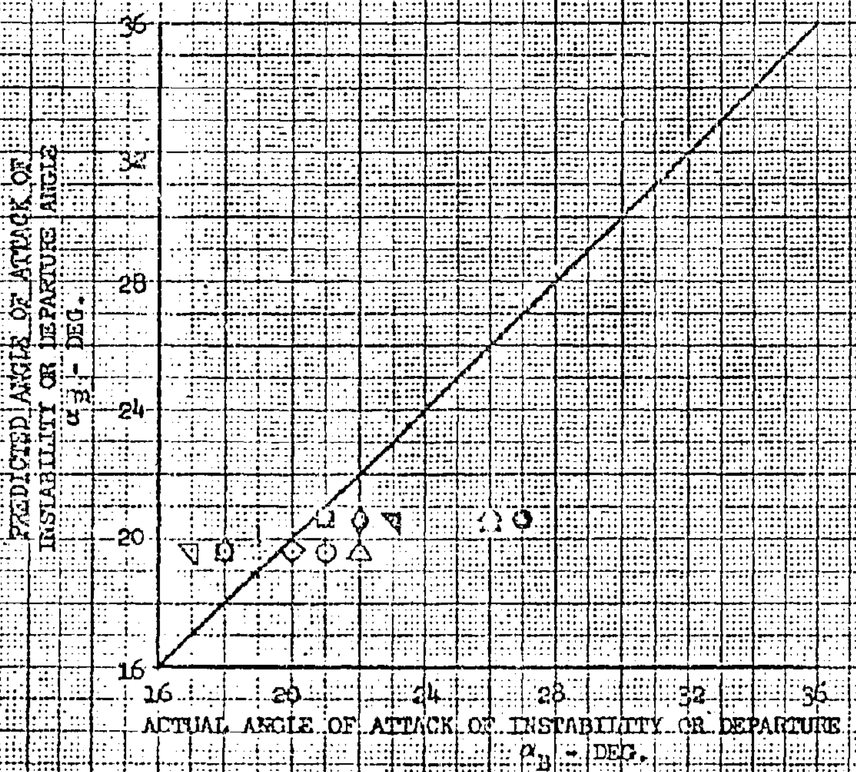

S-04-A-1-036

## MODEL F-4E
## AILERON/RUDDER DIVERGENCE PARAMETER

$$C_{n_\beta} - C_{l_\beta}\left(\frac{C_{n_{\delta a}}}{C_{l_{\delta a}}}\right) + K_1\left(\frac{C_{n_{\delta a}}}{C_{l_{\delta a}}} C_{l_{\delta r}} - C_{n_{\delta r}}\right) > 0$$

| SYMBOL | FIGURE | MANEUVER | $K_1$ | $\dot{\alpha}$ (DEG/SEC) |
|---|---|---|---|---|
| ○ | 3.3 | 1g Stall | 2.0 | 2.4 |
| □ | 3.4 | Turn | " | 1.2 |
| ◇ | 3.12 | " | " | 1.3 |
| ▲ | 3.3 | 1g Stall | " | 2.4 |
| ◆ | 3.4 | Turn | " | 1.2 |
| ◥ | 3.12 | " | " | 1.3 |

where $\delta_r = -K\beta$

NOTE: Open symbols denote basic F-4E and solid symbols denote slatted F-4E.

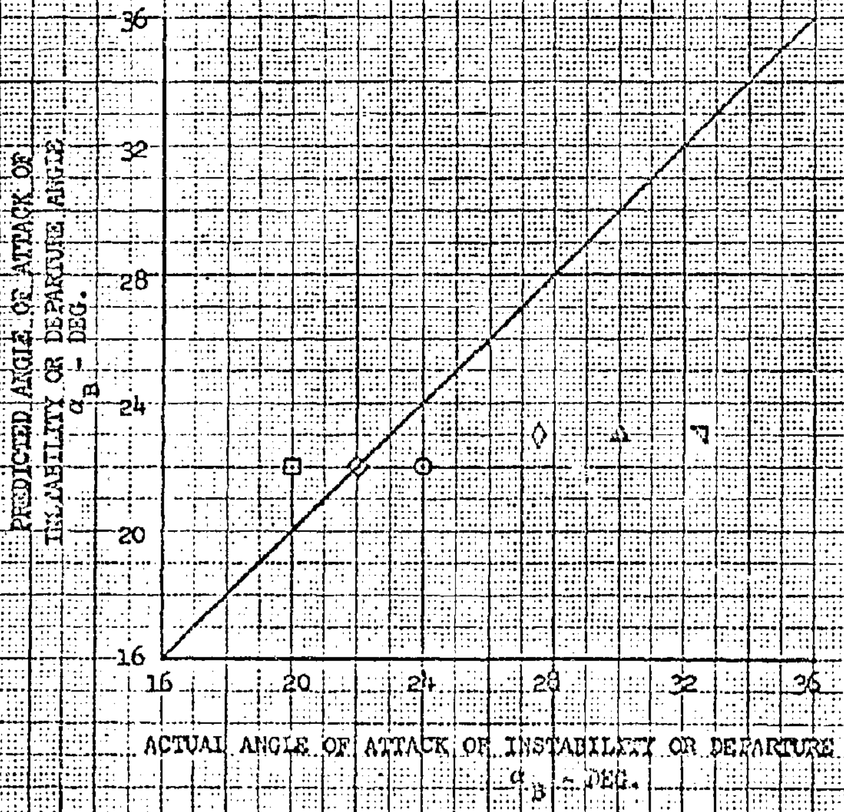

S40.1L/L.057

Figure 5.3

## MODEL F-4E

## AILERON PROPORTIONAL TO RUDDER

$$C_{n_\beta} - C_{l_\beta}\left(\frac{C_{n_{\delta_a}} + K_2\, C_{n_{\delta_r}}}{C_{l_{\delta_a}} + K_2\, C_{l_{\delta_r}}}\right) > 0$$

| SYMBOL | FIGURE | MANEUVER | $\delta_a$ | $\delta_r$ | $K_2$ | $\dot{\alpha}$ (DEG/SEC) |
|---|---|---|---|---|---|---|
| ○ | 3.3 | 1g Stall | -8° | 0 | 0 | 2.4 |
| □ | 3.4 | Turn | +3° | 0 | 0 | 1.2 |
| ◇ | 3.12 | " | +3° | -1° | -.33° | 1.3 |
| ▲ | 3.3 | 1g Stall | -25° | -4° | .16° | 2.4 |
| ◆ | 3.4 | Turn | +7° | +.35° | .05° | 1.2 |
| ◀ | 3.12 | " | +6° | 0 | 0 | 1.3 |

Where $K_2 = \delta_r / \delta_a$ @ Departure

NOTE: Open symbols denote basic F-4E and solid symbols denote slatted F-4E.

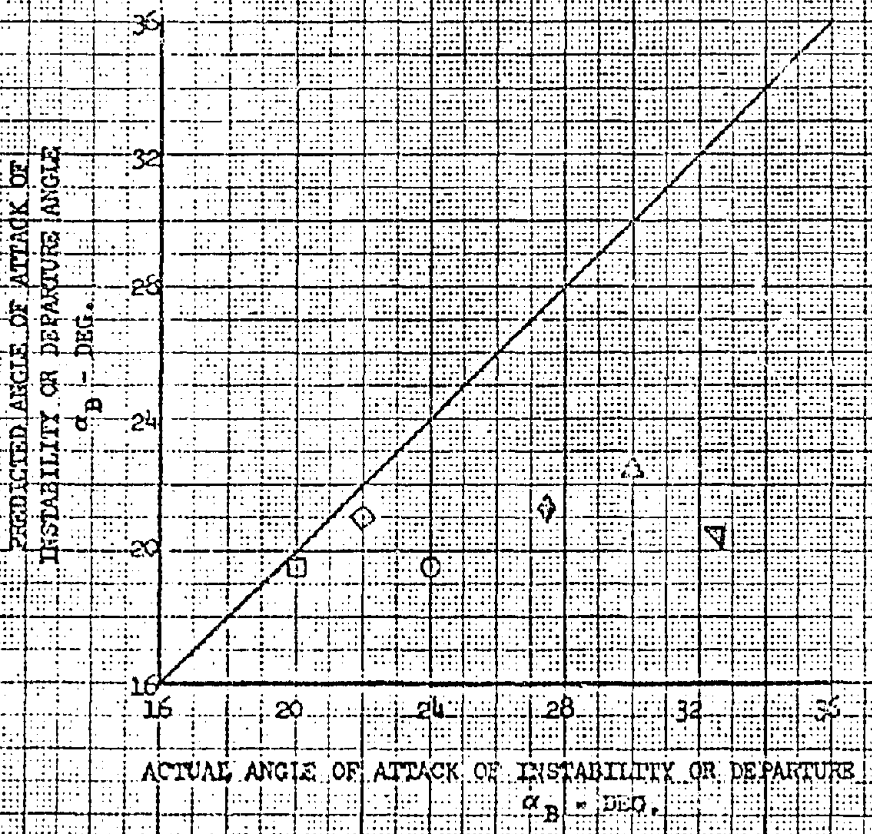

5-607-11-0256

NATIONAL TRACING PAPER
INDIANAPOLIS, INDIANA
LITHO IN U.S.A.

Figure 5.4

## MODEL F-4E

## $\beta$ PLUS $\delta$ AXIS STABILITY INDICATOR SUMMARY

| Symbol | Figure | Maneuver | Controls | $\dot{\alpha}$ (Deg/Sec) |
|---|---|---|---|---|
| ○ | 3.7 | 1g Stall | None | 1.2 |
| △ | 3.8 | " " | " | 2.4 |
| □ | 3.9 | " " | " | 5.6 |
| ◇ | 3.1 | " " | Aileron Only | 1.2 |
| ◁ | 3.15 | " " | " " | 1.3 |
| ◇ | 3.16 | " " | " " | 1.3 |
| ◇ | 3.3 | " " | Aileron/Rudder | 2.4 |
| ◇ | 3.5 | " " | Rudder Only | 2.4 |
| ● | 3.2 | Turn | Aileron Only | 1.2 |
| ▲ | 3.17 | " | " " | 1.2 |
| ■ | 3.18 | " | " " | 1.5 |
| ◆ | 3.4 | " | Aileron/Rudder | 1.2 |
| ◀ | 3.12 | " | " " | 1.3 |
| ◆ | 3.16 | " | Rudder Only | 1.2 |

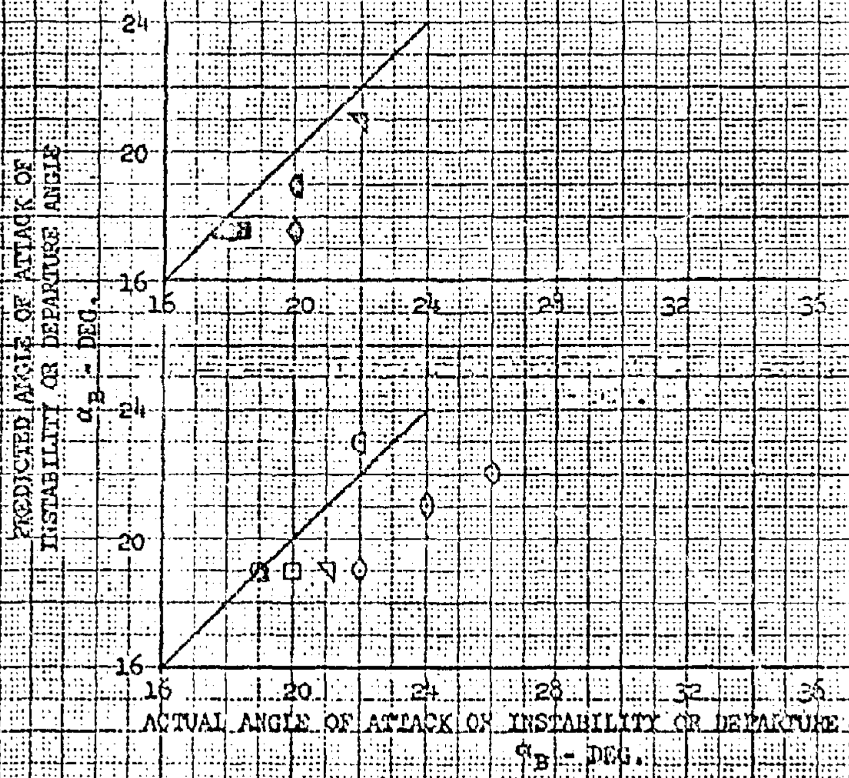

Figure 5.5

## MODEL F-4E
## WITH LEADING EDGE SLATS
## $\beta$ PLUS $\delta$ AXIS STABILITY INDICATOR SUMMARY

| Symbol | Figure | Maneuver | Controls | $\dot{\alpha}$(Deg/Sec) |
|---|---|---|---|---|
| (1) | 3.7 | 1g Stall | None | 1.2 |
| (1) | 3.8 | " " | " | 2.4 |
| (1) | 3.9 | " " | " | 5.6 |
| ○ | 3.1 | " " | Aileron Only | 1.2 |
| △ | 3.15 | " " | " " | 1.3 |
| □ | 3.16 | " " | " " | 1.3 |
| ◇ | 3.3 | " " | Aileron/Rudder | 2.4 |
| (1) | 3.5 | " " | Rudder Only | 2.4 |
| ● | 3.2 | Turn | Aileron Only | 1.2 |
| ▲ | 3.17 | " | " " | 1.2 |
| ■ | 3.18 | " | " " | 1.5 |
| ♦ | 3.4 | " | Aileron/Rudder | 1.2 |
| ▼ | 3.12 | " | " " | 1.3 |
| (1) | 3.6 | " | Rudder Only | 1.2 |

NOTE: (1) No instability has been predicted and no Departure has occurred.

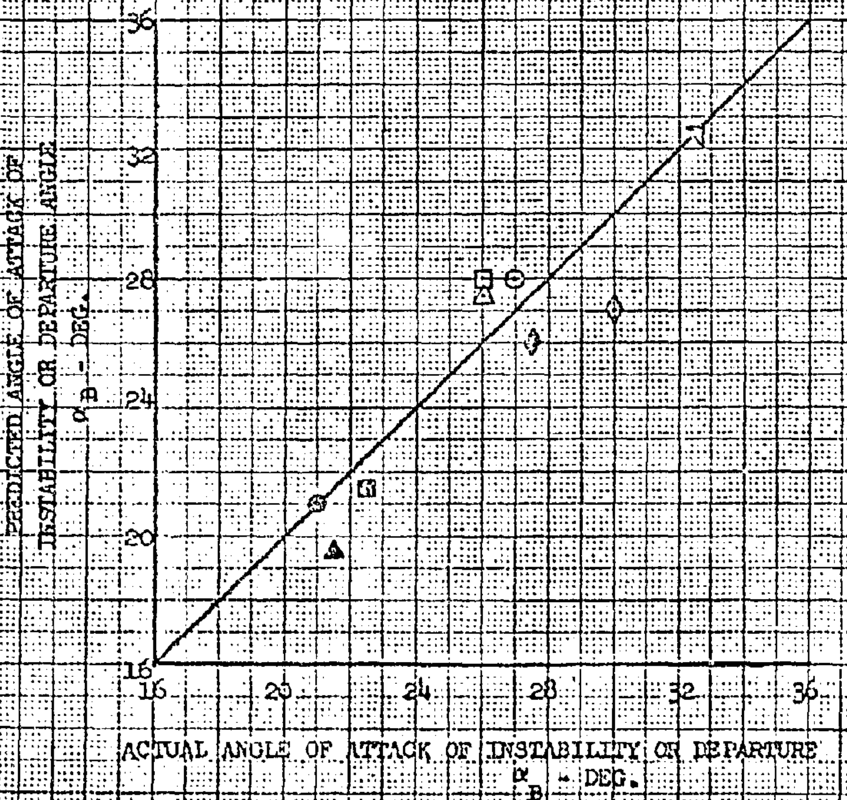

8404-6-051

LITHO IN U.S.A.
INDIANAPOLIS, INDIANA

Figure 5.6

## 6. Conclusions

The following conclusions are presented based on the results of this investigation.

6.1 Stall/Near Stall/Departure - The slatted F-4E shows markedly improved stall characteristics relative to the basic F-4E. The angle of attack at departure is higher in all cases than the basic F-4E and the roll and yaw accelerations at departures are much less than with the basic F-4E. The departure characteristics of the basic F-4E usually starts with an abrupt divergence in yaw coupled with a high roll rate. The slatted F-4E usually departs in roll, with little yaw divergence. The above analytically determined characteristics agree with the results obtained during flight test of the two configurations.

Application of full aircraft nose down stabilator on the slatted F-4E departure results in a faster airplane response in reducing angle of attack. The basic F-4E has a rapid increase in angle of attack just after departure resulting in a longer time to reduce the angle of attack.

Departures for the same entry rate ($\dot{\alpha}$) in the constant bank angle turn occur at a lower angle of attack than the 1g stall. The higher Mach number constant bank angle turn causes higher roll and yaw acceleration for both the basic and slatted F-4E.

Increasing the entry rate ($\dot{\alpha}$) on both the basic and the slatted F-4E results in an increase in the angle of attack at departure. The amplitude of lateral-directional oscillations increases with increasing entry rates and roll and yaw accelerations are higher. However, above moderately high entry rates ($\dot{\alpha} = 5$ to 10 deg/sec) the amplitude of lateral-directional oscillations and the roll and yaw accelerations do not increase.

In summary the slatted F-4E departures will occur at greater angles of attack than the basic F-4E with the rudder or rudder with restricted aileron controls and can be recovered by using full foward longitudinal control. It is also shown that with this type of aileron/rudder control inputs and slow entry rates that departures may not occur with the slatted F-4E airplane.

6.2 Spin Characteristics - The spin mode characteristics of the basic F-4E and the slatted F-4E are in general the same. When using pro-spin controls both aircraft obtained a flat spin ($\alpha_B = 74^\circ$-$84^\circ$) mode regardless of the c.g. or mass configuration. The slatted F-4E has a slightly higher rate of rotation and angle of attack in the flat spin. Recovery from the flat spin mode could not be made with either the basic or slatted F-4E airplane.

The differences in spin entry characteristics of the basic and slatted F-4E are small when pro-spin controls are used to enter the spin. However, in a normal spin resulting from constant bank angle turn, the basic F-4E is far more prone to enter a spin than the slatted F-4E.

6.3 Divergence Criteria - The departure criterion "$C_{n_\beta}$ dynamic" predicts the angle of attack for departure reasonably well. This parameter should only be used when the aileron and rudder are fixed. The lateral control divergence parameters are unsatisfactory in predicting departure angles of attack. The $\beta$ plus $\delta$ axis stability indicator shows good agreement with the computer time history departures for both lateral-directional controls fixed and free.

## 7. Recommendations

(1) The Out-of-Control departure recovery method of applying aircraft-nose-down stabilator, ailerons and rudder neutral as recommended in the flight manual, is the best technique to use to recover from a departure with the slatted F-4E airplane.

(2) Recovery from a fully developed spin was studied using the computer results. Since the aerodynamic characteristics of the basic F-4E and the slatted F-4E are about the same in the spin regions ($\alpha_B = 50^\circ$ to $90^\circ$), the basic F-4E recommended spin recovery technique should be retained. This recovery method is full aircraft-nose-down stabilator, ailerons full with the spin, and rudder neutralized. For a flat spin with either the basic or the slatted F-4E, recovery with the normal aircraft control surfaces is not possible.

(3) Only rudder control should be used in the high angle of attack region to prevent departures. However, rudder control in combination with restricted aileron can be used with almost the same results as the rudder alone.

(4) The analytical studies of a fully developed spin for the basic F-4E and slatted F-4E indicate little difference in the spin characteristics. The stall/near stall studies for the two aircraft indicate the slatted F-4E airplane departs at higher angles of attack and is more responsive to pitch and lateral-directional control motions than the basic F-4E airplane. Therefore, with improved high angle of attack characteristics for the slatted F-4E airplanes, it is recommended that a stall/spin flight test program not be conducted on the slatted F-4E aircraft.

## 8.0 REFERENCES

1. MCAIR Report MDC A0005, "Model F-4 Spin Evaluation Program," Volume I, C.C. Brady, W.A. Moran. 15 August 1969
2. MCAIR Report MDC A0005, "Model F-4 Spin Evaluation Program," Volume II, C.C. Brady, W.A. Moran. 15 August 1969
3. NASA TM SX-2337, "Free - Flight Investigation of Effects of Slats on Lateral-Directional Stability of A 0.13-Scale Model of the F-4E Airplane," William A. Newsom, Jr., Sue B. Grafton. July 1971
4. T.O. 1F-4C-1 "Flight Manual", USAF Series F-4C, F-4D and F-4E Aircraft. 15 August 1971
5. NASA RM L58E16, "Dynamic Lateral Behavior of High Performance Aircraft,: Martin T. Moul, John W. Paulson August 5, 1958
6. MCAIR Report EN844, "Lateral and Directional Static Stability At High Angles of Attack," J. Hodgkinson. 15 October 1971
7. AFFTC Report FTC-SD-70-20, "Stall/Near Stall Investigation of the F-4E Aircraft," C.G. McElroy, First Lieutenant USAF, G.R. Gentry, Major USAF. October 1970
8. MCAIR Report MDC A1571, "Aerodynamic Stability And Control Characteristics Report," W.C. Bottoms, J.G. Carmichael Jr., C.R. Hobbs, R.J. Pelikan, J.W. Shepherd. 1 March 1972

# APPENDIX A

## SLATTED F-4E AERODYNAMIC DATA

Inclusive Pages: A.1 thru A.47

## Table Of Contents

| Section | Title | Page |
|---|---|---|
| A | Slatted F-4E Aerodynamic Data | A.3 |
| | A.1 Force and Moment Wind Tunnel Data | A.3 |
| | A.1.1 Adjustments in Static Pitching Moment Coefficient | A.4 |
| | A.1.2 Adjustments in Yawing Moment Asymmetries | A.5 |
| | A.2 Forced Oscillation Wind Tunnel Data | A.5 |
| | A.2.1 Adjustment in Roll Damping Due to Roll Velocity | A.5 |
| | A.3 Rotary Balance Wind Tunnel Data | A.6 |
| | A.3.1 Rotary Balance Data Below 35° Angle of Attack | A.6 |

# APPENDIX A

## A. Slatted F-4E Aerodynamic Data

The data as presented in this appendix were used in the six-degree-of-freedom computer simulation of the slatted F-4E for both the stall/near stall and spin studies. All the data are input independent of Mach number and flexibility effects. The aerodynamic coefficients are presented, in the body axis system, as a function of angle of attack ranging from 0° to 90°. All data is presented at a C.G. of $33\%\bar{c}$.

A.1 Force and Moment Wind Tunnel Data - High angle of attack static force and moment data on the slatted F-4E was obtained from two wind tunnel tests. A 5% scale model force & moment test was conducted at NASA LRC in the 7 x 10 Foot High Speed Wind Tunnel. The force and moment coefficient data were obtained at various sideslip angles from 0° to 40° angle of attack at .23 Mach number and a Reynolds number of $1.5 \times 10^6$ per ft. The 6.67% scale model force and moment test was conducted at NASA ARC in the 12-Foot Pressure Wind Tunnel. These test data were obtained for an angle of attack variation from 20° to 90° at various sideslip angles for .23 Mach number and a Reynolds number of $4.0 \times 10^6$ per ft.. The data from these two tests along with some of the data presented in Appendix B were used in generating the slatted F-4E aerodynamic curves presented in this appendix.

The static longitudinal and lateral-directional parameters $C_z$, $C_x$, $C_m$, $C_l$, and $C_y$ are presented in Figures A.1 through A.5, at zero degrees control surface deflection ($\delta_s$, $\delta_r$, $\delta_a = 0$). The yawing moment coefficient $C_n$, is presented in Figure A.6 as a function of sideslip angle for various stabilator deflections. The yawing moment asymmetries ($\beta = 0$) of the wind tunnel model are presented in Figure A.7.

The static longitudinal and lateral-directional control derivatives $C_{z_{\delta_s}}$, $C_{x_{\delta_s}}$, $C_{m_{\delta_s}}$, $C_{n_{\delta_a}}$, $C_{l_{\delta_a}}$, $C_{n_{\delta_r}}$, $C_{l_{\delta_r}}$, and $C_{y_{\delta_r}}$ are presented in Figure A.8 through A.15. The sign convention used is that a positive force or moment is generated by a negative value for control deflection. The control derivatives $C_{l_{\delta_a}}$ and $C_{n_{\delta_a}}$ contain both the aileron and spoiler contribution referenced to the aileron deflection.

A.1.1 Adjustments in Static Pitching Moment Coefficient - Above 50° angle of attack the wind tunnel pitching moment coefficient curve is adjusted in the same manner as was done in Reference 1. That is, for a steady spin at a given angle of attack the following equation was used:

$$C_m = \frac{\Omega_V^2 \left[\sin\alpha\cos\alpha\,(I_Z - I_X) + I_{xz}\,(1 - 2\cos^2\alpha)\right] - (I\Omega_e)\ \Omega_V \sin\alpha}{-q_o S\bar{c}} \qquad \text{Equation A.1}$$

where the rate or rotation, angle of attack, and inertia characteristics were obtained from Reference 7. This basic pitching moment coefficient is then adjusted for c.g., pitching moment coefficient due to rotation, and stabilator deflection. The results ($C_{m_{33}}$ @ $\delta_s = 0$) are presented in Figure A.16. It is assumed that these pitching moment coefficient values obtained from the basic F-4E flight test in the spin regions would be applicable to the slatted F-4E, since there is little difference found in the wind tunnel pitching moment curves between the basic and slatted F-4E.

The pitching moment coefficients below 26° angle of attack are obtained by taking slatted F-4E flight test stabilator required to trim versus angle of attack data (Reference 8) and applying these results to wind tunnel stabilator power ($C_{m_{\delta_s}}$) to generate a pitching moment coefficient versus angle of attack. These results along with the final pitching moment curve used in the study is presented in Figure A.16.

A.1.2 Adjustments in Yawing Moment Asymmetries - Since the adjustment of yawing moment asymmetries was done in the same manner for both the slatted and the basic F-4E, the modifications are described in Appendix B.

A.2 Forced Oscillation Wind Tunnel Data - Forced oscillation testing was conducted in the NASA-LRC Full Scale Tunnel on a 13% scale Model F-4E with leading edge slats. Three axis lateral-directional data were obtained from 0° to 40° angle of attack in 5° increments at a dynamic pressure of 5.00 psf and a Reynolds number of $0.505 \times 10^6$ per ft.. The frequency was 1.0 cps and the amplitude was ±5° ($\phi,\psi$). These data along with the curves presented in Appendix B for the basic F-4E were used to generate the forced oscillation dynamic derivatives for the slatted F-4E. The dynamic forced oscillation derivatives $C_{l_p}$, $C_{l_r}$, $C_{n_p}$, $C_{y_p}$, and $C_{y_r}$ are presented in Figures A.17 through A.22. The longitudinal damping derivative $C_{m_q}$ is the same as the basic F-4E and is presented in Appendix B.

A.2.1 Adjustment in Roll Damping Due to Roll Velocity - A comparison of flight test slatted F-4E (A/C 284 slatted prototype) data with SDF computer time history results shows a much higher level of roll-yaw damping in the 20° to 40° angle region from the computer results. Therefore, a parametric study was made using a linear lateral-directional dynamic stability program in the 20° to 40° angle of attack region to determine the most critical factor involved and the amount of change needed to match flight test results. As expected, $C_{l_p}$ is the most senitive parameter in determining the roll-yaw damping characteristics. The magnitude of $C_{l_p}$ was reduced in the 20° to 40° angle of attack region to obtain more neutral to unstable damping level. The original and revised curves of roll damping are presented in Figure A.23.

A.3 Rotary Balance Wind Tunnel Data - The rotary balance testing was conducted at the NASA-LRC Vertical Spin Tunnel with a 9.1% scale Model F-4B with leading edge slats. Three axis components lateral-directional data were obtained from 35° to 90° angle of attack in 5° increments at a dynamic pressure of 1.295 psf and a Reynolds number of 0.3097 x $10^6$ per ft.. The axis of rotation was parallel to the velocity vector therefore $\Omega = \Omega_v$. Data were obtained at spin rate coefficients ($\Omega_v b/2V$) of 0.0, 0.075, 0.10, 0.15, 0.2, 0.25, and 0.30. The dynamic rotary balance coefficients $\Delta C_n$, $\Delta C_l$, and $\Delta C_y$ are presented as a function of $\Omega_v b/2V$ at various angles of attack in Figures A.24 through A.26. The longitudinal parameters $\Delta C_m$, $\Delta C_z$, and $\Delta C_x$, are the same as the basic F-4E and are presented in Appendix B.

A.3.1 Rotary Balance Data Below 35° Angle of Attack - A detail discussion of the method used in generating rotary balance data and adjustments made to the rotary balance wind tunnel data are presented in Appendix D.

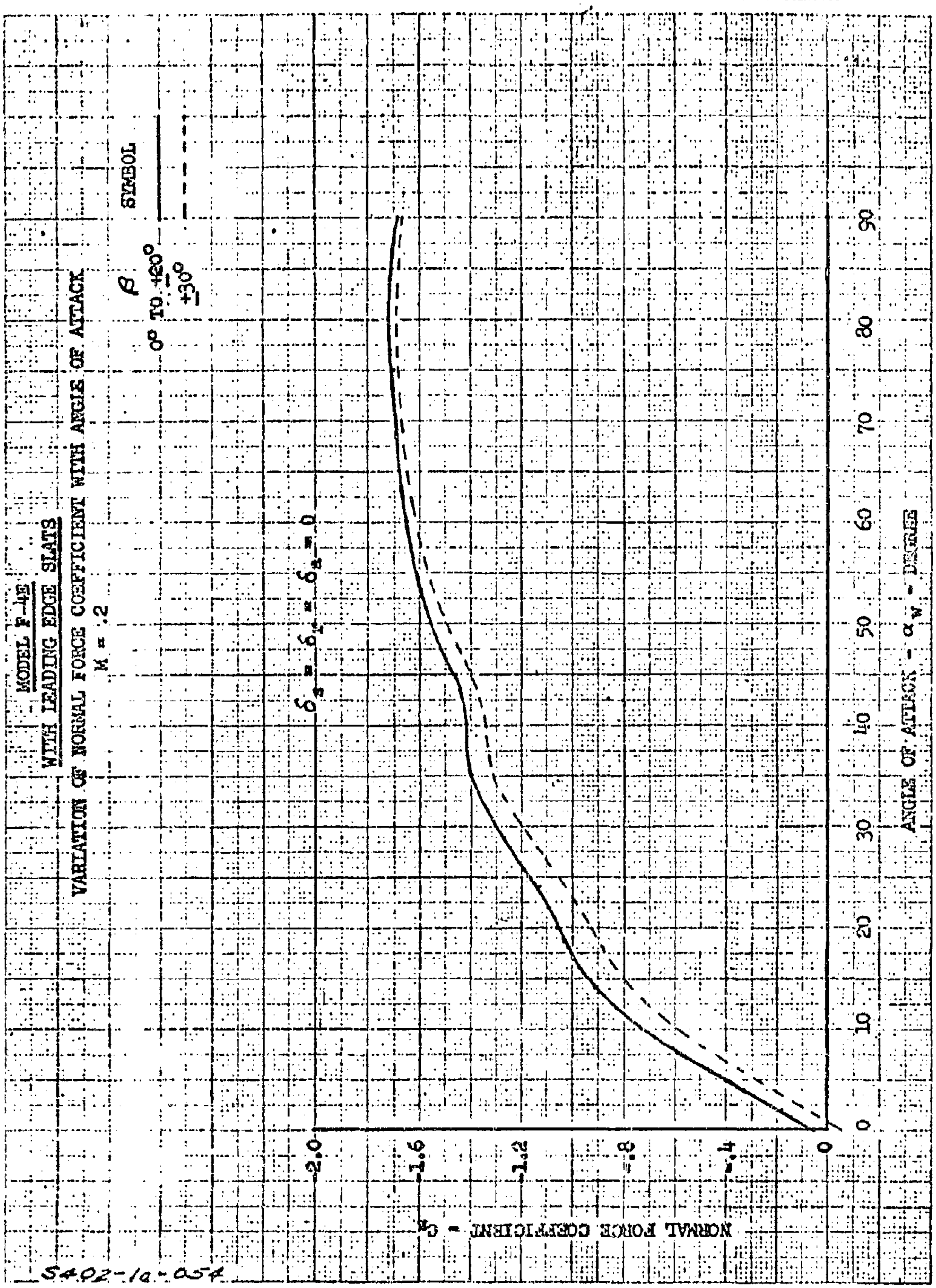

5402-1a-054

Figure A.1

MODEL F-4E
WITH LEADING EDGE SLATS
VARIATION OF AXIAL FORCE COEFFICIENT WITH ANGLE OF ATTACK

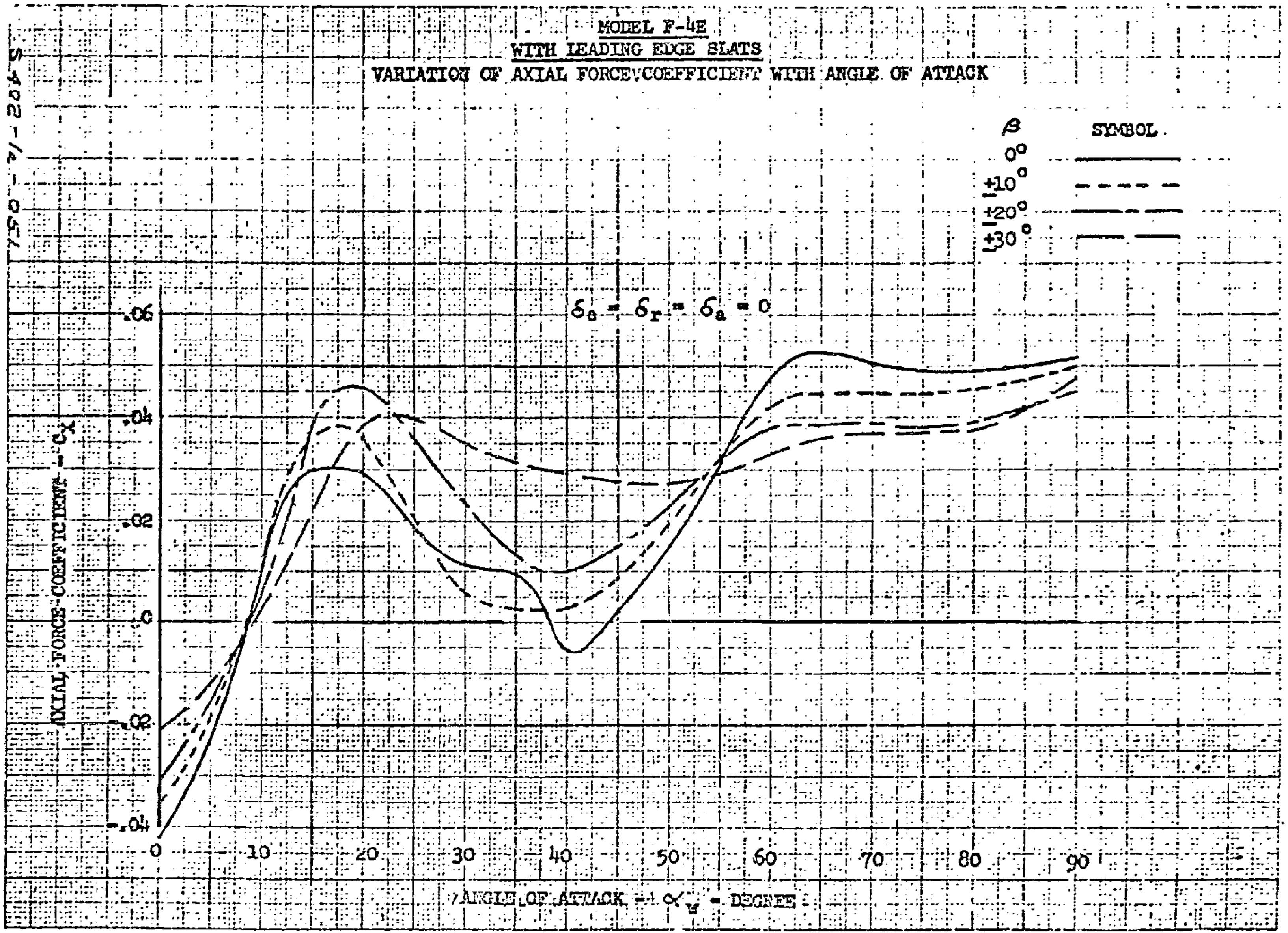

S 402-1/2-051

NATIONAL TRACING PAPER
INDIANAPOLIS, INDIANA

UN 330135M 10X10 TO CM
LITHO IN U.S.A.

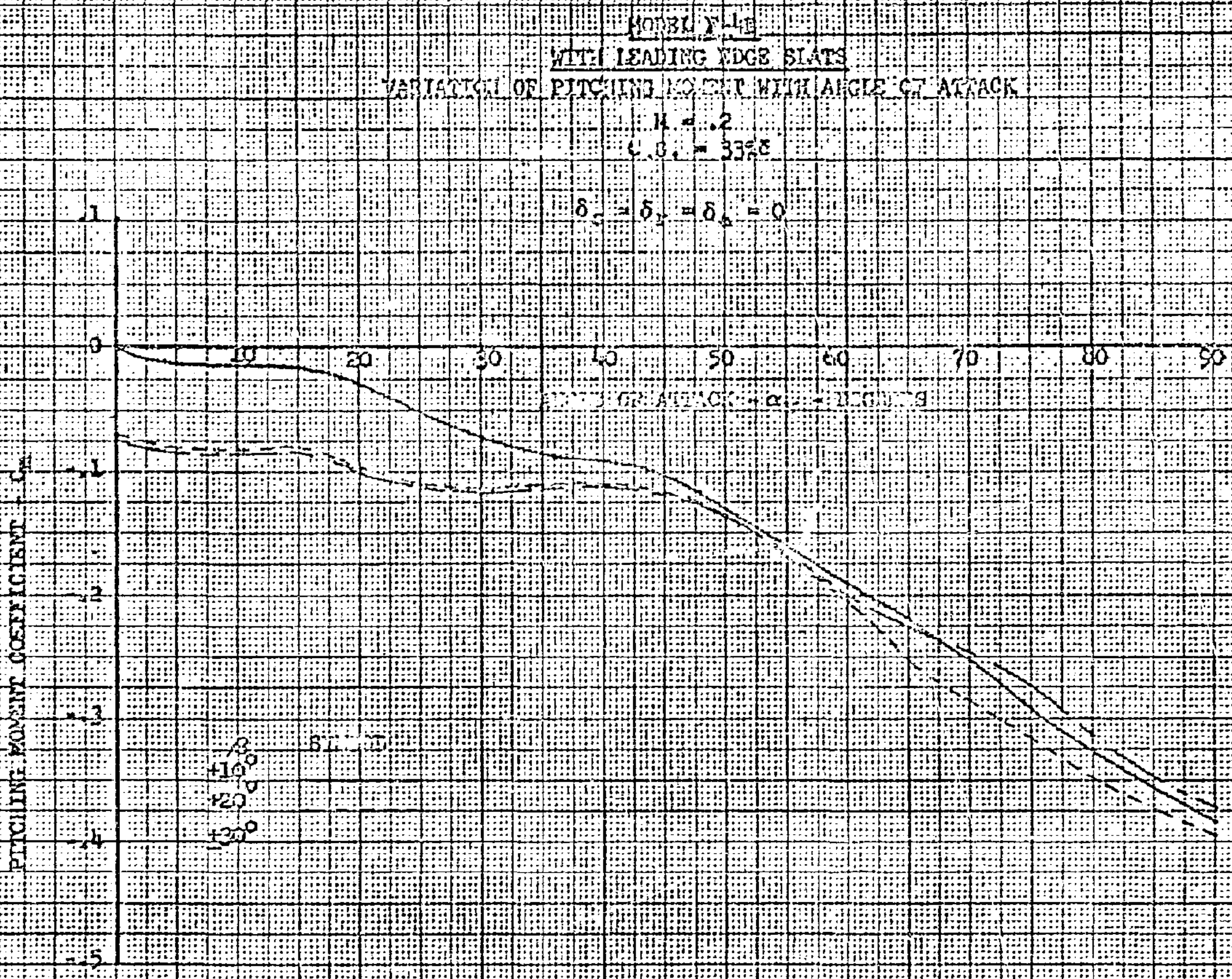

Figure A.3

[illegible]

VARIATION OF ROLLING MOMENT COEFFICIENT WITH SIDESLIP ANGLE

M = .2

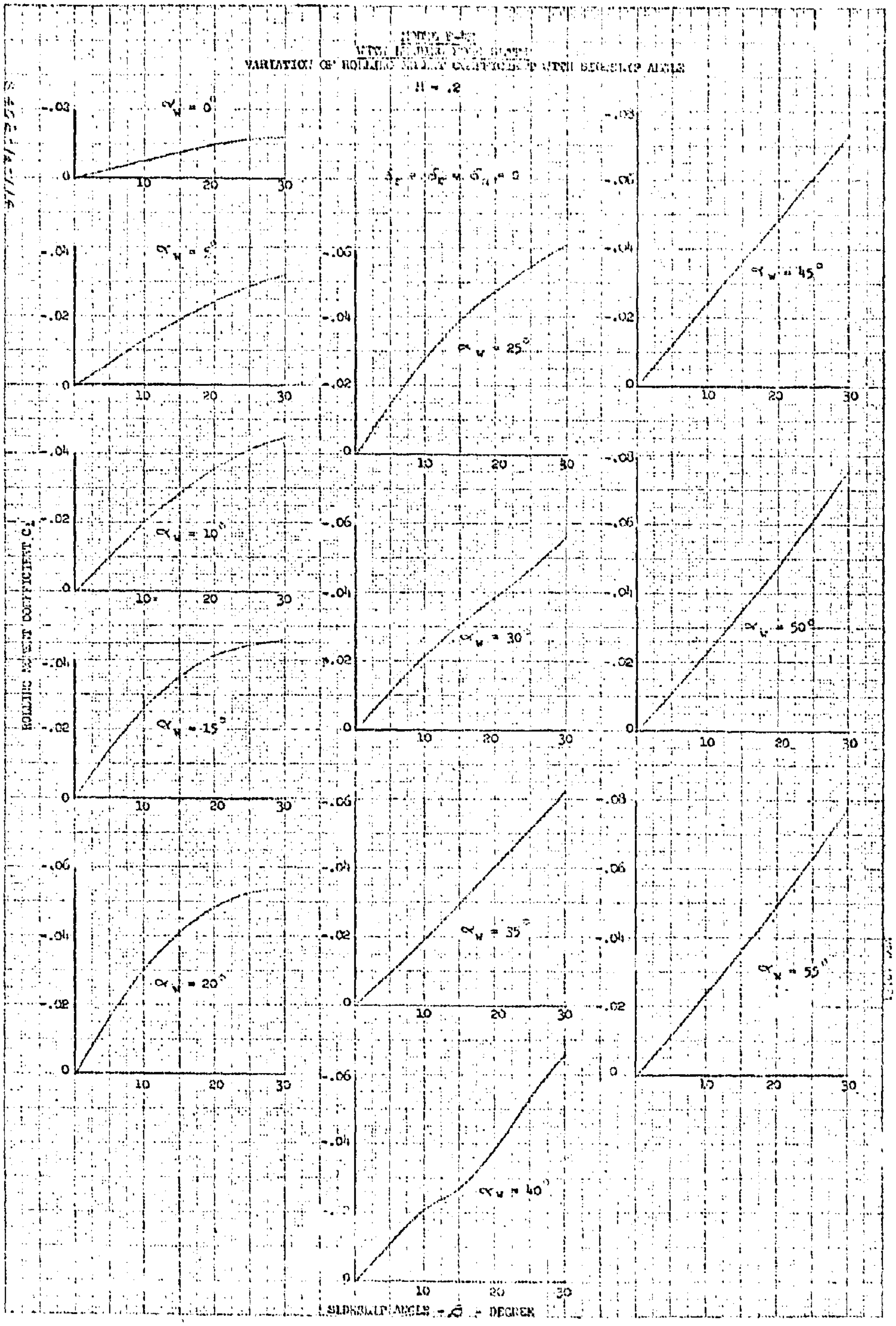

FIGURE 5-[illegible]

[illegible]

VARIATION OF ROLLING MOMENT COEFFICIENT WITH SIDESLIP ANGLE

M = .2

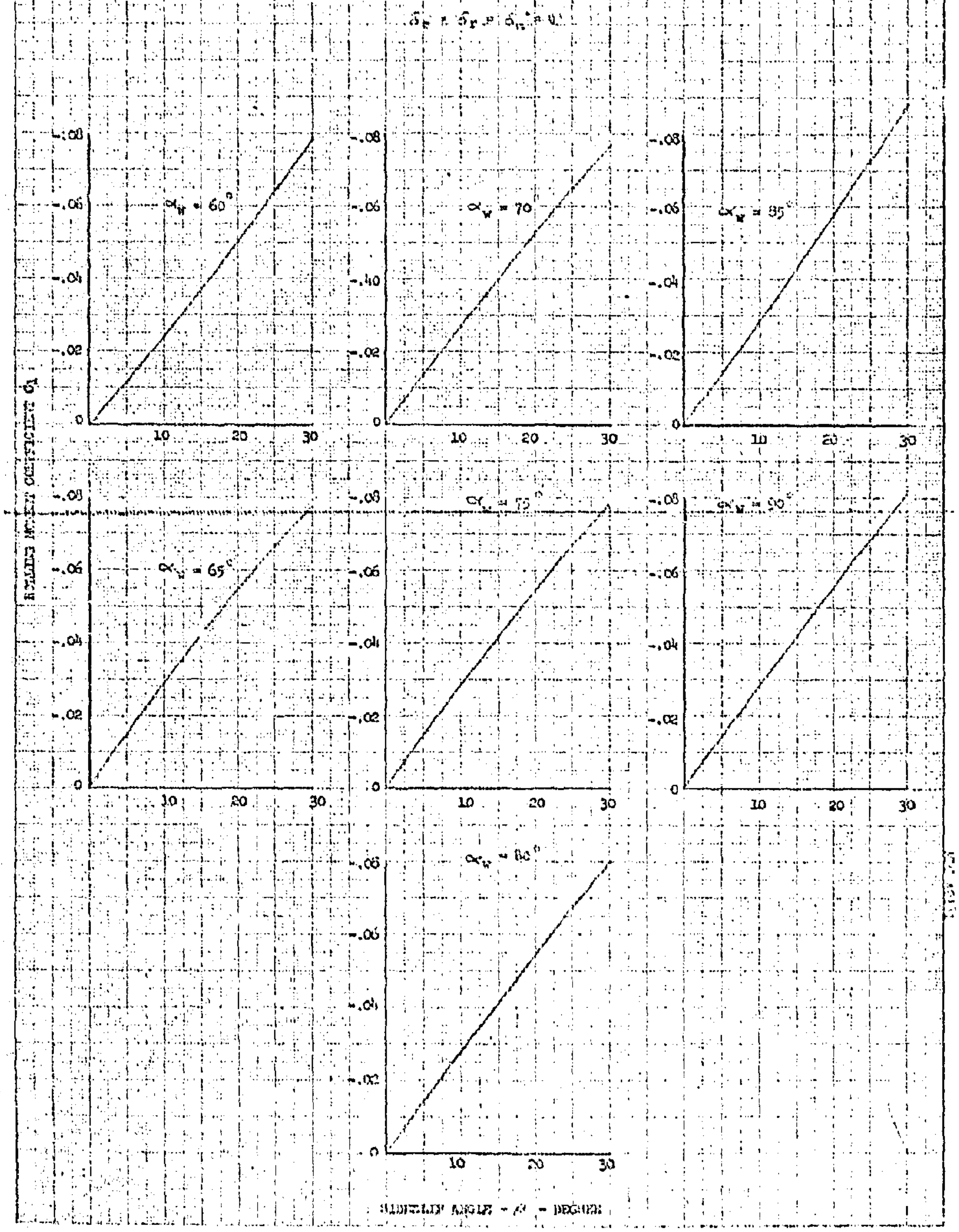

VARIATION OF SIDE FORCE COEFFICIENT WITH SIDESLIP ANGLE

M = .8

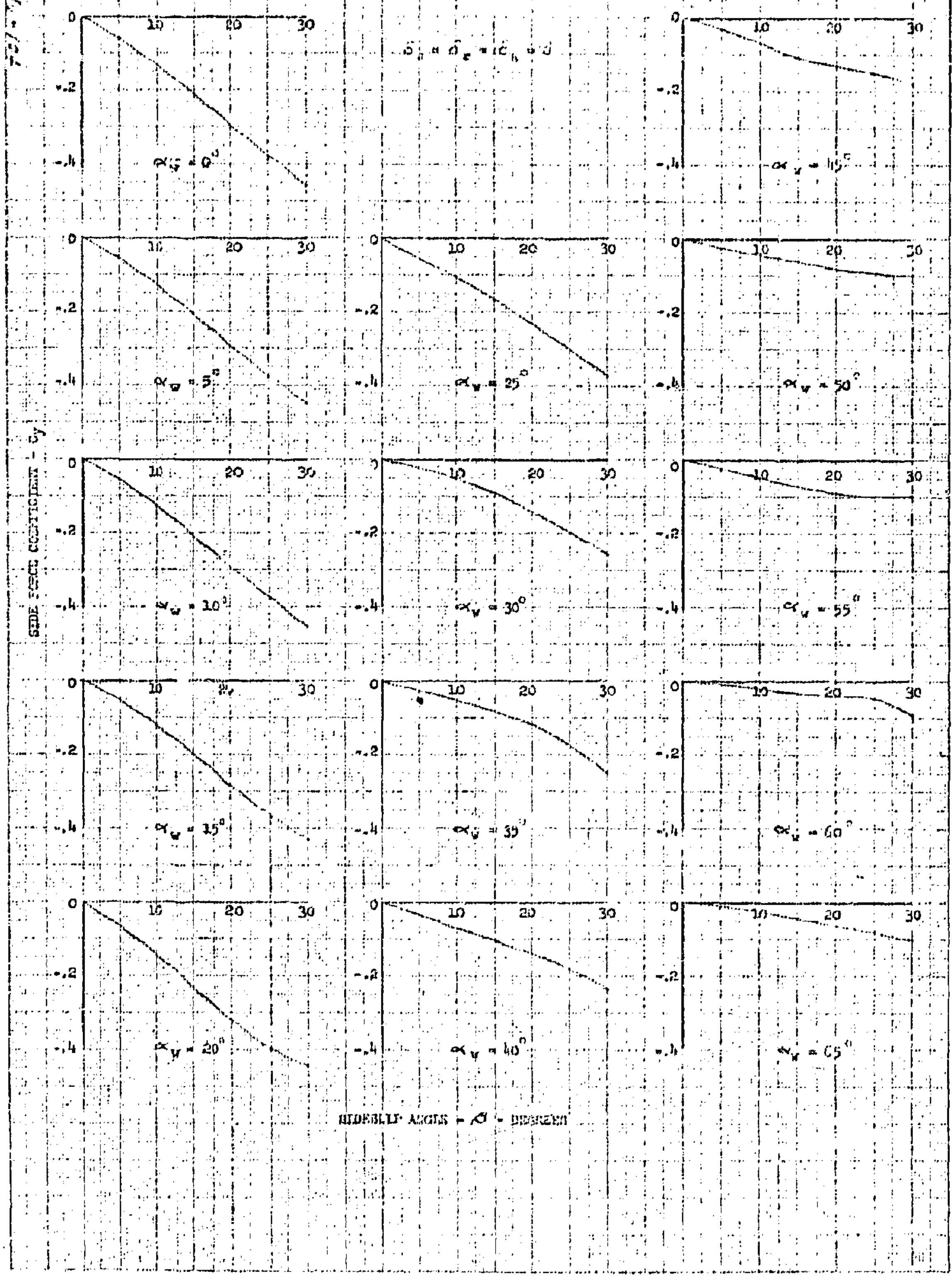

## MODEL F-4E
## WITH LEADING EDGE SLATS
## VARIATION OF SIDE FORCE COEFFICIENT WITH SIDESLIP ANGLE

$M = .2$

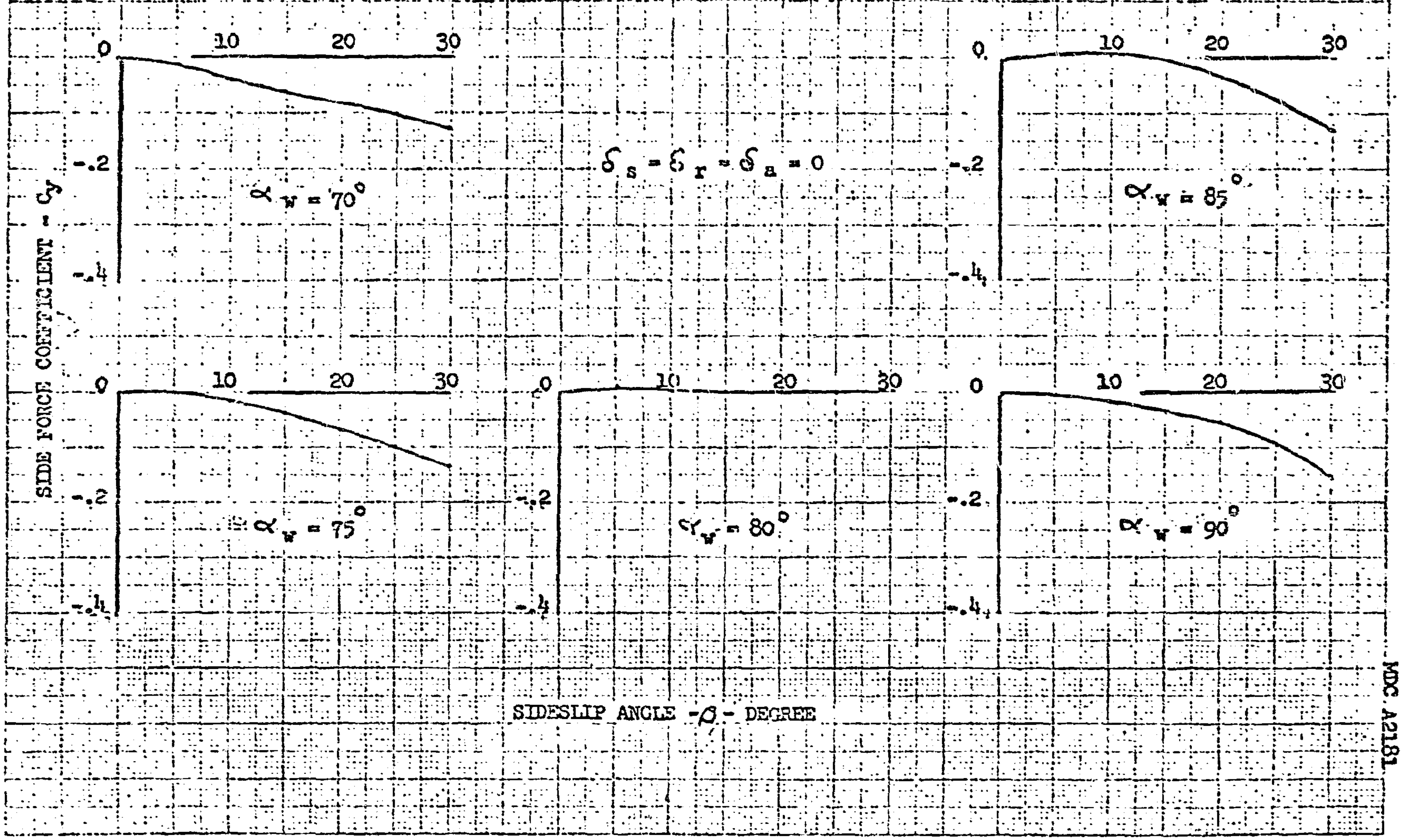

Figure A.5 Con

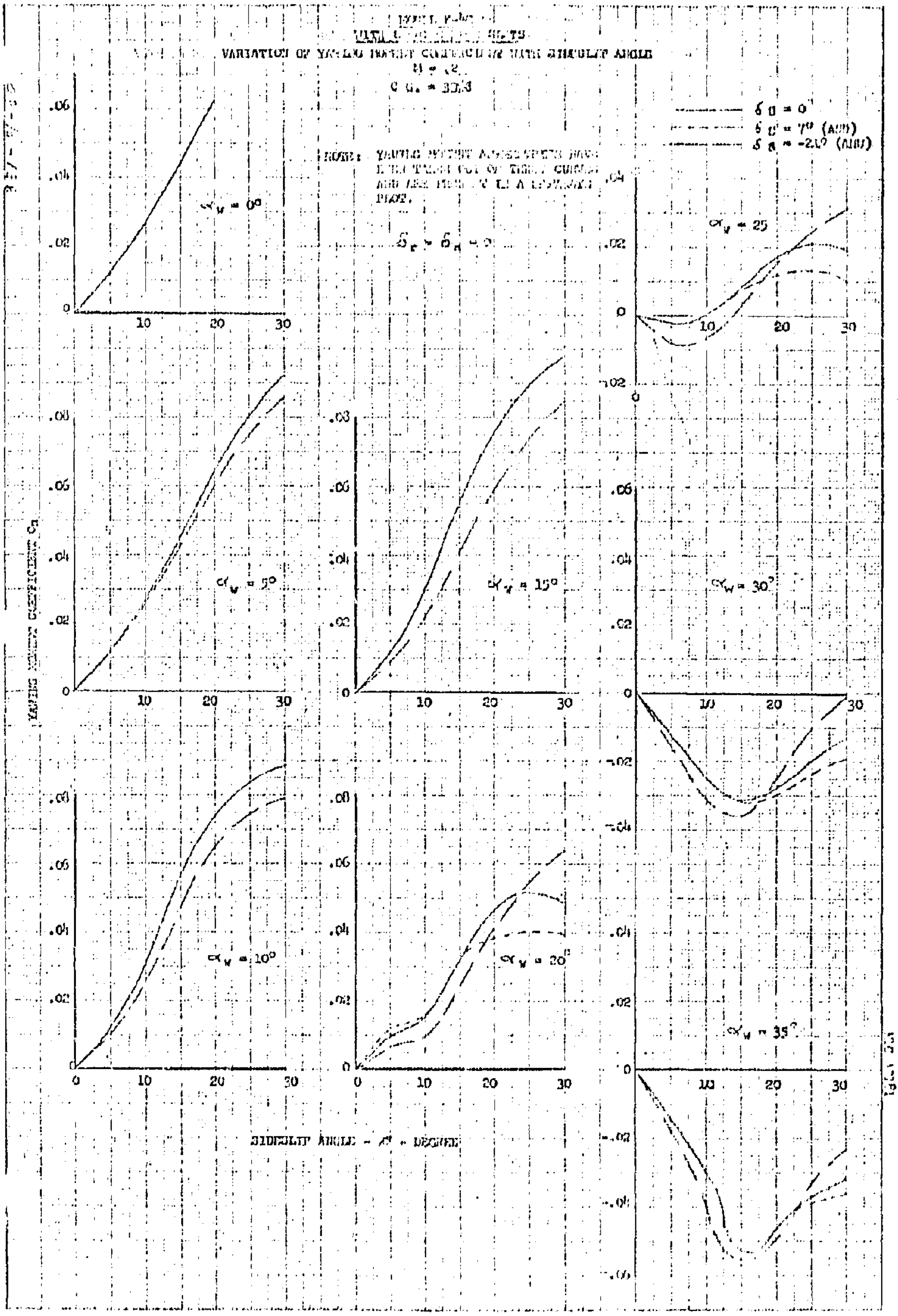
VARIATION OF YAWING MOMENT COEFFICIENT WITH SIDESLIP ANGLE
M = .2
C.G. = 33.3
δ R = 0°
δ R = 7° (AUD)
δ R = -21° (AUD)
NOTE: YAWING MOMENT ... HAVE BEEN TAKEN OUT OF THESE CURVES AND ARE PLOTTED ON A SEPARATE PLOT.
δ e = δ a = 0
αW = 0°
αW = 5°
αW = 10°
αW = 15°
αW = 20°
αW = 25
αW = 30°
αW = 35°
YAWING MOMENT COEFFICIENT Cn
SIDESLIP ANGLE - β - DEGREE
0
.02
.04
.06
.08
-.02
-.04
-.06
10
20
30

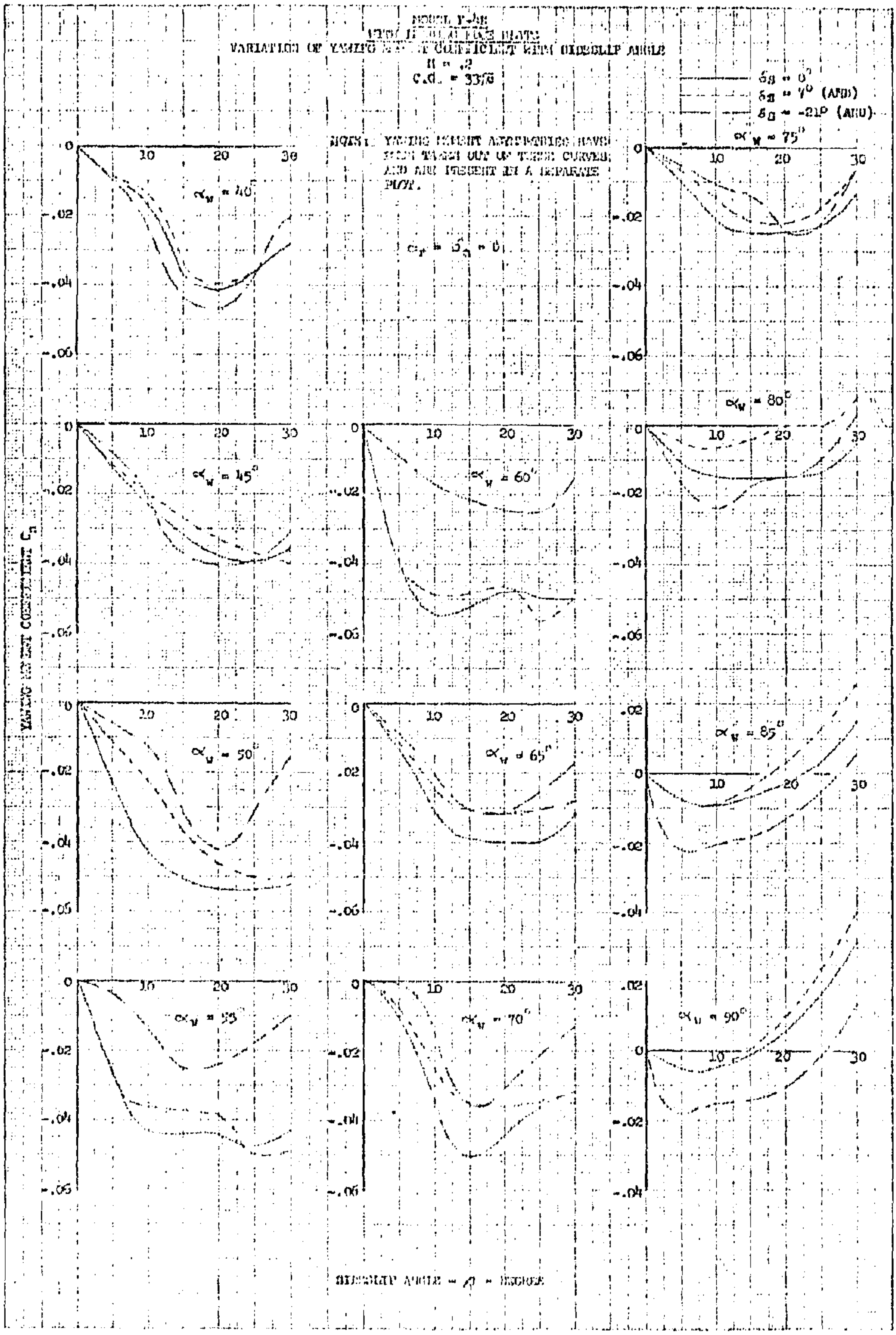

Figure 4.6 Con't

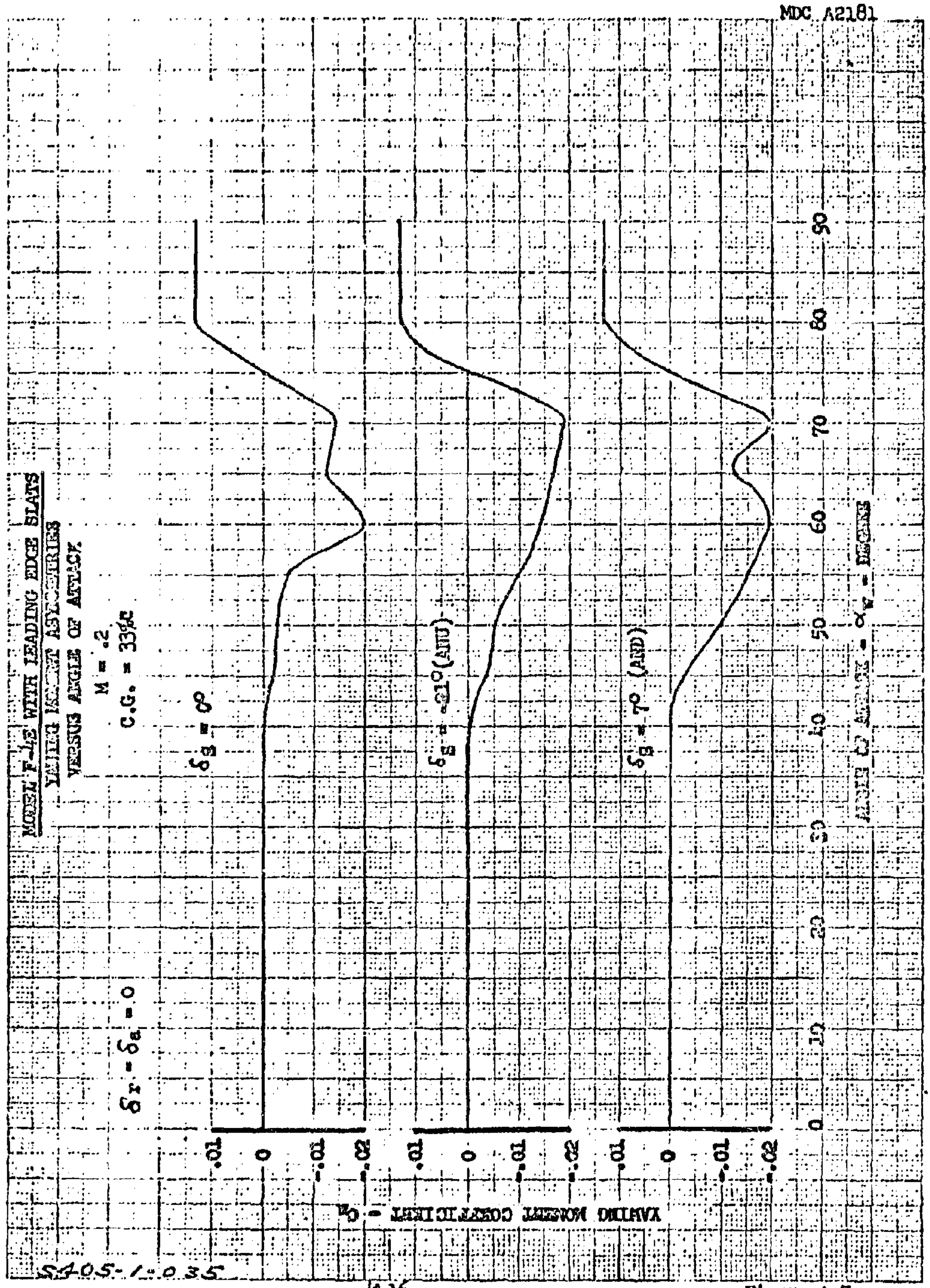

S405-1-035

Figure A.7

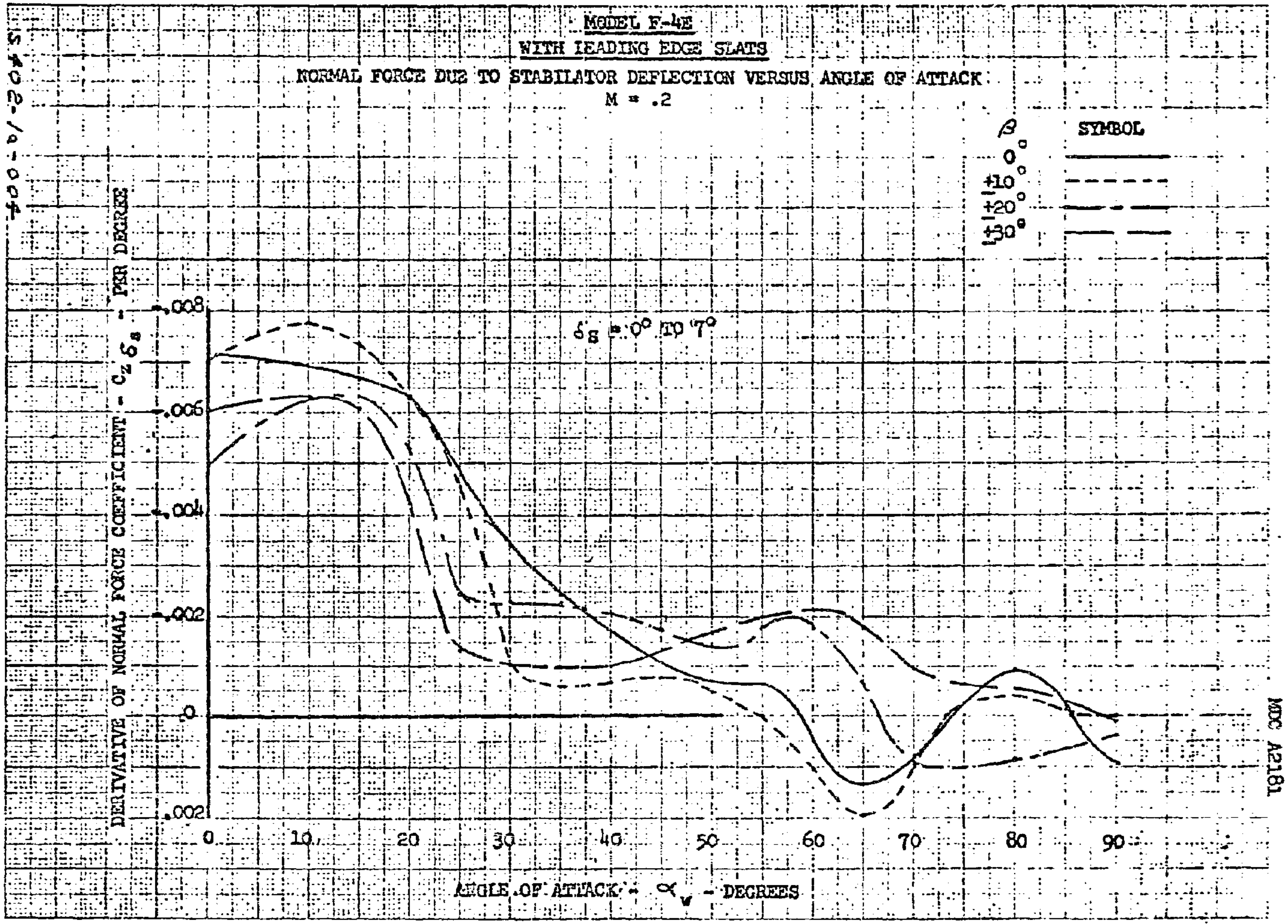

MODEL F-4E

WITH LEADING EDGE SLATS

NORMAL FORCE DUE TO STABILATOR DEFLECTION VERSUS ANGLE OF ATTACK

M = .2

S402-/a-004

Figure A.8

MODEL F-4E

WITH LEADING EDGE SLATS

NORMAL FORCE DUE TO STABILATOR DEFLECTION VERSUS ANGLE OF ATTACK

M = .2

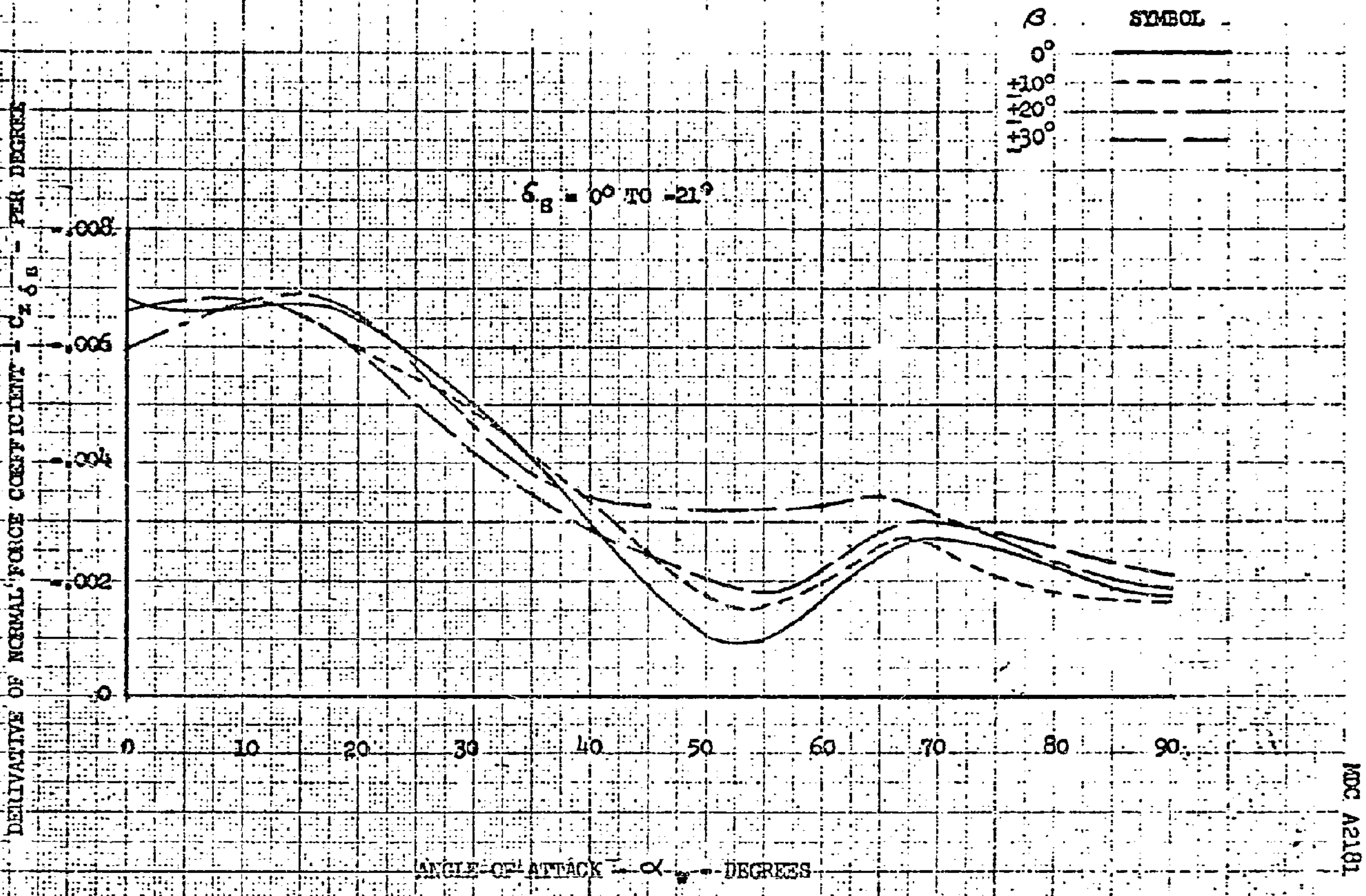

5402-6-004

Figure A.8 Con't

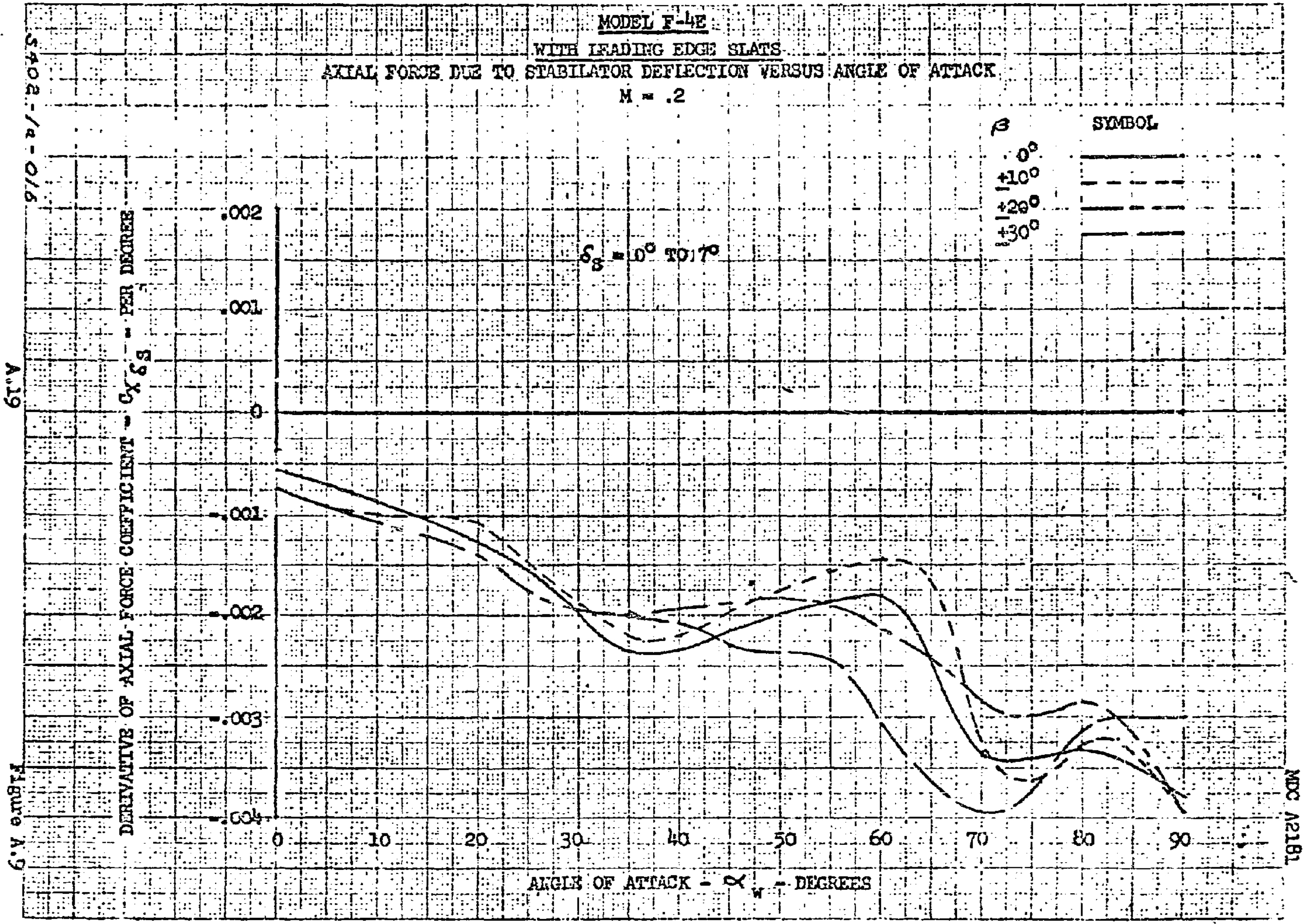

MODEL F-4E
WITH LEADING EDGE SLATS
AXIAL FORCE DUE TO STABILATOR DEFLECTION VERSUS ANGLE OF ATTACK
M = .2

5402-1a-016

Figure A.9

MODEL F-4E

WITH LEADING EDGE SLATS

AXIAL FORCE DUE TO STABILATOR DEFLECTION VERSUS ANGLE OF ATTACK

M = .2

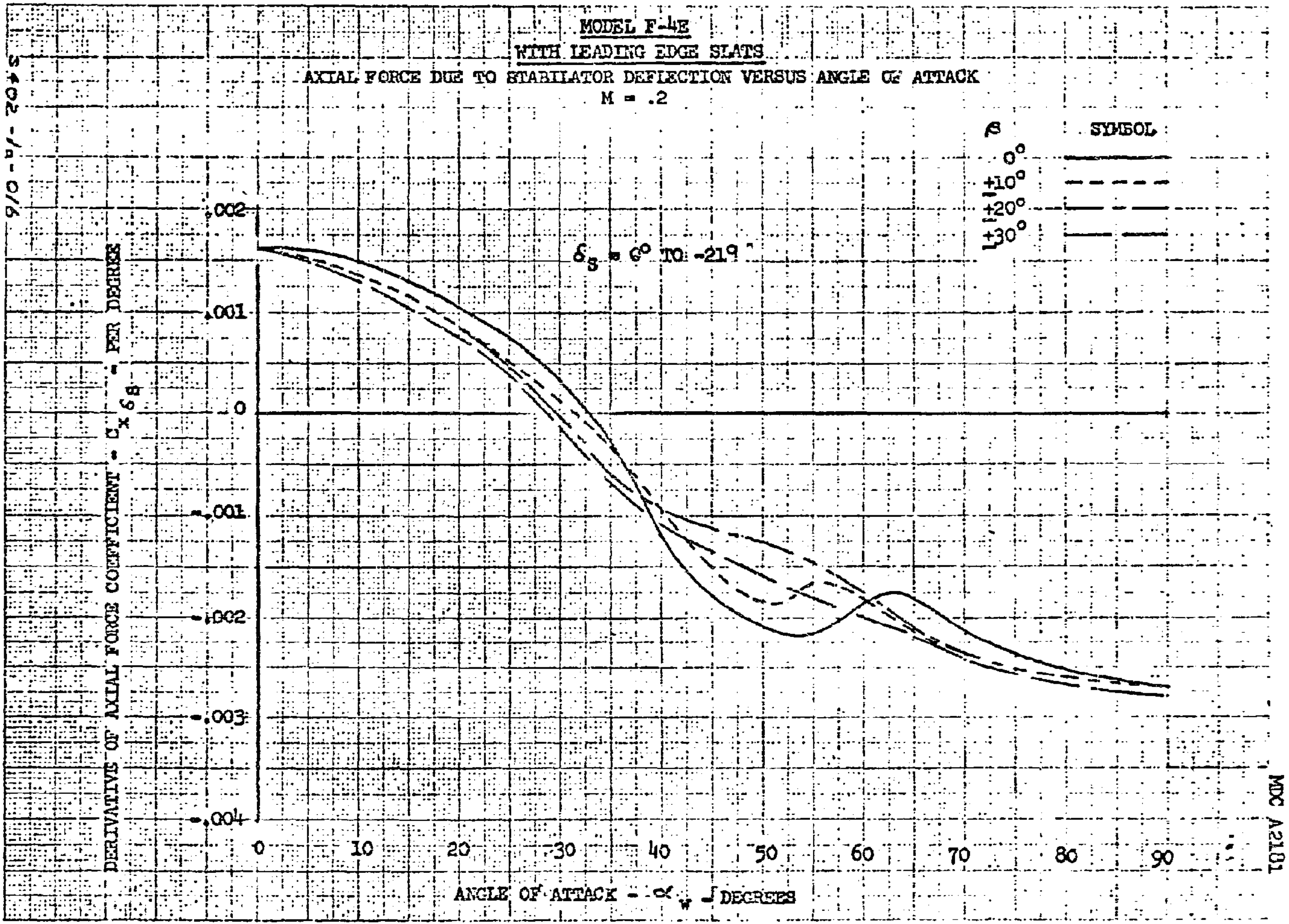

3402-1a-016

Figure A.9 Con't

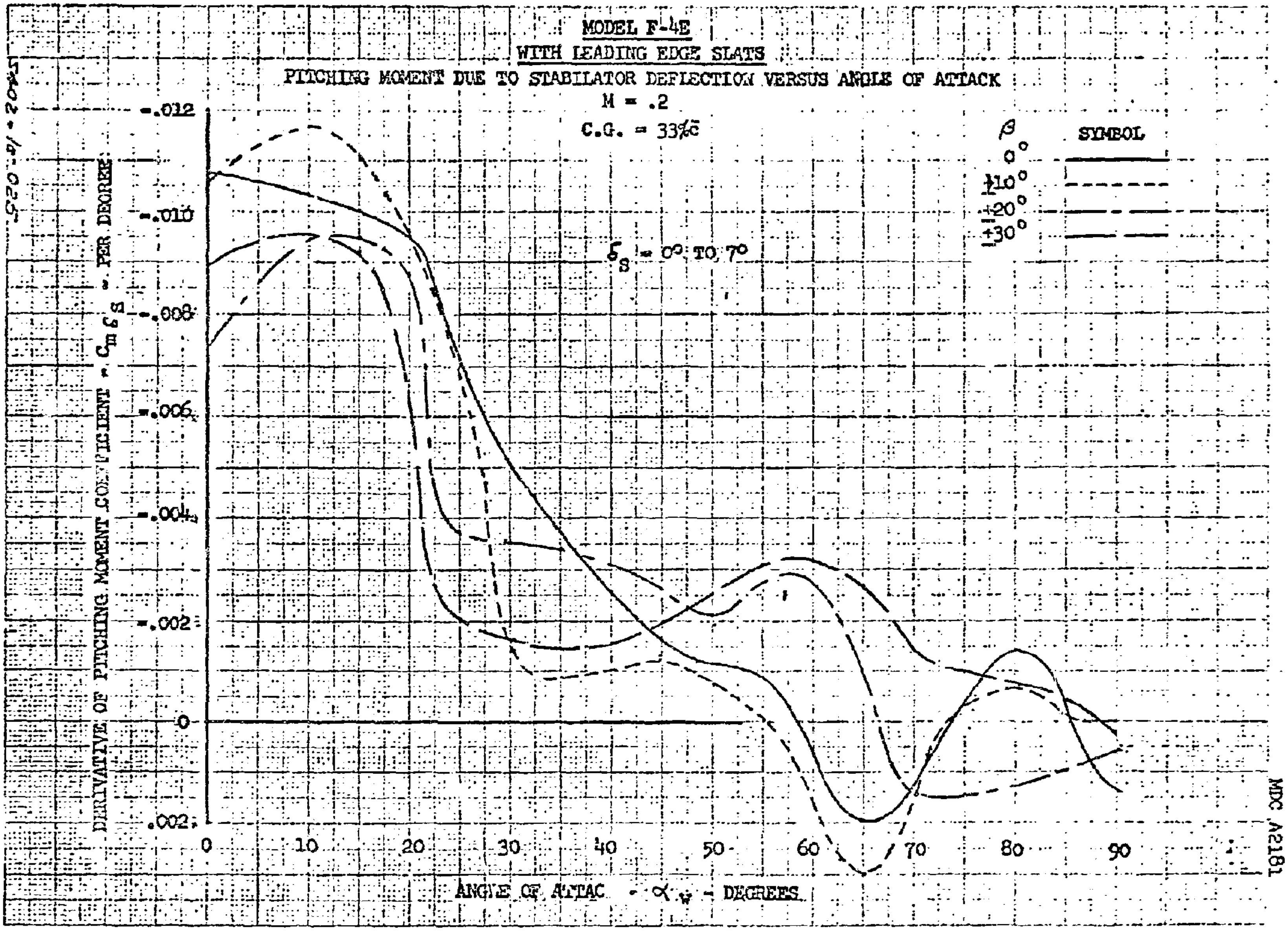

MODEL F-4E
WITH LEADING EDGE SLATS
PITCHING MOMENT DUE TO STABILATOR DEFLECTION VERSUS ANGLE OF ATTACK
M = .2
C.G. = 33%c̄

5402 • 16 • 025

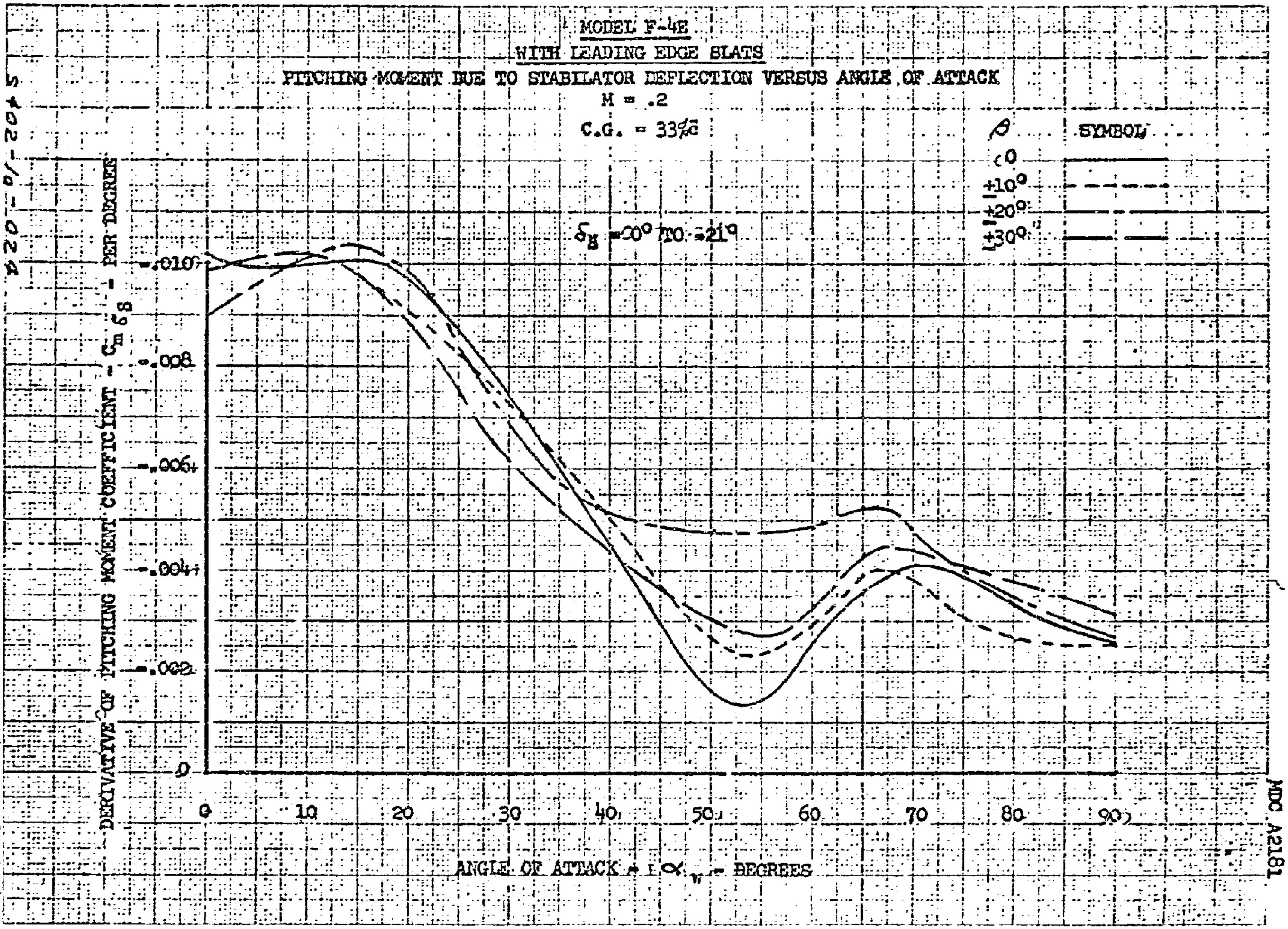

S 402-10-024

Figure A.10 Cont

YAWING MOMENT DUE TO AILERON DEFLECTION VERSUS ANGLE OF ATTACK

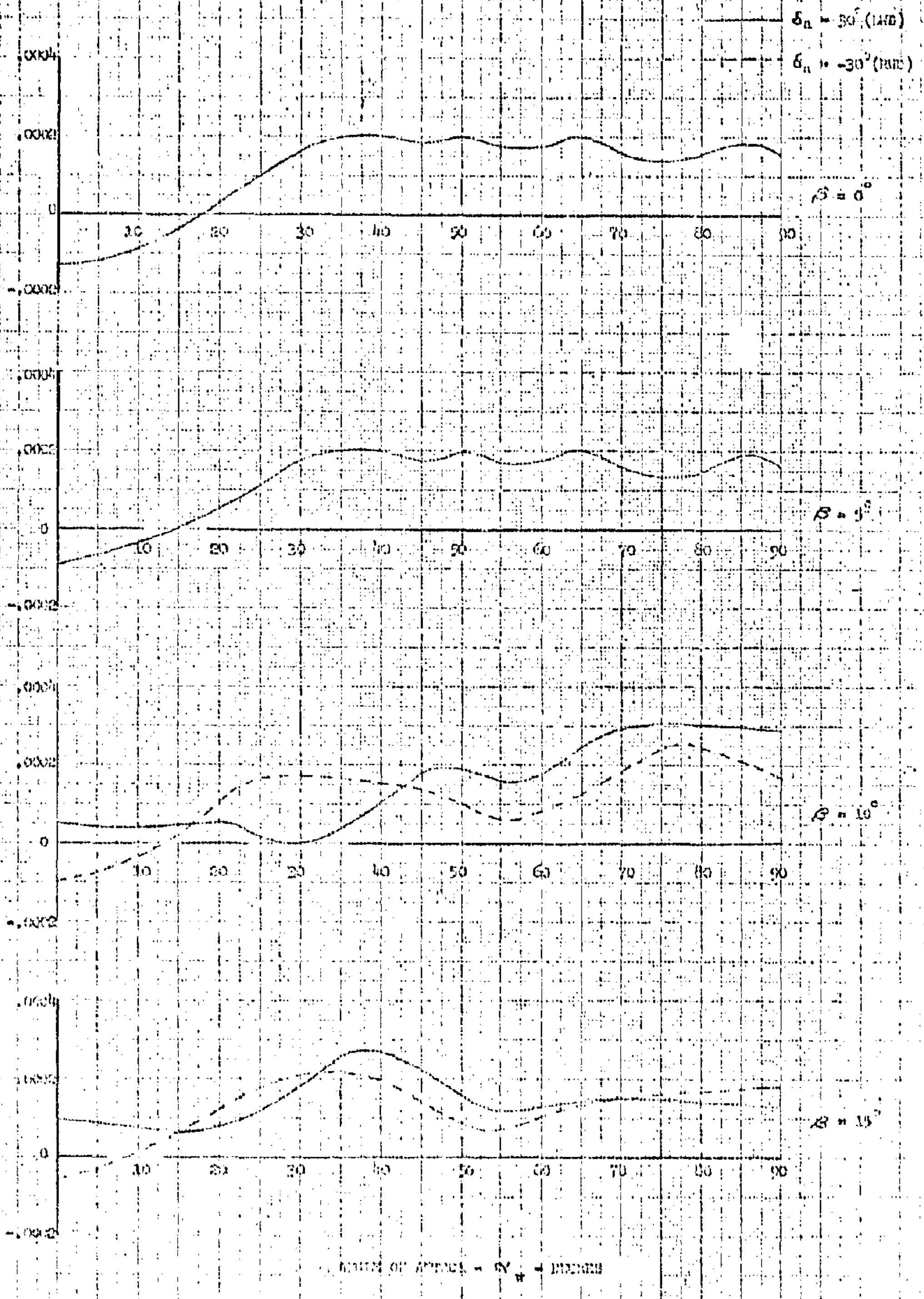

A-25

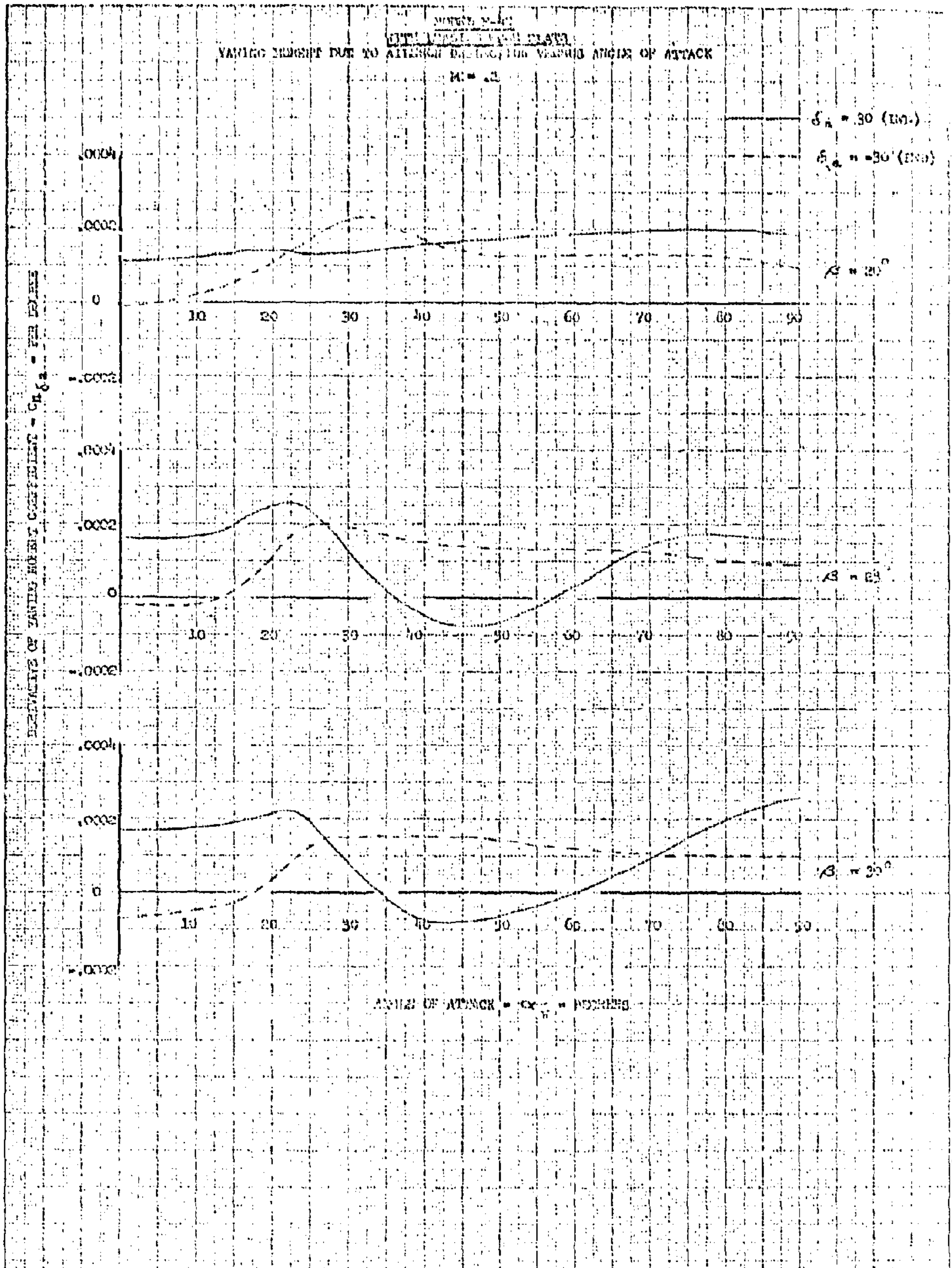

Figure 4.11 Cont'd

5402-16-096

MODEL P-47

WITH [illegible] SLATS

ROLLING MOMENT DUE TO AILERON DEFLECTION VERSUS ANGLE OF ATTACK

M = .2

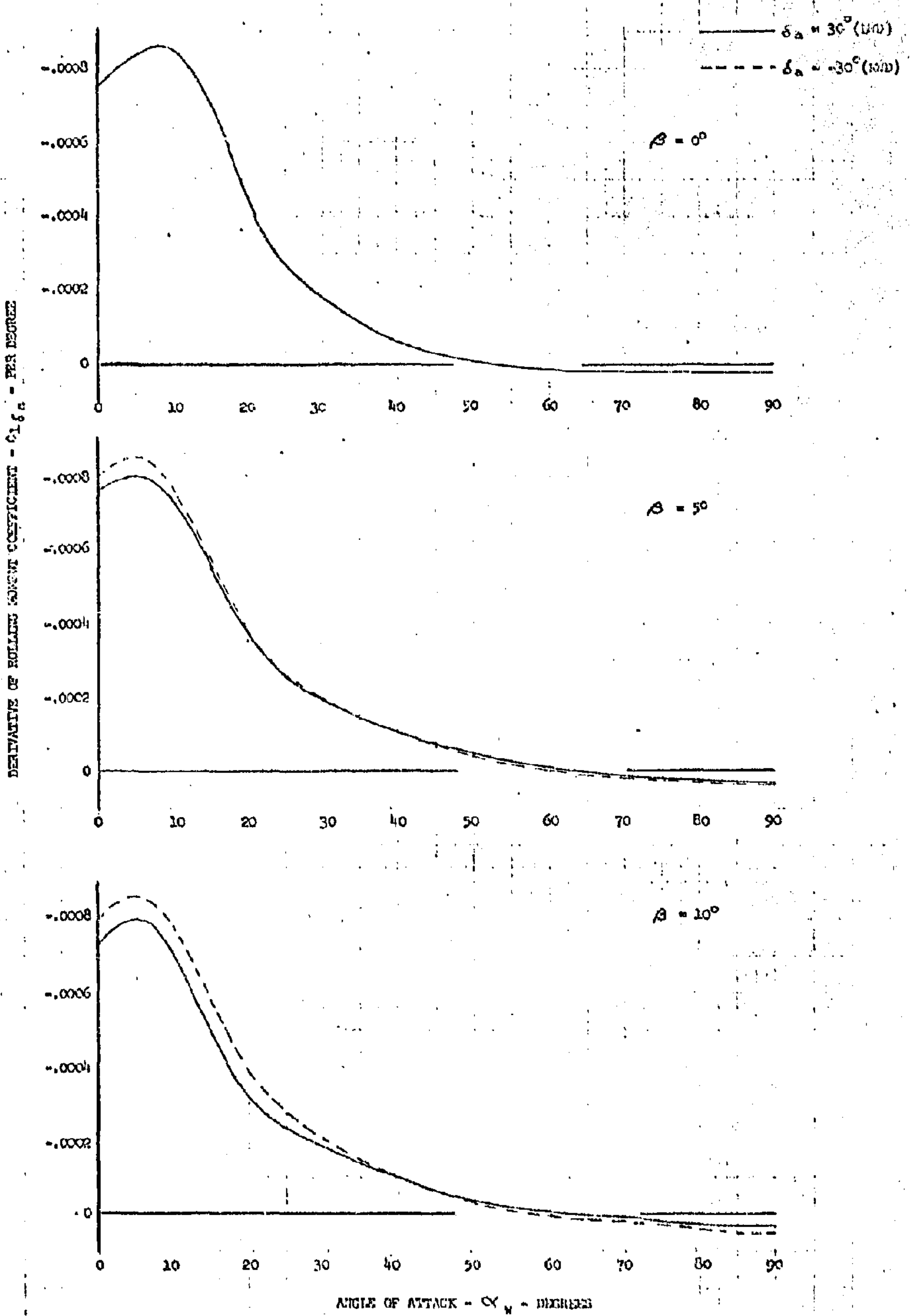

Figure A.12

A.25

XOC A2181

FIGURE F-48

[illegible]

ROLLING MOMENT DUE TO AILERON DEFLECTION VERSUS ANGLE OF ATTACK

M = .2

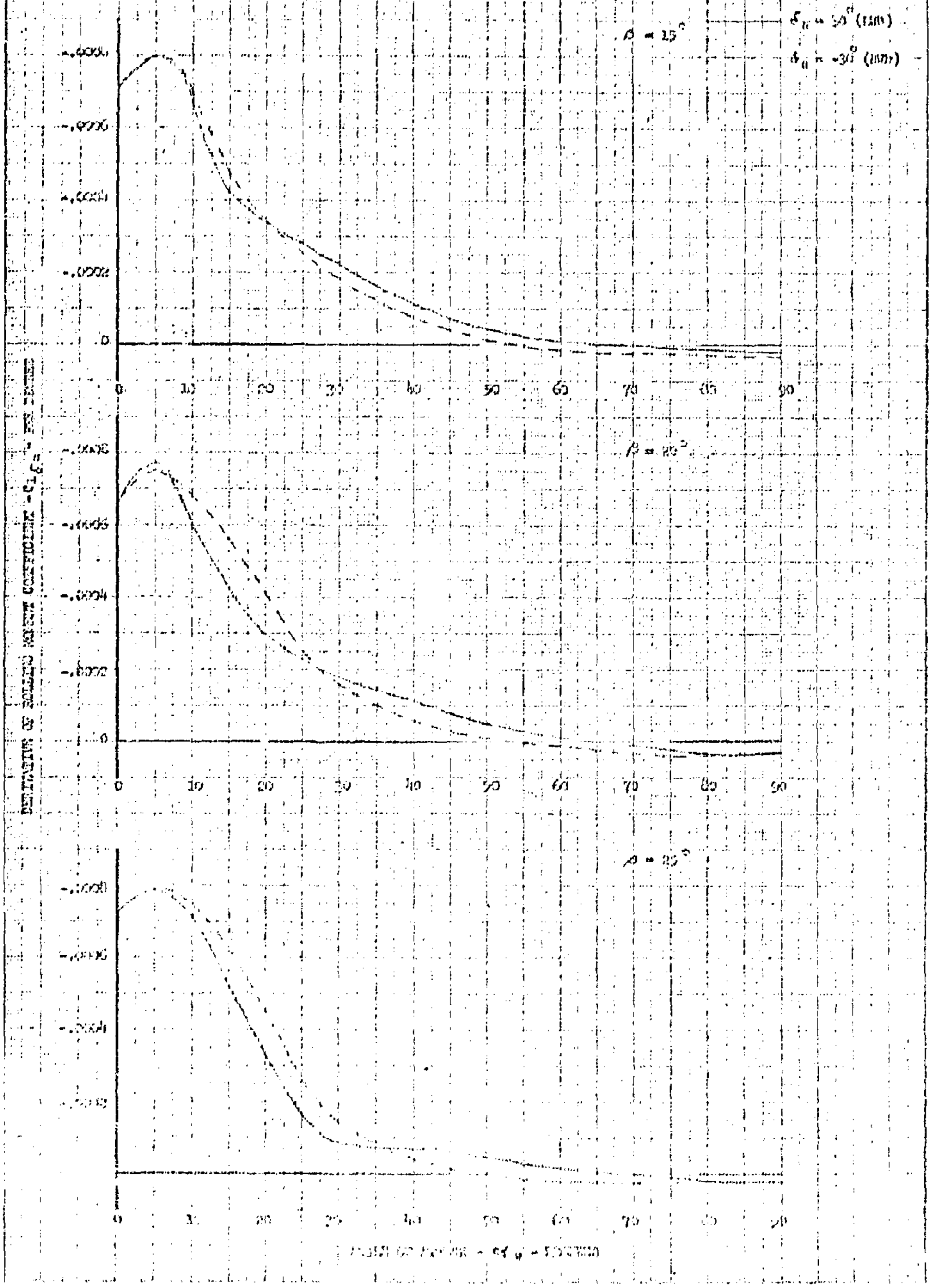

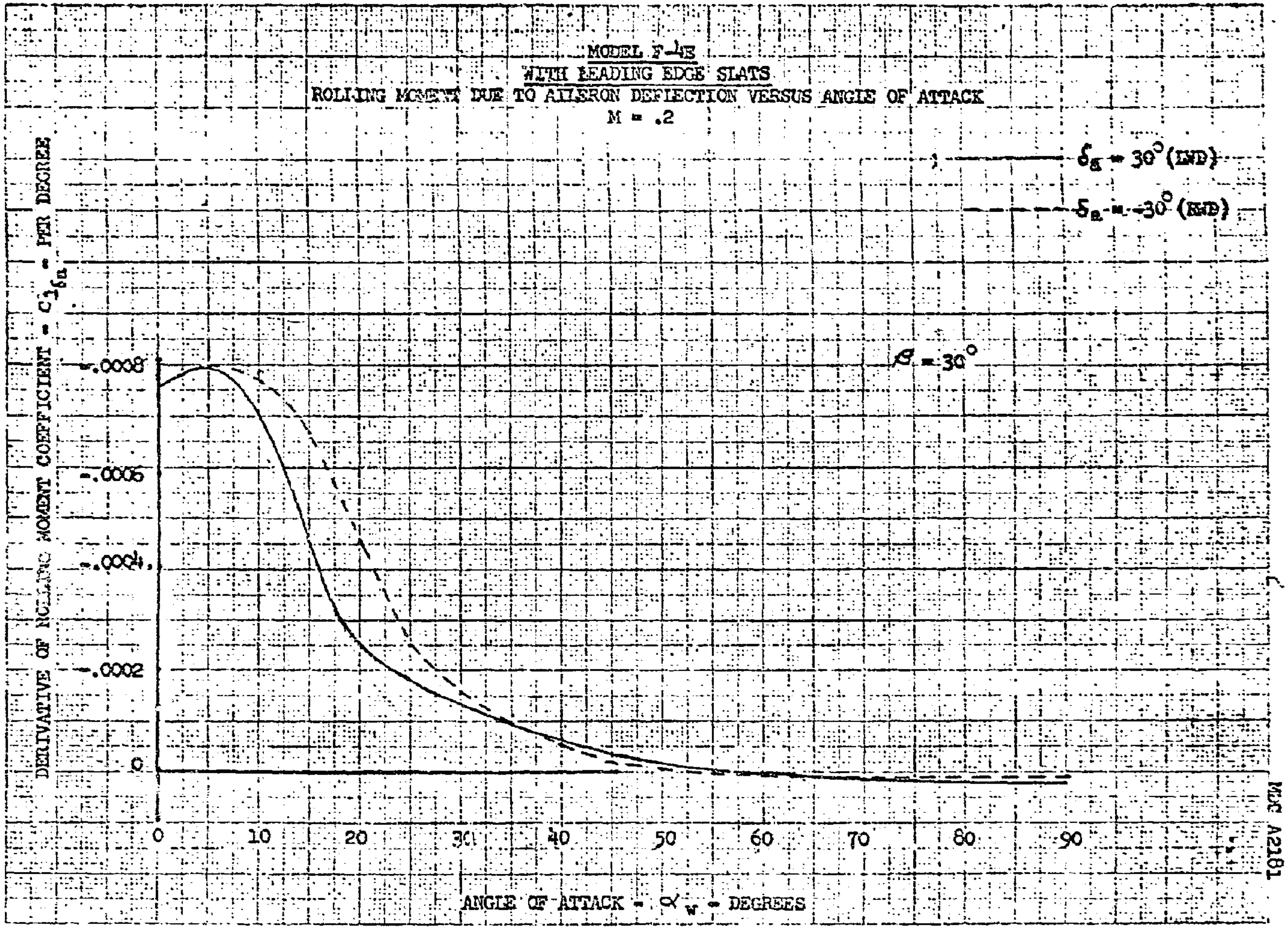

MODEL F-4E
WITH LEADING EDGE SLATS
ROLLING MOMENT DUE TO AILERON DEFLECTION VERSUS ANGLE OF ATTACK
M = .2

Figure A.12 Con't

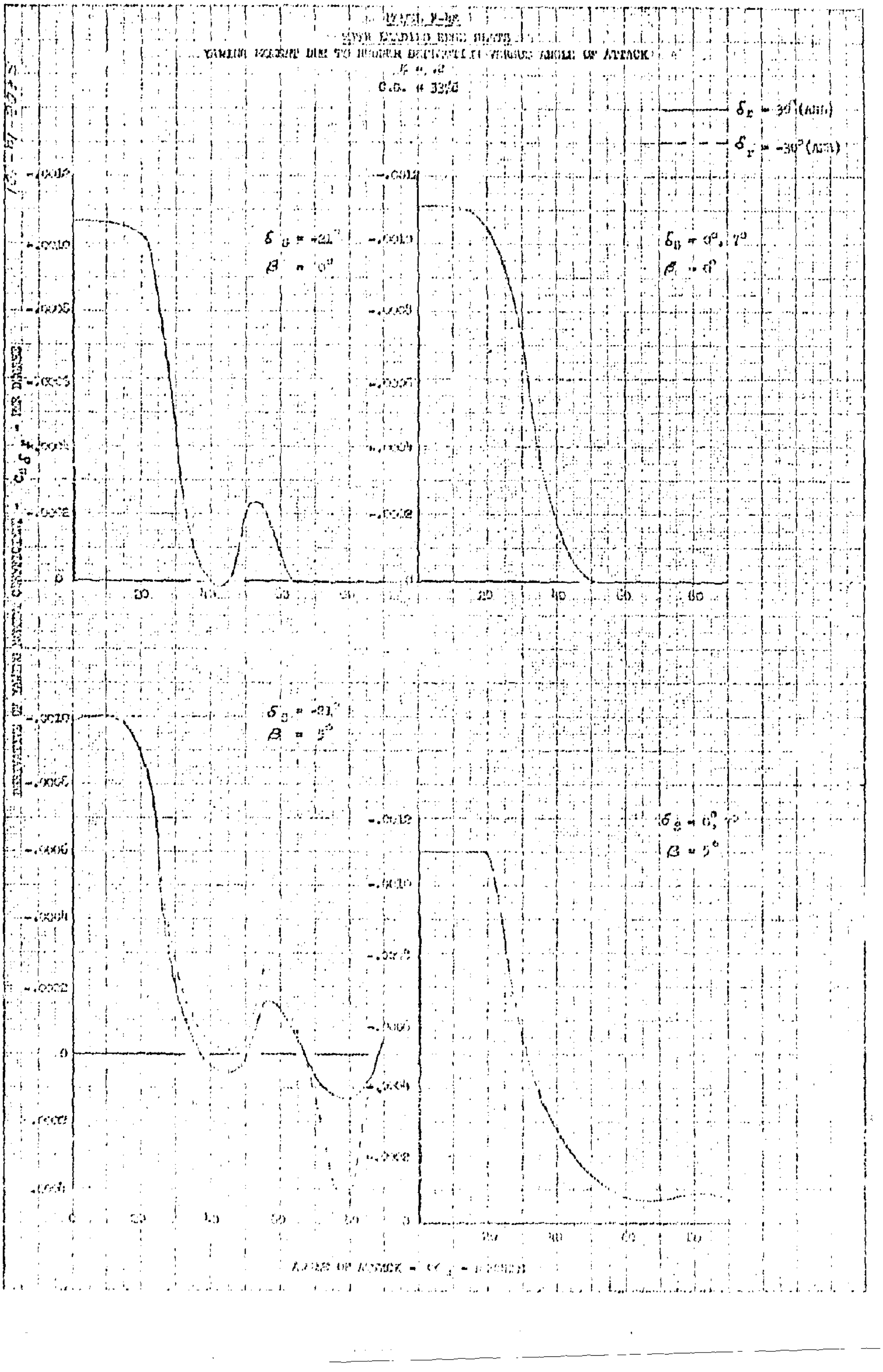
PLATE V-
WITH LEADING EDGE SLATS
YAWING MOMENT DUE TO RUDDER DEFLECTION VERSUS ANGLE OF ATTACK
C.G. @ 33%
$\delta_r$ = 30°
$\delta_r$ = -30°
$\delta_s$ = 21°
$\beta$ = 0°
$\delta_s$ = 0°, 7°
$\beta$ = 0°
$\delta_s$ = 21°
$\beta$ = 5°
$\delta_s$ = 0°, 7°
$\beta$ = 5°
-.0012
-.0010
-.0008
-.0006
-.0004
-.0002
0
.0002
.0004
20
40
60
80
DERIVATIVE OF YAWING MOMENT COEFFICIENT, $C_{n_{\delta r}}$ - PER DEGREE
ANGLE OF ATTACK - $\alpha_F$ - DEGREES

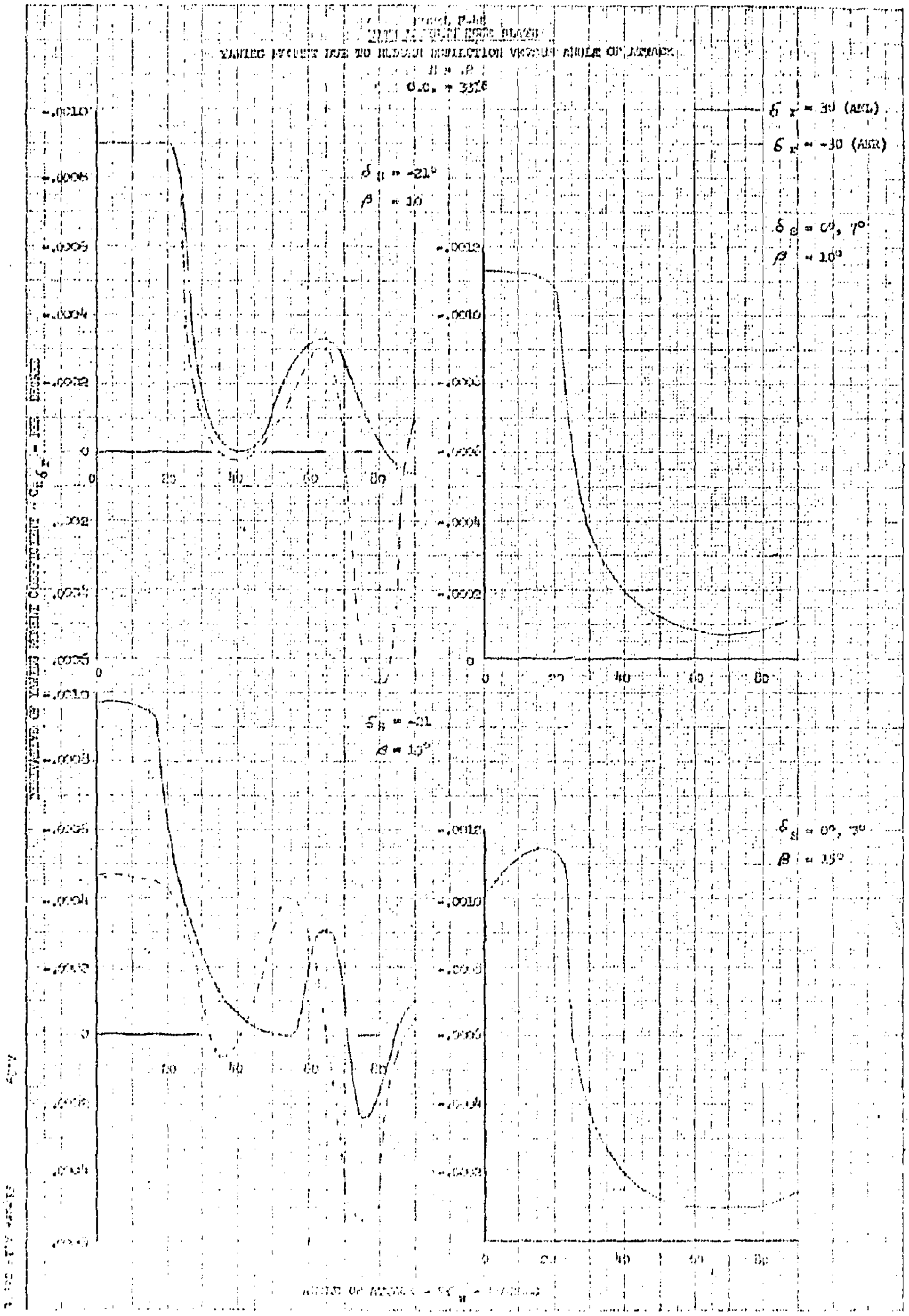

YAWING MOMENT DUE TO RUDDER DEFLECTION VERSUS ANGLE OF ATTACK

M = .8

C.G. = 33%

FIGURE F-15

[illegible]

YAWING MOMENT DUE TO RUDDER DEFLECTION VERSUS ANGLE OF ATTACK

R = [illegible]

C.G. = 33.8

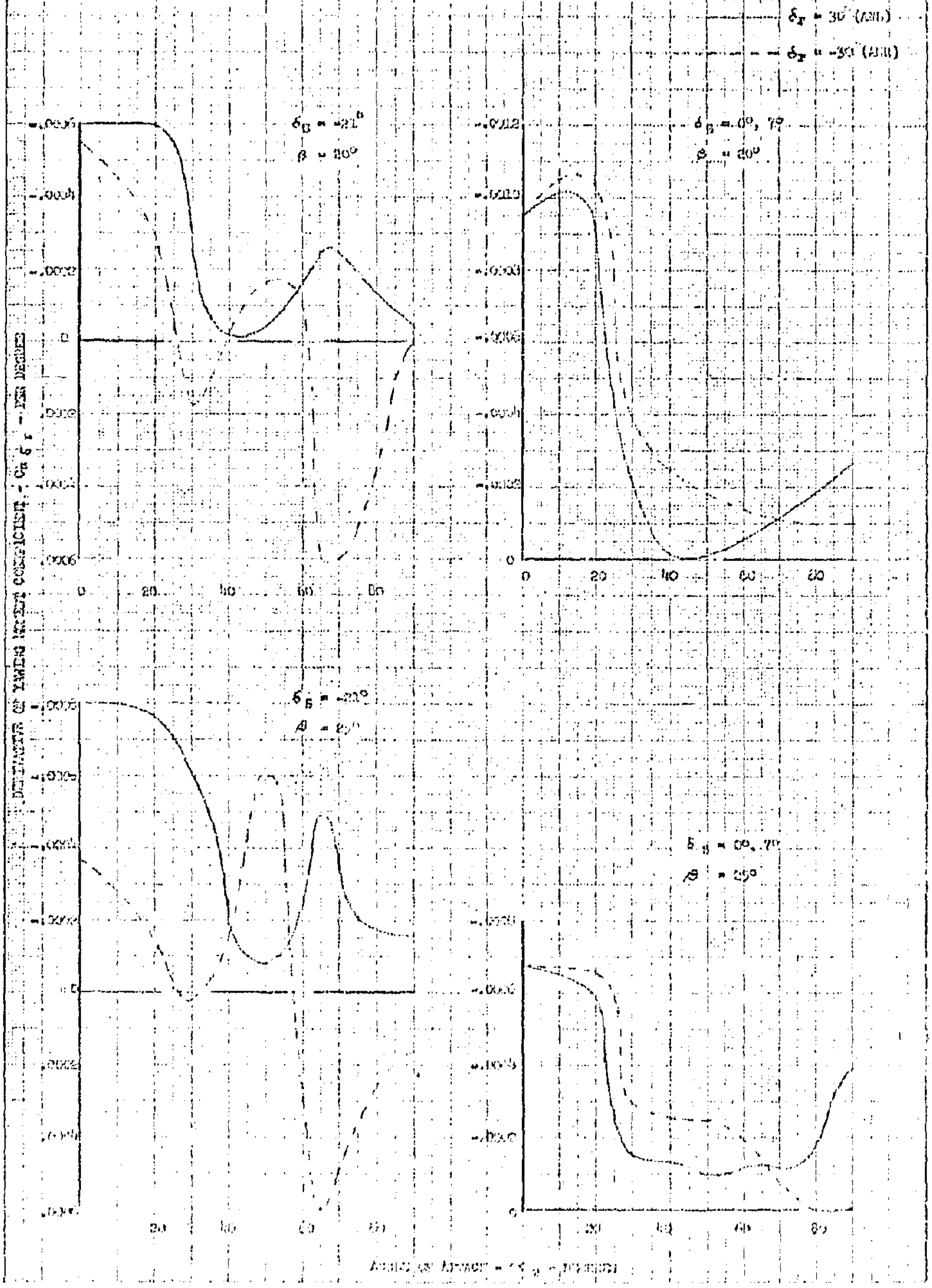

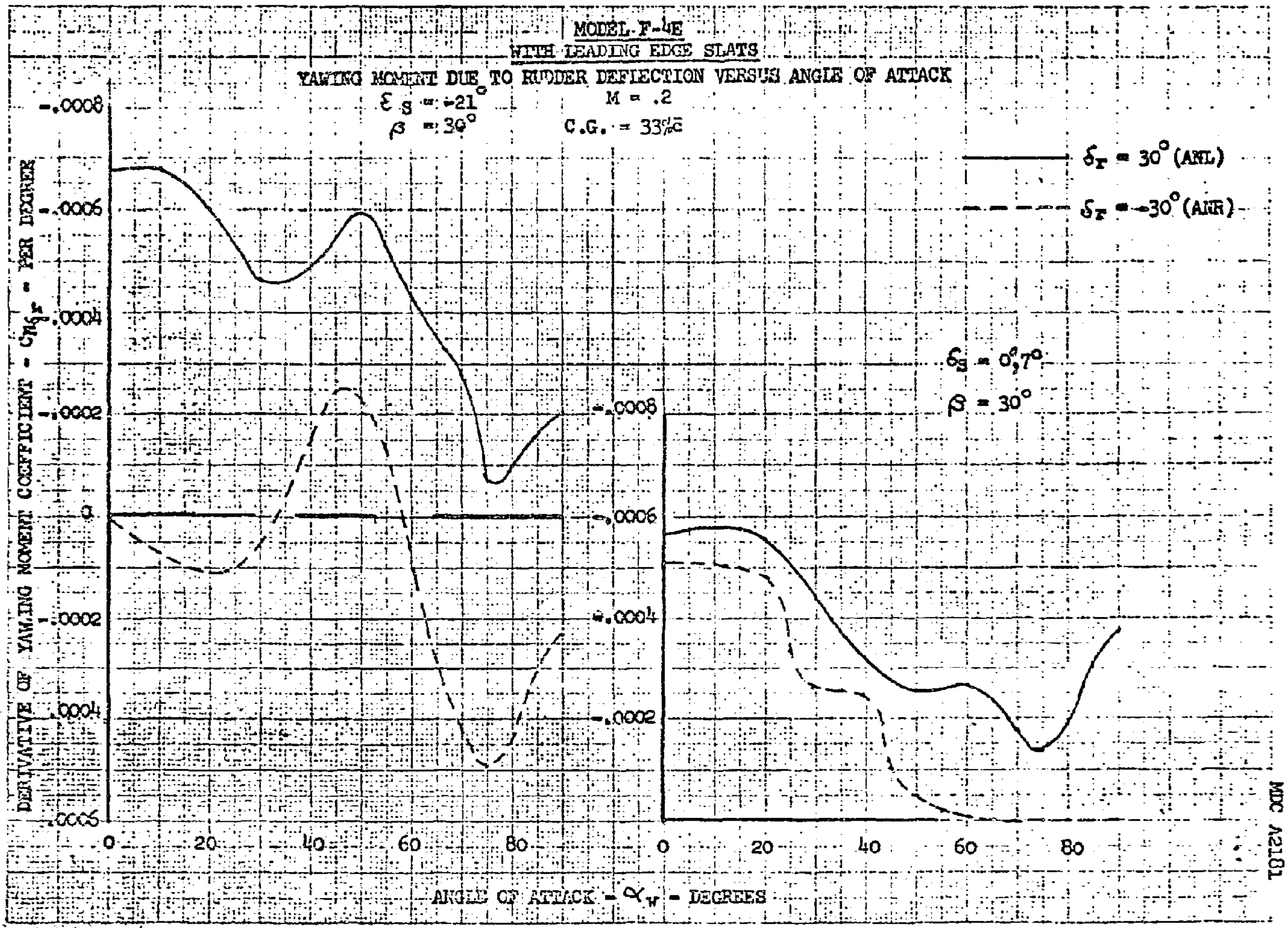

MODEL F-4E
WITH LEADING EDGE SLATS
YAWING MOMENT DUE TO RUDDER DEFLECTION VERSUS ANGLE OF ATTACK

Figure A.13 Cont

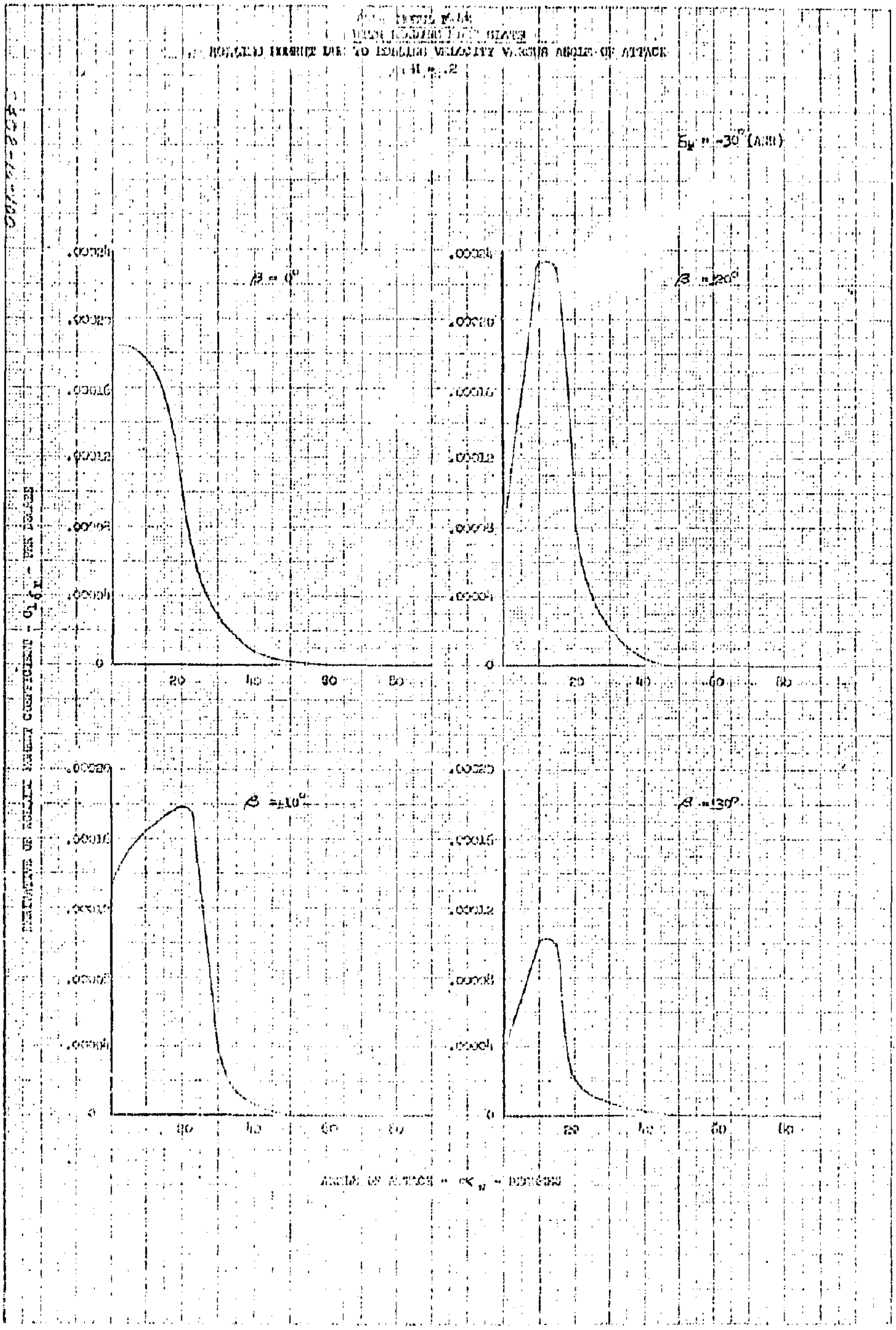

ROLLING MOMENT DUE TO ROLLING VELOCITY VERSUS ANGLE OF ATTACK

M = .2

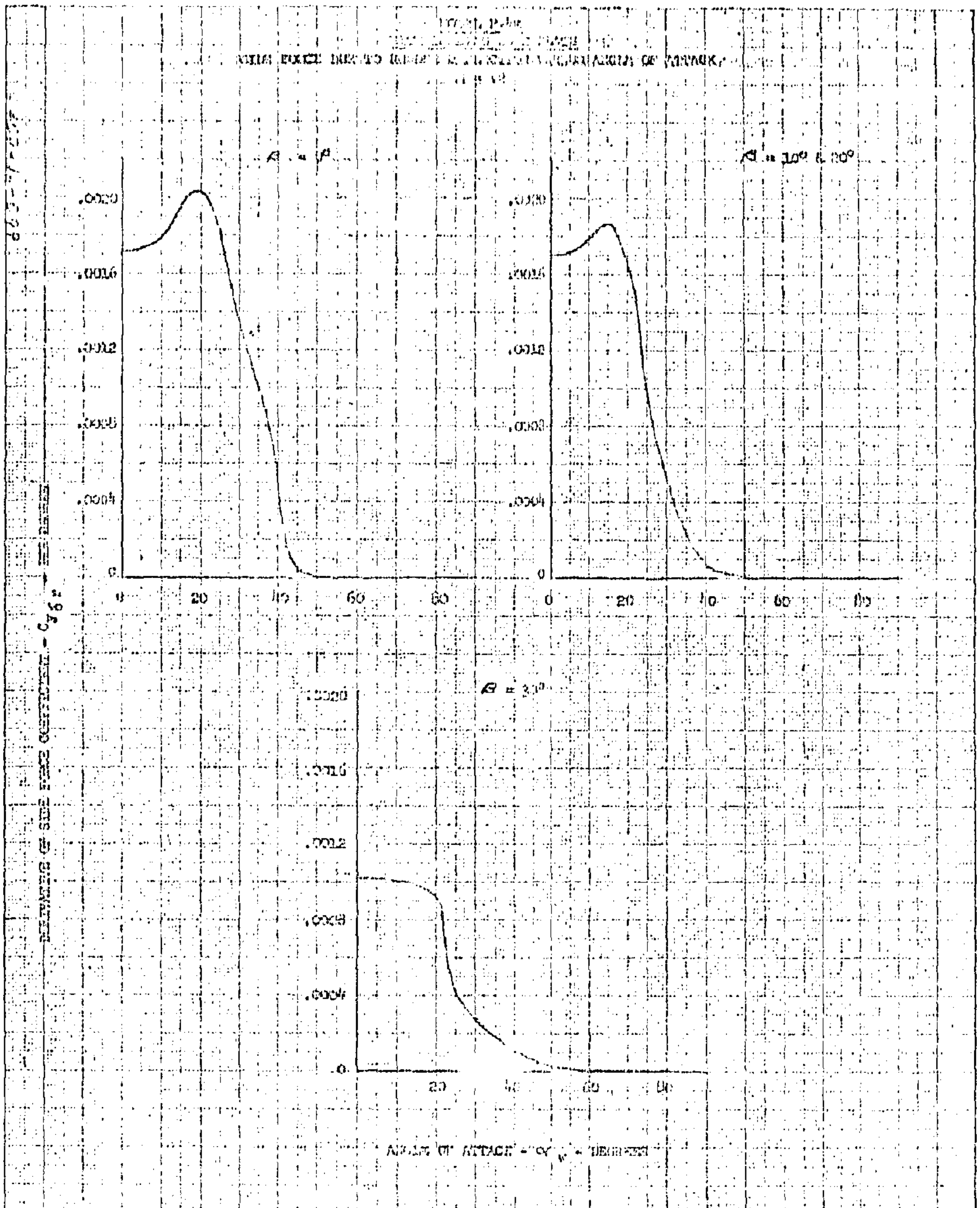
.0020
.0016
.0012
.0008
.0004
0
0
20
40
60
80
ANGLE OF ATTACK - α - DEGREES

Figure A.15

NATIONAL TRACING PAPER
INDIANAPOLIS, INDIANA

UN 22019CM 10X10 TO CM
LITHO IN U.S.A.

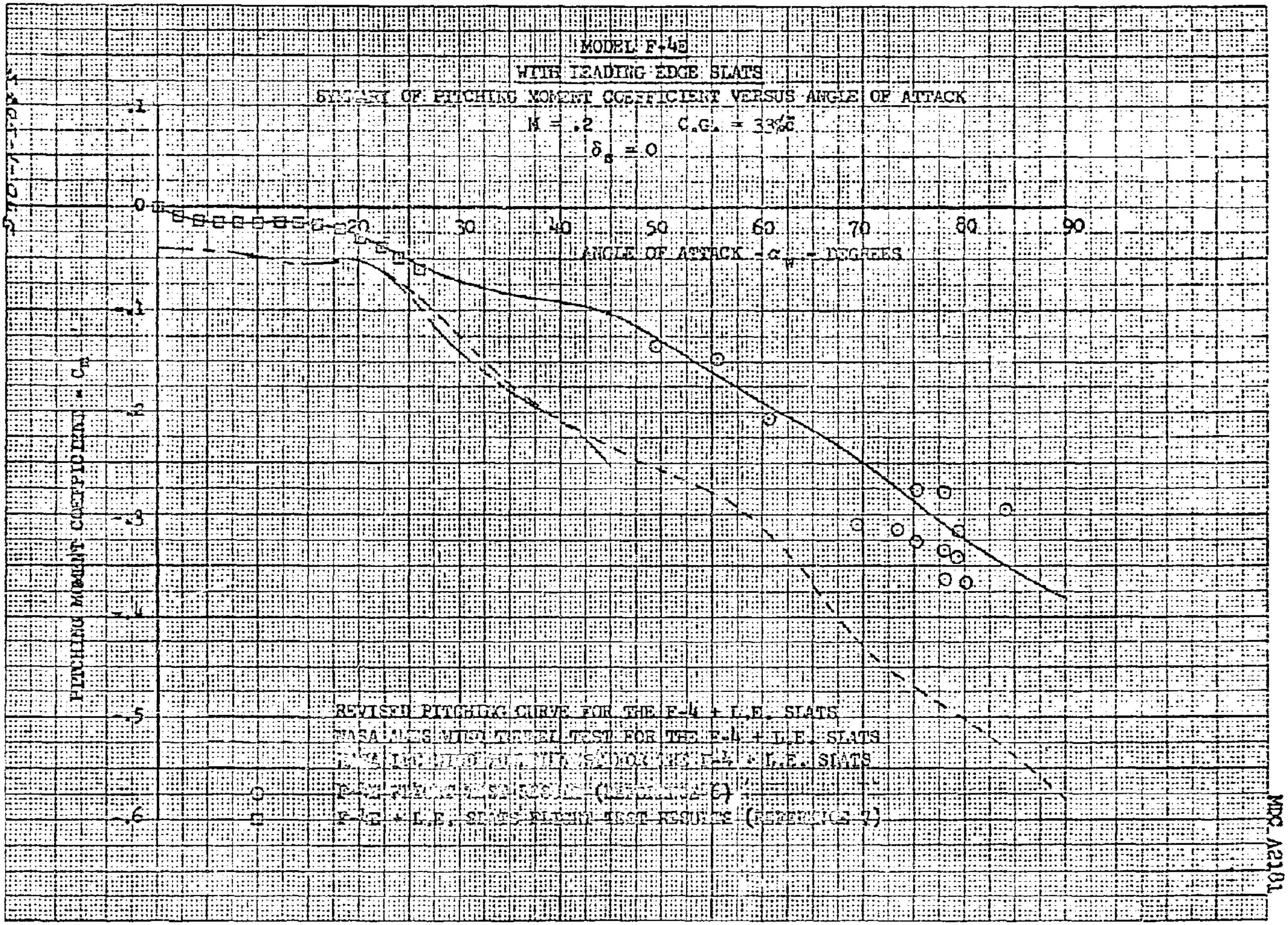

Figure A.16

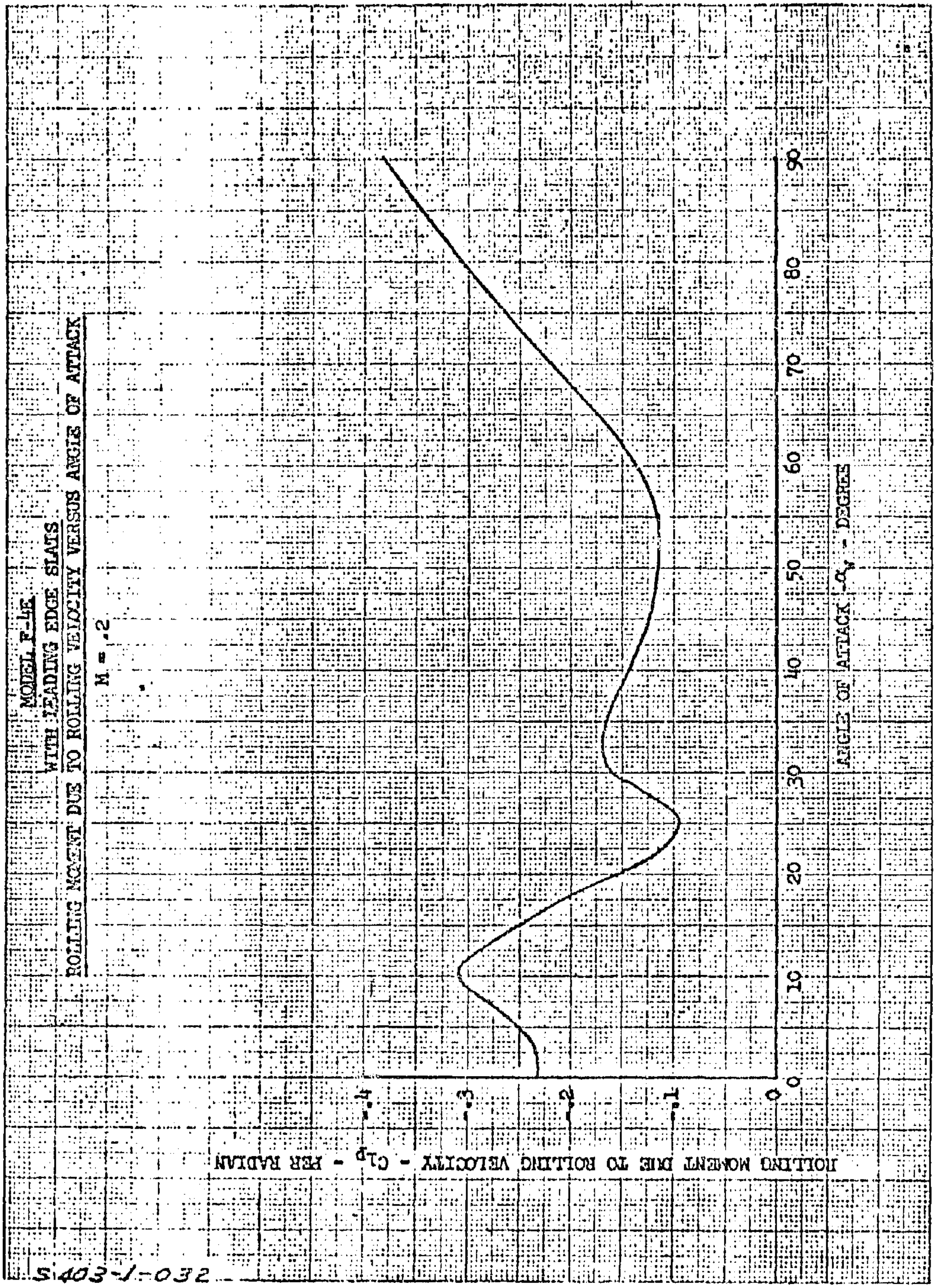

MODEL F-4E

WITH LEADING EDGE SLATS

ROLLING MOMENT DUE TO ROLLING VELOCITY VERSUS ANGLE OF ATTACK

M = .2

S403-1-032

MODEL F-4E

WITH LEADING EDGE SLATS

ROLLING MOMENT DUE TO YAWING VELOCITY VERSUS ANGLE OF ATTACK

M = .2

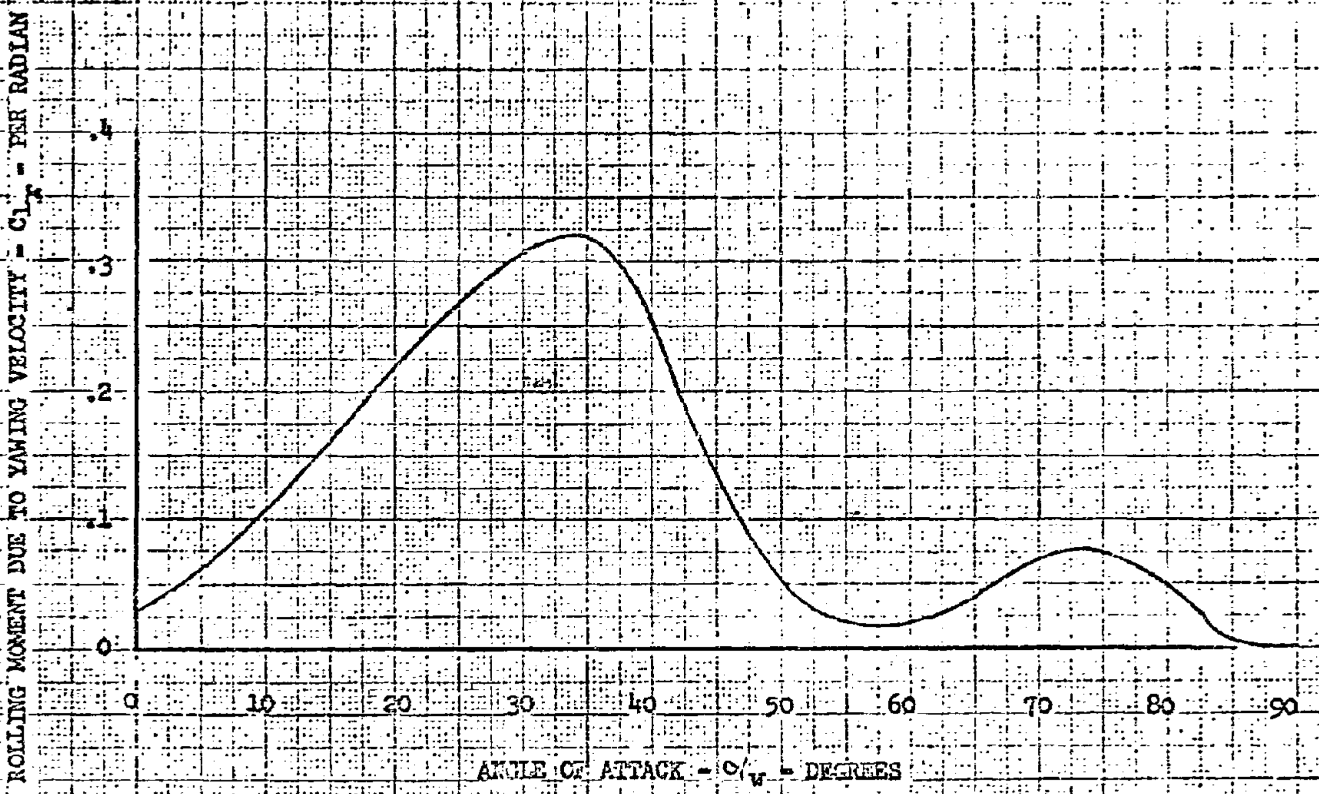

S402-16

Figure A.18

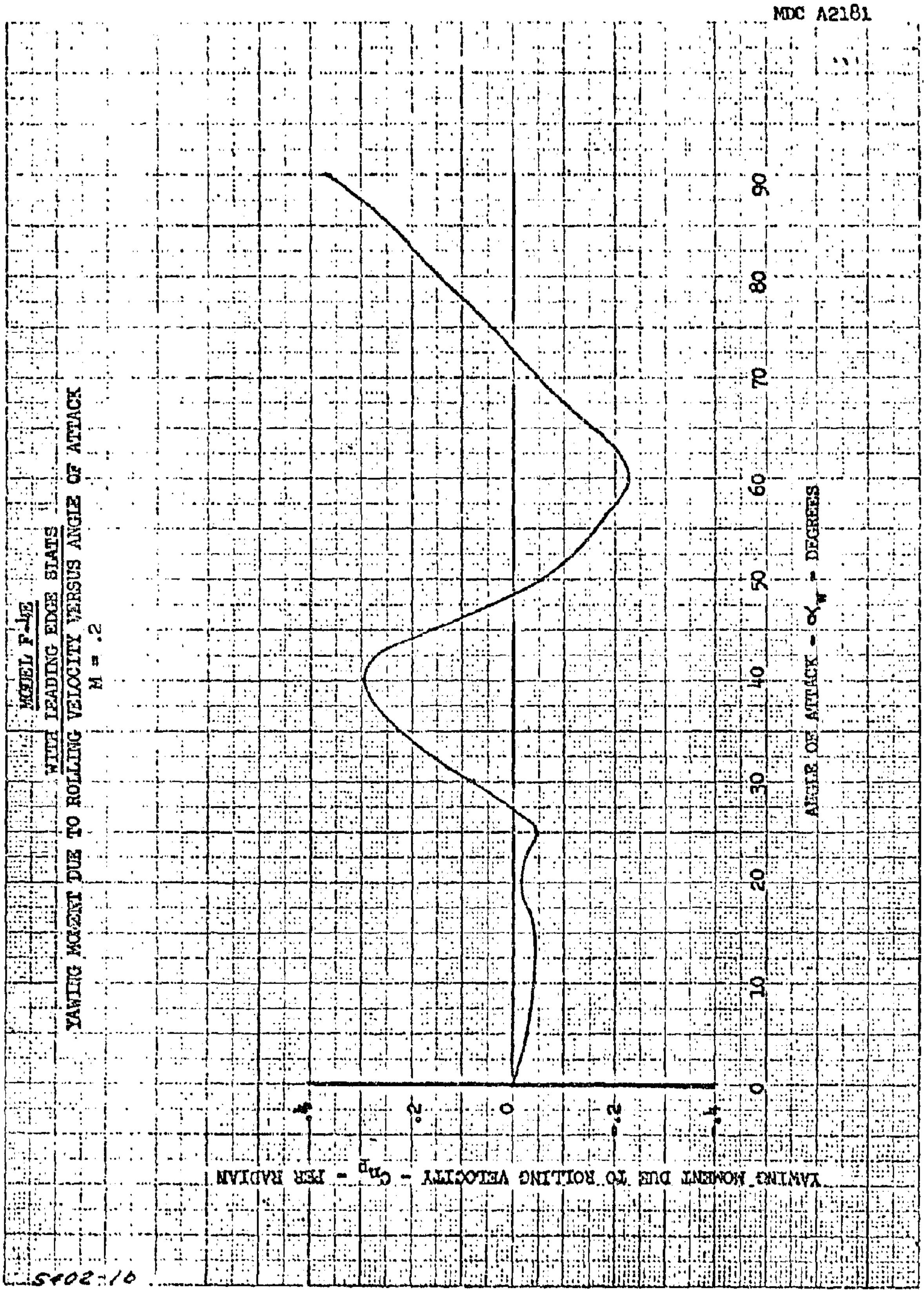

5402-10

Figure A.19

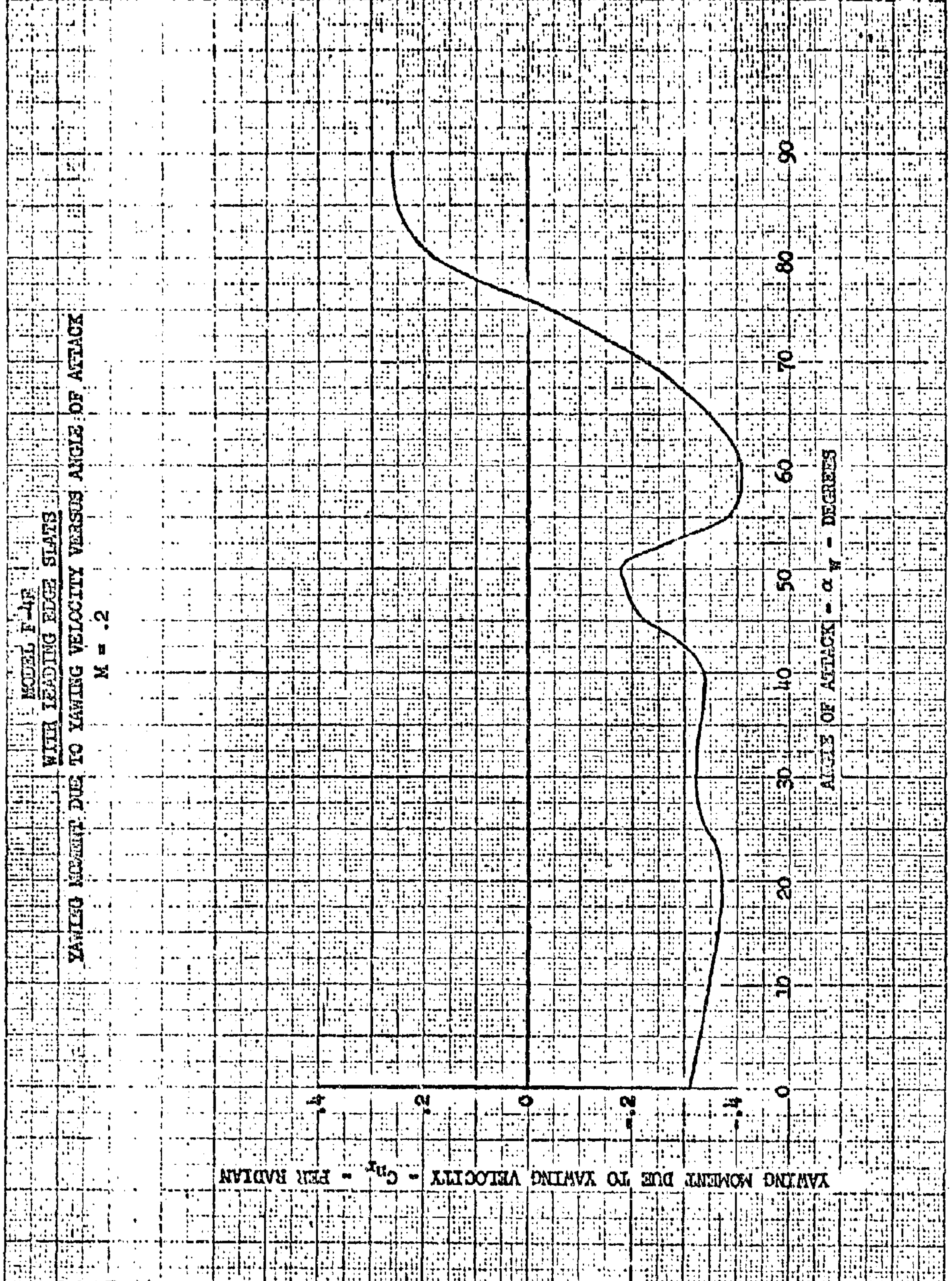
MODEL F-4E
WITH LEADING EDGE SLATS
YAWING MOMENT DUE TO YAWING VELOCITY VERSUS ANGLE OF ATTACK
M = .2

5.402-16

Figure A.20

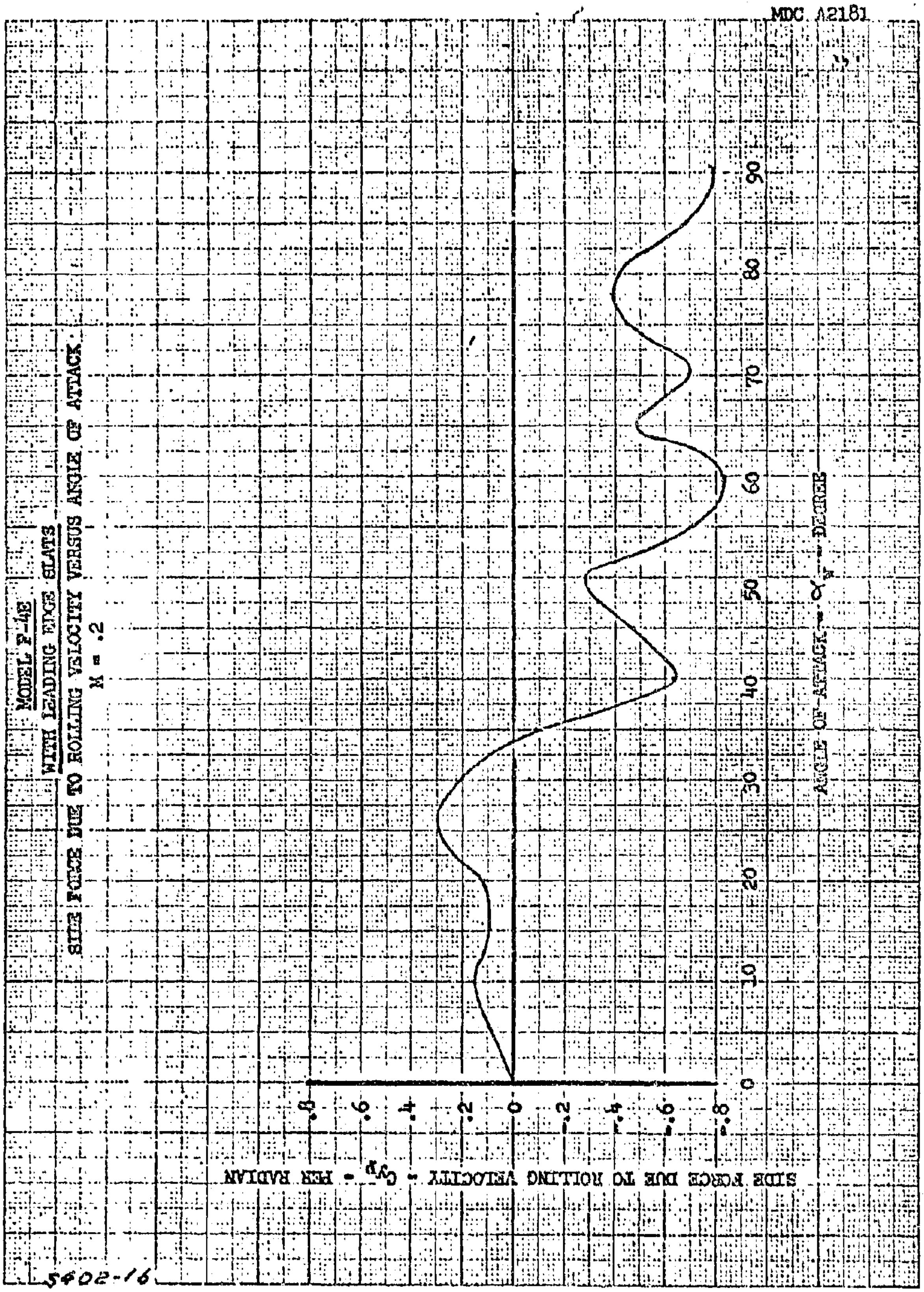

5402-16

Figure A.21

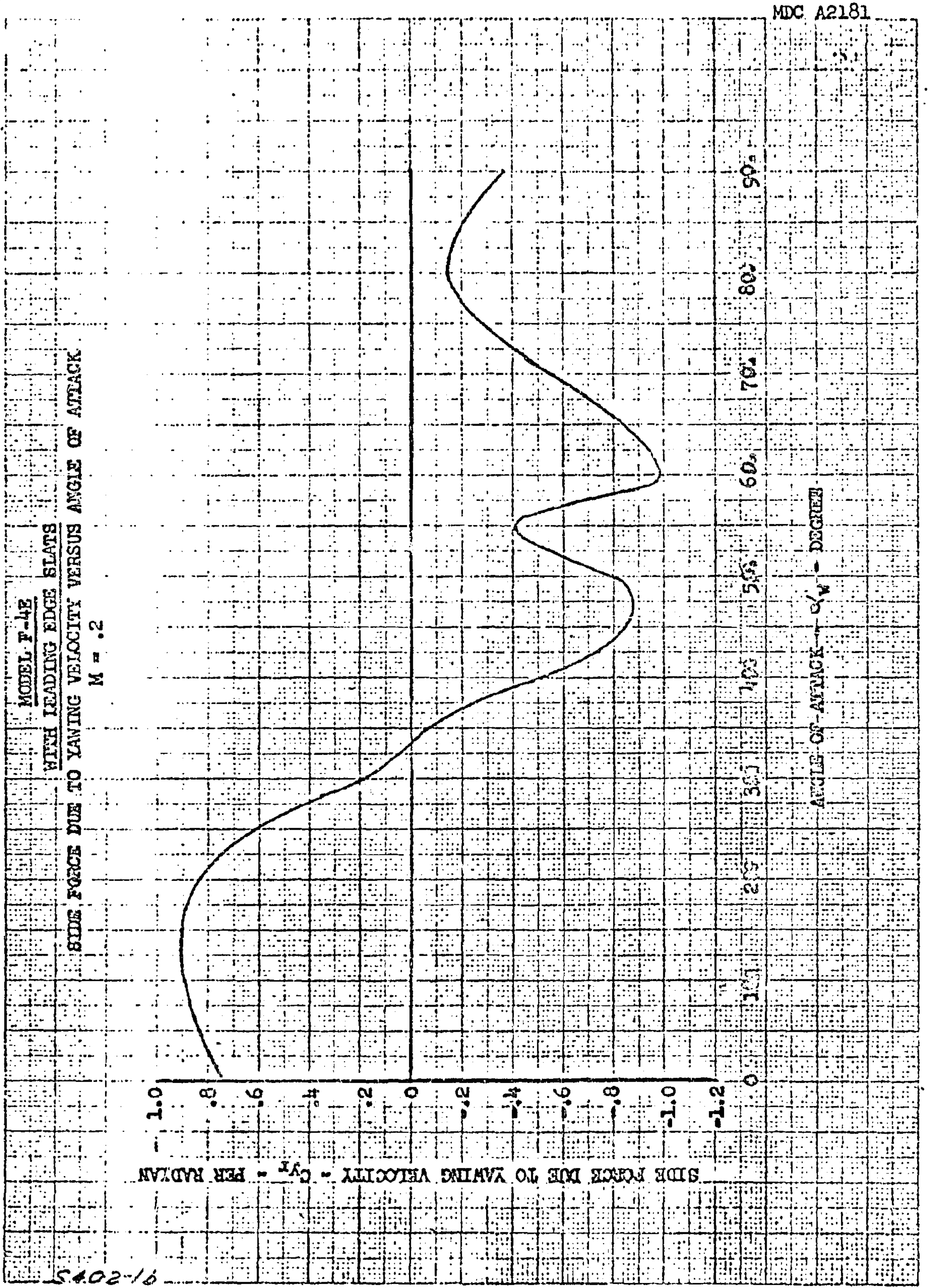

MODEL F-4E

WITH LEADING EDGE SLATS

SIDE FORCE DUE TO YAWING VELOCITY VERSUS ANGLE OF ATTACK

M = .2

S402-16

Figure A.22

MODEL F-4E
WITH LEADING EDGE SLATS
ROLLING MOMENT DUE TO ROLLING VELOCITY VERSUS ANGLE OF ATTACK
M = .2 C.G. = 33%c

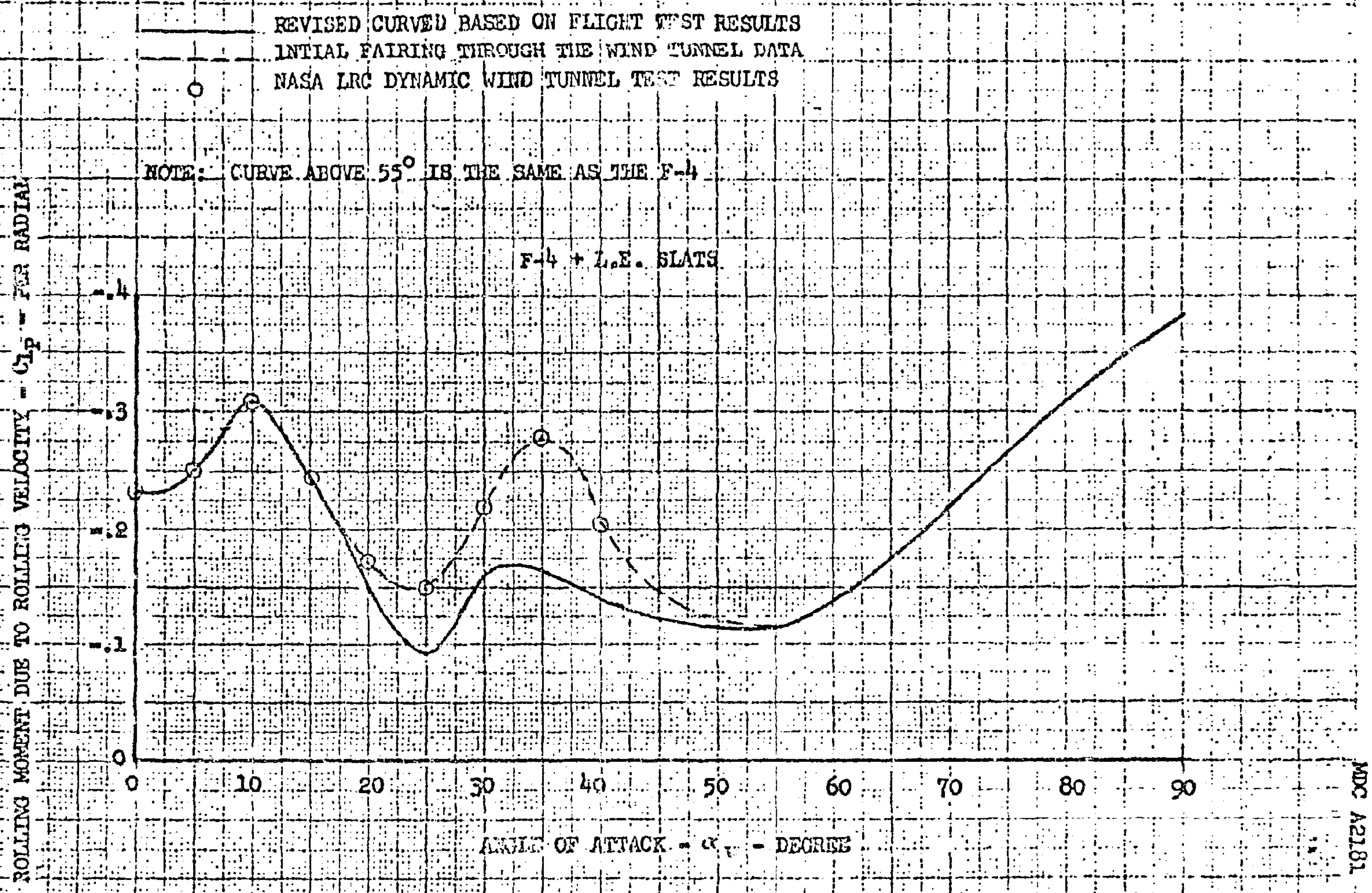

5403-1-032

Figure A.23

MODEL [illegible]

[illegible] SLATS

VARIATION OF YAWING MOMENT COEFFICIENT WITH SPIN COEFFICIENT

M = .2

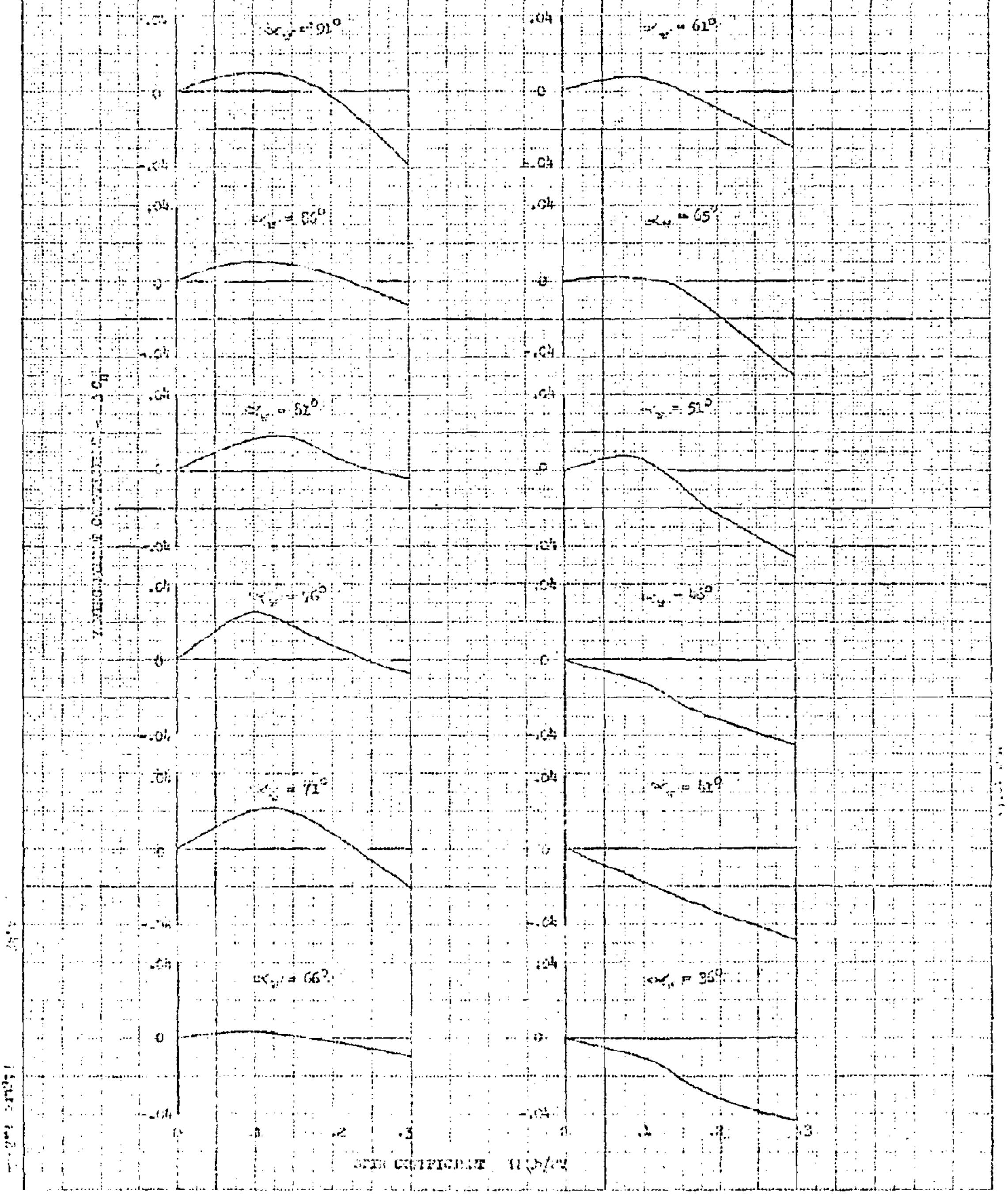

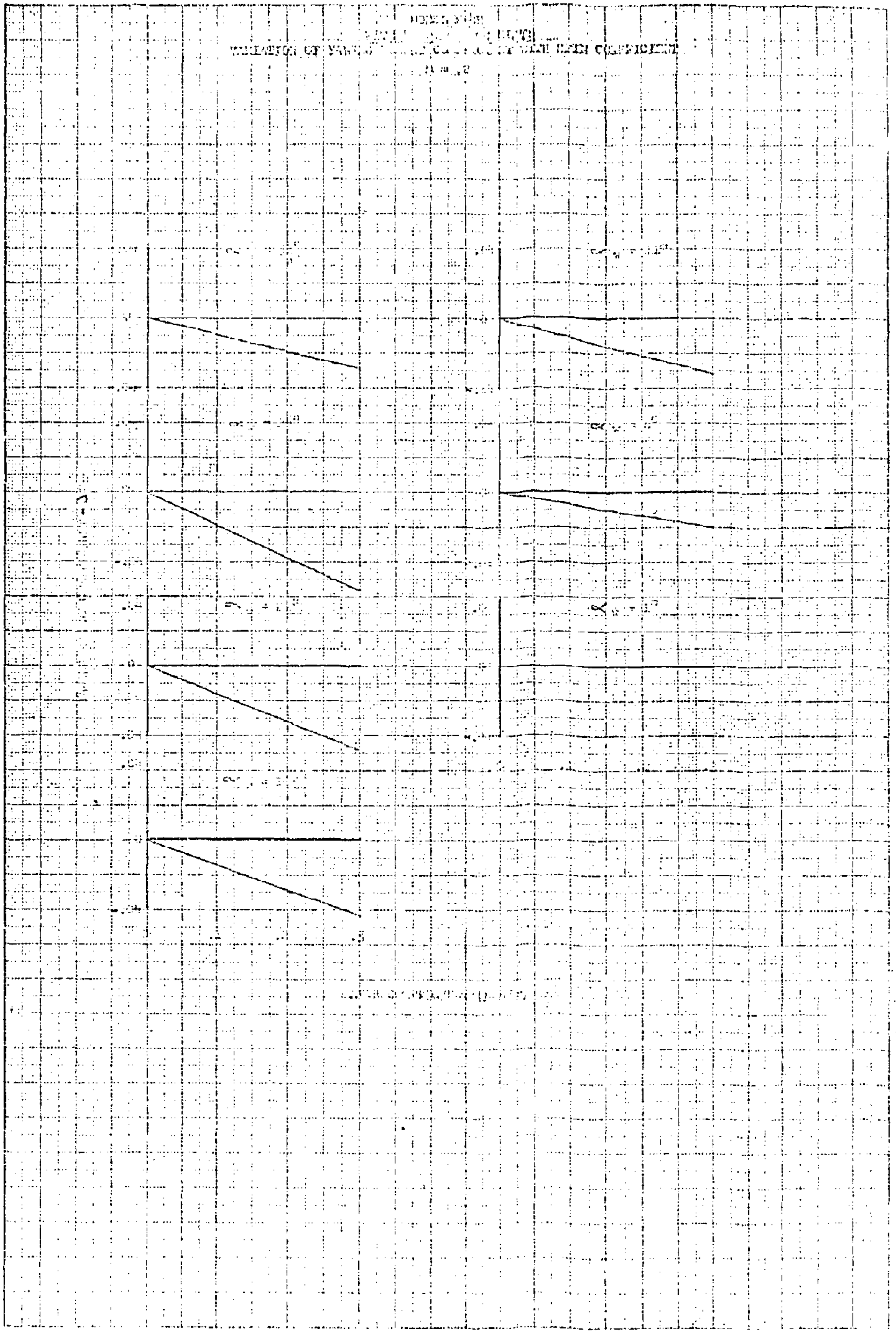
VARIATION OF YAW
COEFFICIENT

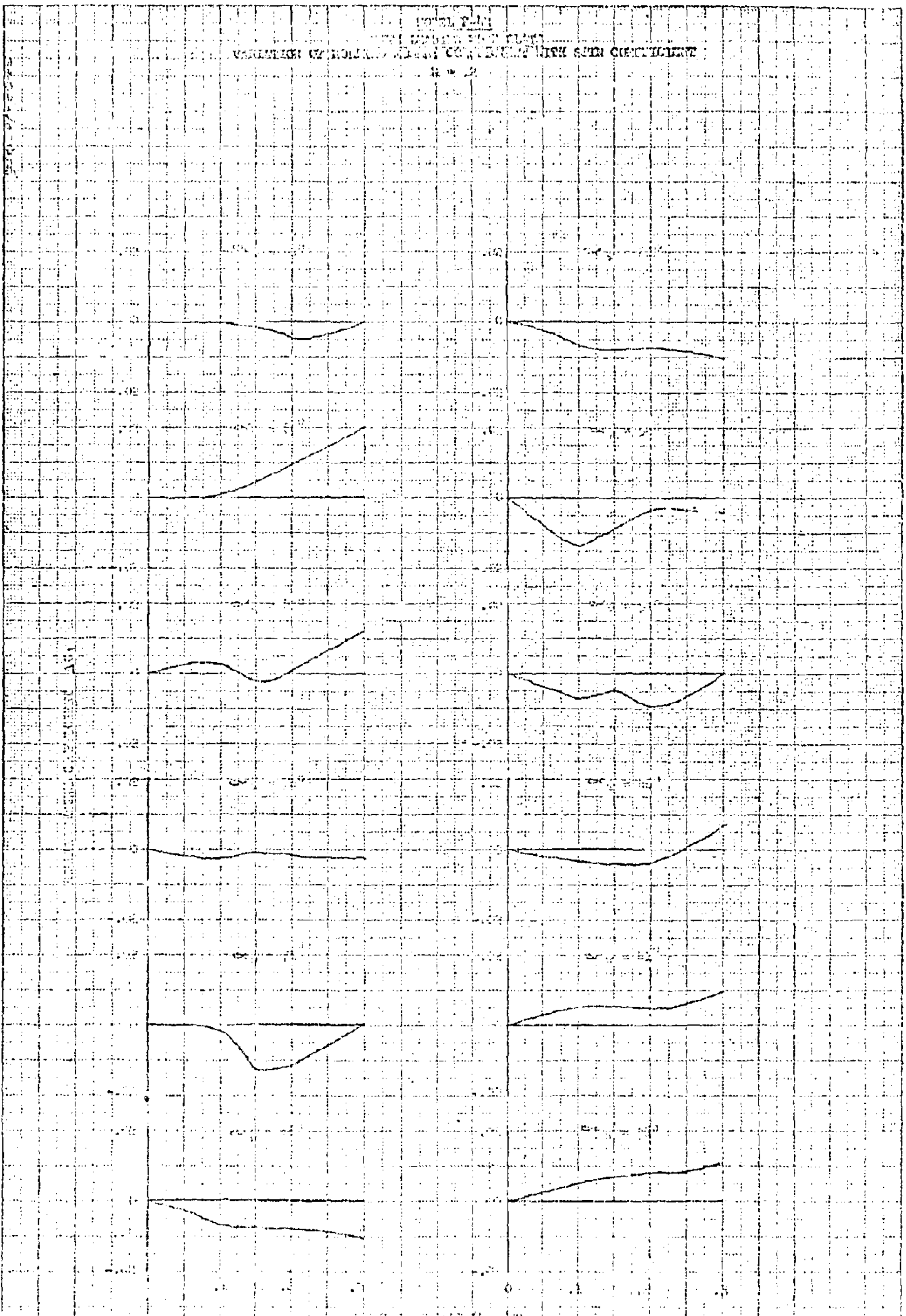

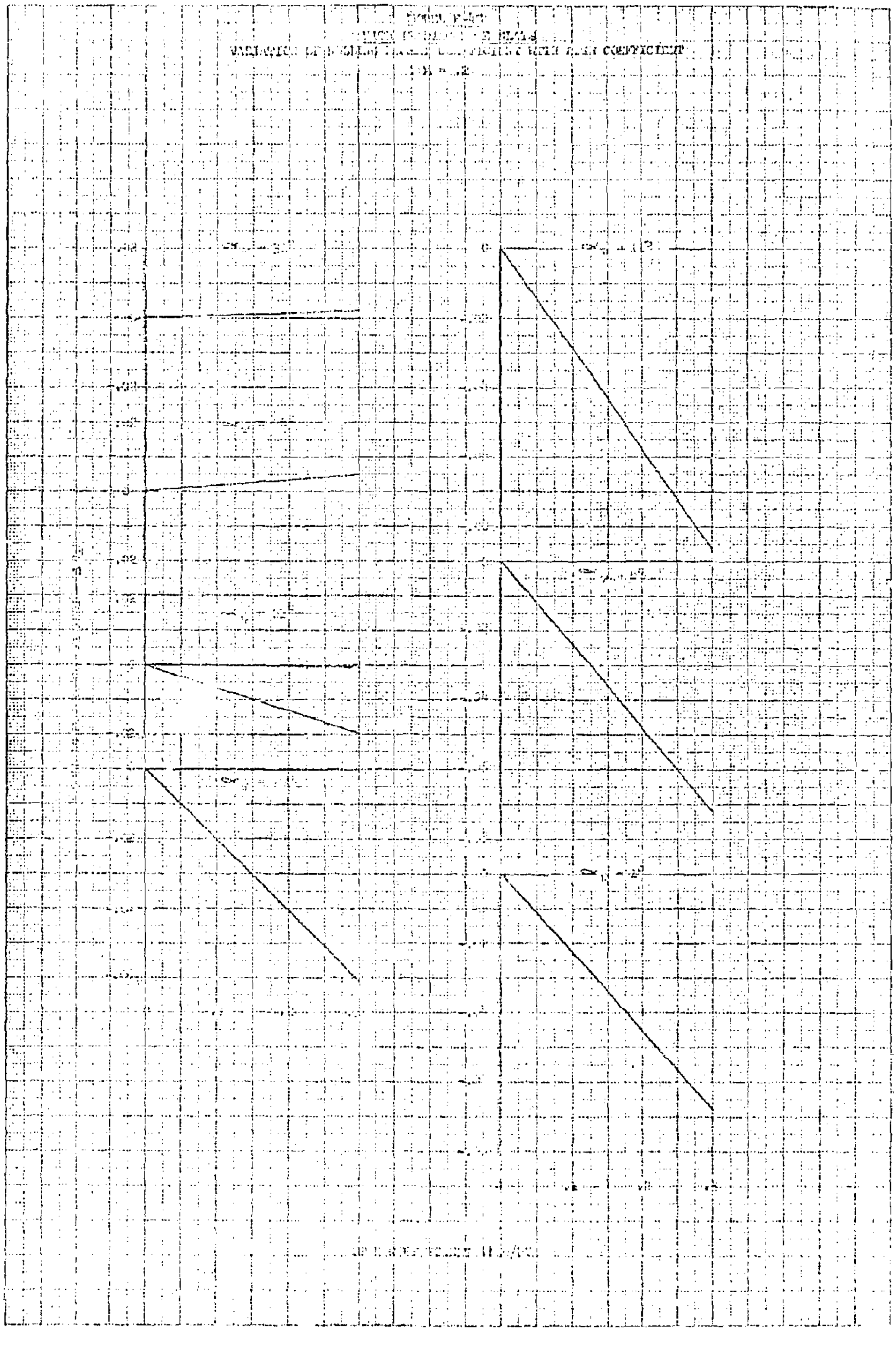
VARIATION OF [illegible] WITH [illegible] COEFFICIENT
.02
0
-.02
.02
0
-.02
0
0
0

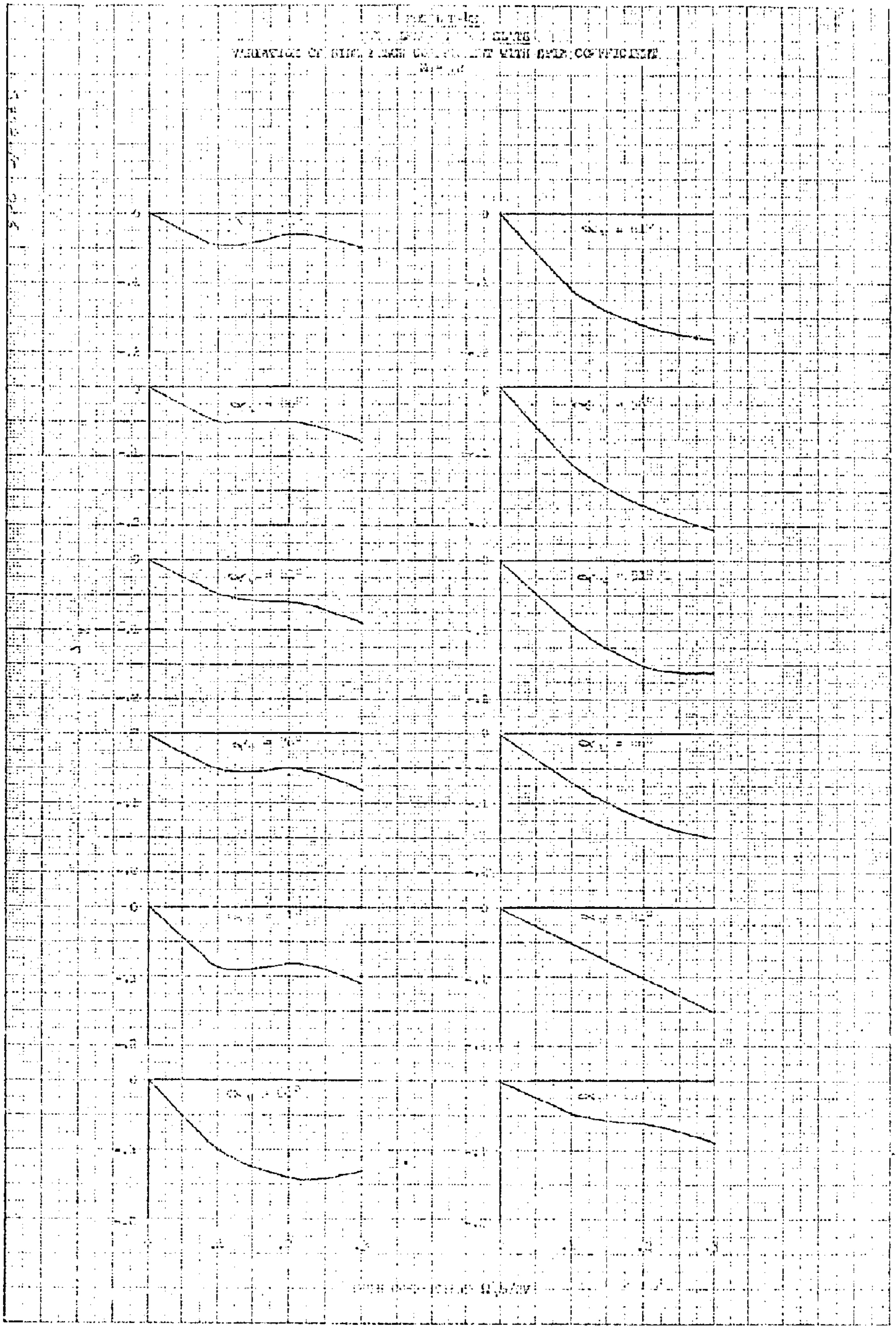VARIATION OF SIDE FORCE COEFFICIENT WITH SPIN COEFFICIENT
0
-.1
-.2
0
.1
.2
.3
SPIN COEFFICIENT Ωb/2V

VARIATION OF SIDE FORCE COEFFICIENT WITH SPIN COEFFICIENT

M = 2.2

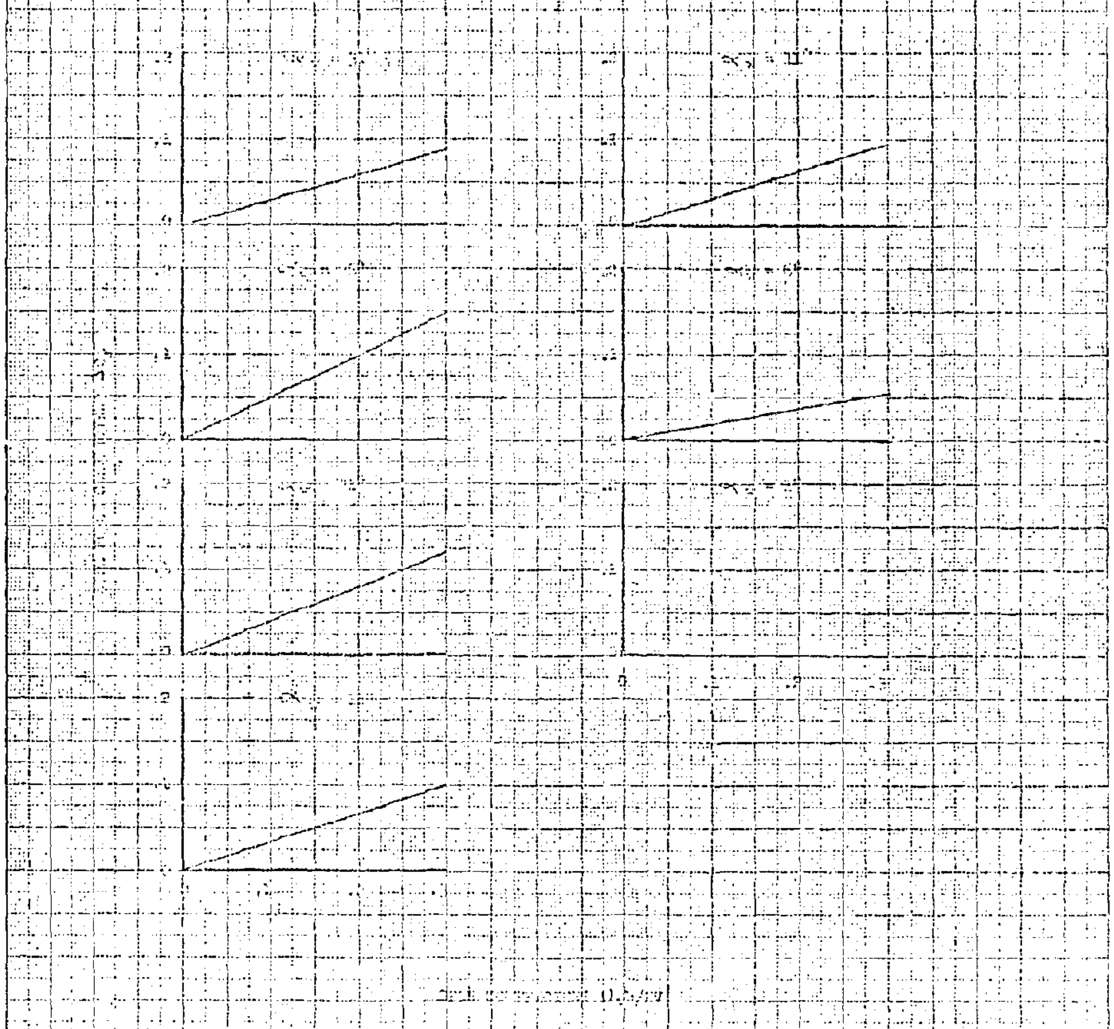

# APPENDIX B

## BASIC F-4E AERODYNAMIC DATA

Inclusive Pages: B.1 Thru B.49

## Table Of Contents

| Section | Title | Page |
|---|---|---|
| B | Basic F-4E Aerodynamic Data | B.3 |
|  | B.1 Force and Moment Wind Tunnel Data | B.3 |
|  | B.1.1 Adjustment in Static Pitching Moment Coefficient | B.4 |
|  | B.1.2 Adjustment in Yawing Moment Asymmetries | B.4 |
|  | B.2 Forced Oscillation Wind Tunnel Data | B.5 |
|  | B.3 Rotary Balance Wind Tunnel Data | B.5 |
|  | B.3.1 Rotary Balance Data Below 35° Angle of Attack | B.6 |

# APPENDIX B

## B. Basic F-4E Aerodynamic Data

The data as presented in this appendix were used in the six-degree-of-freedom computer simulation of the basic F-4E for both the stall and spin studies. All the data are input independent of Mach number and flexibility effects. The aerodynamic coefficients are in the body axis system as a function of angle of attack ranging from 0° to 90°. All data are presented at C.G. of 33%$\bar{c}$.

B.1 Force and Moment Wind Tunnel Data - High angle of attack static force and moment data on the basic F-4E were obtained from wind tunnel testing. A 6.67% scale model force and moment test was conducted at NASA ARC in the 12-Foot Pressure Wind Tunnel. These data were obtained with an angle of attack variation from 0° to 90° at various sideslip angles for .23 Mach number and a Reynolds number of $4.0 \times 10^6$ per foot. The results of this test was used as a bases for the curves presented in this appendix for the basic F-4E. They are the same curves as those found in Reference 2.

The static longitudinal and lateral-directional parameters $C_z$, $C_x$, $C_m$, $C_l$, and $C_y$ are presented in Figures B.1 through B.5, at zero degrees control surface deflection ( $\delta_s$, $\delta_r$, $\delta_a = 0$). The yawing moment coefficient $C_n$, is presented in Figure B.6 as a function of sideslip angle for various stabilator deflections. The yawing moment asymmetries ($\beta = 0$) of the wind tunnel model are presented in Figure B.7.

The static longitudinal and lateral-directional control derivatives $C_{z_{\delta_s}}$, $C_{x_{\delta_s}}$, $C_{m_{\delta_s}}$, $C_{n_{\delta_a}}$, $C_{l_{\delta_a}}$, $C_{n_{\delta_r}}$, $C_{l_{\delta_r}}$, and $C_{y_{\delta_r}}$ are presented in Figures B.8 through B.15. The sign convention used is that a positive force or moment is generated by a negative value for control deflection. The control derivatives $C_{l_{\delta_a}}$ and $C_{n_{\delta_a}}$ contain both the aileron and spoiler contribution referenced to the aileron deflection.

B.1.1 Adjustment in Static Pitching Moment Coefficient - The basic F-4E adjusted pitching moment curve is the same as was used in Reference 1.

B.1.2 Adjustments in Yawing Moment Asymmetries - Both the basic and slatted F-4E have similar wind tunnel asymmetric yawing moments coefficient above 40° angle of attack. These asymmetries are positive and therefore promote a right spin. However, the engine gyroscopic effects promote a left spin. Thus the sign of the asymmetries was changed to create a left spin simulating a more critical condition. This is justified in that some aircraft will always spin to the left and some always to the right, which indicates that the asymmetries are aircraft dependent and can be applied in any manner.

An additional modification is made to the yawing moment asymmetries above 70° angle of attack. This was done in order to obtain the same intermediate spin mode as experienced in flight test. Thus by making the asymmetries more positive (left spin only) the angle of attack and the associated rate or rotation is reduced to agree better with the results obtained from the basic F-4E stall/spin flight test program (Reference 7). The same modification is made to the slatted F-4E asymmetries. The original wind tunnel asymmetries along with the revised curves used in this analytical study are presented in Figure B.16 for both the basic and slatted F-4E.

## APPENDIX B

B.2 Forced Oscillation Wind Tunnel Data - Forced oscillation testing was conducted in the NASA LRC 12-Foot Tunnel on a 9.1% scale Model F-4D. Pitch, roll, and yaw data were obtained from 0° to 90° angle of attack in 5° increments at a dynamic pressure of 5.28 psf and a Reynolds number of $.25 \times 10^6$ per ft.. The forced oscillation investigation was conducted for frequencies of 0.7 cps and 1.0 cps and angular amplitudes of 5° and 10°. The results of this test was used as a base for the curves presented in this appendix for the basic F-4E. They are the same curves as those found in Reference 2. The dynamic forced oscillation derivatives $C_{m_q}$, $C_{l_p}$, $C_{l_r}$, $C_{n_p}$, $C_{n_r}$, $C_{y_p}$, and $C_{y_r}$ are presented in Figures B.17 through B.23.

B.3 Rotary Balance Wind Tunnel Data - Two separate rotary balance tests were conducted at NASA-LRC Vertical Spin Tunnel with a 9.1% scale Model F-4B. In the first test six axes data (Reference 2) were obtained from 35° to 90° angle of attack in 5° increments at a dynamic pressure 1.295 psf and a Reynolds number of $.3097 \times 10^6$ per ft.. The axis of rotation was parallel to the velocity vector, therefore $\Omega = \Omega_v$. Data were obtained at spin coefficients ($\Omega_v b/2V$) of 0.0, 0.075, 0.1, 0.15, 0.20, 0.25, and 0.30. The axial force $\Delta C_x$, and pitching moment $\Delta C_m$ rotary balance coefficients are presented in Figures B.24 and B.25. These curves are the same as those presented in Reference 2. The remaining coefficients have been changed from that presented in Reference 2 based on the second more current series rotary balance tests. The updated coefficients $\Delta C_z$, $\Delta C_n$, $\Delta C_l$, and $\Delta C_y$ are presented as a function $\Omega_v b/2V$ at various angles of attack in Figures B.26 through B.29.

APPENDIX B

B.3.1. Rotary Balance Data Below 35° Angle of Attack - A detail discussion of the method used in generating rotary balance data and adjustments made to the rotary balance wind tunnel data are presented in Appendix D.

COPY AVAILABLE TO DDC DOES NOT
PERMIT FULLY LEGIBLE PRODUCTION

## MODEL F-4E

## VARIATION OF NORMAL FORCE COEFFICIENT WITH ANGLE OF ATTACK

M = .2

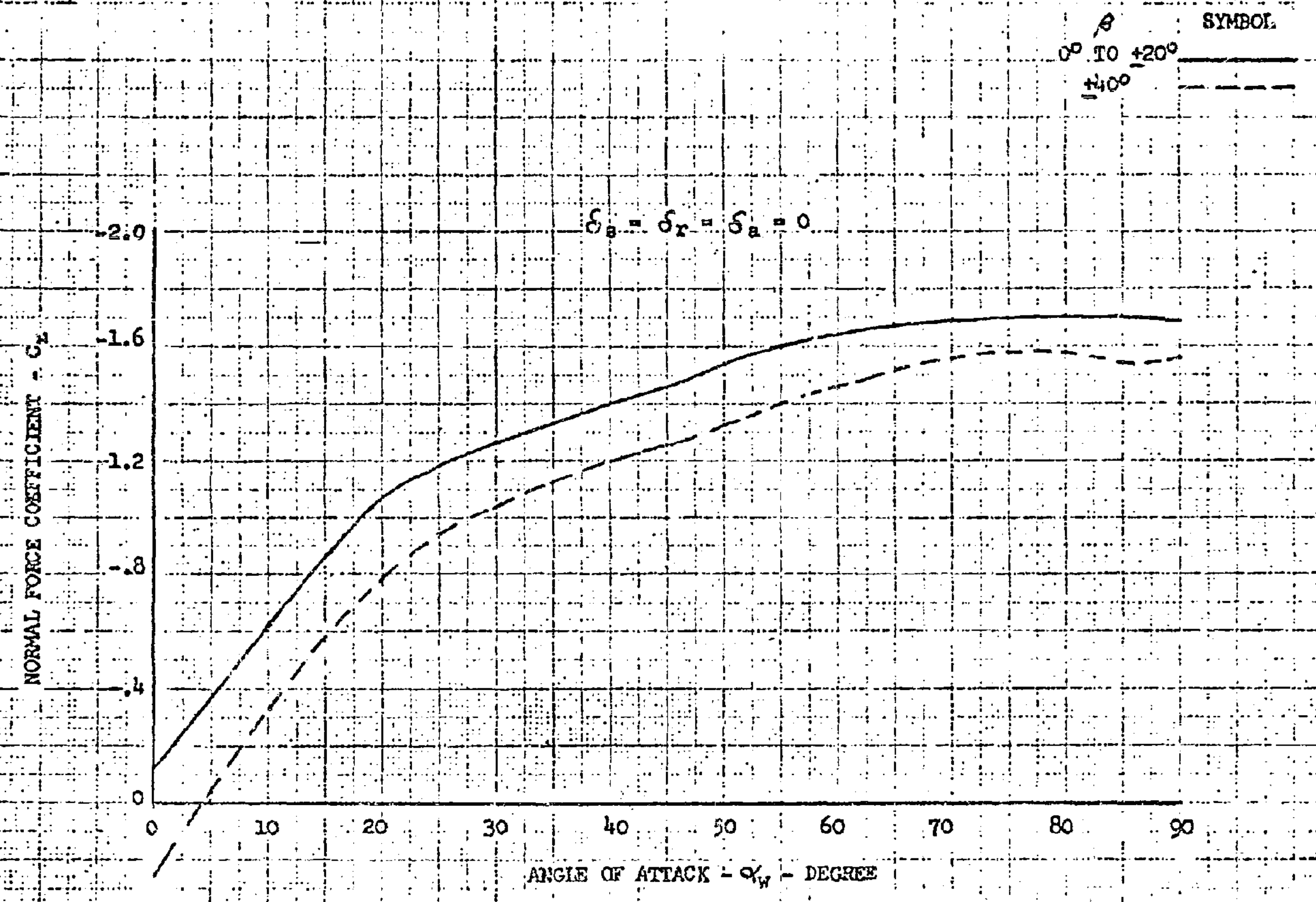

Figure B.1

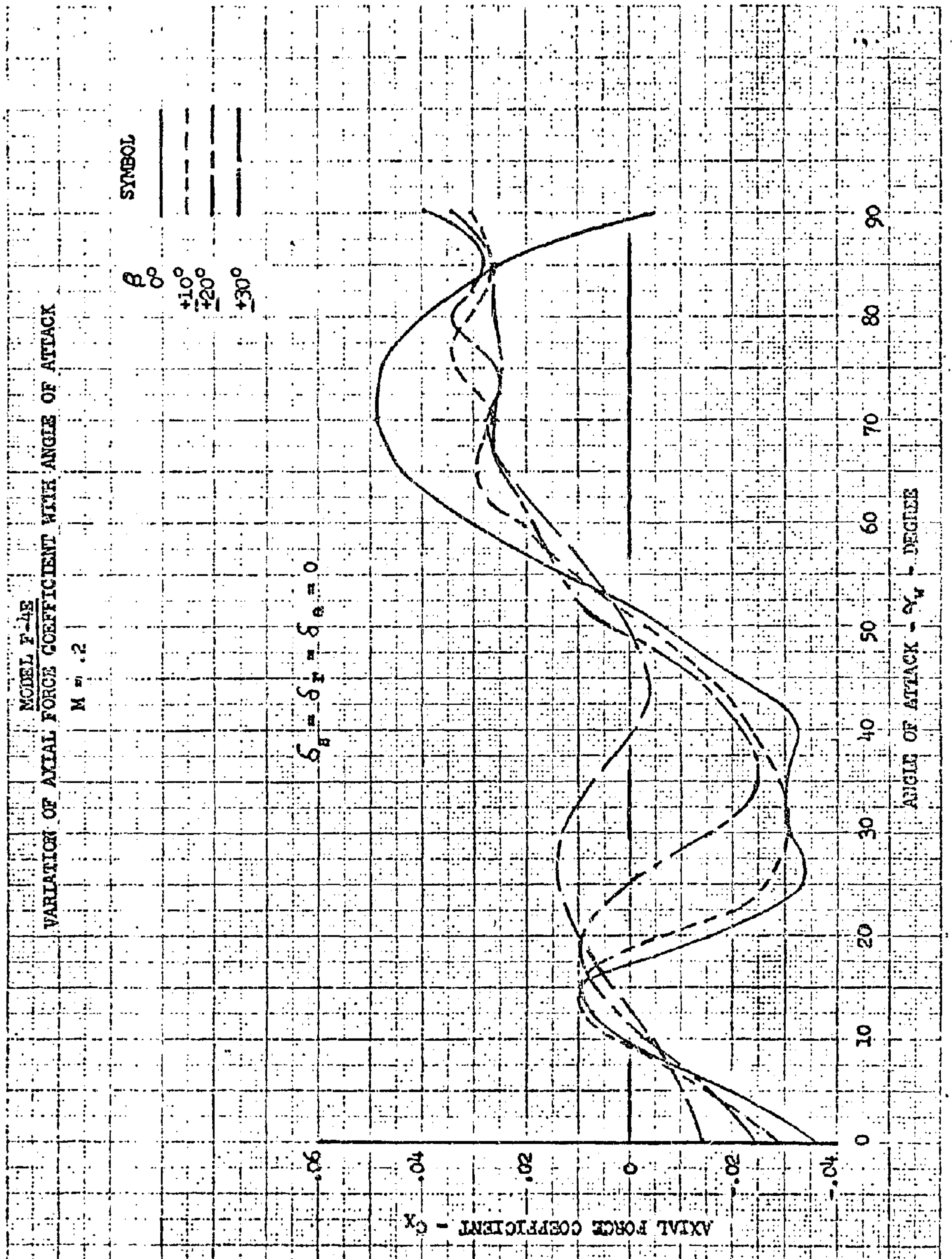

MODEL F-4E

VARIATION OF AXIAL FORCE COEFFICIENT WITH ANGLE OF ATTACK

M = .2

$\delta_s = \delta_r = \delta_a = 0$

Figure B.2

NATIONAL TRACING PAPER
INDIANAPOLIS, INDIANA

LITHO IN U.S.A.

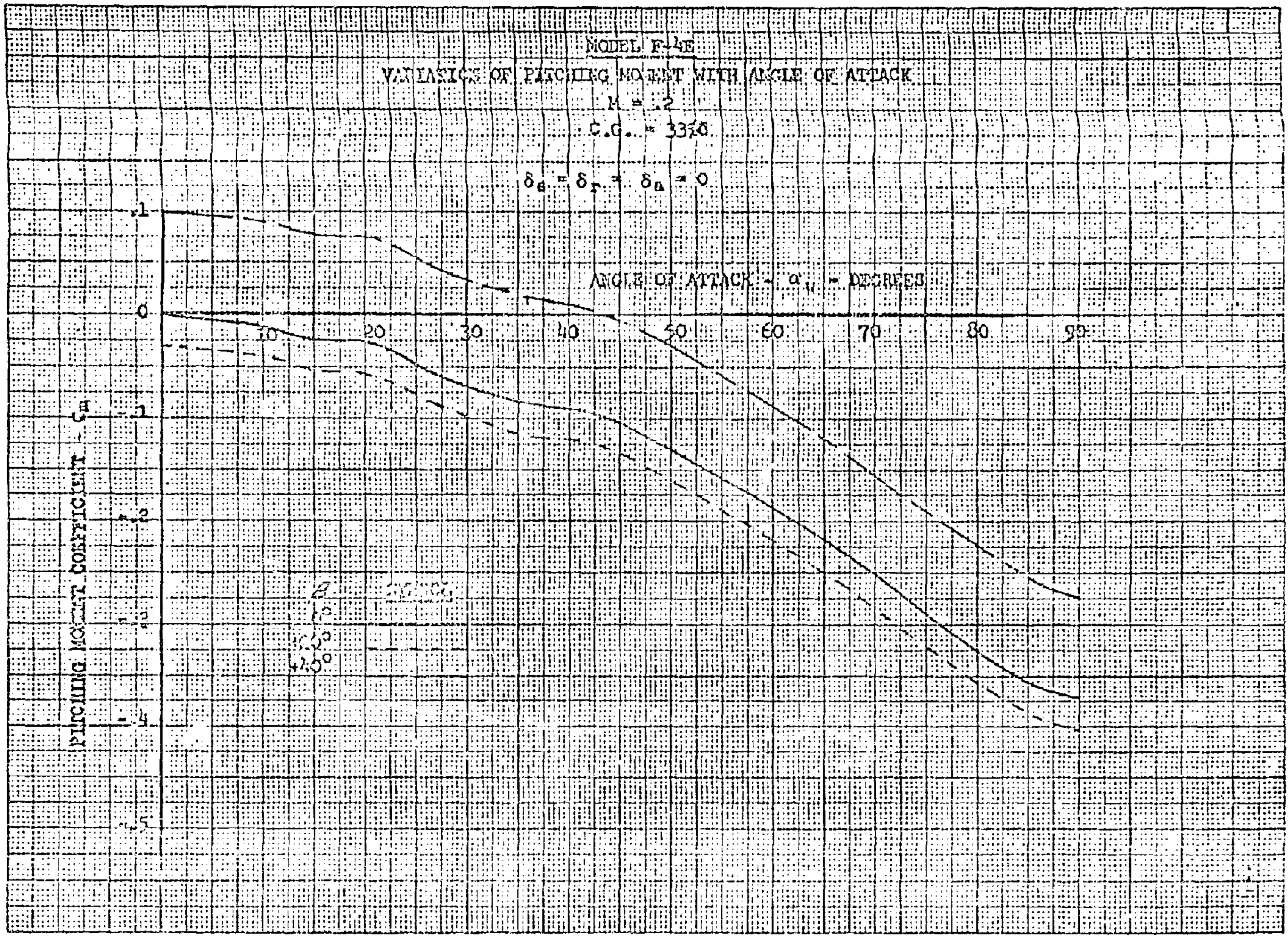

Figure B.3

[illegible]

VARIATION OF ROLLING MOMENT COEFFICIENT WITH SIDESLIP ANGLE

M = .2

$\delta_a = \delta_r = \delta_e = 0$

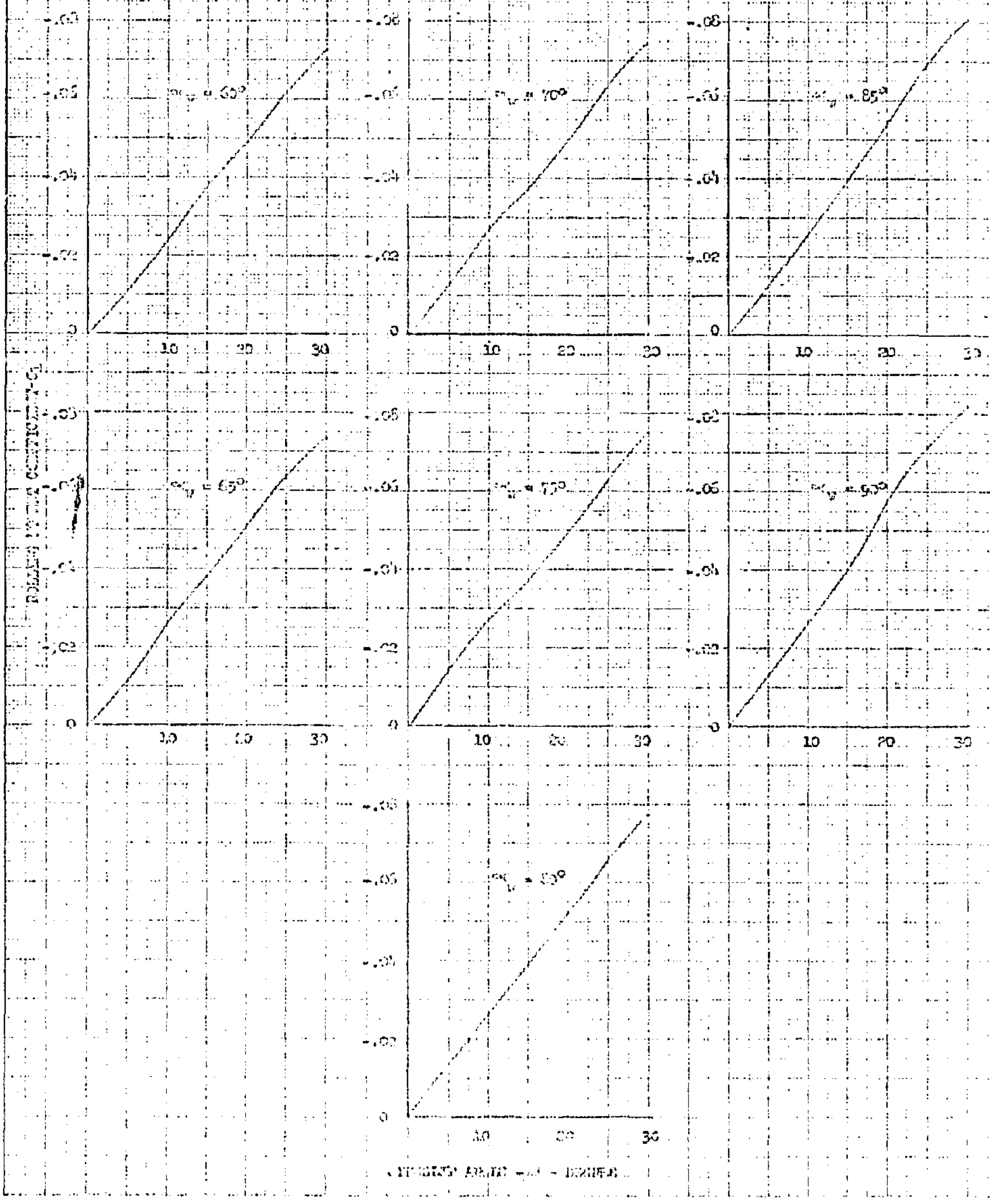

VARIATION OF ROLLING [illegible] COEFFICIENT WITH SIDESLIP ANGLE [illegible]

M = .2

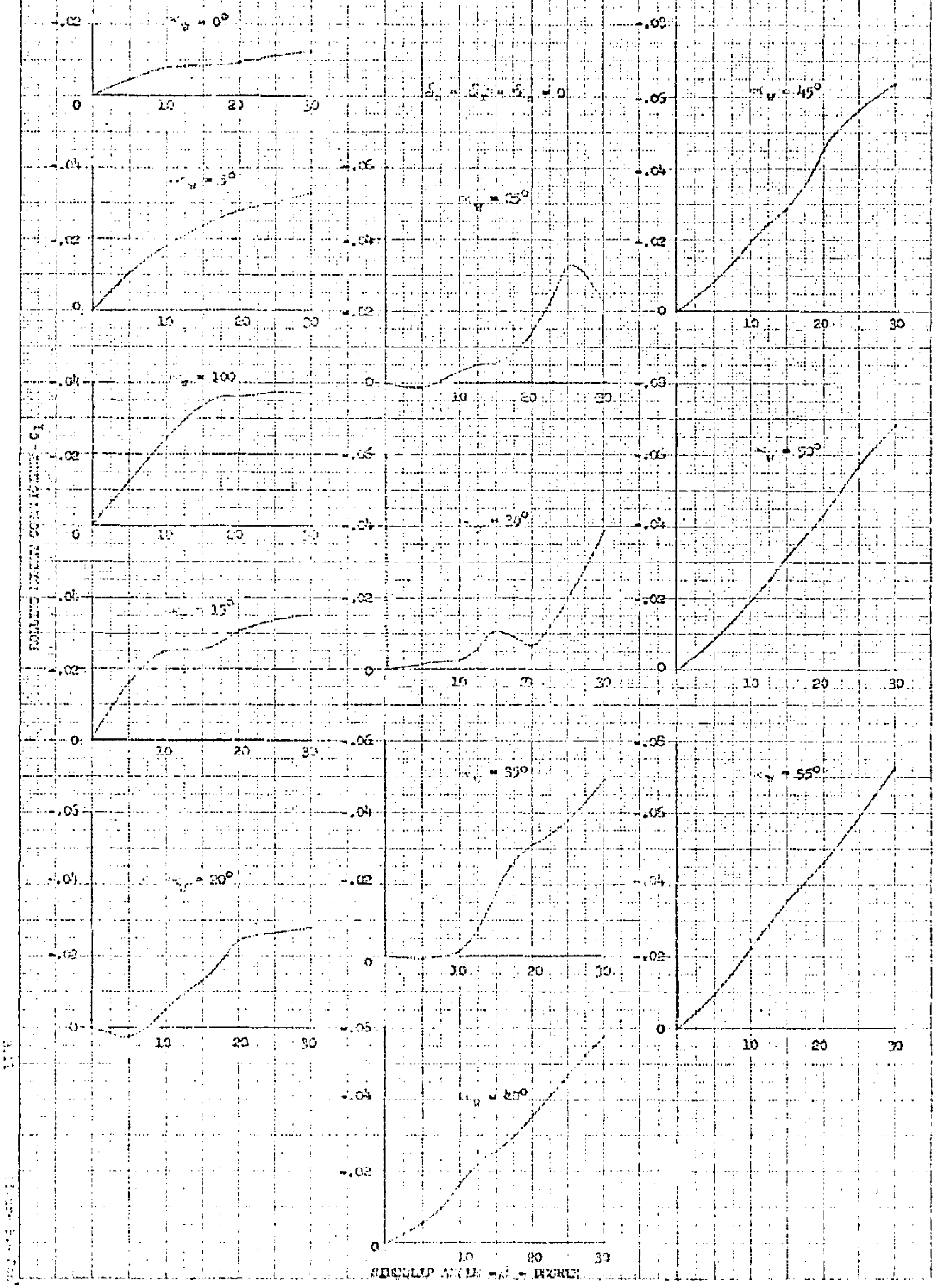

[illegible]

VARIATION OF SIDE FORCE COEFFICIENT WITH DIHEDRAL ANGLE

[illegible]

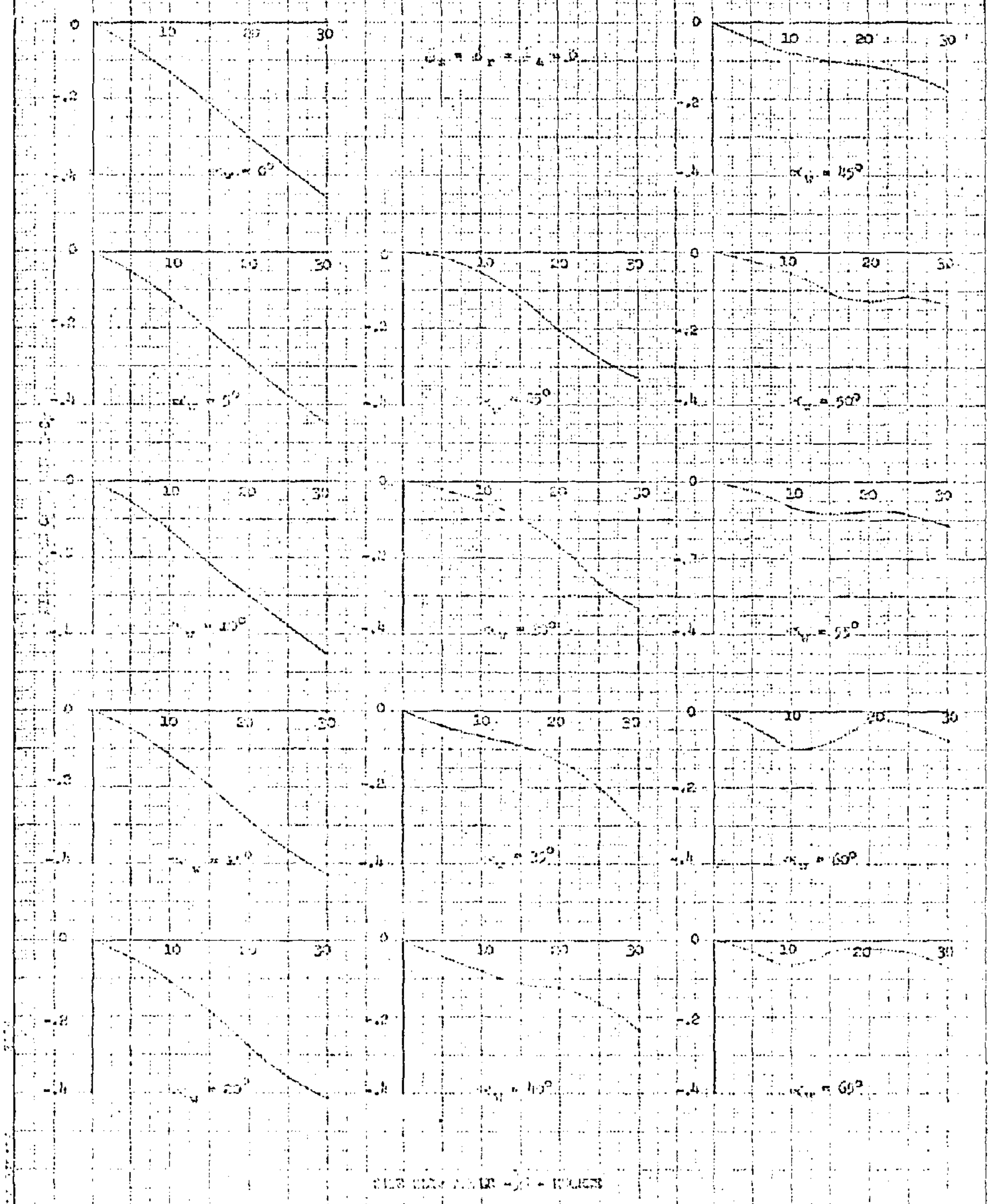

MODEL F-4E

VARIATION OF SIDE FORCE COEFFICIENT WITH SIDESLIP ANGLE

M = .2

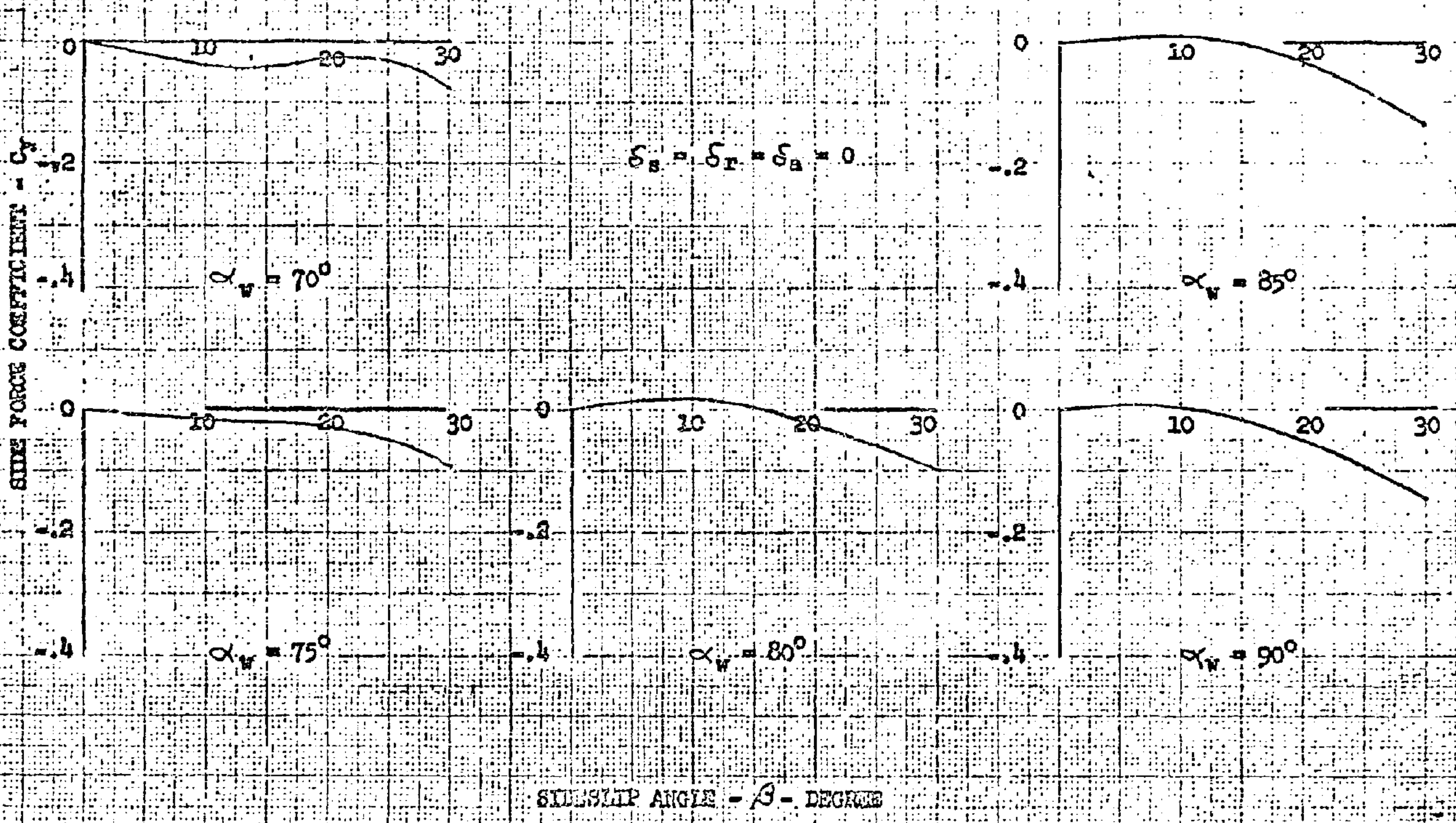

Figure B.5 Con't

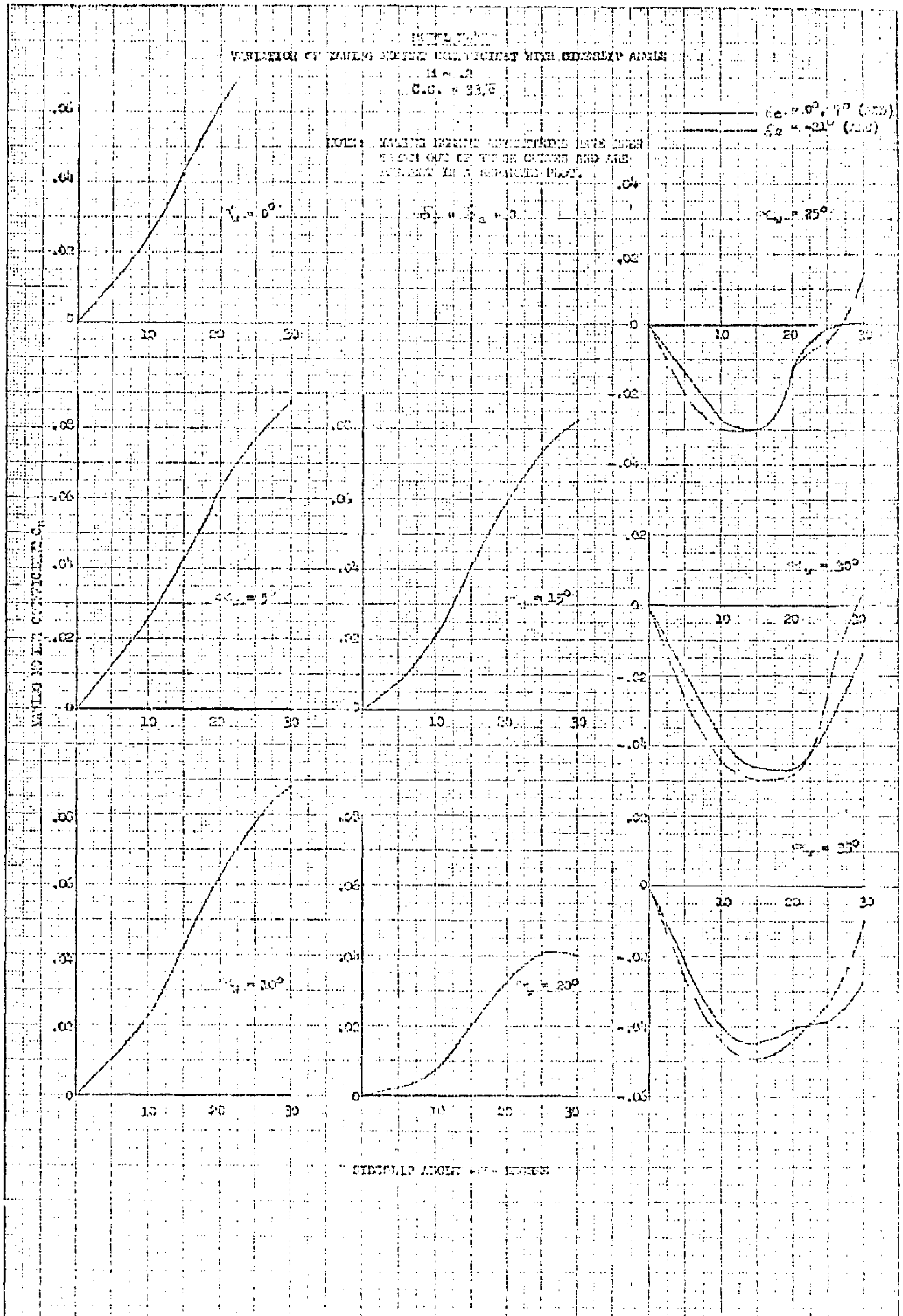
VARIATION OF YAWING MOMENT COEFFICIENT WITH SIDESLIP ANGLE
C.G. = 33%
NOTE: YAWING MOMENT INCREMENTS HAVE BEEN TAKEN OUT OF THESE CURVES AND ARE PLOTTED IN A SEPARATE PLOT.
δe = 0°, 7° (·)
δa = -21° (·)
δr = δa = 0
αw = 0°
αw = 5°
αw = 10°
αw = 15°
αw = 20°
αw = 25°
αw = 30°
αw = 35°
YAWING MOMENT COEFFICIENT, Cn
SIDESLIP ANGLE ψ - DEGREES
0
.02
.04
.06
.08
-.02
-.04
-.06
10
20
30

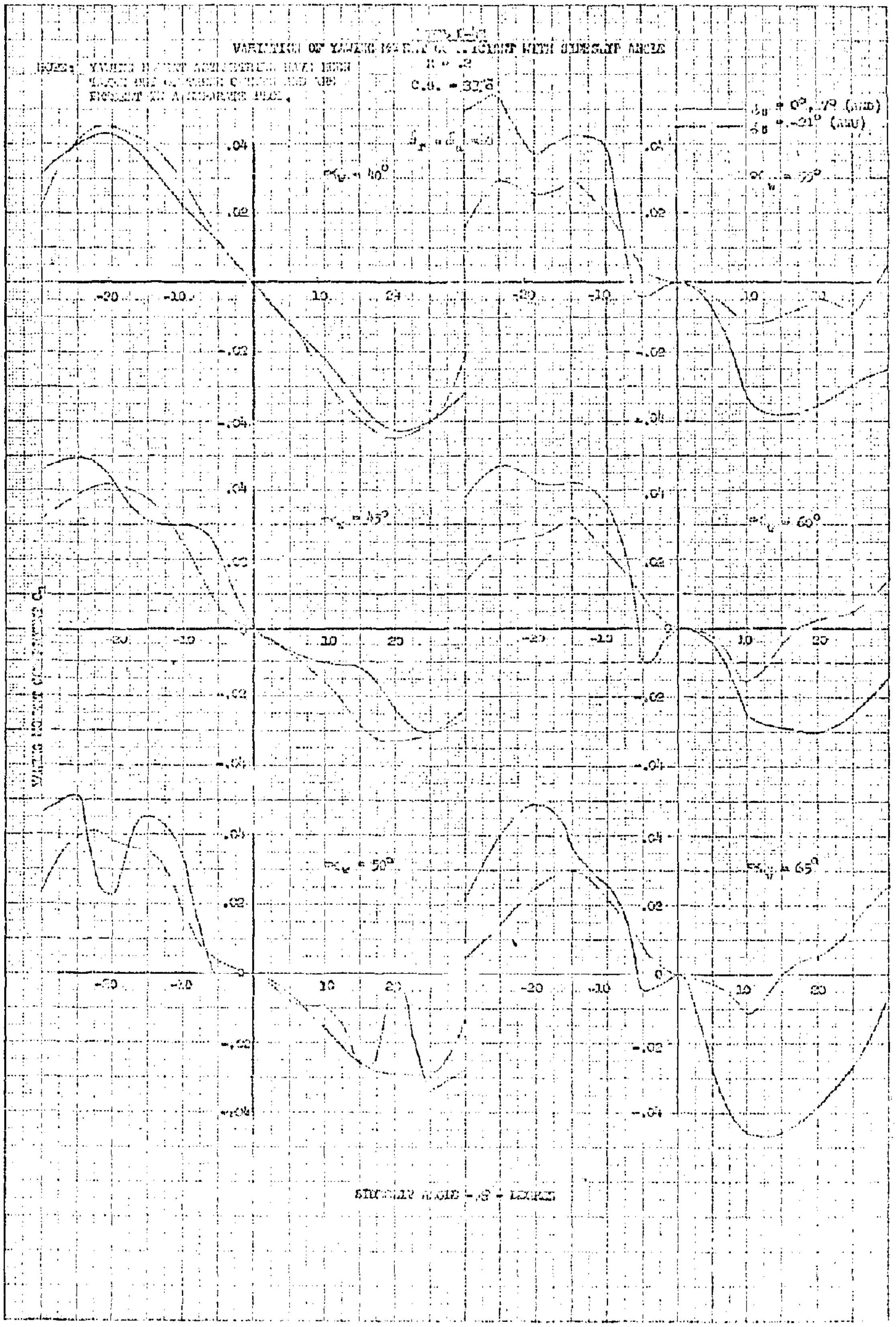

Figure 1.1 Cont'd

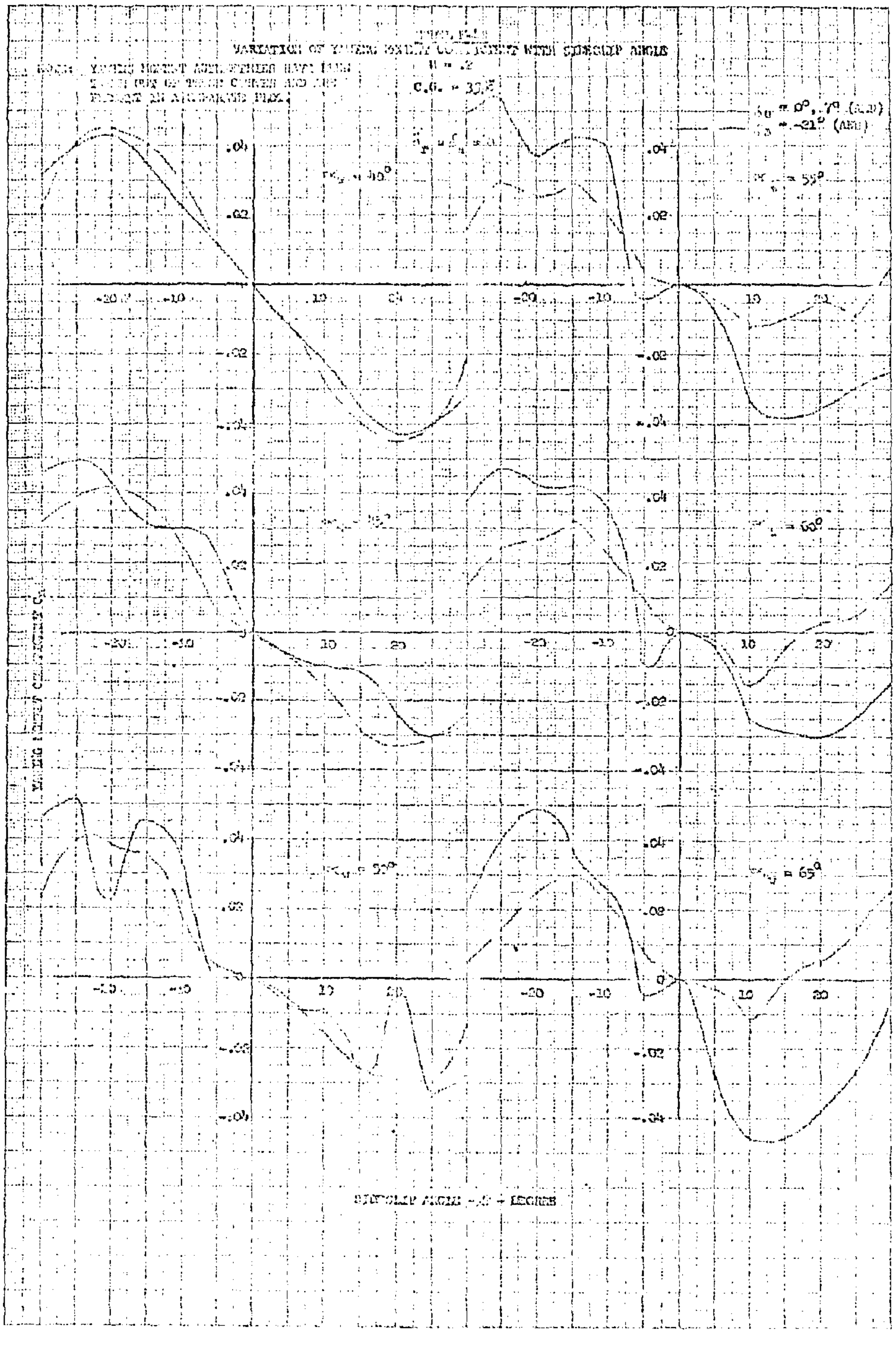

VARIATION OF YAWING MOMENT COEFFICIENT WITH SIDESLIP ANGLE
M = .2
C.G. = 30%
NOTE: YAWING MOMENT ASYMMETRIES HAVE BEEN ... OUT OF THESE CURVES AND ARE ... IN APPENDIX ...
$\delta_r = \delta_a = 0$
$\delta_e = 0°, -7°$
$\delta_a = -21°$
$\alpha_u = 40°$
$\alpha_u = 45°$
$\alpha_u = 50°$
$\alpha_u = 55°$
$\alpha_u = 60°$
$\alpha_u = 65°$
.04
.02
0
-.02
-.04
-20
-10
10
20
YAWING MOMENT COEFFICIENT $C_n$
SIDESLIP ANGLE -β- DEGREES

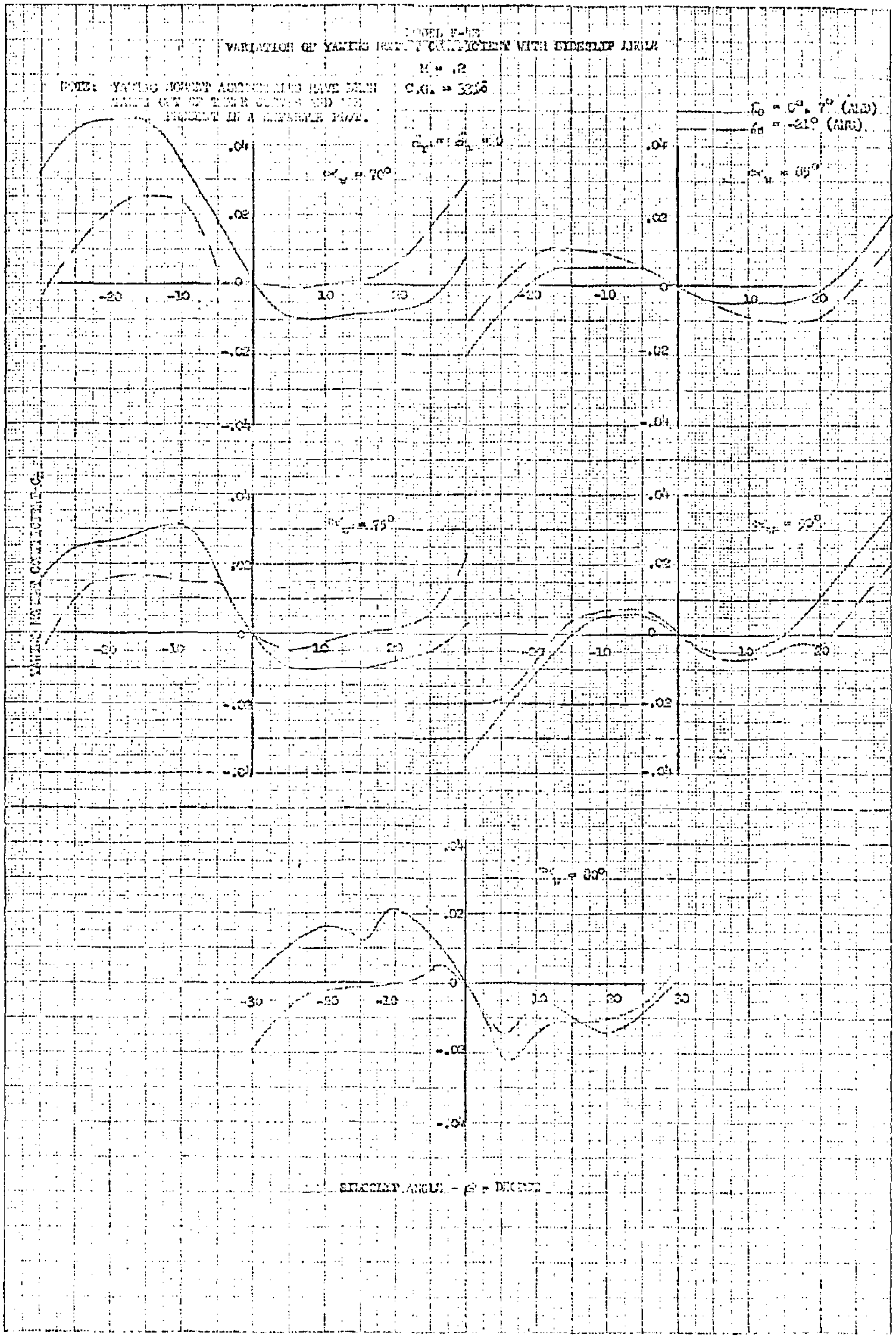

Figure 9.6 Cont'd.

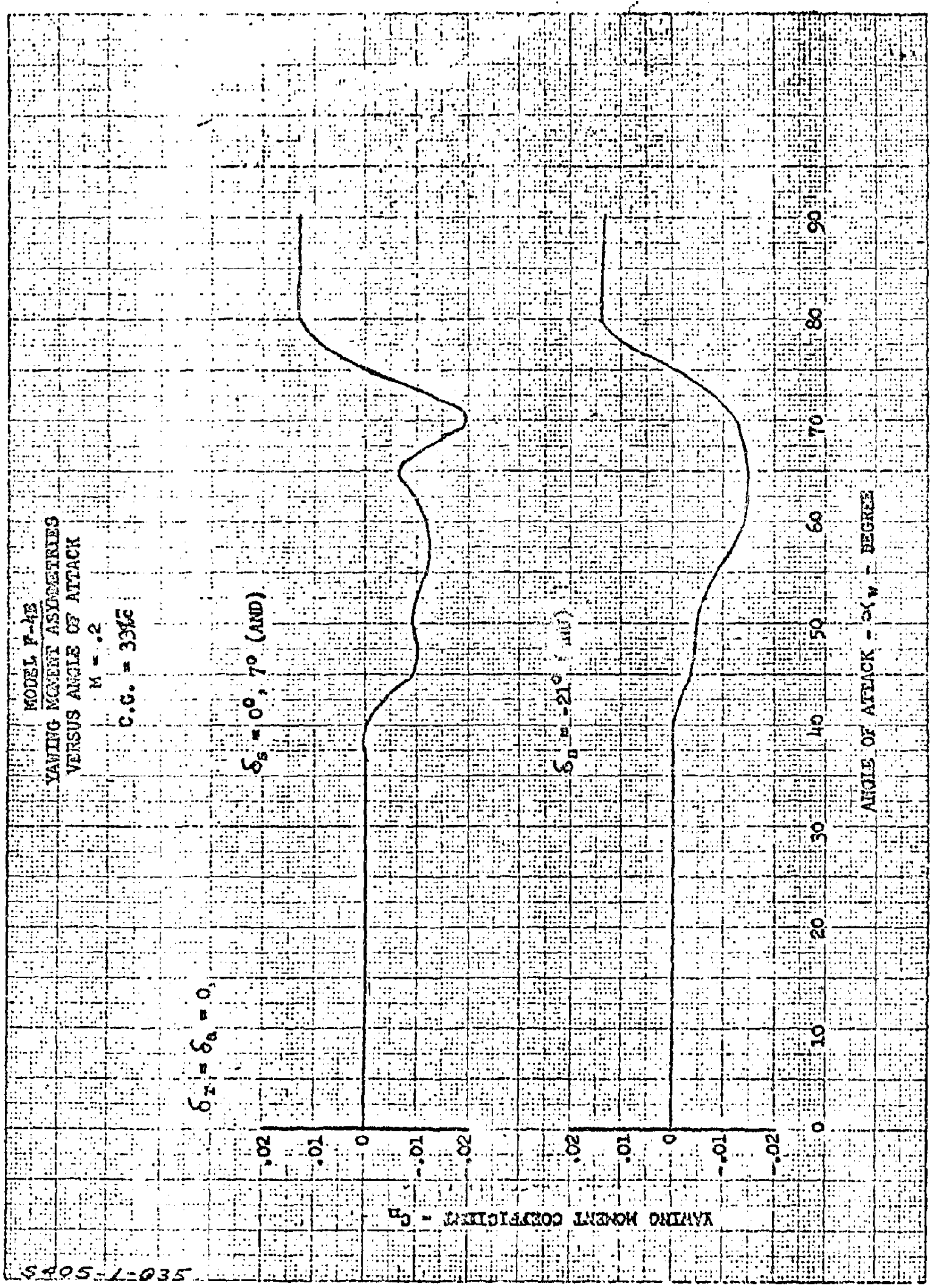
MODEL F-4E
YAWING MOMENT ASYMMETRIES
VERSUS ANGLE OF ATTACK
M = .2
C.G. = 33%c
$\delta_r = \delta_a = 0$
$\delta_a = 0°, 7°$ (AND)
$\delta_a = -21°$ (AND)
.02
.01
0
-.01
-.02
YAWING MOMENT COEFFICIENT - $C_n$
ANGLE OF ATTACK - $\alpha_W$ - DEGREE
0
10
20
30
40
50
60
70
80
90
S405-1-035

Figure B.7

## MODEL F-4E

## NORMAL FORCE DUE TO STABILATOR DEFLECTION VERSUS ANGLE OF ATTACK

M = .2

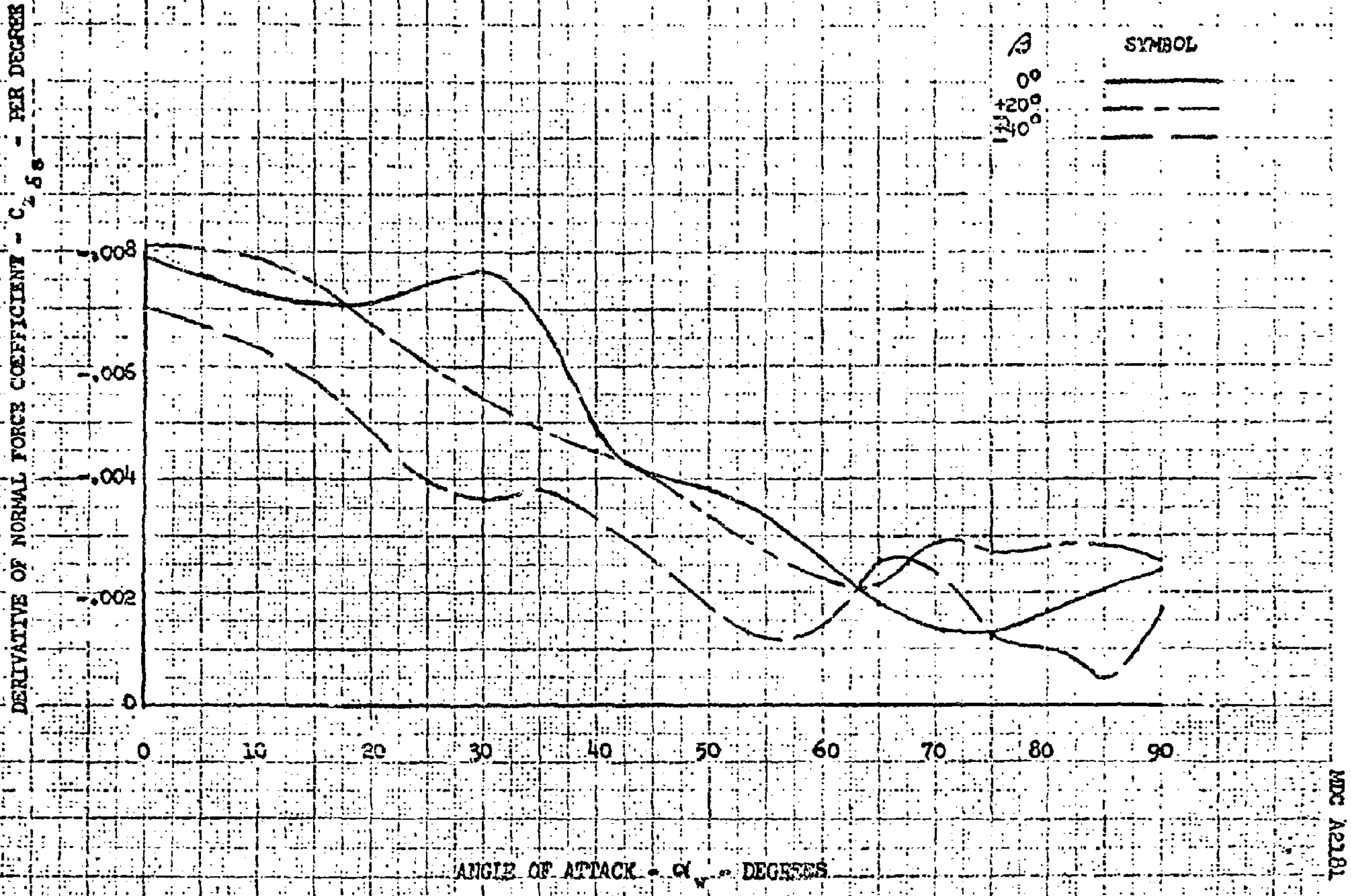

Figure B.8

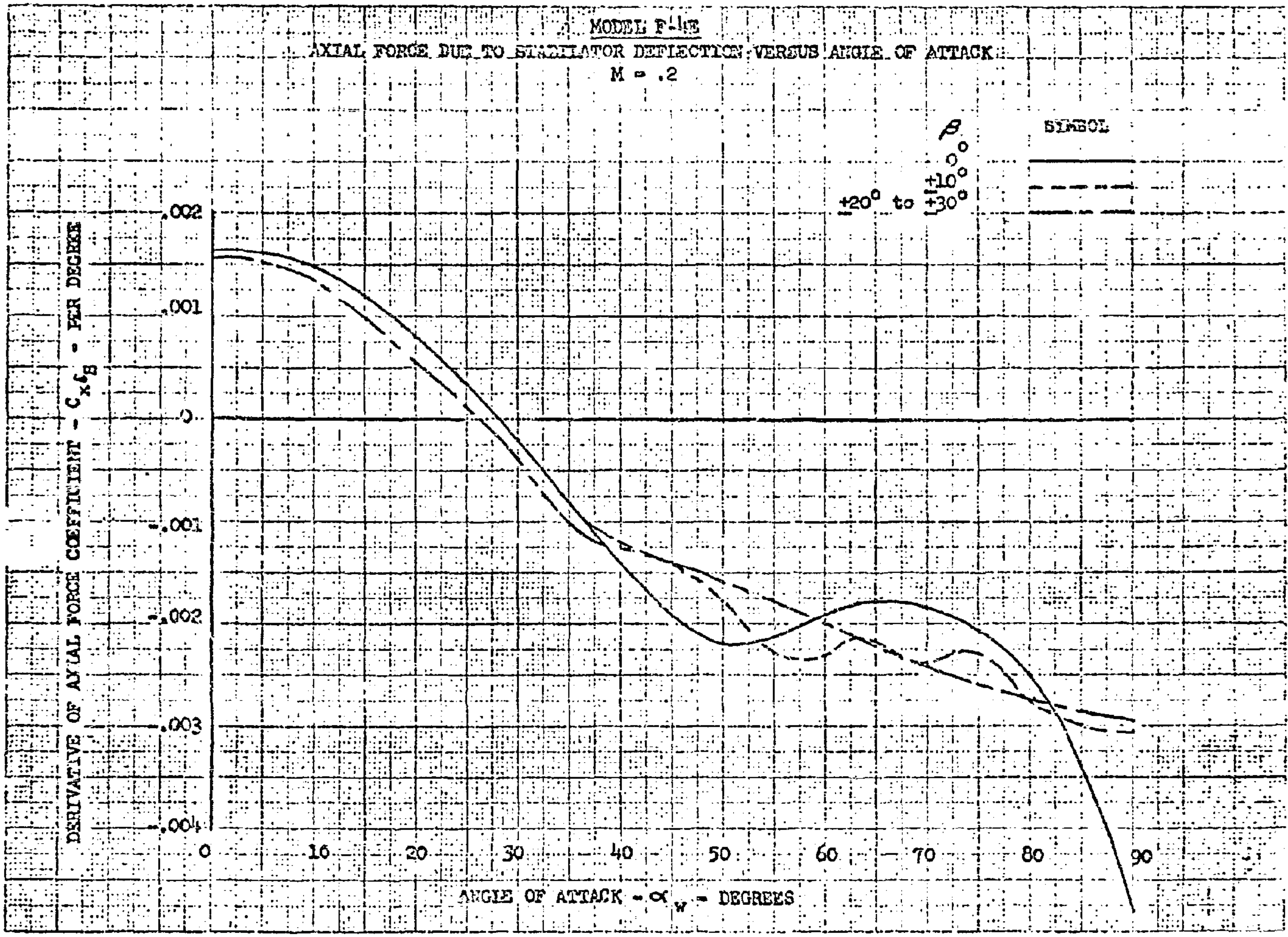
MODEL F-4E

AXIAL FORCE DUE TO STABILATOR DEFLECTION VERSUS ANGLE OF ATTACK

M = .2

Figure B.9

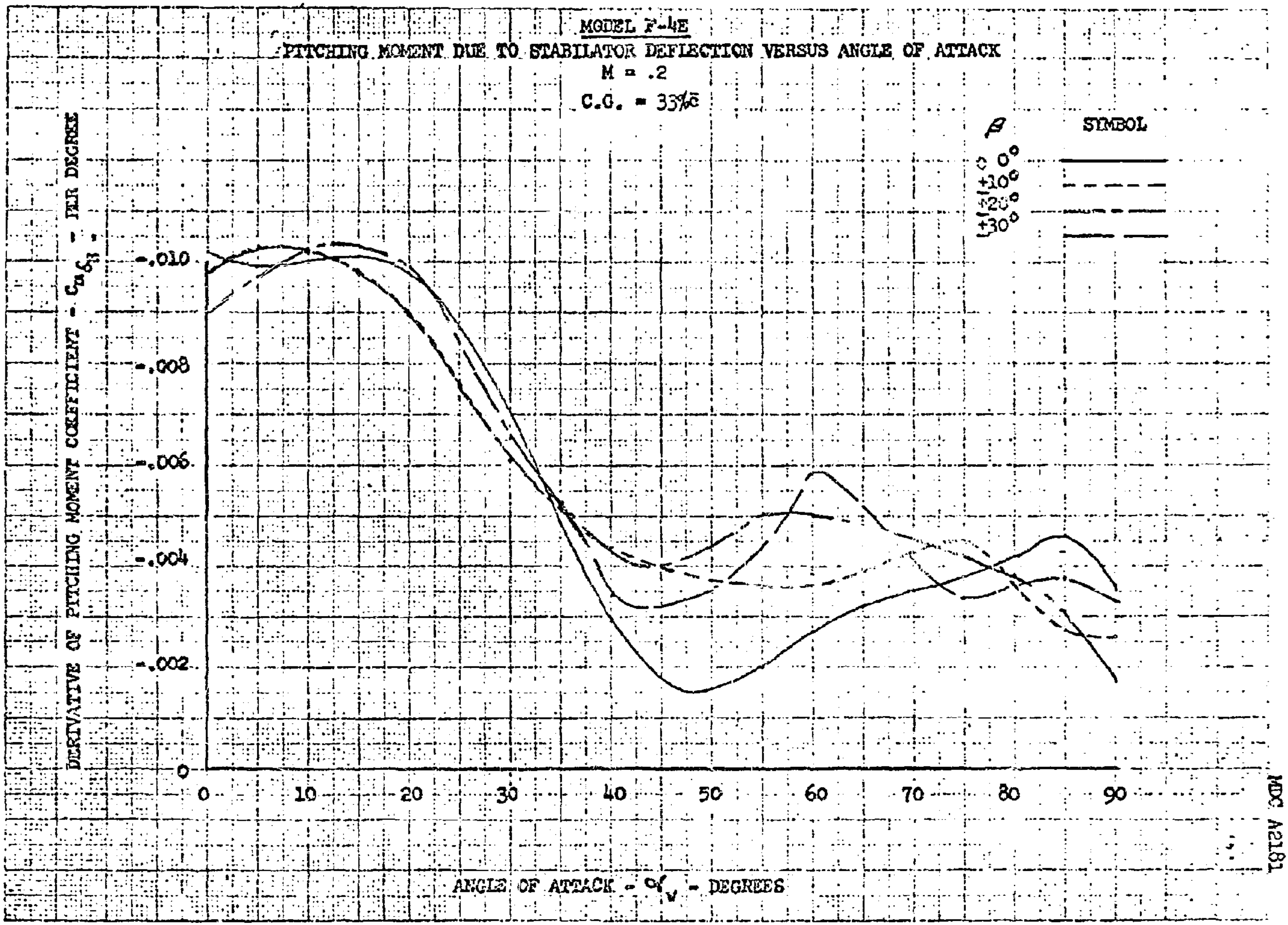

MODEL F-4E

PITCHING MOMENT DUE TO STABILATOR DEFLECTION VERSUS ANGLE OF ATTACK

M = .2

C.G. = 33%c̄

Figure B.10

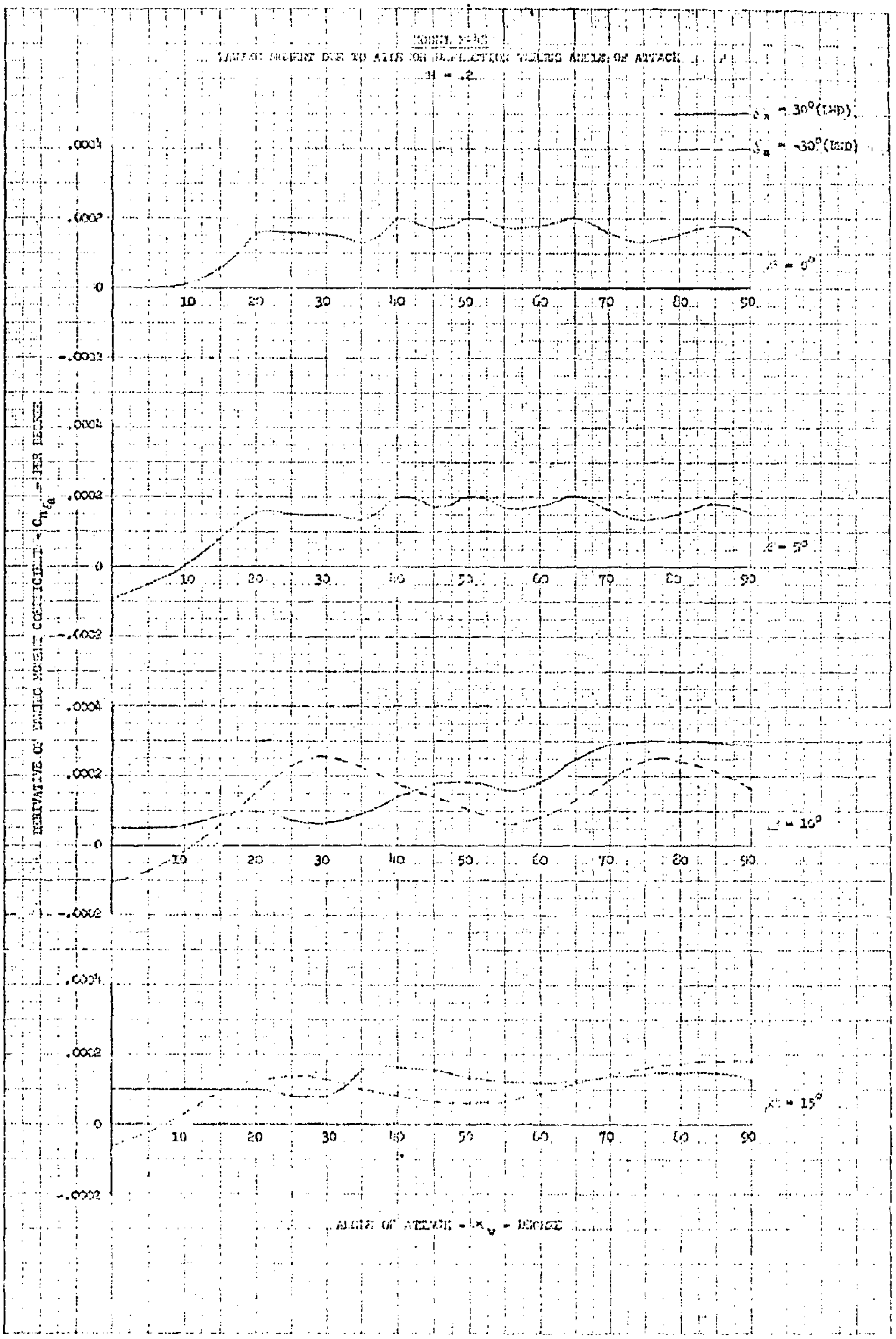MODEL [illegible]
YAWING MOMENT DUE TO AILERON DEFLECTION VERSUS ANGLE OF ATTACK
M = .2
δa = 30°(LHD)
δa = -30°(LHD)
.0004
.0002
0
-.0002
β = 0°
β = 5°
β = 10°
β = 15°
10
20
30
40
50
60
70
80
90
DERIVATIVE OF YAWING MOMENT COEFFICIENT - $C_{n_{\delta a}}$ - PER DEGREE
ANGLE OF ATTACK - $\alpha_v$ - DEGREE

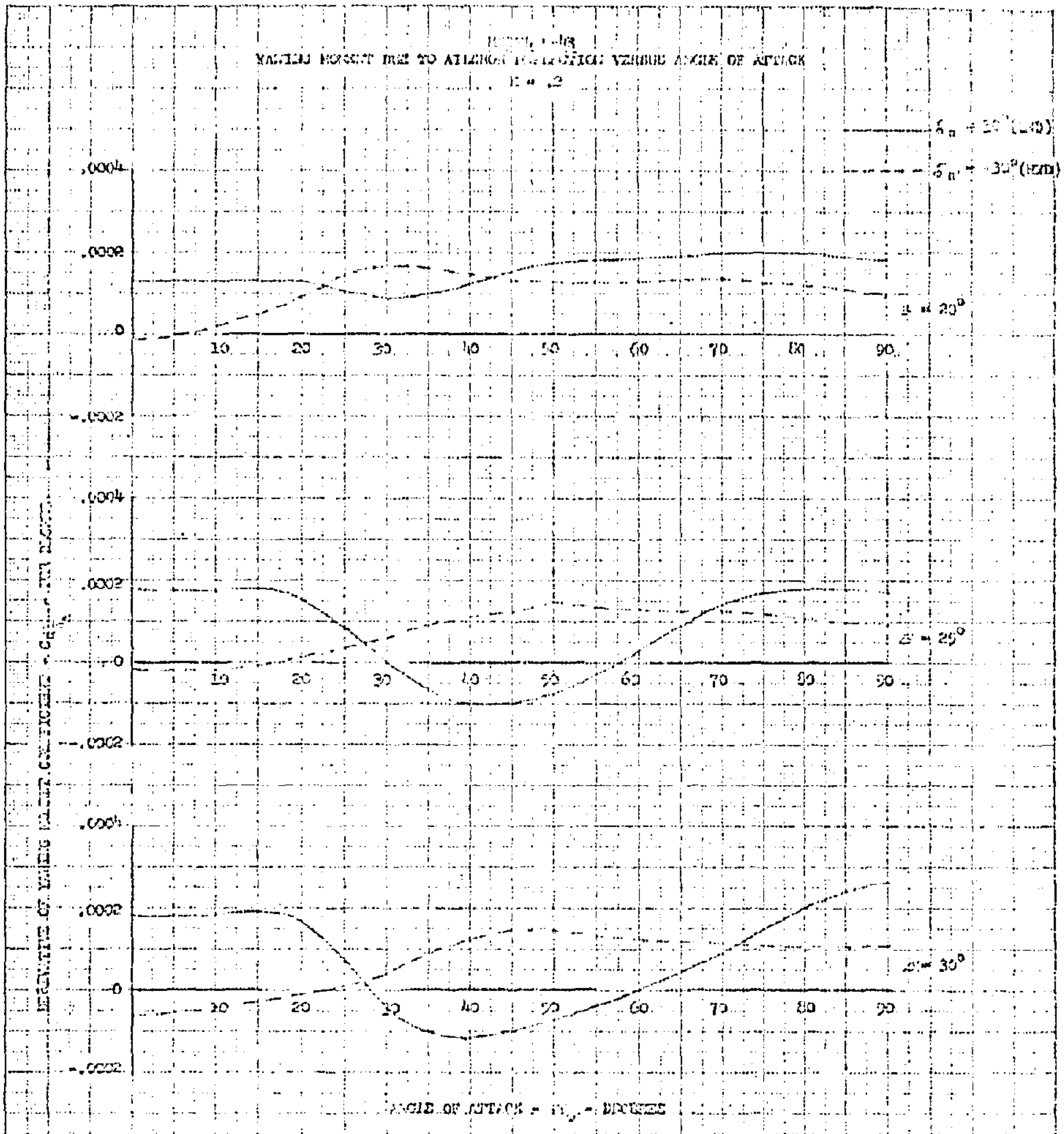
FIGURE 4-48

YAWING MOMENT DUE TO AILERON DEFLECTION VERSUS ANGLE OF ATTACK

M = .2

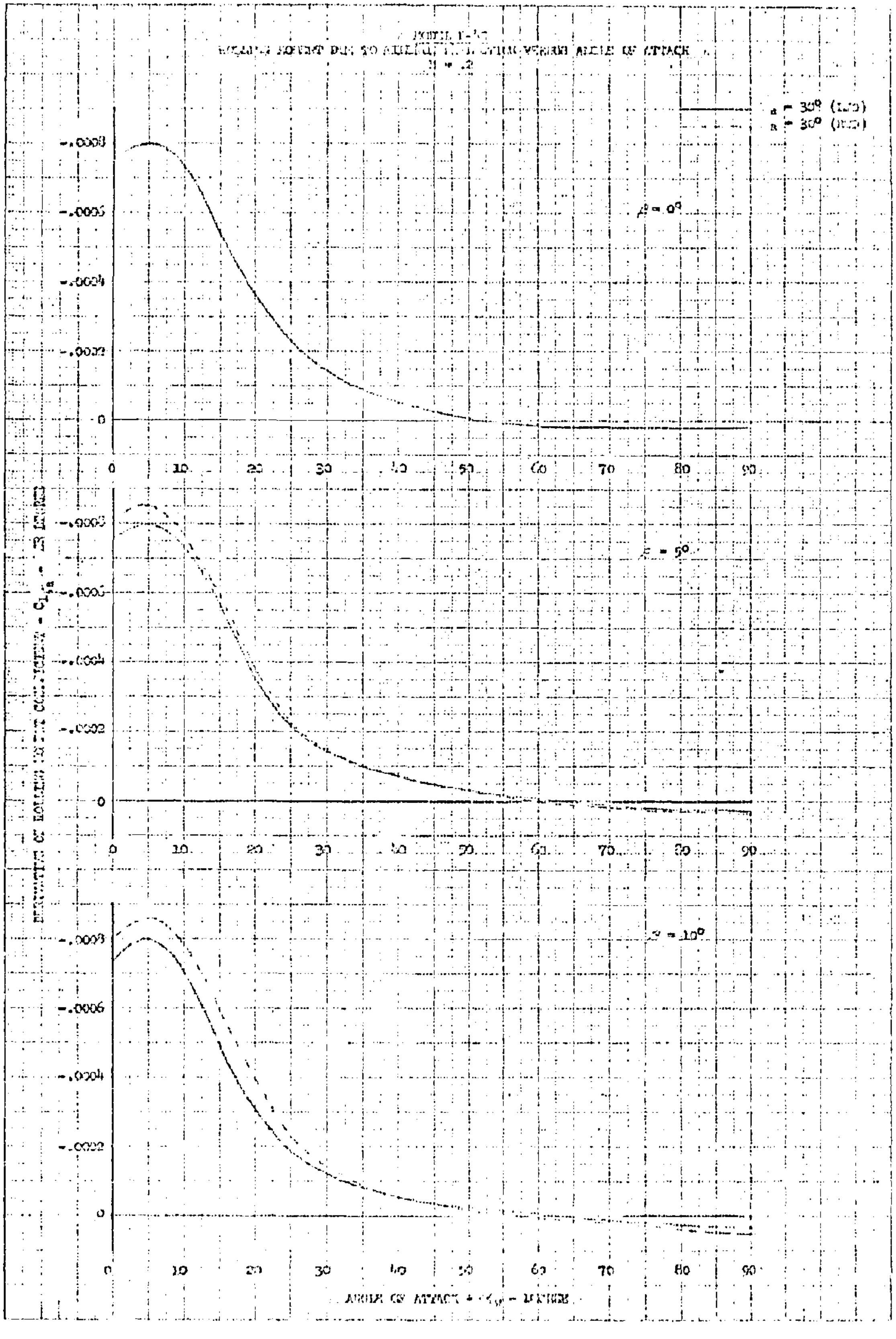
FIGURE I-57
ROLLING MOMENT DUE TO AILERON DEFLECTION VERSUS ANGLE OF ATTACK
M = .2

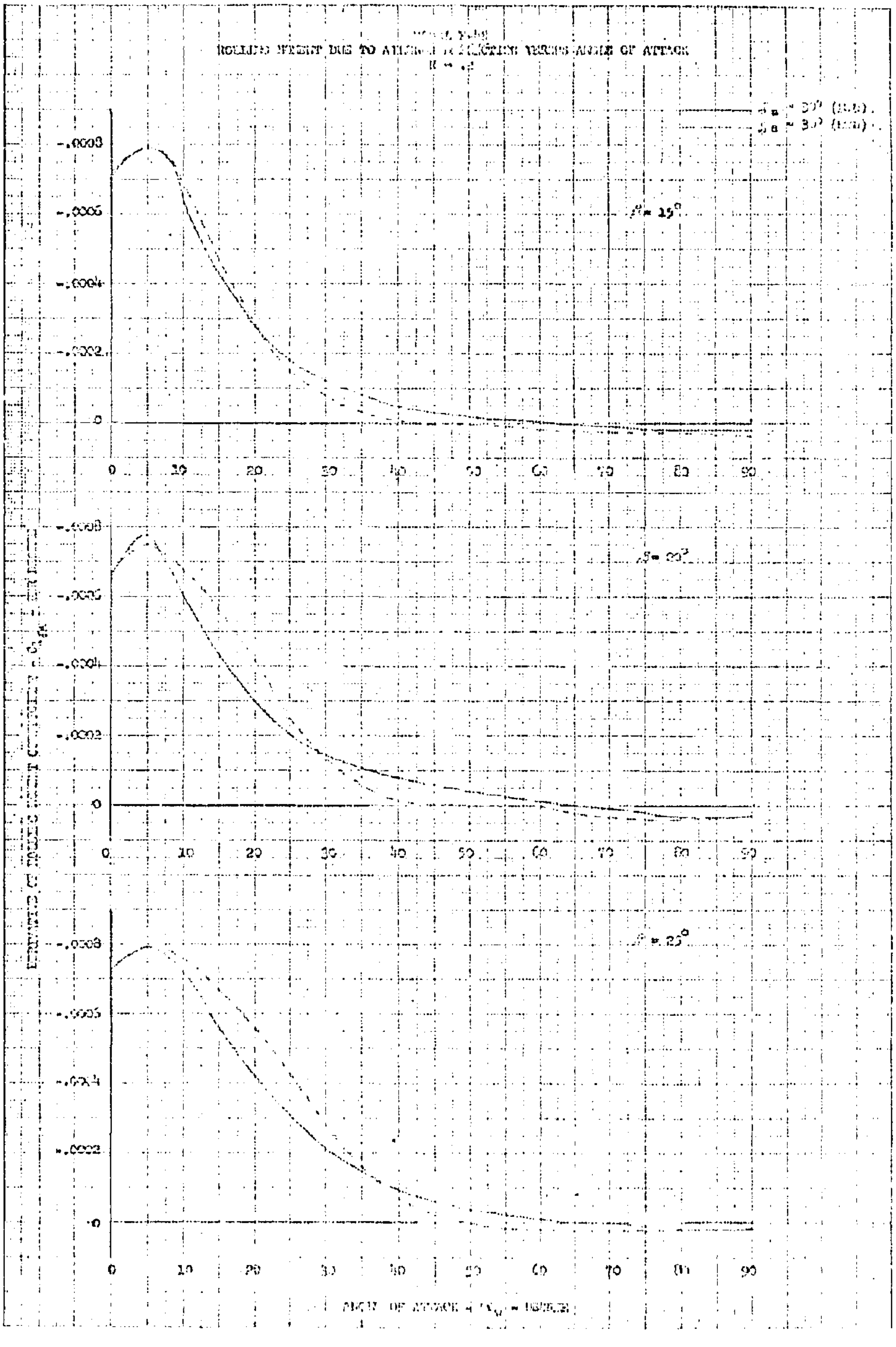

ROLLING MOMENT DUE TO AILERON DEFLECTION VERSUS ANGLE OF ATTACK

M = .2

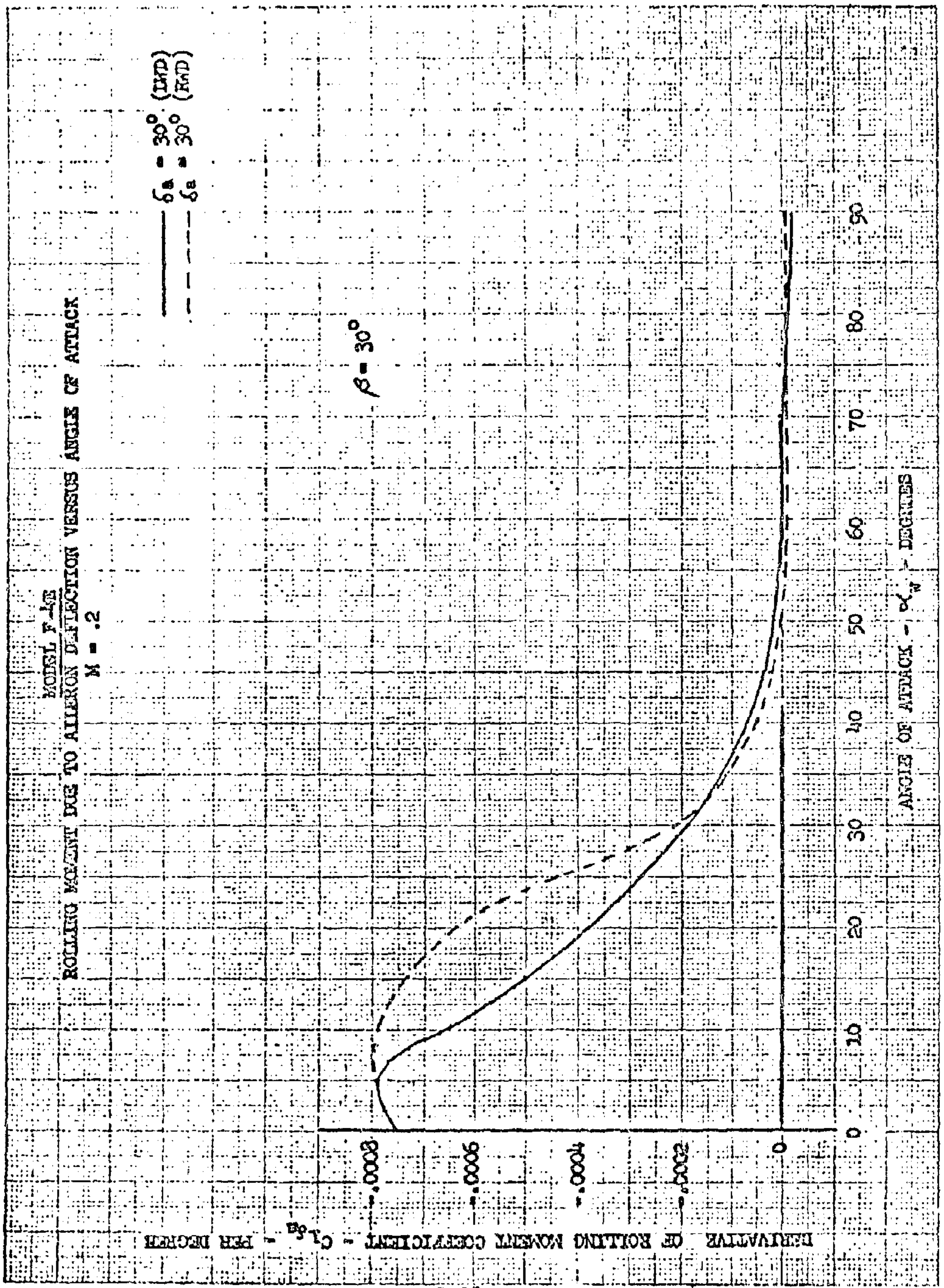

Figure B.12 Con't

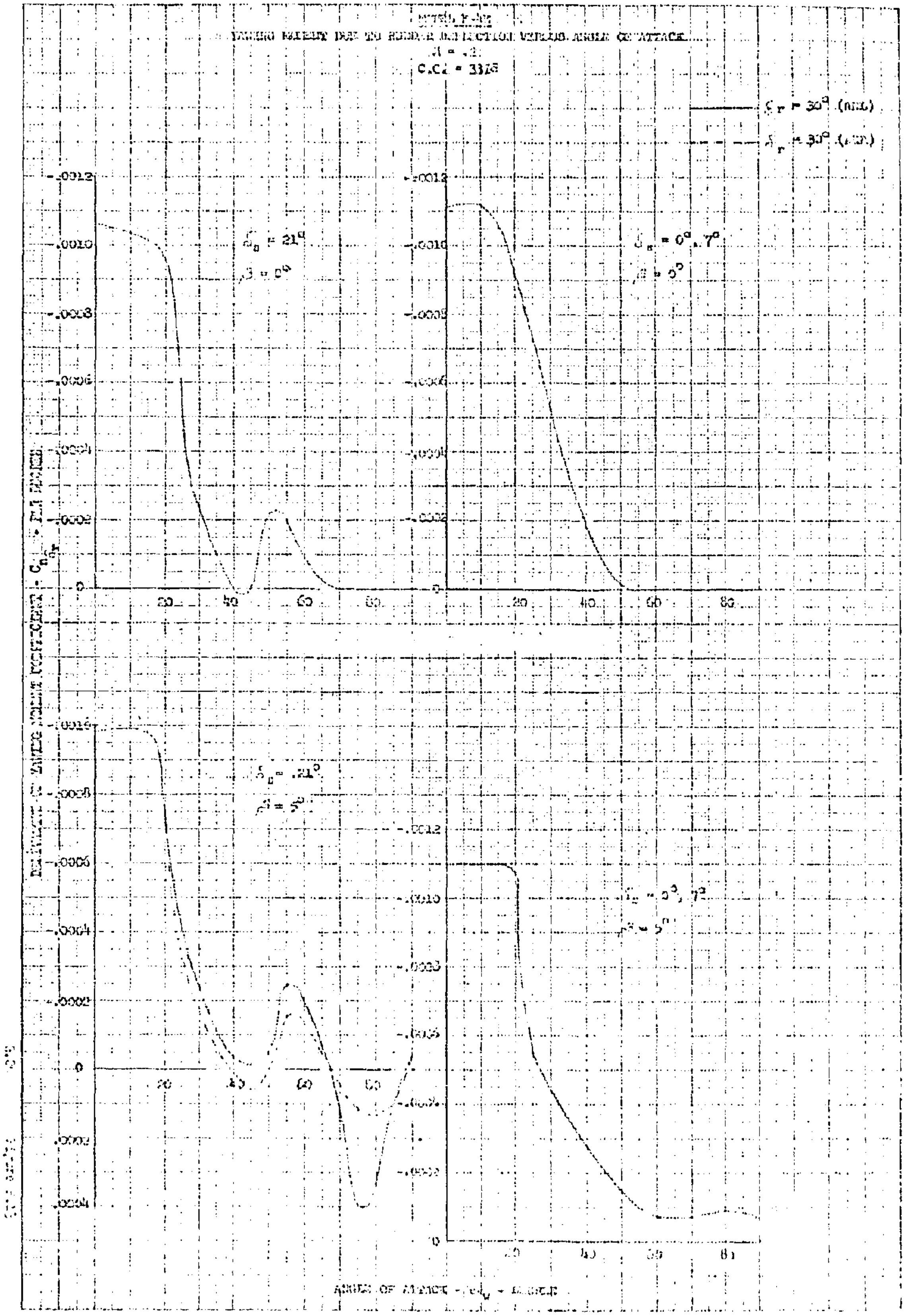

YAWING MOMENT DUE TO RUDDER DEFLECTION VERSUS ANGLE OF ATTACK

M = .2

C.G. = 33%

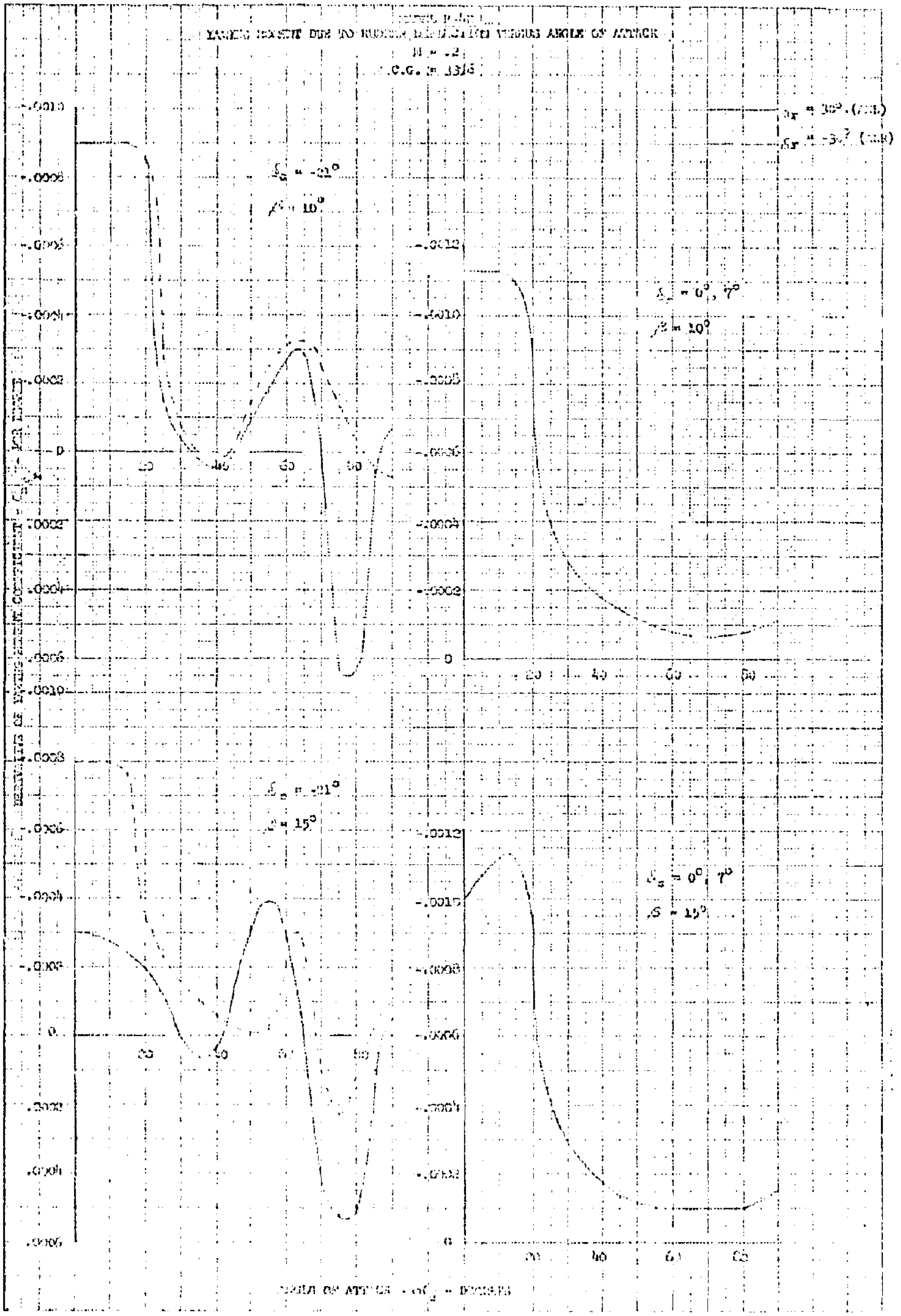

YAWING MOMENT DUE TO RUDDER DEFLECTION VERSUS ANGLE OF ATTACK

M = .2

C.G. = 33%

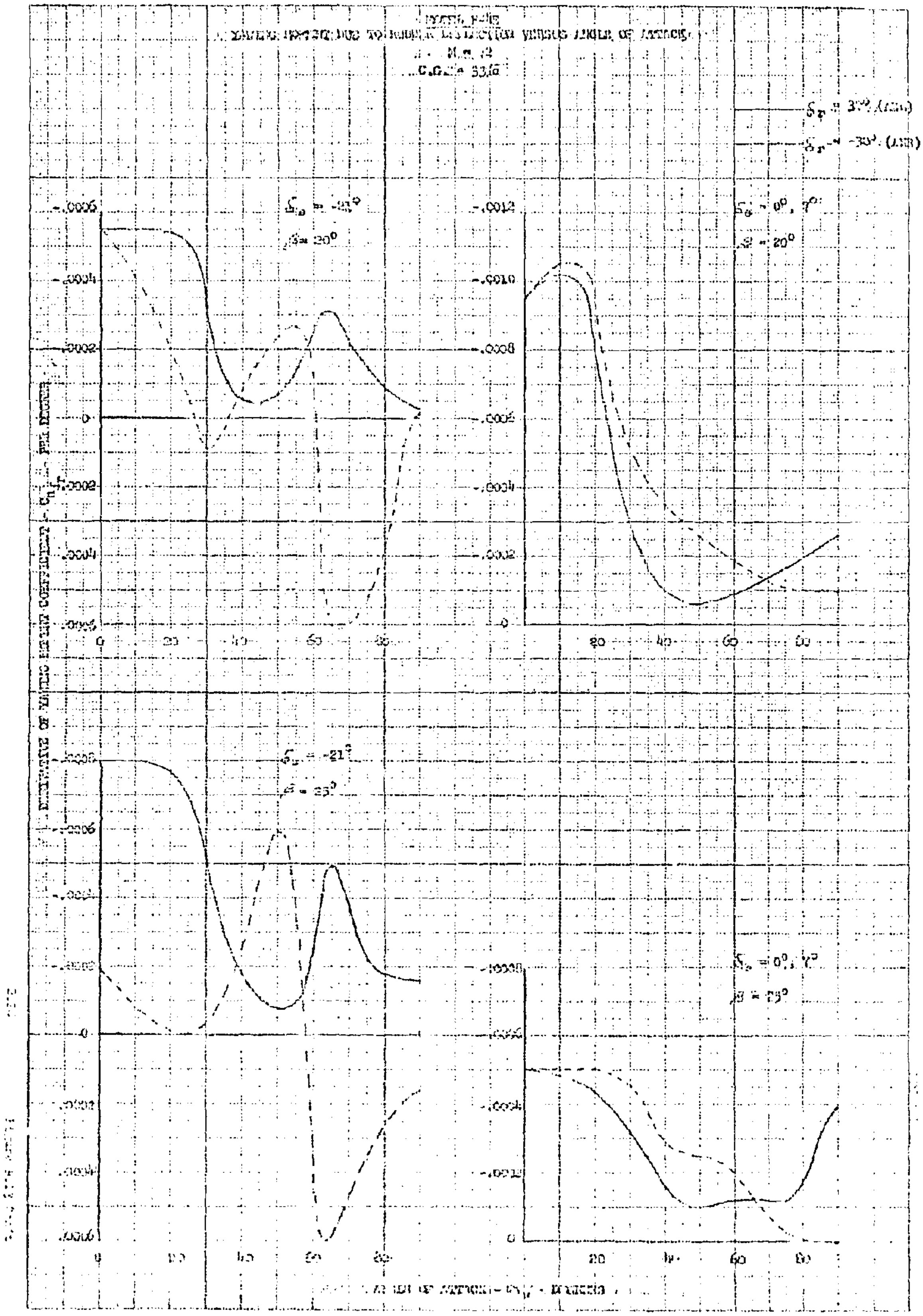
YAWING MOMENT DUE TO RUDDER DEFLECTION VERSUS ANGLE OF ATTACK
M = .2
C.G. = 33%
δr = 30° (AVG)
δr = -30° (AVG)
δa = -21°
β = 20°
δa = 0°, 7°
β = 20°
δa = -21°
β = 25°
δa = 0°, 7°
β = 25°
-.0006
-.0004
-.0002
0
.0002
.0004
.0006
-.0012
-.0010
-.0008
-.0006
-.0004
-.0002
0
-.0008
-.0006
-.0004
-.0002
0
.0002
.0004
.0006
-.0008
-.0006
-.0004
-.0002
0
0
20
40
60
80
20
40
60
80
ANGLE OF ATTACK - α - DEGREES

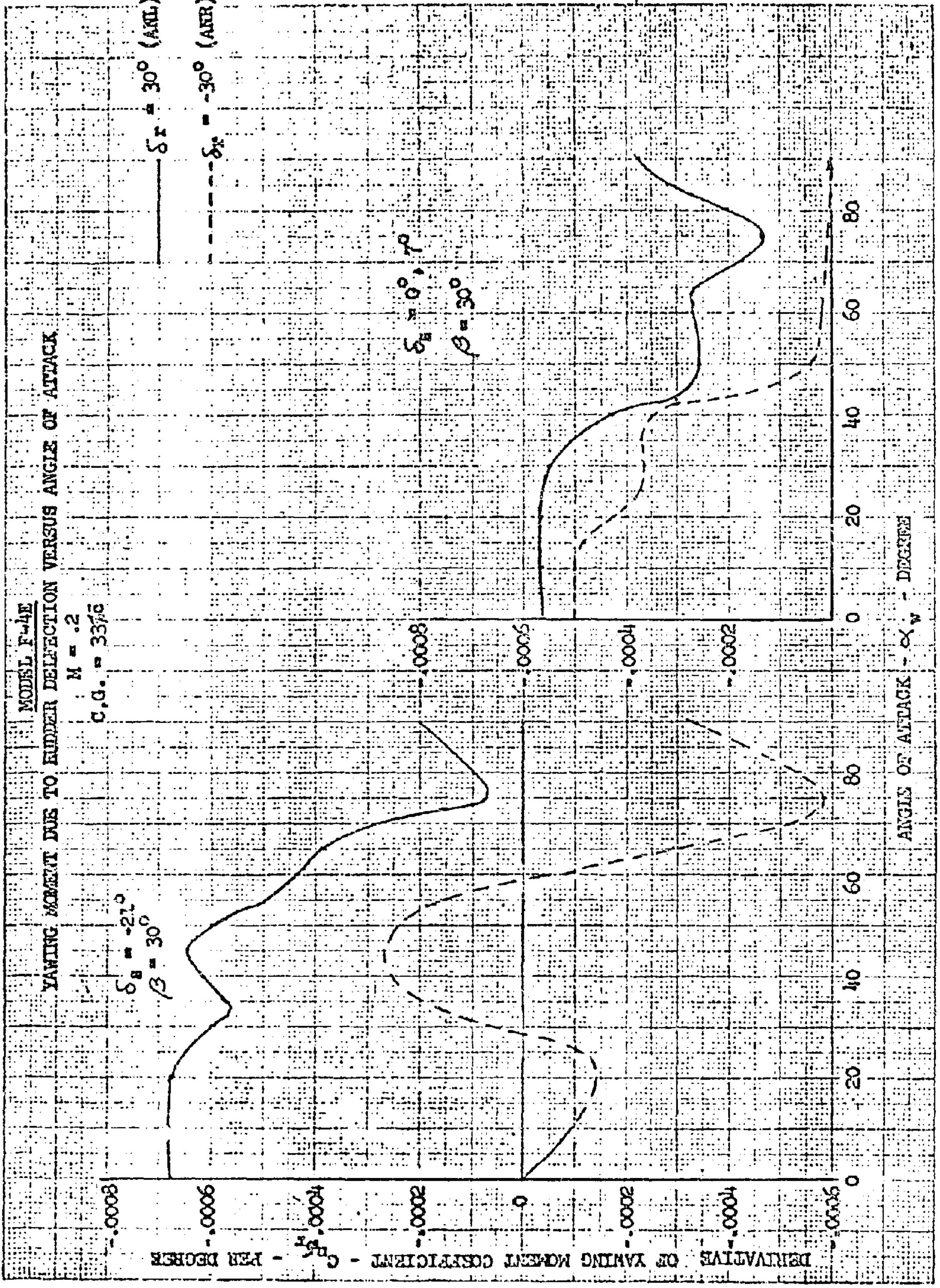

MODEL F-4E

YAWING MOMENT DUE TO RUDDER DEFLECTION VERSUS ANGLE OF ATTACK

M = .2

c.g. = 33%c

Figure B.13 Con't

FIGURE V-48

ROLLING MOMENT DUE TO RUDDER DEFLECTION VERSUS ANGLE OF ATTACK

$M = 12$

$\delta_R = 30°$ (AFT)

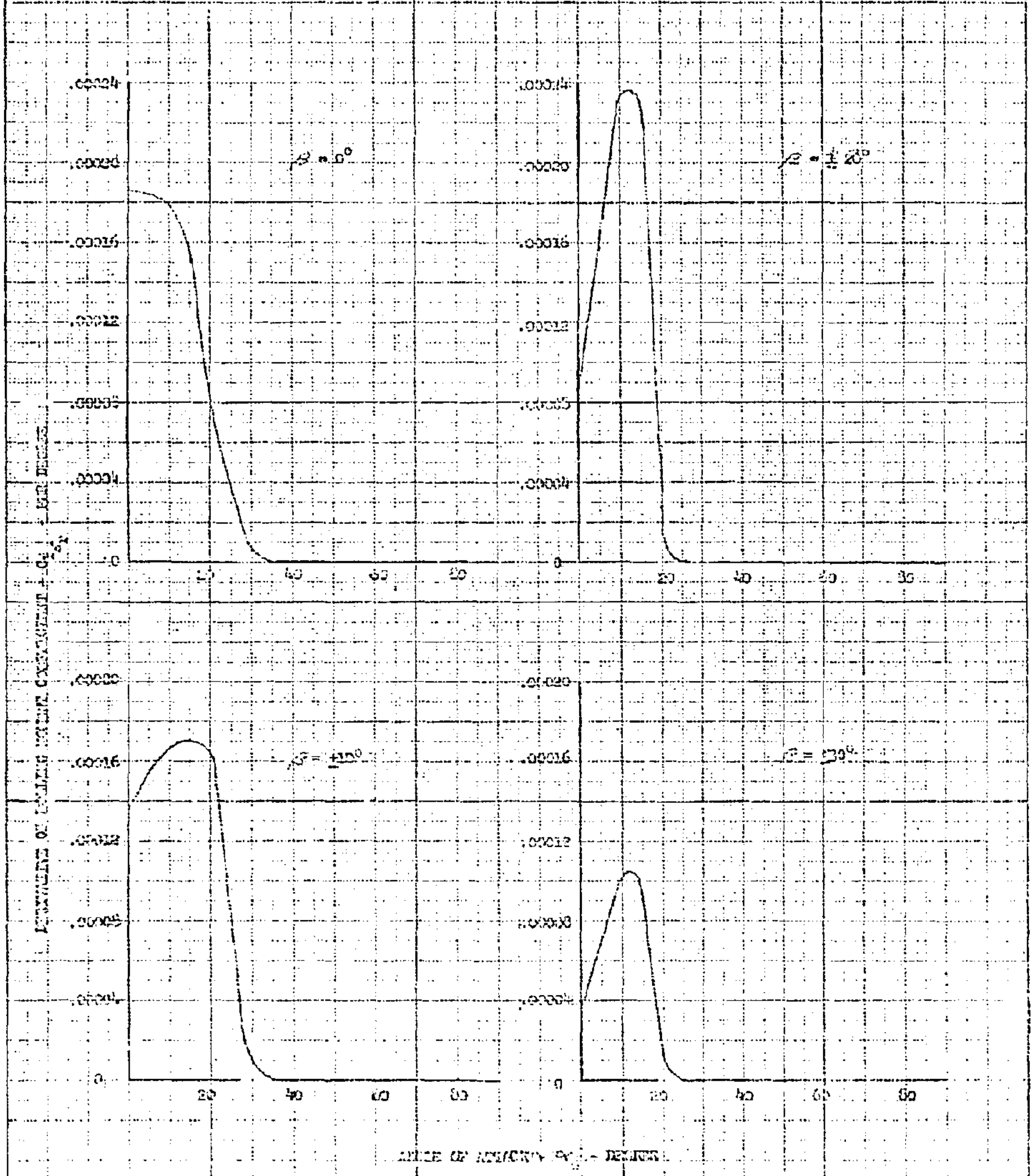

FIGURE F-4

SIDE FORCE DUE TO RUDDER DEFLECTION VERSUS ANGLE OF ATTACK

M = .2

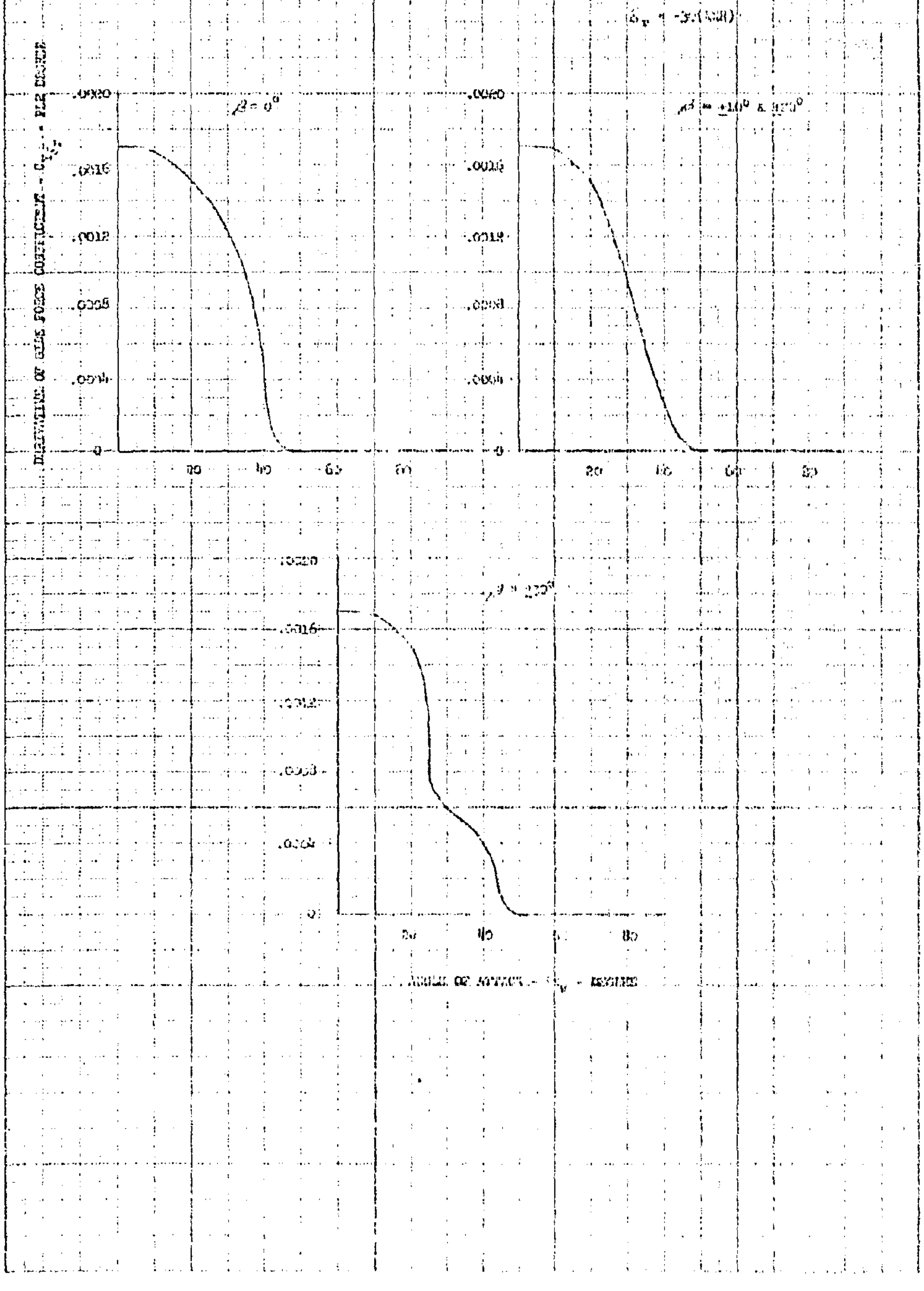

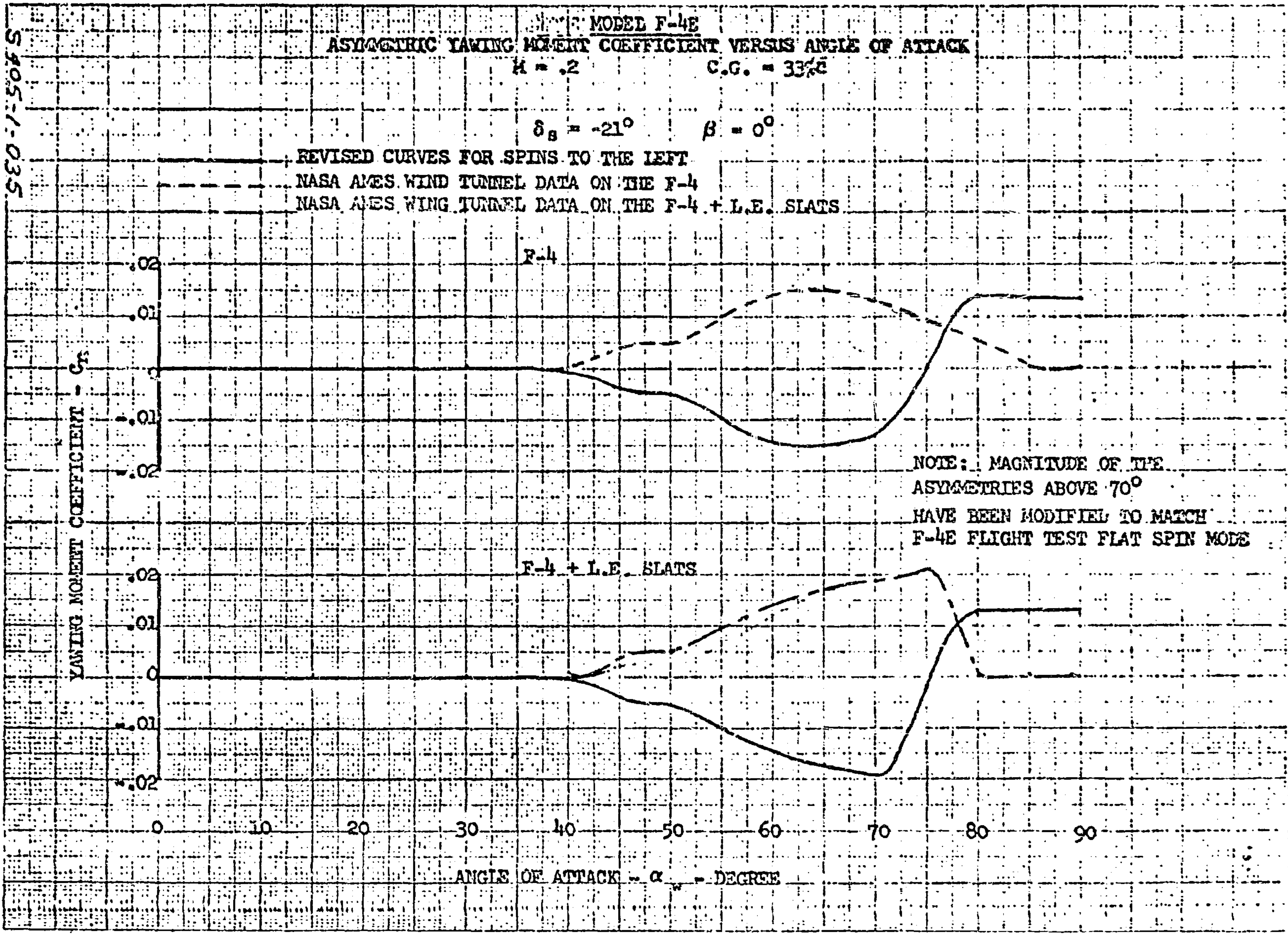

MODEL F-4E

ASYMMETRIC YAWING MOMENT COEFFICIENT VERSUS ANGLE OF ATTACK

S405-1-035

Figure B.16

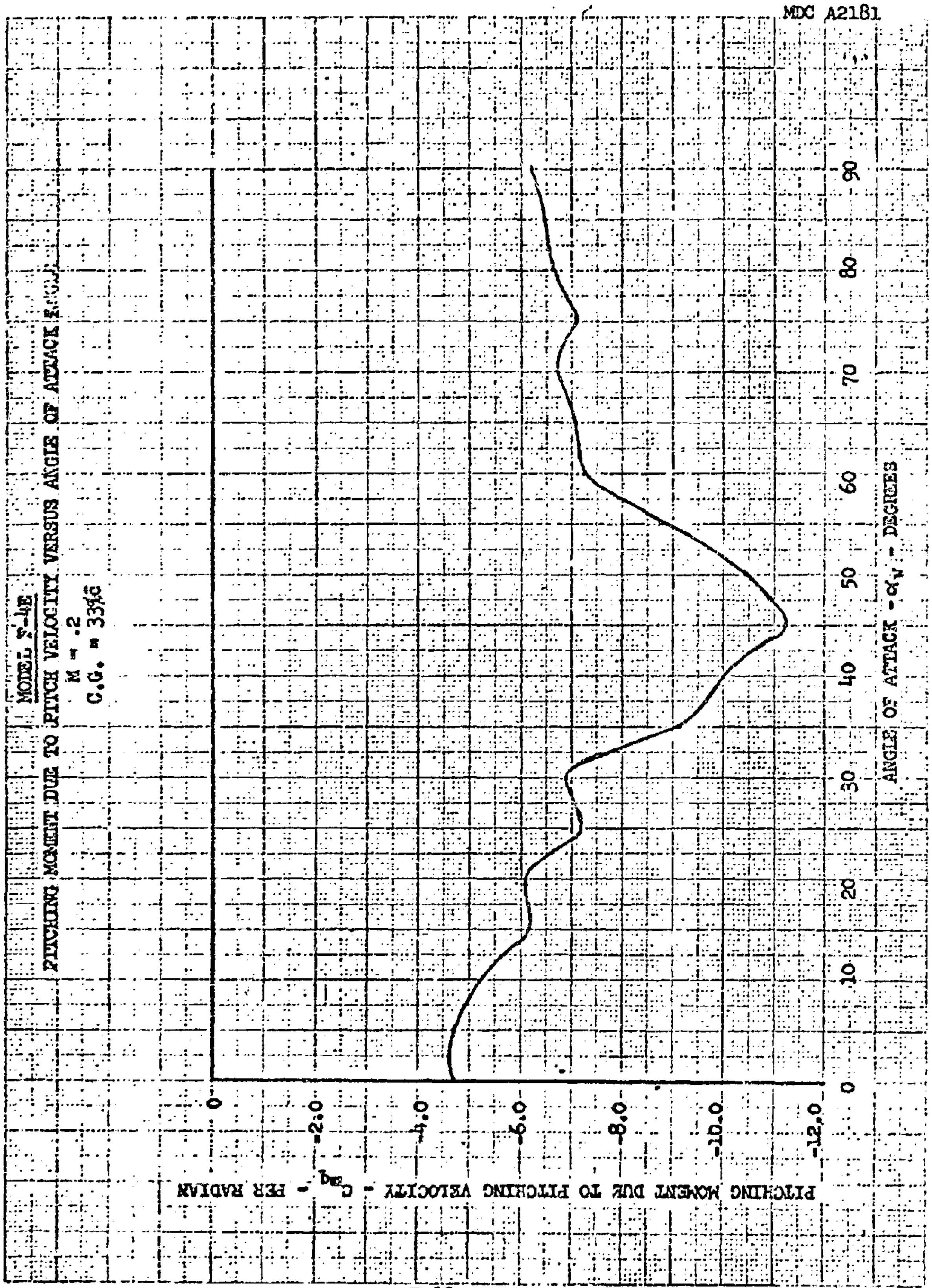
MODEL F-4E
PITCHING MOMENT DUE TO PITCH VELOCITY VERSUS ANGLE OF ATTACK [illegible]
M = .2
C.G. = 33%c
0
-2.0
-4.0
-6.0
-8.0
-10.0
-12.0
PITCHING MOMENT DUE TO PITCHING VELOCITY - $C_{m_q}$ - PER RADIAN
0
10
20
30
40
50
60
70
80
90
ANGLE OF ATTACK - $\alpha_W$ - DEGREES

Figure B.17

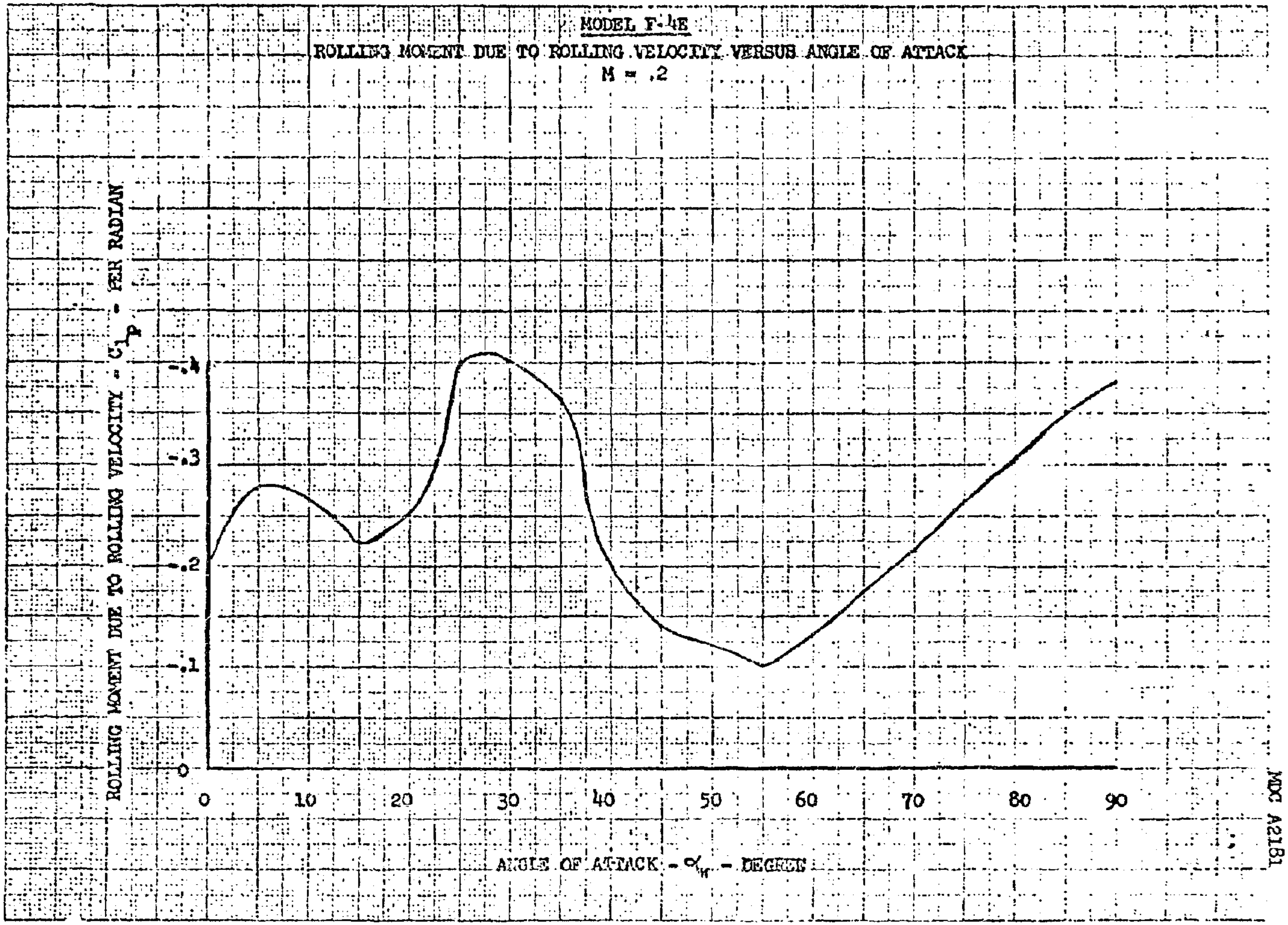

MODEL F-4E

ROLLING MOMENT DUE TO ROLLING VELOCITY VERSUS ANGLE OF ATTACK

M = .2

Figure B.18

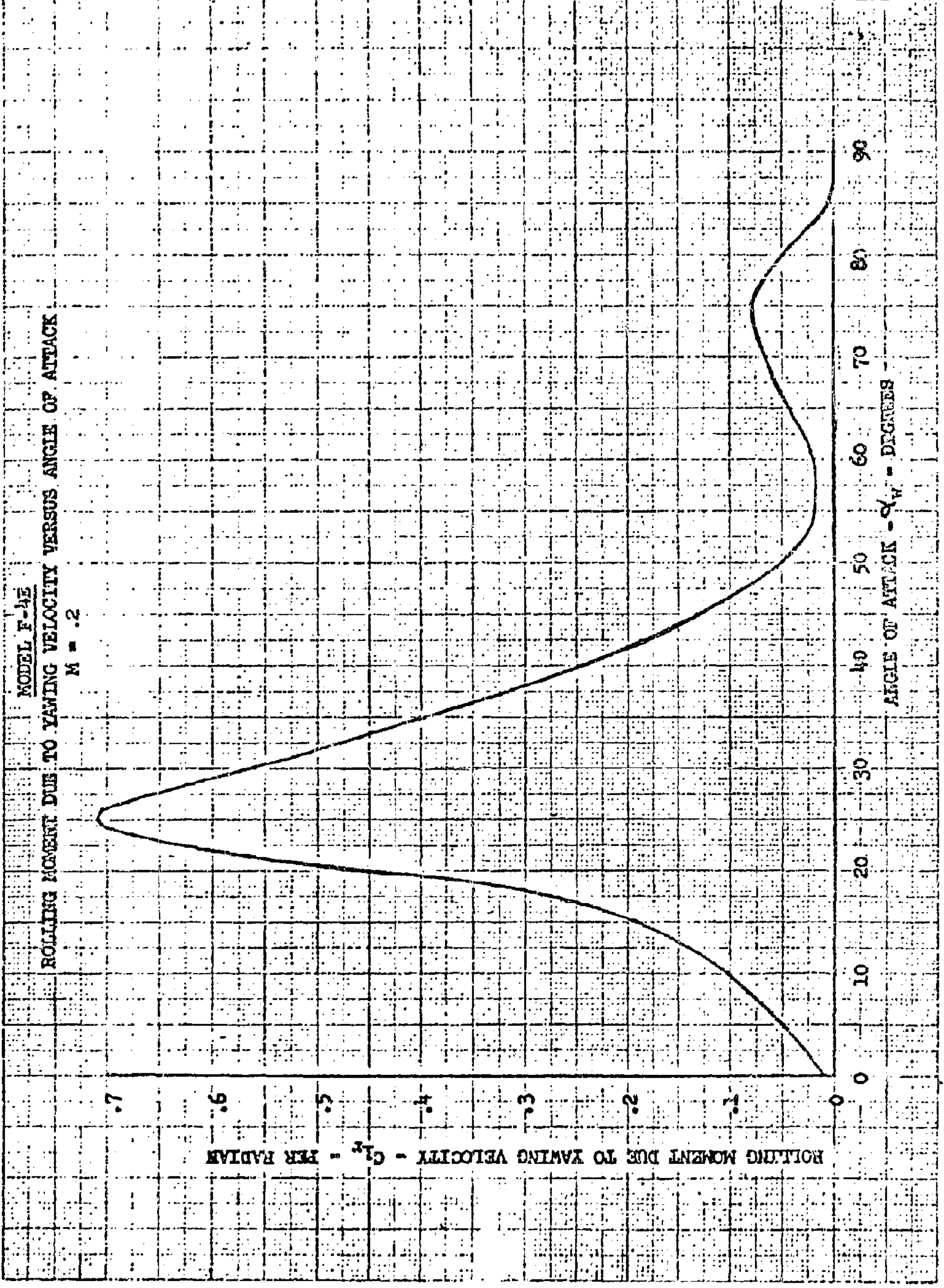
MODEL F-4E
ROLLING MOMENT DUE TO YAWING VELOCITY VERSUS ANGLE OF ATTACK
M = .2
ROLLING MOMENT DUE TO YAWING VELOCITY - $C_{l_r}$ - PER RADIAN
.7
.6
.5
.4
.3
.2
.1
0
ANGLE OF ATTACK - $\alpha_W$ - DEGREES
0
10
20
30
40
50
60
70
80
90

Figure B.19

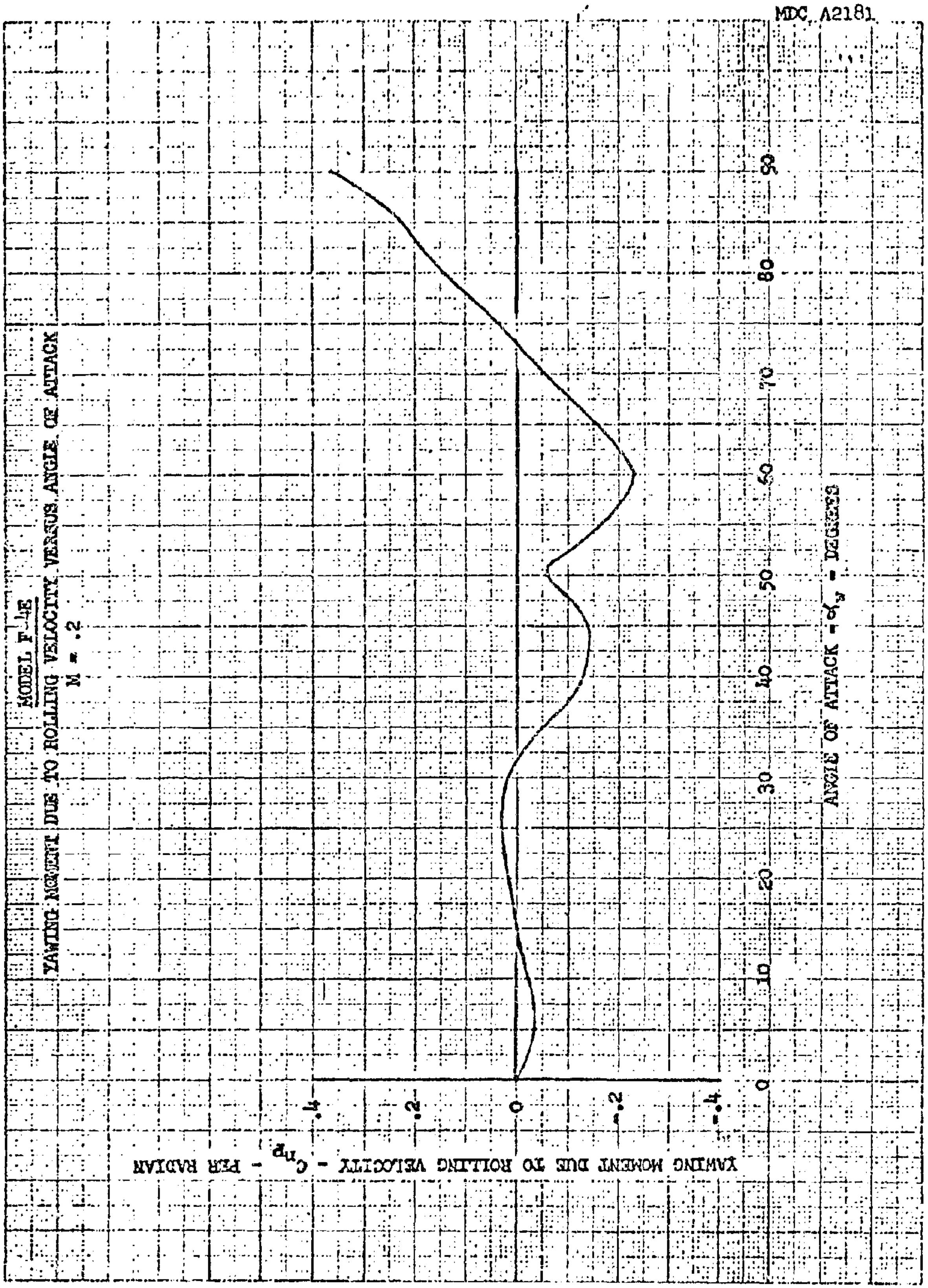

MODEL F-4E

YAWING MOMENT DUE TO ROLLING VELOCITY VERSUS ANGLE OF ATTACK

M = .2

Figure B.20

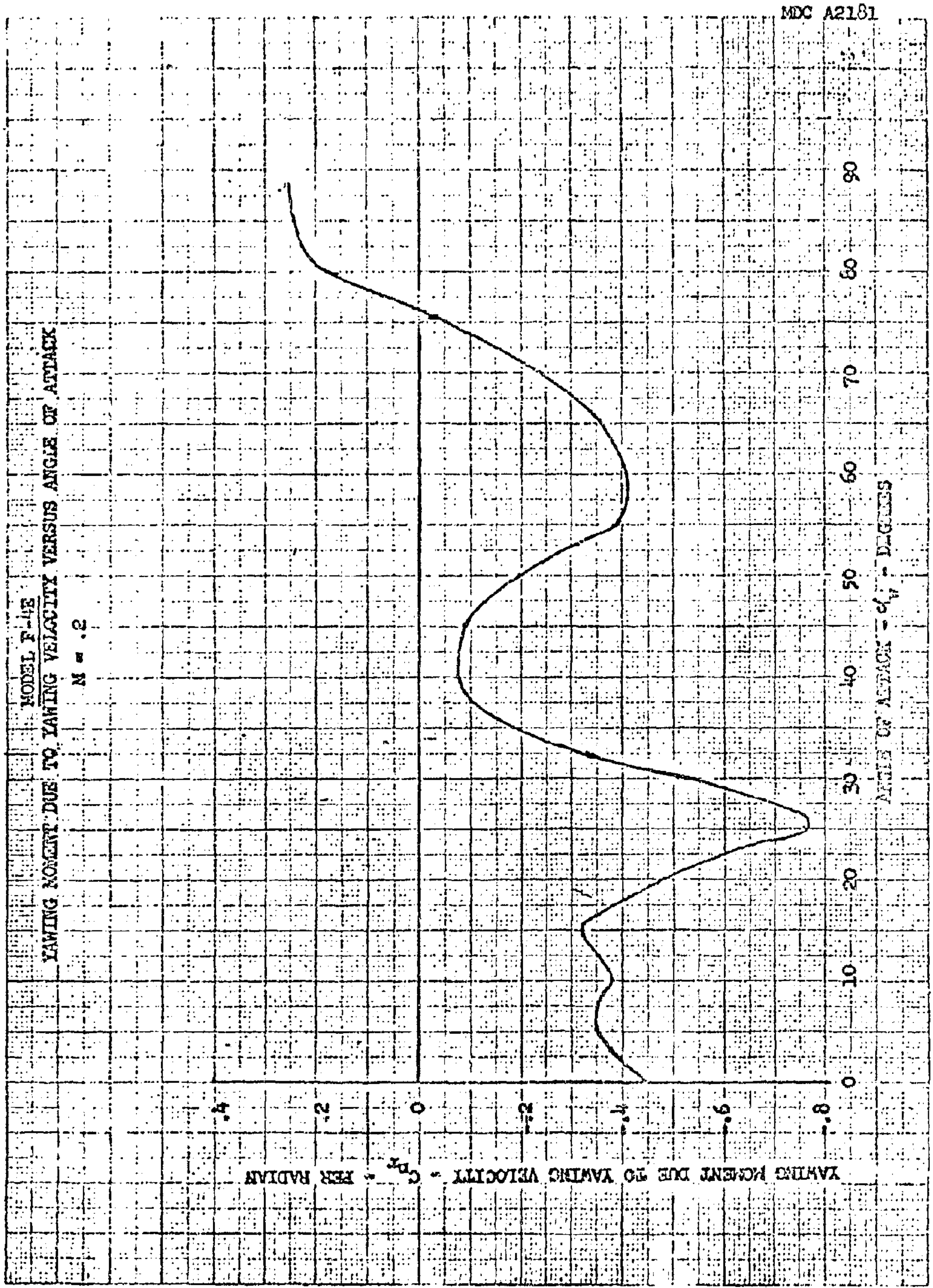

MODEL F-4E

YAWING MOMENT DUE TO YAWING VELOCITY VERSUS ANGLE OF ATTACK

M = .2

Figure B.21

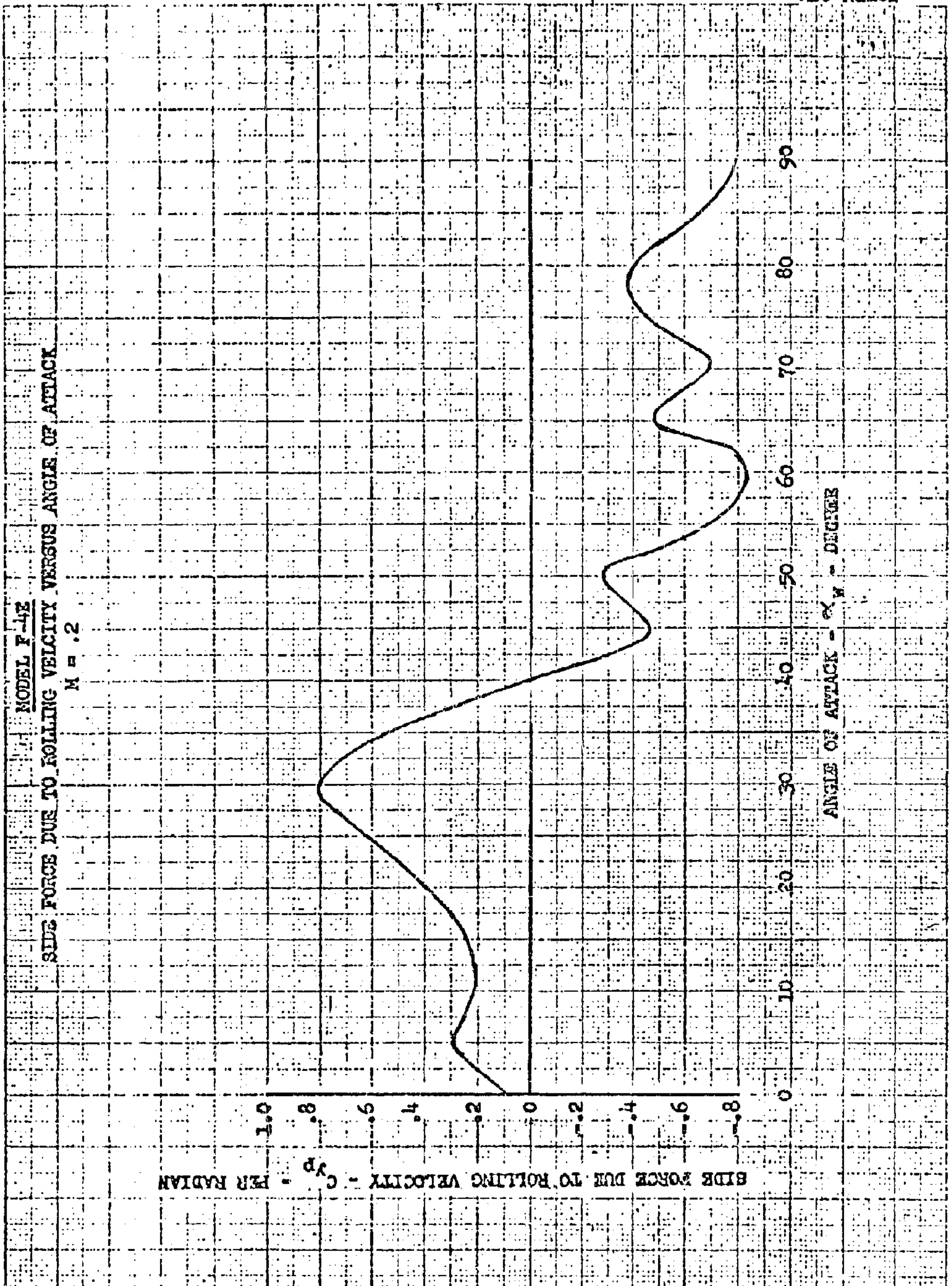

MODEL F-4E

SIDE FORCE DUE TO ROLLING VELCITY VERSUS ANGLE OF ATTACK

M = .2

Figure B.22

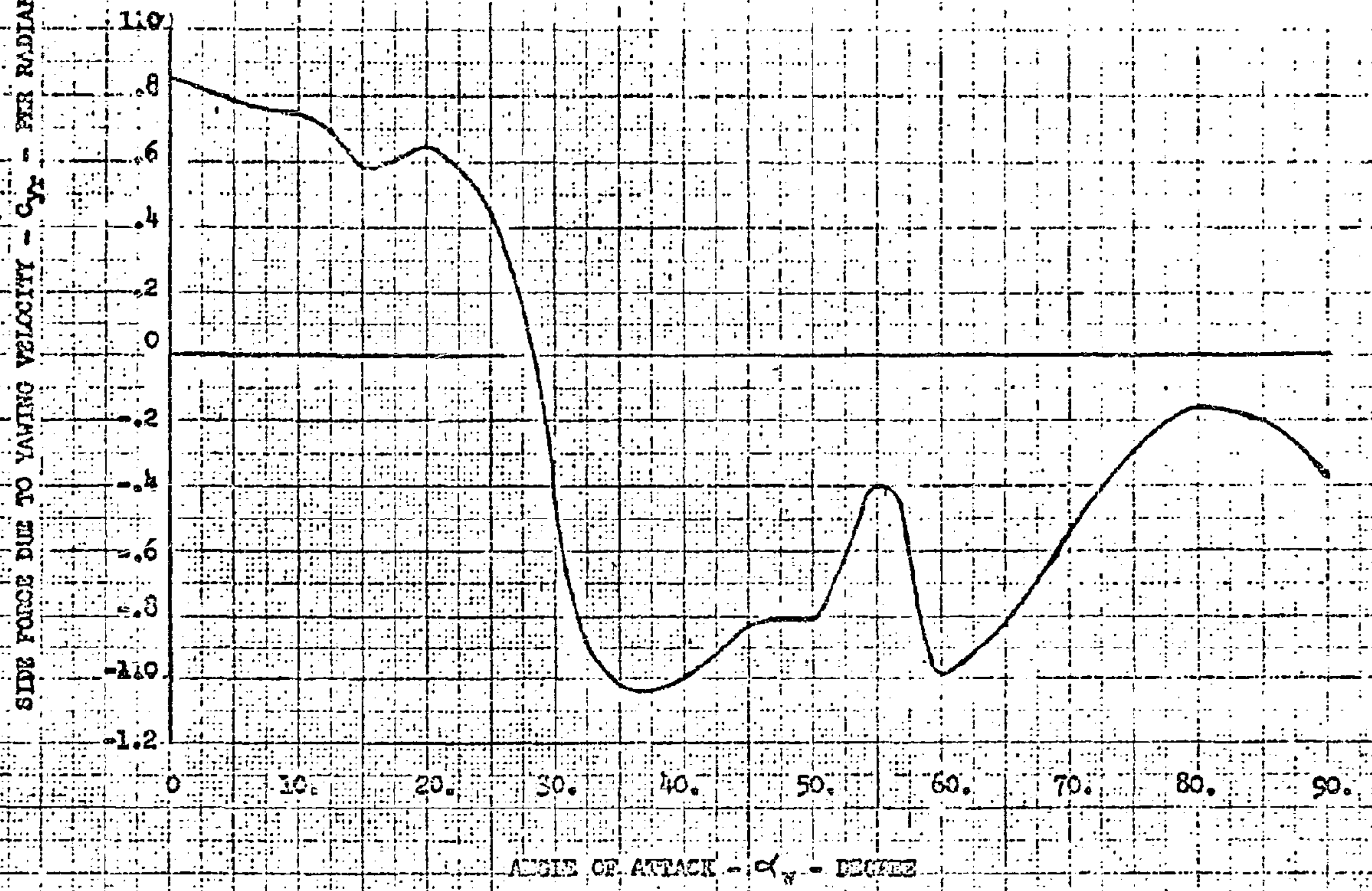

MODEL F-4E

SIDE FORCE DUE TO YAWING VELOCITY VERSUS ANGLE OF ATTACK

M = .2

Figure B.23

FIGURE B-18

VARIATION OF AXIAL FORCE COEFFICIENT WITH LIFT COEFFICIENT

M = .2

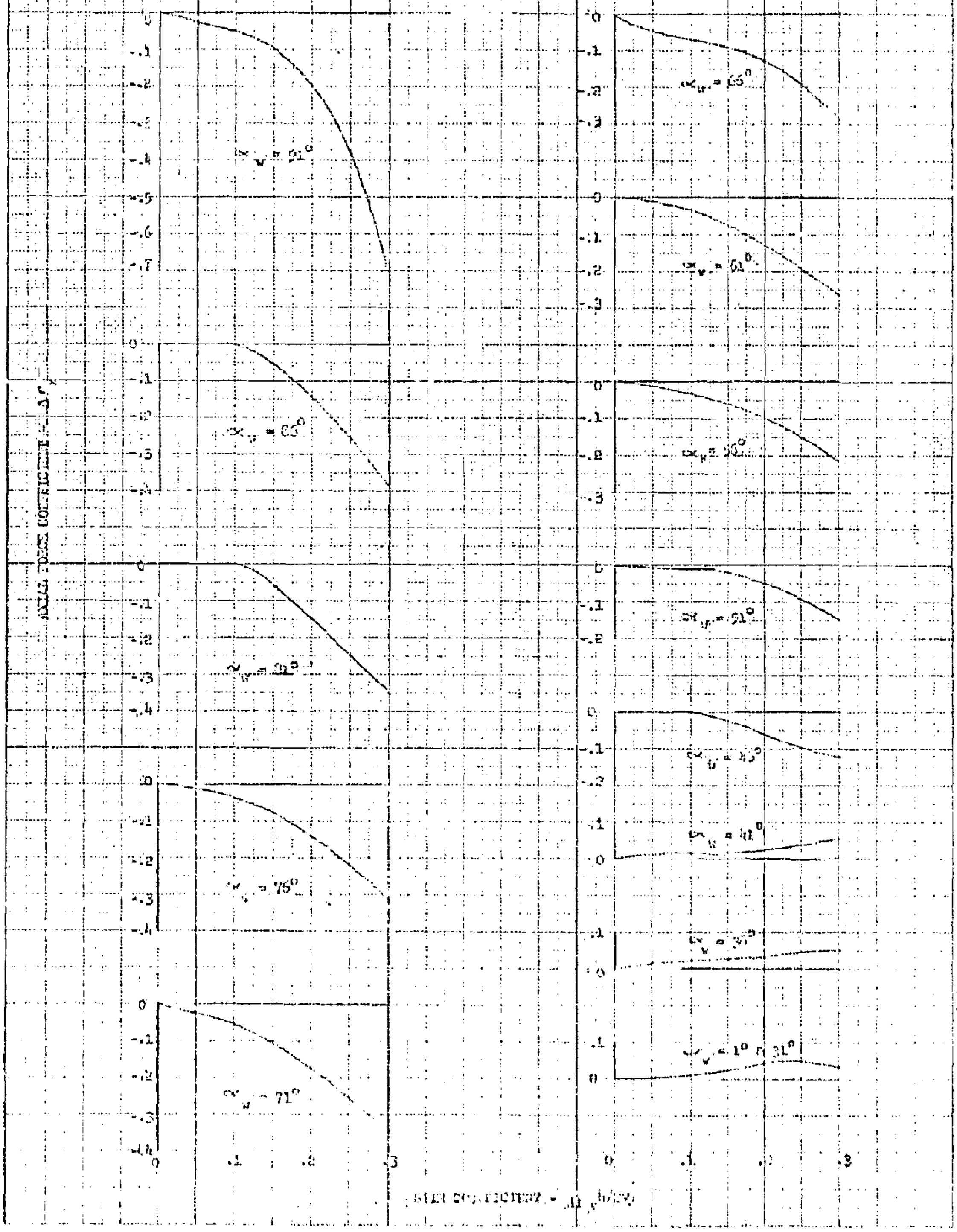

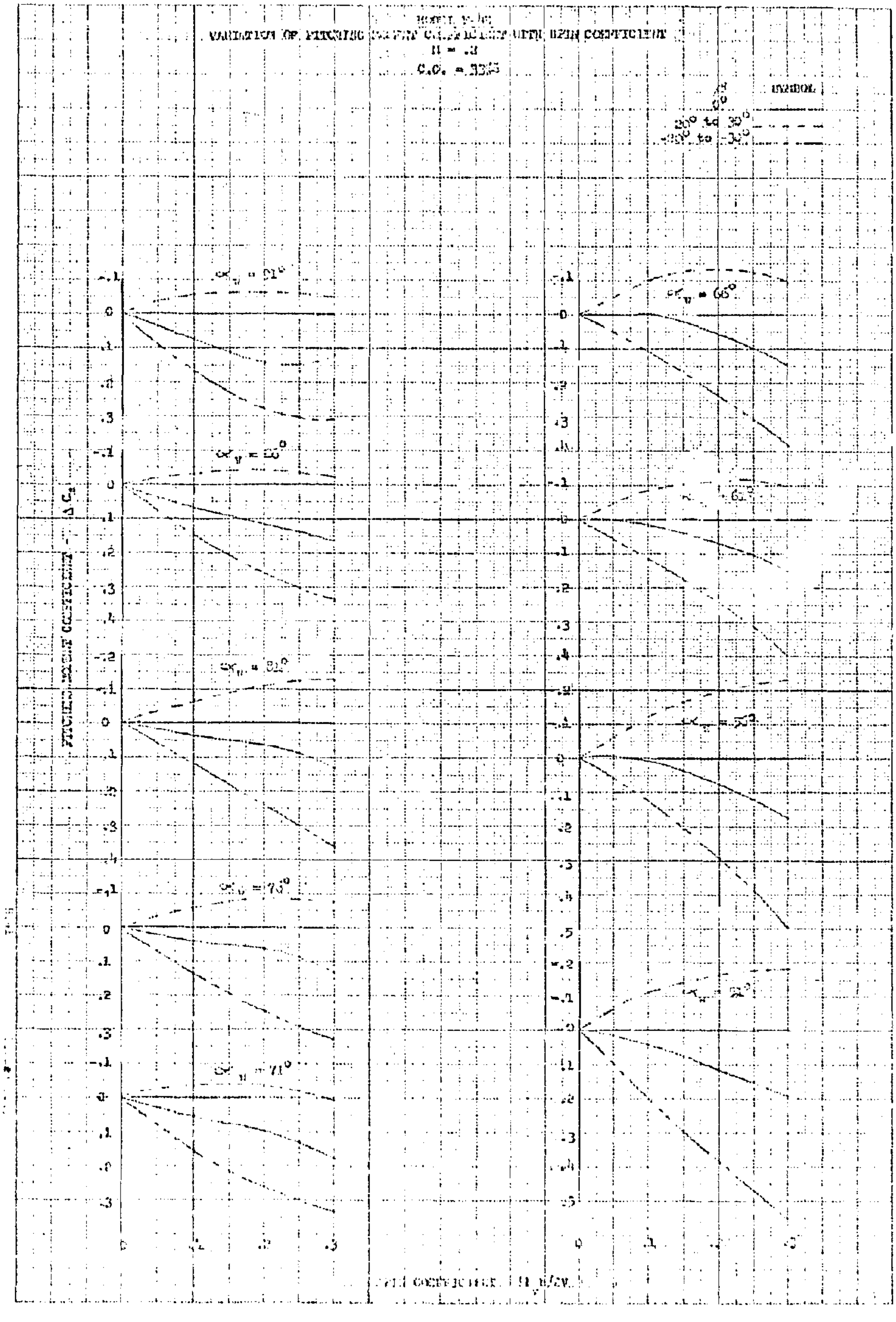MODEL
VARIATION OF PITCHING MOMENT COEFFICIENT WITH SPIN COEFFICIENT
μ = .3
C.G. = 33%
SYMBOL
0°
20° to 30°
-20° to -30°
α = 51°
α = 55°
α = 62°
α = 70°
α = 71°
α = 65°
α = 52°
PITCHING MOMENT COEFFICIENT - ΔC_m
SPIN COEFFICIENT, Ωb/2V
0
.1
.2
.3

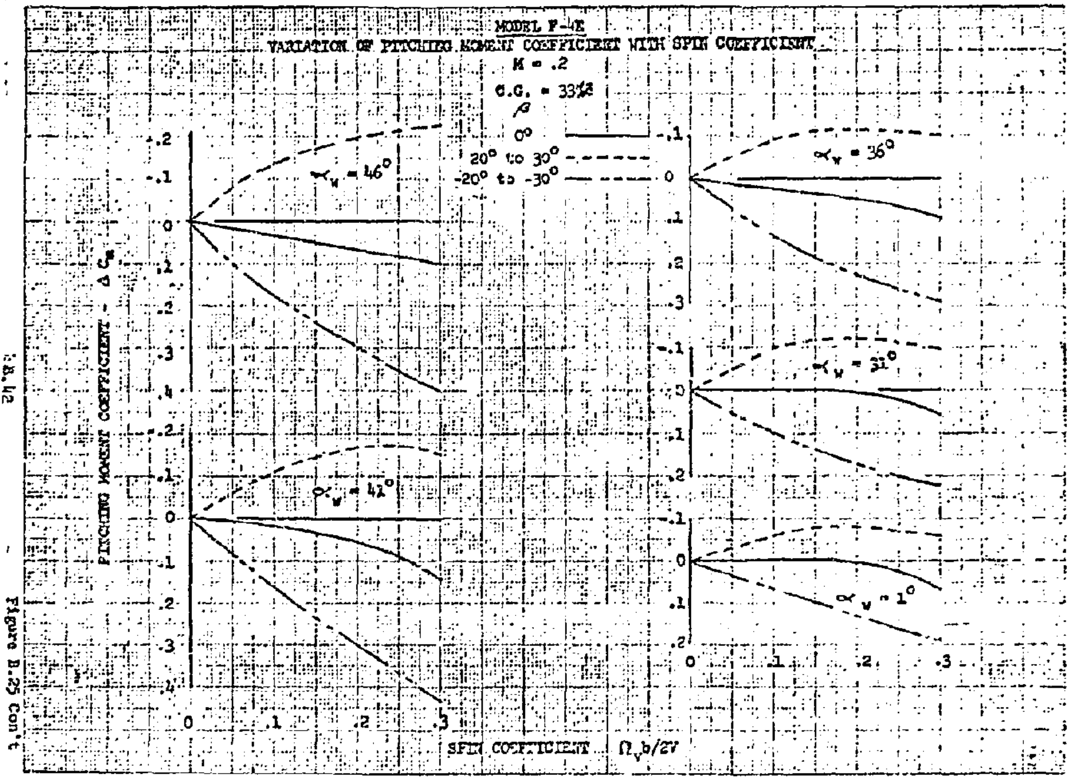

Figure B.25 Con't

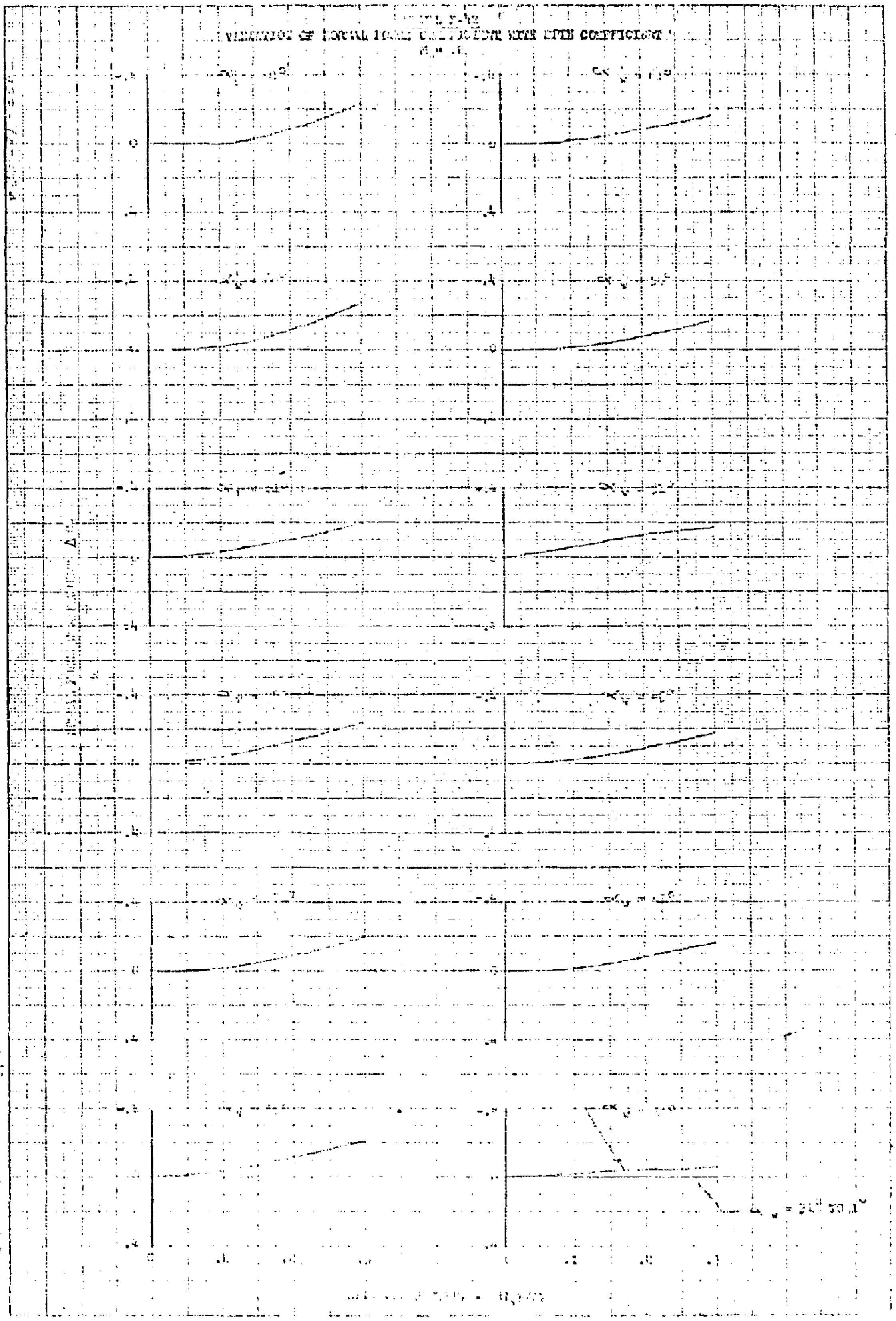

VARIATION OF NORMAL FORCE COEFFICIENT WITH LIFT COEFFICIENT

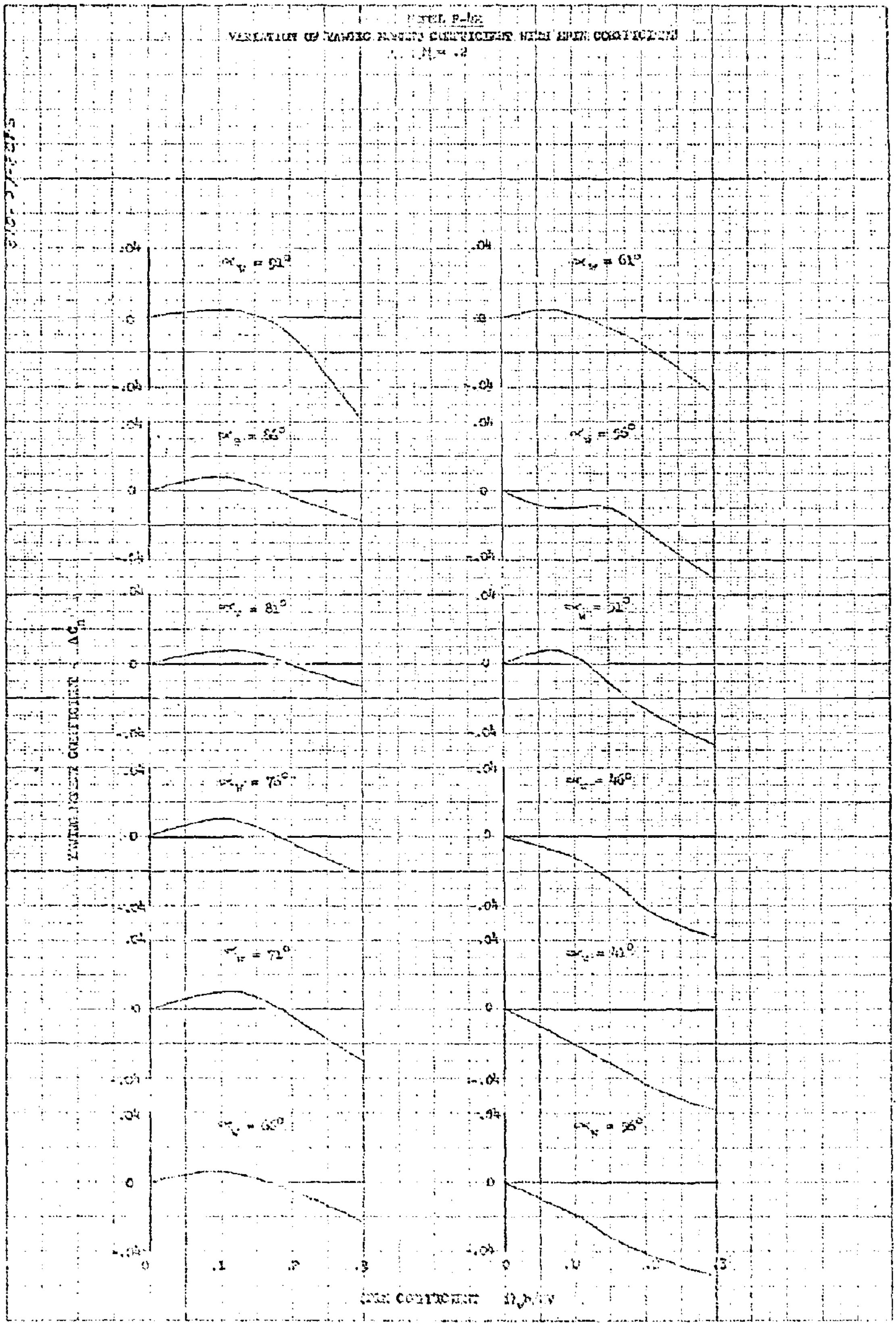

MODEL P-[illegible]

VARIATION OF YAWING MOMENT COEFFICIENT WITH SPIN COEFFICIENT

$M = .2$

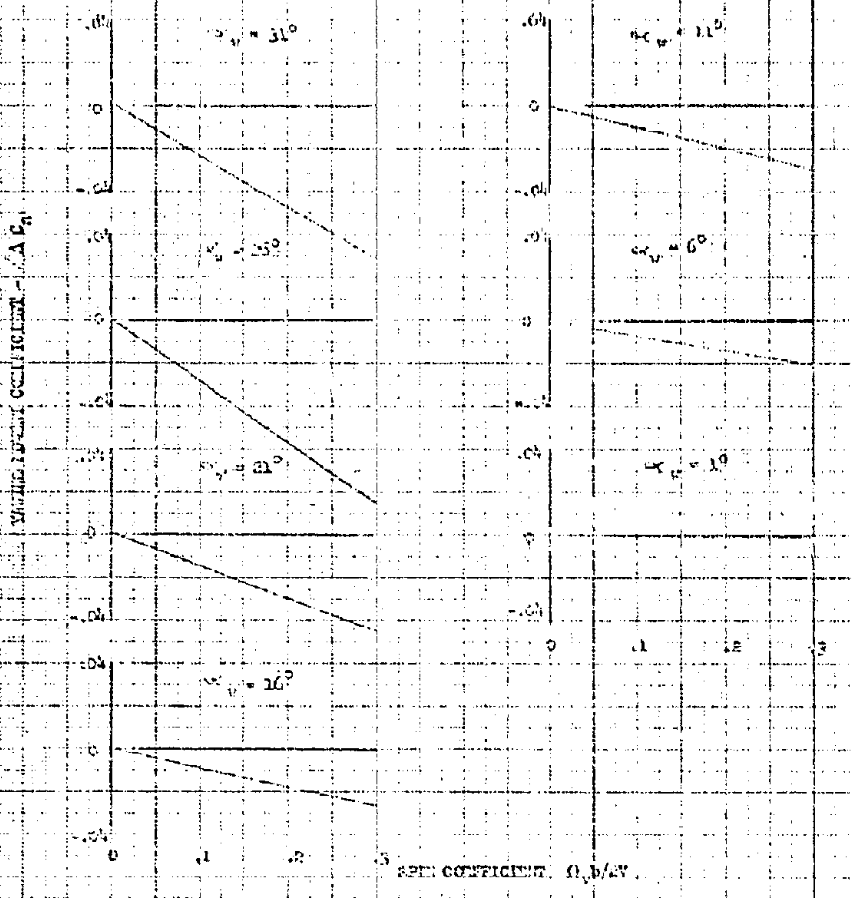

VARIATION OF YAWING MOMENT COEFFICIENT WITH SPIN COEFFICIENT

R = .3

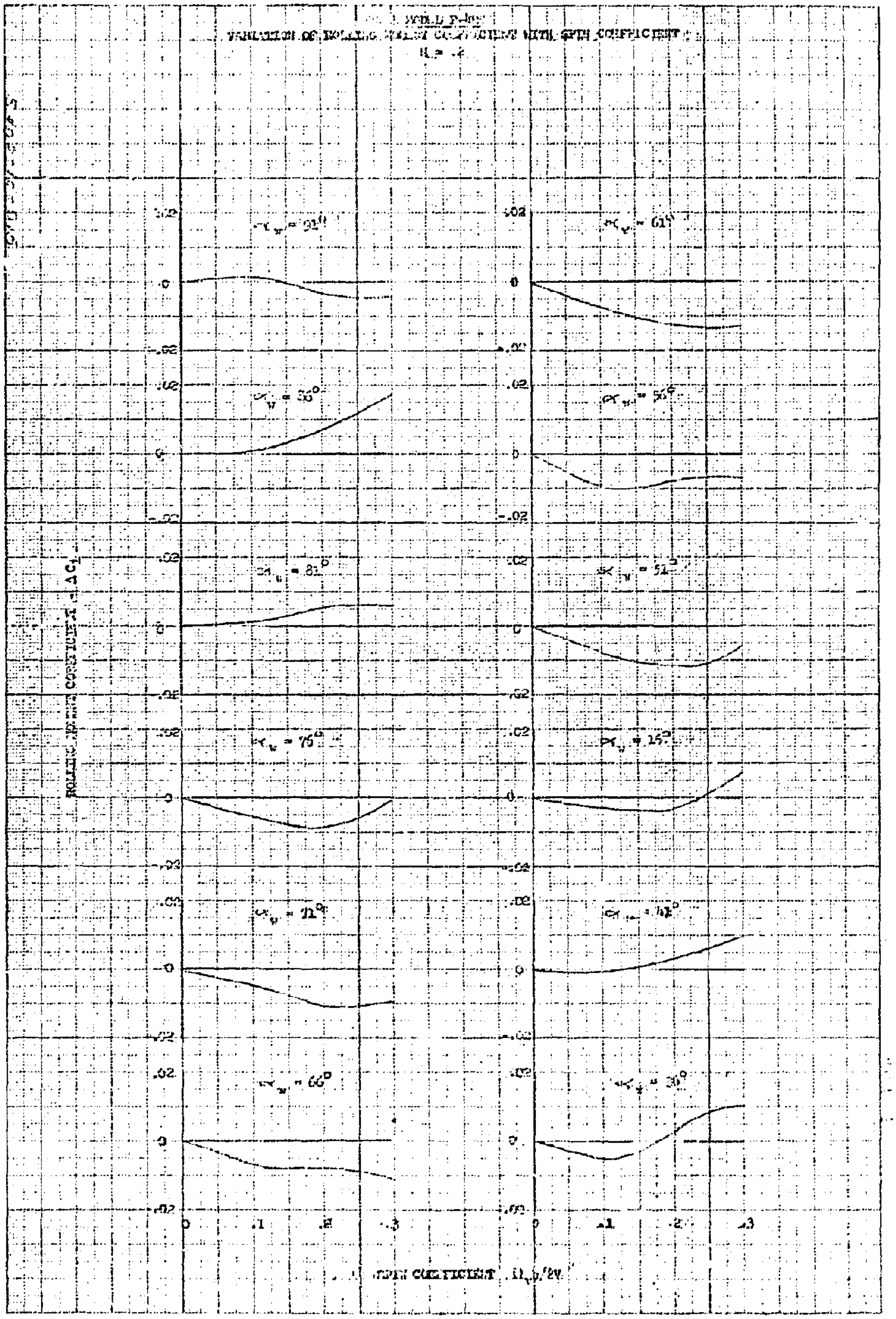
MODEL P-
VARIATION OF ROLLING MOMENT COEFFICIENT WITH SPIN COEFFICIENT
R = .2

VARIATION OF ROLLING MOMENT COEFFICIENT WITH SPIN COEFFICIENT

M = .2

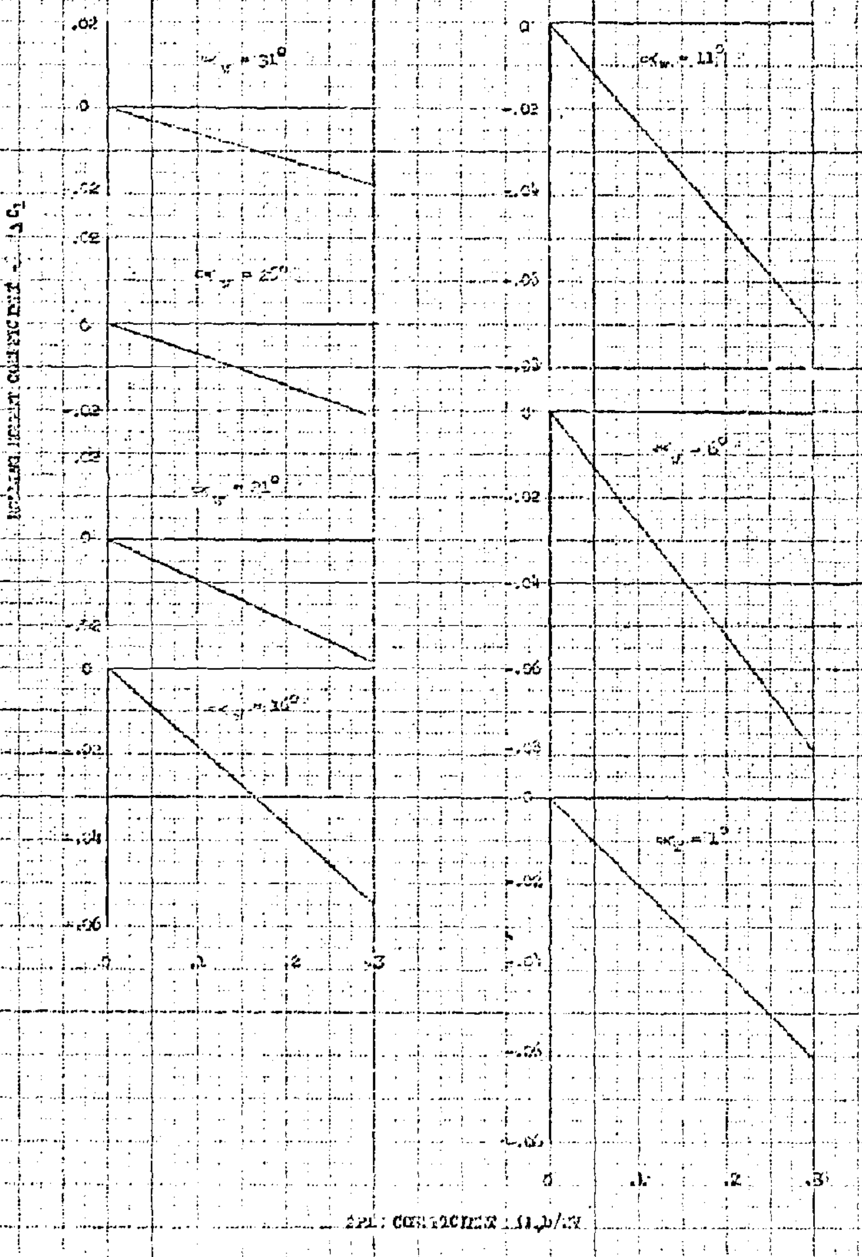

FIGURE P-[illegible]
VARIATION OF SIDE FORCE COEFFICIENT WITH SPIN COEFFICIENT
($\mu$ = .2)

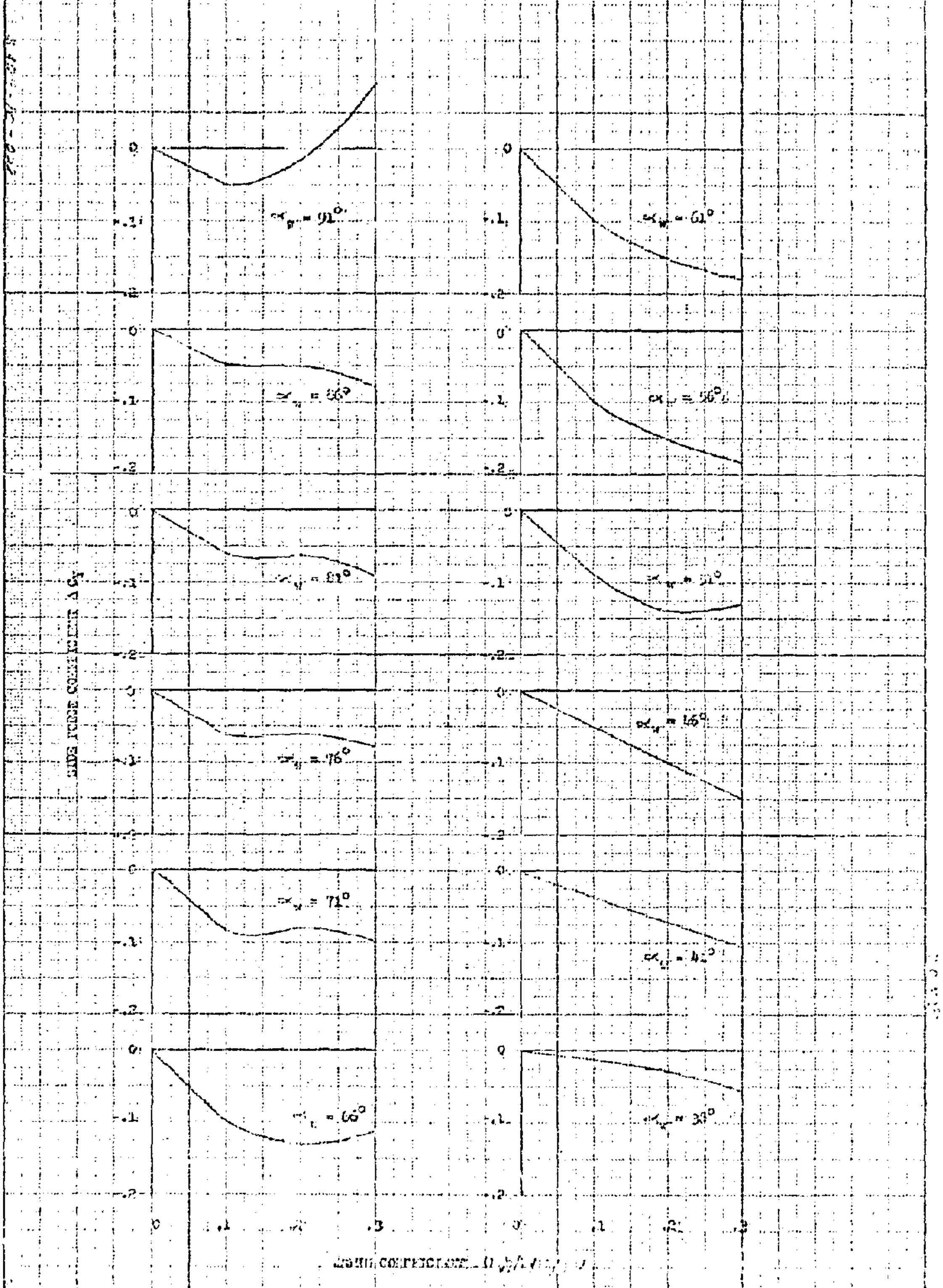

VARIATION OF SIDE FORCE C[illegible] WITH SPIN COEFFICIENT, [illegible]

M = .2

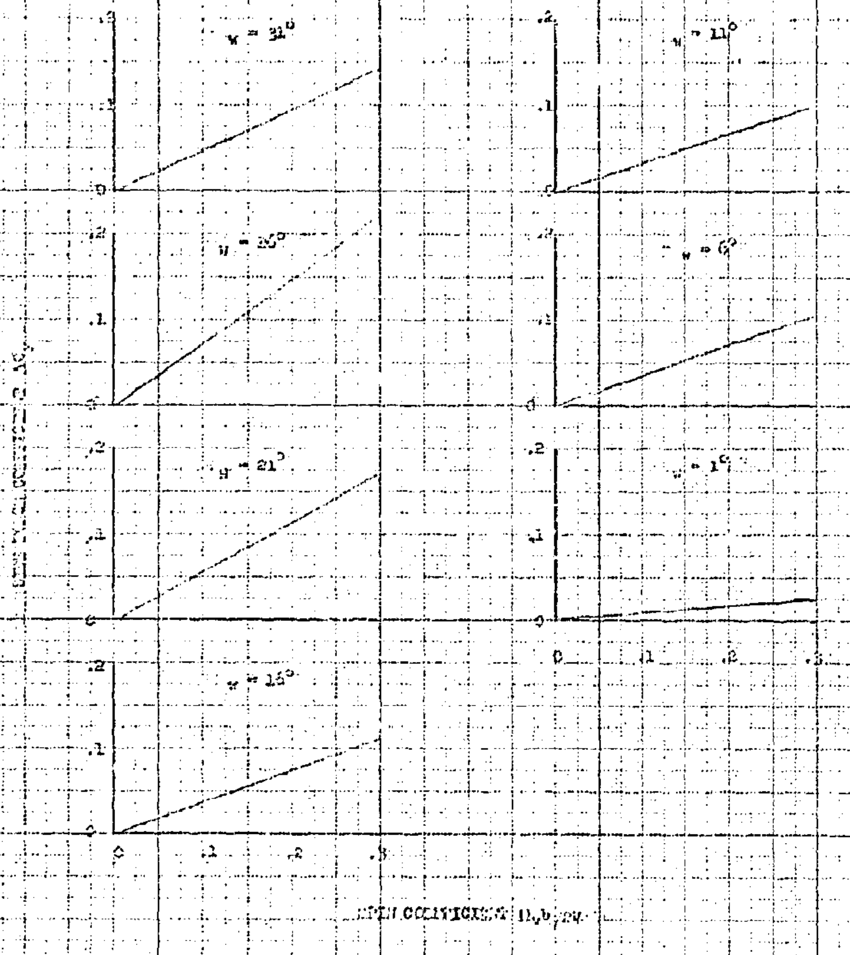

# APPENDIX C

## EQUATIONS OF MOTION

Inclusive Pages: C.1 thru C.7

## Table Of Contents

| Section | Title | Page |
|---|---|---|
| C | Description of the SDF Computer Program | C.3 |
| | C.1 The Basic Program Equations of Motion | C.3 |
| | C.2 Modification of The Equations of Motion For Rotary Balance Data | C.4 |

# APPENDIX C

## C. Description of the SDF Computer Program

The time history data presented in this report were calculated using the six-degree-of-freedom computer program (SDF). The program is designed to determine vehicle performance throughout the entire flight regime of speed and altitude in an atmosphere and gravity field. A description of the basic program equations of motion and the modifications made to these equations for rotary balance data are presented in the following paragraphs.

C.1 The Basic Program Equation of Motion - The equations of motion as normally used in the SDF Program are presented below.

$$\dot{p} = \frac{I_y - I_z}{I_x} qr + \frac{I_{xz}}{I_x} \dot{r} + \frac{I_{xz}}{I_x} pq + \frac{M_x}{I_x} \tag{Equation C.1}$$

$$\dot{q} = \frac{I_z - I_x}{I_y} pr + \frac{I_{xz}}{I_y} r^2 - \frac{I_{xz}}{I_y} p^2 - \frac{I_{eng}\Omega_{eng}}{I_y} r + \frac{M_y}{I_y} \tag{Equation C.2}$$

$$\dot{r} = \frac{I_x - I_y}{I_z} pq + \frac{I_{xz}}{I_z} \dot{p} - \frac{I_{xz}}{I_z} pr + \frac{I_{eng}\Omega_{eng}}{I_z} q + \frac{M_z}{I_z} \tag{Equation C.3}$$

$$\dot{u} = vr - wq + \frac{F_y}{m} \tag{Equation C.4}$$

$$\dot{v} = wp - ur + \frac{F_y}{m} \tag{Equation C.5}$$

$$\dot{w} = uq - vp + \frac{F_z}{m} \tag{Equation C.6}$$

where

$$M_x = -T\sin\lambda_T \sin\phi_T Y_N + T\sin\lambda_T \cos\phi_T Z_N + \frac{1}{2}\rho V^2 Sb\left[C_l + C_{l_{\delta_r}}\delta_r + C_{l_{\delta_a}}\delta_a + \frac{b}{2V}\left(C_{l_r} r + C_{l_p} p\right)\right] \tag{Equation C.7}$$

$$M_y = T\cos\lambda_T Z_N + T\sin\lambda_T \sin\phi_T X_N + \frac{1}{2}\rho V^2 S\bar{c}\left[C_{m_{\delta_s}}\delta_s + C_m + \frac{\bar{c}}{2V}\left(C_{m_q} q\right)\right] \tag{Equation C.8}$$

$$M_z = -T\sin\lambda_T \cos\phi_T X_N - T\cos\lambda_T Y_N + \tfrac{1}{2}\rho V^2 Sb \left[C_n + C_{n_{\delta_r}}\delta r + C_{n_{\delta_a}}\delta a + \frac{b}{2V}(C_{n_r} r + C_{n_p} p)\right] \qquad \text{(Equation C.9)}$$

$$F_x = -W\sin\Theta + T\cos\lambda_T + \tfrac{1}{2}\rho V^2 S\left[C_x + C_{x_{\delta_s}}\delta s\right] \qquad \text{(Equation C.10)}$$

$$F_y = W\cos\Theta\sin\phi - T\sin\lambda_T\cos\phi_T + \tfrac{1}{2}\rho V^2 S\left[C_{y_{\delta_r}}\delta r + \frac{b}{2V}(C_{y_r} r + C_{y_p} p)\right] \qquad \text{(Equation C.11)}$$

$$F_z = W\cos\Theta\cos\phi - T\sin\lambda_T\sin\phi_T + \tfrac{1}{2}\rho V^2 S\left[(C_z + C_{z_{\delta_s}}\delta s + \frac{c}{2V}(C_{z_q} q)\right] \qquad \text{(Equation C.12)}$$

Where $C_l$, $C_m$, $C_n$, $C_x$, $C_y$, and $C_z$ are values at zero control deflections and are a function of $\alpha$ and $\beta$. These curves are presented in Appendix A and B.

C.2 Modification of Equations of Motion For Rotary Balance Data - The aerodynamic characteristics of the F-4 vary nonlinearly with rotation rate in a spin. Since forced oscillation derivatives are linear it is necessary to use rotary balance wind tunnel data instead, so that the aerodynamic force and moment coefficients could be obtained as a function of rotation rate. As described in Appendix A and B rotary balance force and moment data were obtained by rotating the model about an axis parallel to the airflow. In order to properly use these data Equations C.7 through C.12 must be modified. The forced oscillation derivatives are applied only to the oscillatory components of rotation and the rotary balance data are applied as a function of steady state rotation. It is assumed that this steady state rotation is the component of rotation parallel to the velocity vector.

## APPENDIX C

A detailed derivation is necessary to obtain the modifications to the equations of motion so that rotary balance data can be used. The vector relationships and individual rates will be discussed in detail. The total rotational velocity is given by

$$\bar{\Omega} = p\bar{i} + q\bar{j} + r\bar{k} \qquad \text{(Equation C.13)}$$

The component of $\Omega$ parallel to the velocity vector is given by

$$\Omega_V = \frac{\bar{\Omega}\cdot\bar{V}}{|V|}$$

where $\bar{V} = u\bar{i} + v\bar{j} + w\bar{k}$

therefore

$$\Omega_V = \frac{up + vq + wr}{V} \qquad \text{(Equation C.14)}$$

but

$$\frac{u}{V} = \cos\beta\cos\alpha$$

$$\frac{v}{V} = \sin\beta$$

$$\frac{w}{V} = \cos\beta\sin\alpha$$

Substituting into Equation C.14 gives

$$\Omega_V = p\cos\beta\cos\alpha + q\sin\beta + r\cos\beta\sin\alpha \qquad \text{(Equation C.15)}$$

The components of $\Omega_V$ along the X, Y, and Z axes are determined as follows:

$$\bar{\Omega}_V = \Omega_V \frac{\bar{V}}{V}$$

$$\bar{\Omega}_V = \Omega_V \cos\beta\cos\alpha\,\bar{i} + \Omega\sin\beta\,\bar{j} + \Omega_V\cos\beta\sin\alpha\,\bar{k} \qquad \text{(Equation C.16)}$$

The resulting three axes rates have been assigned the name steady state rotation rates and are:

$$p_s = \Omega_V\cos\beta\cos\alpha$$

$$q_s = \Omega_V\sin\beta$$

$$r_s = \Omega_V\cos\beta\sin\alpha \qquad \text{(Equation C.17)}$$

## APPENDIX C

The rate components of the vector perpendicular to the velocity vector $\bar{\Omega}_o$ have been assigned the name oscillatory components. The oscillatory components are obtained by subtracting the steady state rates $p_s$, $q_s$, and $r_s$ from the total rates p, q, and r.

$$p_o = p - p_s$$

$$q_o = q - q_s \qquad \text{(Equation C.18)}$$

$$r_o = r - r_s$$

where $\Omega_o = \sqrt{p_o^2 + q_o^2 + r_o^2}$

$\Omega_V = \sqrt{p_s^2 + q_s^2 + r_s^2}$

When using rotary balance data, only the oscillatory components of p, q, and r are applied to the forced oscillation derivatives. The changes in force and moment coefficients due to steady state rotation rate are included as a function of $\Omega_V b/2V$. These rotary balance coefficients are presented as a function of $\alpha$, $\beta$, and $\frac{\Omega_V b}{2V}$.

Modifying Equations C.7 through C.12 to utilize the rotary balance data in the manner described above gives the following results.

$$M_x = -T\sin\lambda_T \sin\phi_T Y_N + T\sin\lambda_T \cos\phi_T Z_N$$
$$+\tfrac{1}{2}\rho V^2 Sb\left[C_l + C_{l_{\delta r}}\delta r + C_{l_{\delta a}}\delta a + \frac{b}{2V}\left(C_{l_r} r_o + C_{l_p} p_o\right) + \Delta C_l\right]$$

$$M_y = T\cos\lambda_T Z_N + T\sin\lambda_T \sin\phi_T X_N$$
$$+\tfrac{1}{2}\rho V^2 S\bar{c}\left[C_{m_{\delta s}}\delta s + C_m + \frac{\bar{c}}{2V}\left(C_{m_q} q_o\right) + \Delta C_m\right]$$

$$M_z = -T\sin\lambda_T \cos\phi_T X_N - T\cos\lambda_T Y_N$$
$$+\tfrac{1}{2}\rho V^2 Sb\left[C_n + C_{n_{\delta r}}\delta r + C_{n_{\delta a}}\delta a + \frac{b}{2V}\left(C_{n_r} r_o + C_{n_p} p_o\right) + \Delta C_n\right]$$

## APPENDIX C

$$F_x = -W\sin\theta + T\cos\lambda_T + \tfrac{1}{2}\rho V^2 S\left[C_x + C_{x_{\delta_s}}\delta s + \Delta C_x\right]$$

$$F_y = W\cos\theta\sin\phi - T\sin\lambda_T\cos\phi_T + \tfrac{1}{2}\rho V^2 S\Big[C_y + C_{y_{\delta_r}}\delta r + \tfrac{b}{2V}\left(C_{y_r}r_o + C_{y_p}p_o\right)$$
$$+\Delta C_y\Big]$$

$$F_z = W\cos\theta\cos\phi - T\sin\lambda_T\sin\phi_T + \tfrac{1}{2}\rho V^2 S\left[C_z + C_{z_{\delta_s}}\delta s + \tfrac{c}{2V}\left(C_{z_q}q_{\dot{o}}\right) + \Delta C_z\right]$$

where

$\Delta C_l$, $\Delta C_m$, $\Delta C_n$, $\Delta C_x$, $\Delta C_y$, and $\Delta C_z$ are functions of $\alpha$, $\beta$, and $\Omega_v b/2V$ and are presented in Appendix A and B.

# APPENDIX D

# The Use of Forced Oscillation Derivatives to Generate Linear Rotary Balance Data Below 35° Angle of Attack

Inclusive Pages: D.1 thru D.18

## Table Of Contents

| Section | Title | Page |
|---|---|---|
| D | Rotary Balance Data Below 35° Angle of Attack | D.3 |
| | D.1 Rotary Balance Data Obtained From Forced Oscillation Derivatives | D.3 |
| | D.2 Adjustment of Lateral-Directional Rotary Balance Wind Tunnel Data | D.5 |
| | D.3 The Effect of Using Rotary Balance Data Below Stall | D.6 |

## APPENDIX D

### D. Rotary Balance Data Below 35° Angle of Attack

As stated in Appendix A and B rotary balance wind tunnel data is only available in the 35° to 90° angle of attack range. These data are necessary because the aerodynamic forces and moments are nonlinear with rotation rate in the spin angle of attack regions. Rotary balance data are also needed below 35° angle of attack in order to ensure a smooth transition from below stalled flight all the way through departure. Using arbitrary or constant values for rotary balance data below 35° gives erratic lateral-directional computer results. Therefore, the method used in generating rotary data below 35° angle of attack is presented in the following section.

D.1 Rotary Balance Data Obtained from Forced Oscillation Derivatives - Rotary balance wind tunnel data is obtained by rotating the model about an axis parallel to the airflow or the velocity vector. The total rotation rate about the velocity is called $\Omega_V$. As derived in Appendix C this rotation rate can be broken down into steady components as

$$\Omega_V = \sqrt{p_s^2 + r_s^2 + q_s^2}$$

where $p_s$, $r_s$, and $q_s$ are with respect to the x, z, and y aircraft body axis system. The total rolling moment coefficient due to $\Omega_V$ can be broken down into the rolling moment coefficients which are due to the individual rate components $p_s$, $r_s$, and $q_s$ as follows

$$C_{l_{(\text{due to } \Omega_V)}} = C_{l_{(\text{due to } p_s)}} + C_{l_{(\text{due to } r_s)}} + C_{l_{(\text{due to } q_s)}}$$

The individual rolling moment components are the same as

$$C_{l_{(\text{due to } p_s)}} = C_{l_p} \frac{p_s b}{2V}$$

$$C_{l_{(\text{due to } r_s)}} = C_{l_r} \frac{r_s b}{2V}$$

APPENDIX D

$$C_{l_{(\text{due to } q_s)}} = C_{l_q} \frac{q_s b}{2V}$$

Also

$$C_{l_{(\text{due to } \Omega_V)}} = \frac{C_l}{\frac{\Omega_V b}{2V}} \frac{\Omega_V b}{2V}$$

Substitution of terms yields

$$\frac{C_l}{\frac{\Omega_V b}{2V}} \frac{\Omega_V b}{2V} = C_{l_p} \frac{p_s b}{2V} + C_{l_r} \frac{p_s b}{2V} + C_{l_q} \frac{q_s b}{2V} \qquad \text{(Equation D.1)}$$

Likewise the same method can be applied to the total yawing moment coefficient and side force coefficient due $\Omega_V$.

$$\frac{C_n}{\frac{\Omega_V b}{2V}} \frac{\Omega_V b}{2V} = C_{n_p} \frac{p_s b}{2V} + C_{n_r} \frac{r_s b}{2V} + C_{n_q} \frac{q_s b}{2V} \qquad \text{(Equation D.2)}$$

$$\frac{C_Y}{\frac{\Omega_V b}{2V}} \frac{\Omega_V b}{2V} = C_{y_p} \frac{p_s b}{2V} + C_{y_r} \frac{r_s b}{2V} + C_{y_q} \frac{q_s b}{2V} \qquad \text{(Equation D.3)}$$

The relationship between the total rotation rate about the velocity vector $\Omega_V$ and its respective components as derived from Appendix C is presented below:

$$p_s = \Omega_V \cos\beta \cos\alpha$$

$$q_s = \Omega_V \sin\beta$$

$$r_s = \Omega_V \cos\beta \sin\alpha$$

Assuming small values of $\beta$ the following approximations are made;

$$p_s = \Omega_V \cos\beta \cos\alpha \approx \Omega_V \cos\alpha$$

$$q_s = \Omega_V \sin\beta \approx 0 \qquad \text{(Equation D.4)}$$

$$r_s = \Omega_V \cos\beta \sin\alpha \approx \Omega_V \sin\alpha$$

APPENDIX D

Substitution of Equation D.4 into the proper Equations D.1 through D.3 and also dividing each equation by $\Omega_v b/2V$ yields

$$\Delta C_l = (C_{l_p} \cos\alpha + C_{l_r} \sin\alpha)\frac{\Omega_v b}{2V} \quad \text{(Equation D.5)}$$

$$\Delta C_n = (C_{n_p} \cos\alpha + C_{n_r} \sin\alpha)\frac{\Omega_v b}{2V} \quad \text{(Equation D.6)}$$

$$\Delta C_y = (C_{y_p} \cos\alpha + C_{y_r} \sin\alpha)\frac{\Omega_v b}{2V} \quad \text{(Equation D.7)}$$

where $C_{l_p}$, $C_{l_r}$, $C_{n_r}$, $C_{n_p}$, $C_{y_r}$, and $C_{y_p}$ are obtained from forced oscillation wind tunnel data. Equations D.5 through D.7 are used to calculate constant slope rotary balance curves from 1° to 31° wing angle of attack. These curves are presented in Appendix A and B.

D.2 Adjustment of Lateral-Directional Rotary Balance Wind Tunnel Data - The SDF computer time history spin characteristics indicates that the spin entry characteristics of the basic F-4E are different from the results from Reference 1 when the unadjusted rotary balance wind tunnel data are used above 35° angle of attack in conjunction with the calculated rotary balance data below 35° angle of attack. Since these latest results were not indicative of the actual airplane, the lateral-directional rotary balance curves for the basic F-4E had to be adjusted.

As a solution to this problem the slopes of the yawing and rolling moment coefficient versus rotation rate curves are determined from both the generated curves (Equations D.5 and D.6) and the wind tunnel curves at $\Omega_v b/2V = 0$. These slopes are plotted versus angle of attack and a smooth transition is faired between 35° and 45° (see Figure D.1). The revised slopes apply to the data between $\Omega_v b/2V$ of 0 and $\pm.05$. This method was also used to adjust the slatted F-4E rotary data (see Figure D.2). The final rotary balance curves are presented in Appendix A and B. A spin time history of the basic F-4E comparing the effect of using the updated rotary balance data in lieu of that used in the previous spin study (Reference 1) is presented in Figure D.3. The results show that the current rotary balance data causes the aircraft to entry a flat spin slightly faster than with the data of Reference 1. This effect is attributed to the wind tunnel rotary balance yawing moment data being more propelling than which was used in Reference 2. The current yawing moment rotary balance data is compared with the corresponding previous data in Figure D.4 at a spin coefficient ($\Omega_V b/2V$) equal to +.05.

D.3 The Effect of Using Rotary Balance Data Below Stall - Rotary balance data is used below stall so that the same modified equations of motion (see Section C.2) which utilize rotary balance data can be used in both the stall/near stall/departure analysis as well as the spin analysis. Using rotary balance data below stall allows a continuous progression from unstalled flight through departure all the way to the spin region. The purpose of this section is to compare the differences in departure characteristics using forced oscillation derivatives in the normal manner (see Section C.1) with results obtained by applying the forced oscillation derivatives to the oscillatory components of rotation and the rotary balance data as a function of steady state rotation. The yawing moment derivatives are used as an example of the forced oscillation derivatives being applied in the normal manner.

$$C_{n_p}\frac{pb}{2V} + C_{n_r}\frac{rb}{2V} = C_{n_1} \qquad \text{(Equation D.8)}$$

where p and r are the total roll rate and total yaw rate. An example of forced oscillation derivatives being applied to the oscillatory components of rotation and the rotary balance data being applied as a function of steady state rotation is presented below assuming $\beta = 0$.

$$C_{n_p} \frac{p_o b}{2V} + C_{n_r} \frac{r_o b}{2V} + C_n f\left(\frac{\Omega_V b}{2V}\right) = C_{n_2} \qquad \text{(Equation D.9)}$$

where $p_o$ and $r_o$ are the oscillatory rate components and

$$p_o = p - p_s$$

$$r_o = r - r_s$$

$$\Omega_V = \sqrt{p_s^2 + r_s^2}$$

$C_n f\left(\frac{\Omega_V b}{2V}\right)$ is calculated from Equation D.6 ($\beta = 0$)

where $p_s$ and $r_s$ are the steady rate components.

Thus combining Equations D.6 and D.9 yields

$$C_{n_p} \frac{p_o b}{2V} + C_{n_r} \frac{r_o b}{2V} + (C_{n_p} \cos\alpha + C_{n_r} \sin\alpha) \frac{\Omega_V b}{2V} = C_{n_2} \qquad \text{(Equation D.10)}$$

Using Equation D.4

$$p_o = p - \Omega_V \cos\alpha$$

$$r_o = r - \Omega_V \sin\alpha$$

Substitution of the above relations into Equation D.10 yields

$$C_{n_p} \left[ \frac{pb}{2V} - \cos\alpha \frac{\Omega_V b}{2V} \right] + C_{n_r} \left[ \frac{rb}{2V} - \sin\alpha \frac{\Omega_V b}{2V} \right]$$

$$+ \left[ C_{n_p} \cos\alpha + C_{n_r} \sin\alpha \right] \frac{\Omega_V b}{2V} = C_{n_2} = C_{n_1}$$

The sine and cosine terms cancel out and the result is the same as Equation D.8.

Thus when using Equations D.5, D.6, and D.7 to generate rotary balance data, the difference between using just forced oscillation data (applied to p and r) and forced oscillation data (applied only to $p_o$ and $r_o$) used to-

APPENDIX D

gether with rotary balance data (applied to $p_s$ and $r_s$) is quite small. The only approximation made was to assume that $\beta = 0$. A time history comparison (Figure D.5) of the two methods of applying dynamic data shows almost identical trajectories up to $30^o$ angle of attack.

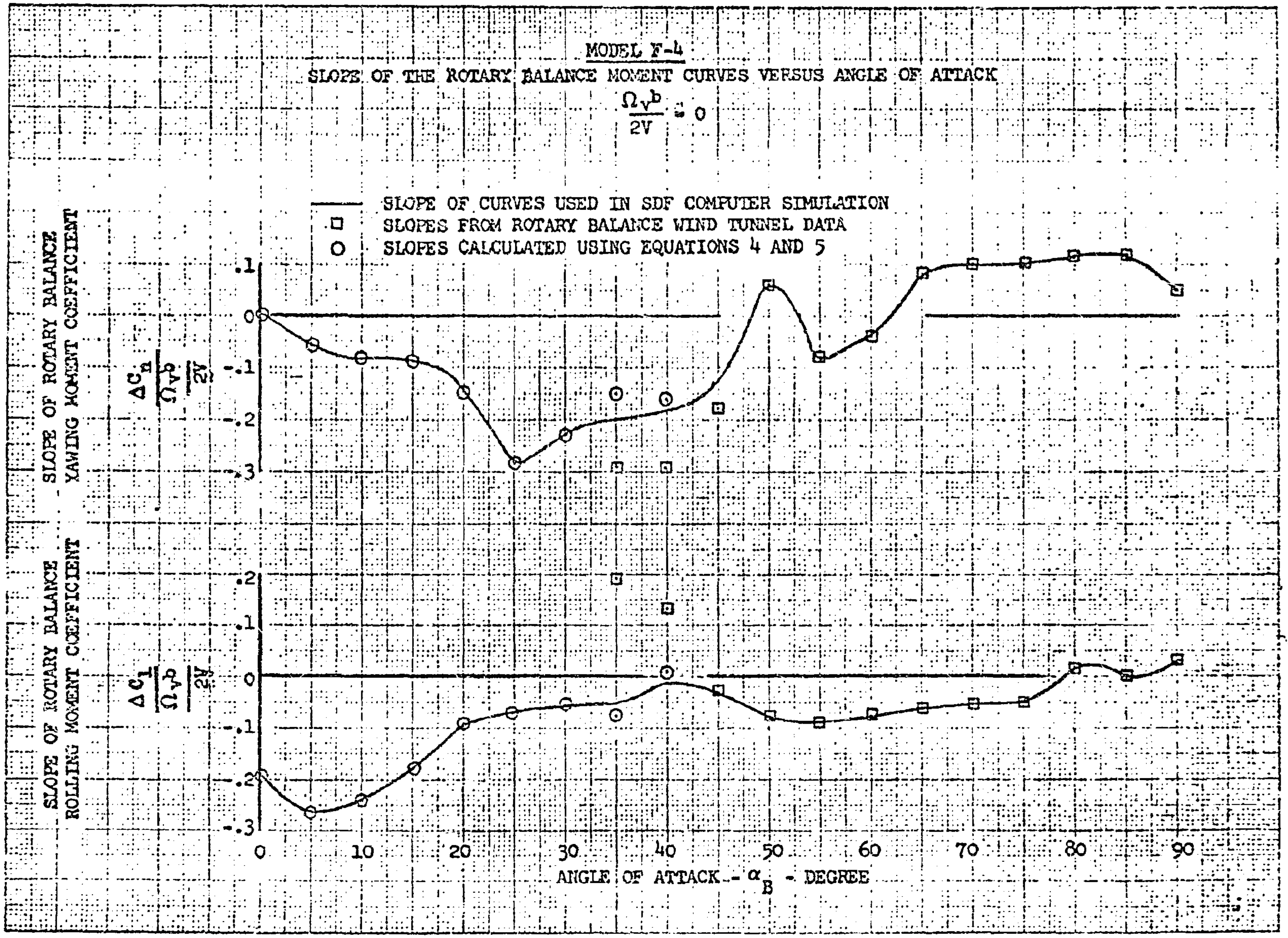

MODEL F-4

SLOPE OF THE ROTARY BALANCE MOMENT CURVES VERSUS ANGLE OF ATTACK

$\frac{\Omega_V b}{2V} \approx 0$

Figure D.1

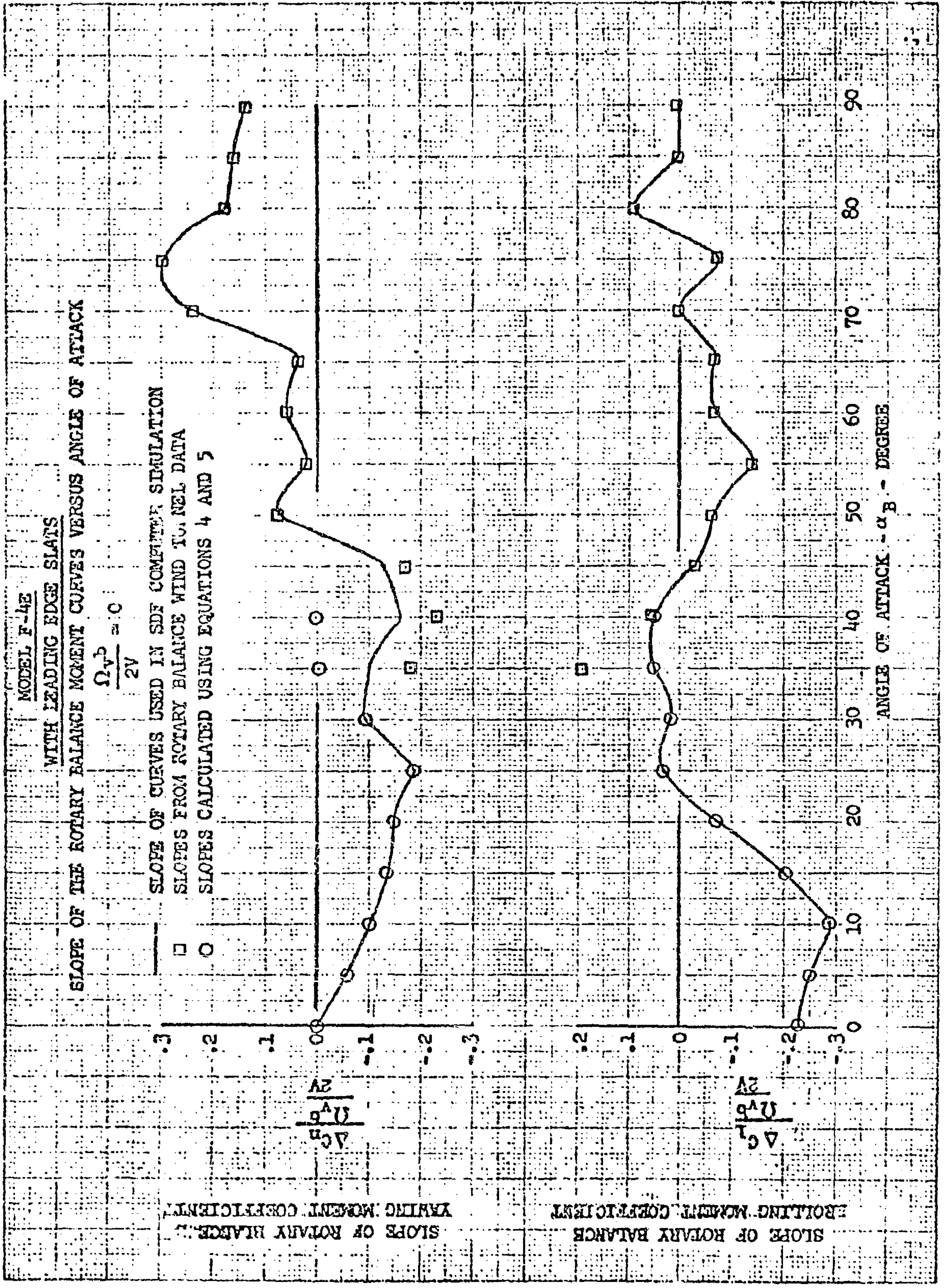

MODEL F-4E

WITH LEADING EDGE SLATS

SLOPE OF THE ROTARY BALANCE MOMENT CURVES VERSUS ANGLE OF ATTACK

$\frac{\Omega_V b}{2V} = 0$

Figure D.2

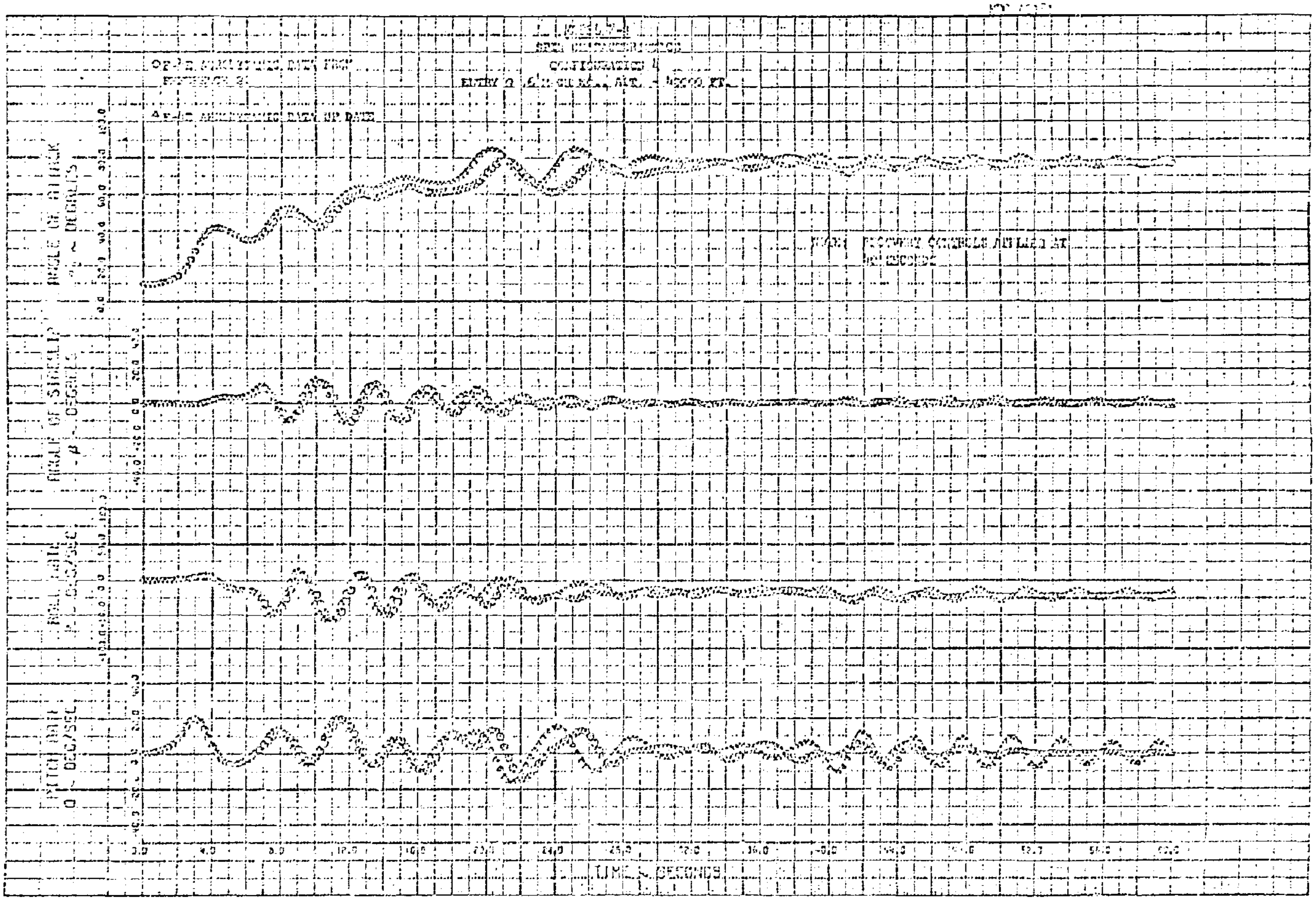
CONFIGURATION 4
NOTE: RECOVERY CONTROLS APPLIED AT
SECONDS
ANGLE OF ATTACK
α ~ DEGREES
ANGLE OF SIDESLIP
β ~ DEGREES
ROLL RATE
P ~ DEG/SEC
PITCH RATE
Q ~ DEG/SEC
0.0
4.0
8.0
12.0
16.0
20.0
24.0
28.0
32.0
36.0
40.0
44.0
48.0
52.0
56.0
60.0
TIME ~ SECONDS

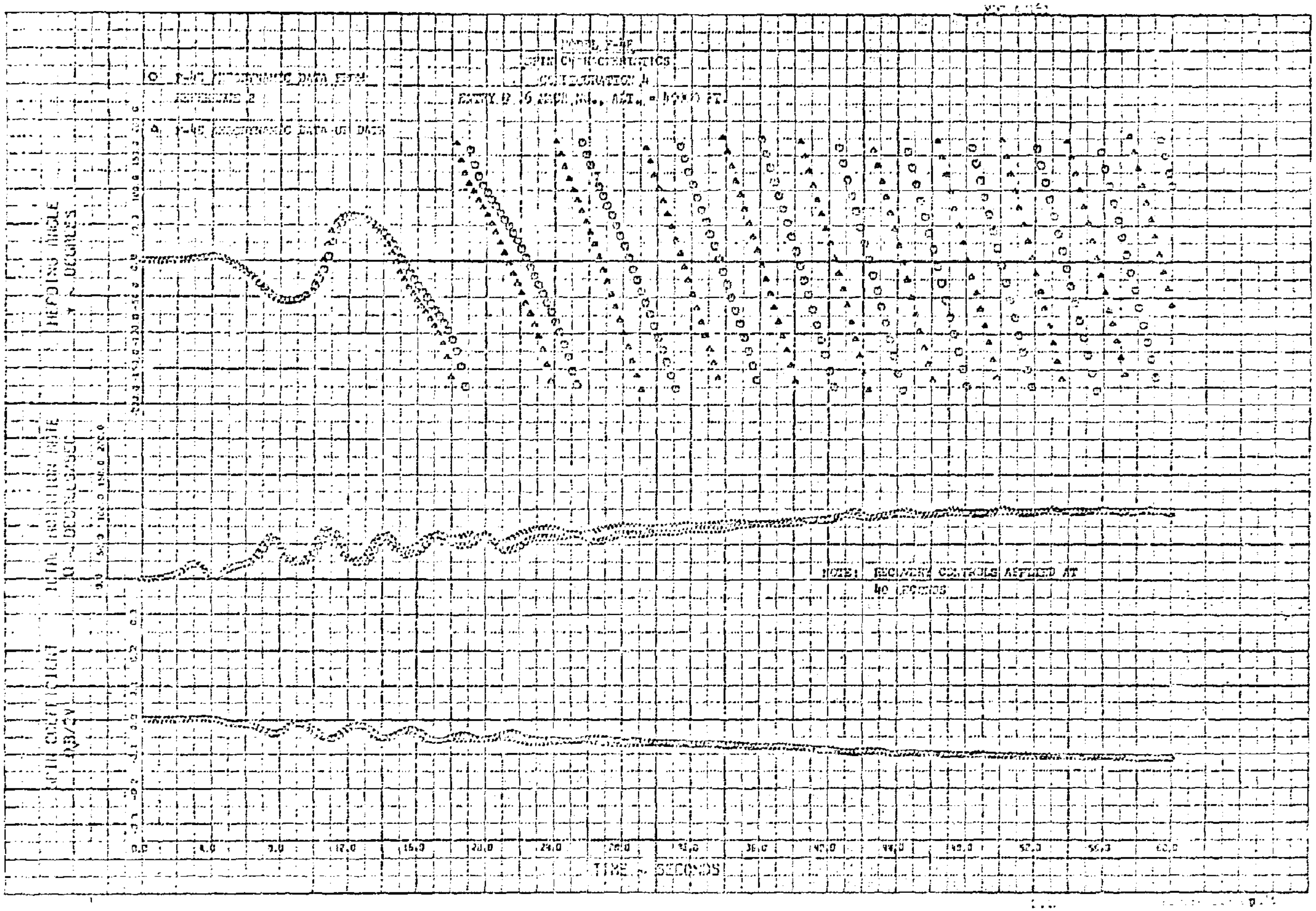
MODEL F-4E
SPIN CHARACTERISTICS
CONFIGURATION 4
ENTRY @ .6 MACH NO., ALT. = 35000 FT.
○ F-4E AERODYNAMIC DATA FROM REFERENCE 2
△ F-4E AERODYNAMIC DATA-UR DATA
HEADING ANGLE ψ ~ DEGREES
-200.0
-150.0
-100.0
-50.0
0.0
50.0
100.0
150.0
200.0
TOTAL ROTATION RATE Ω ~ DEGREES/SEC
0.0
50.0
100.0
150.0
200.0
SPIN COEFFICIENT Ωb/2V
-0.3
-0.2
-0.1
0.0
0.1
0.2
0.3
NOTE: RECOVERY CONTROLS APPLIED AT 40 SECONDS
0.0
4.0
8.0
12.0
16.0
20.0
24.0
28.0
32.0
36.0
40.0
44.0
48.0
52.0
56.0
60.0
TIME ~ SECONDS

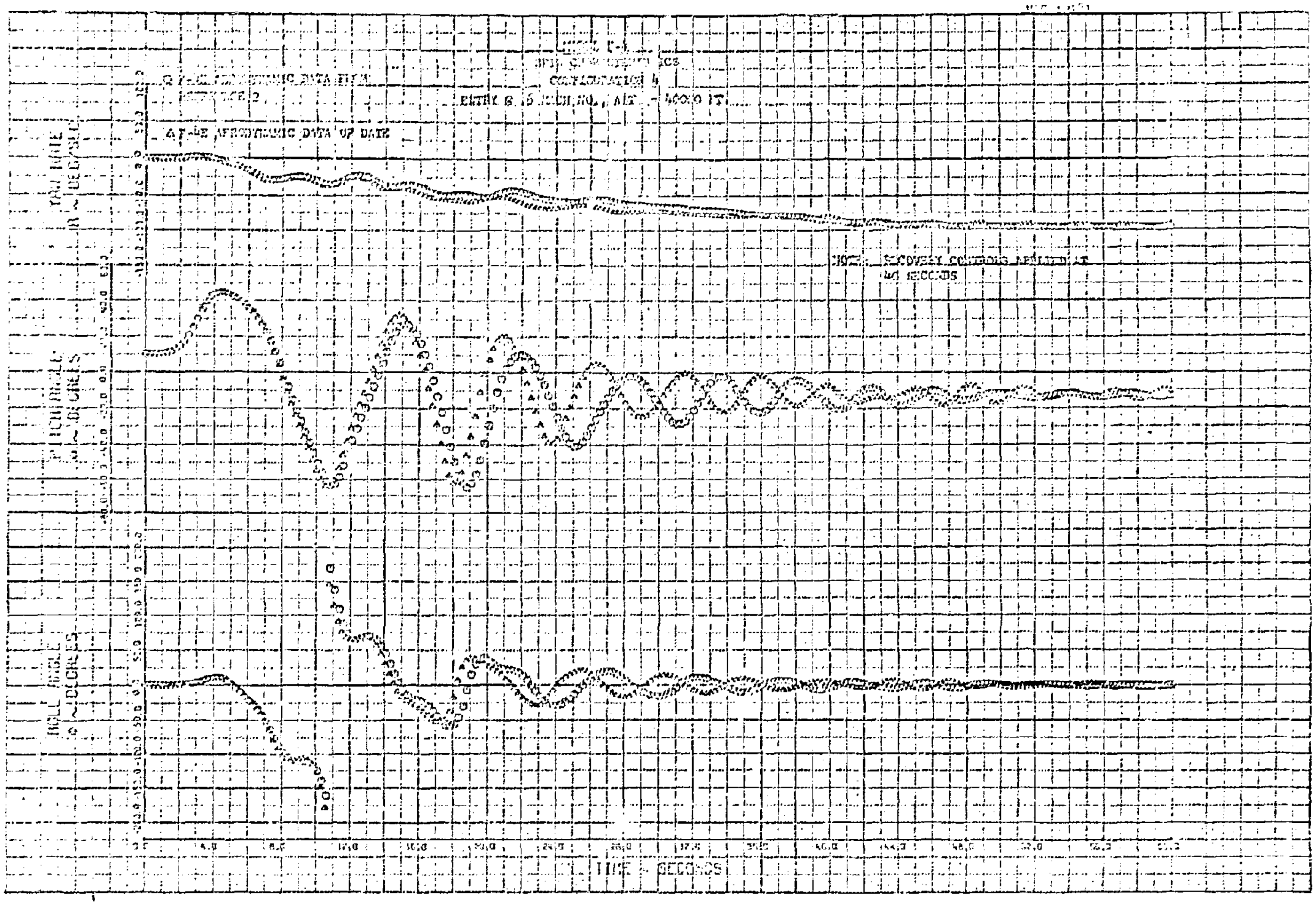

CONFIGURATION 4
ENTRY @ 15 MACH NO., ALT. = 4000.0 FT
PAGE 2
○ F-4E AERODYNAMIC DATA
△ F-4E AERODYNAMIC DATA UP DATE
NOTE: RECOVERY CONTROLS APPLIED AT 40 SECONDS
YAW RATE
R ~ DEG/SEC
PITCH ANGLE
θ ~ DEGREES
ROLL ANGLE
φ ~ DEGREES
0.0
4.0
8.0
12.0
16.0
20.0
24.0
28.0
32.0
36.0
40.0
44.0
48.0
52.0
56.0
60.0
TIME ~ SECONDS

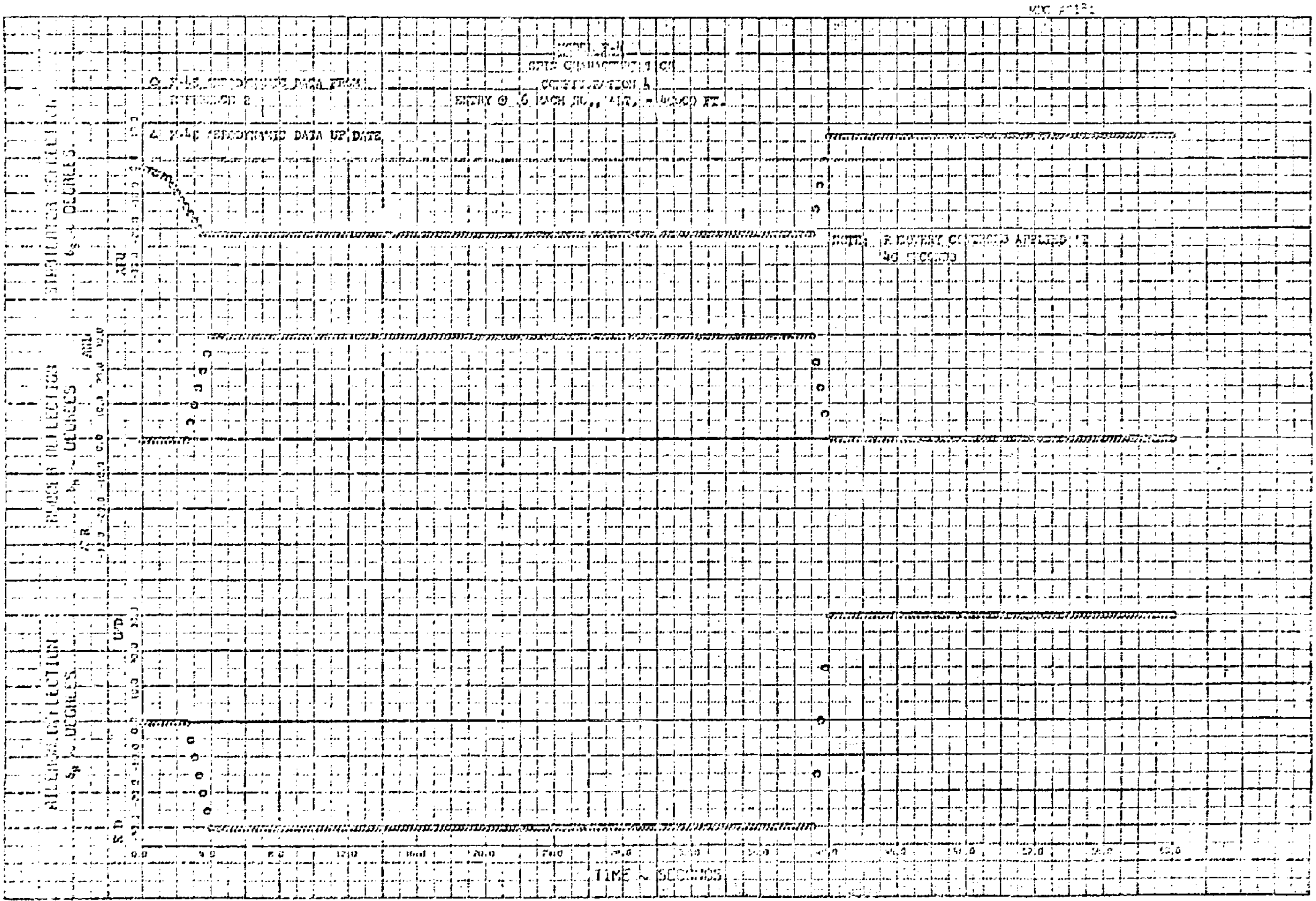

B.14

Figure B.3 Con't

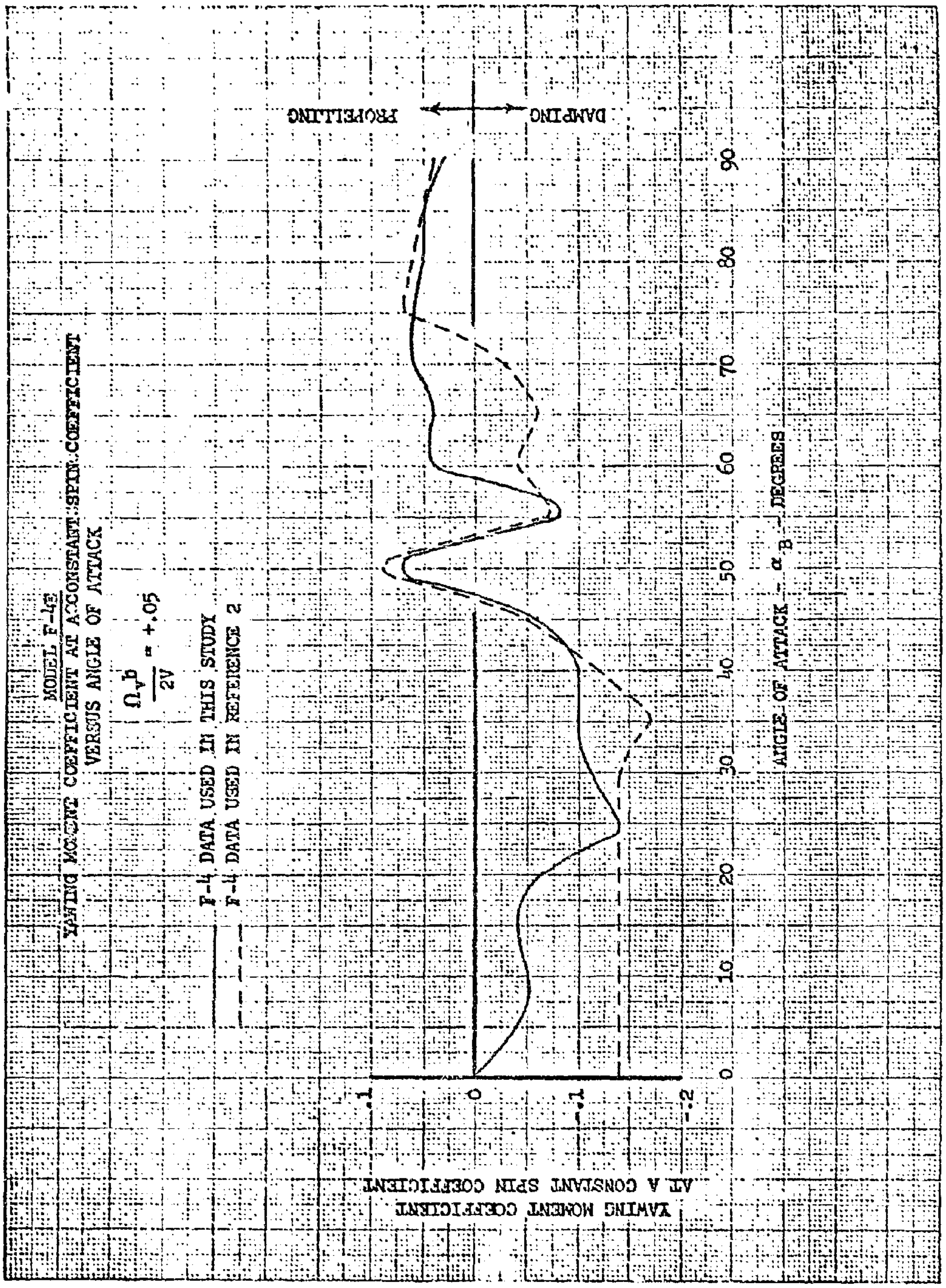
MODEL F-4E
YAWING MOMENT COEFFICIENT AT A CONSTANT SPIN COEFFICIENT
VERSUS ANGLE OF ATTACK
$\frac{\Omega_v b}{2V} = +.05$
F-4 DATA USED IN THIS STUDY
F-4 DATA USED IN REFERENCE 2
PROPELLING
DAMPING
.1
0
-.1
-.2
YAWING MOMENT COEFFICIENT
AT A CONSTANT SPIN COEFFICIENT
0
10
20
30
40
50
60
70
80
90
ANGLE OF ATTACK – $\alpha_B$ – DEGREES

Figure D.4

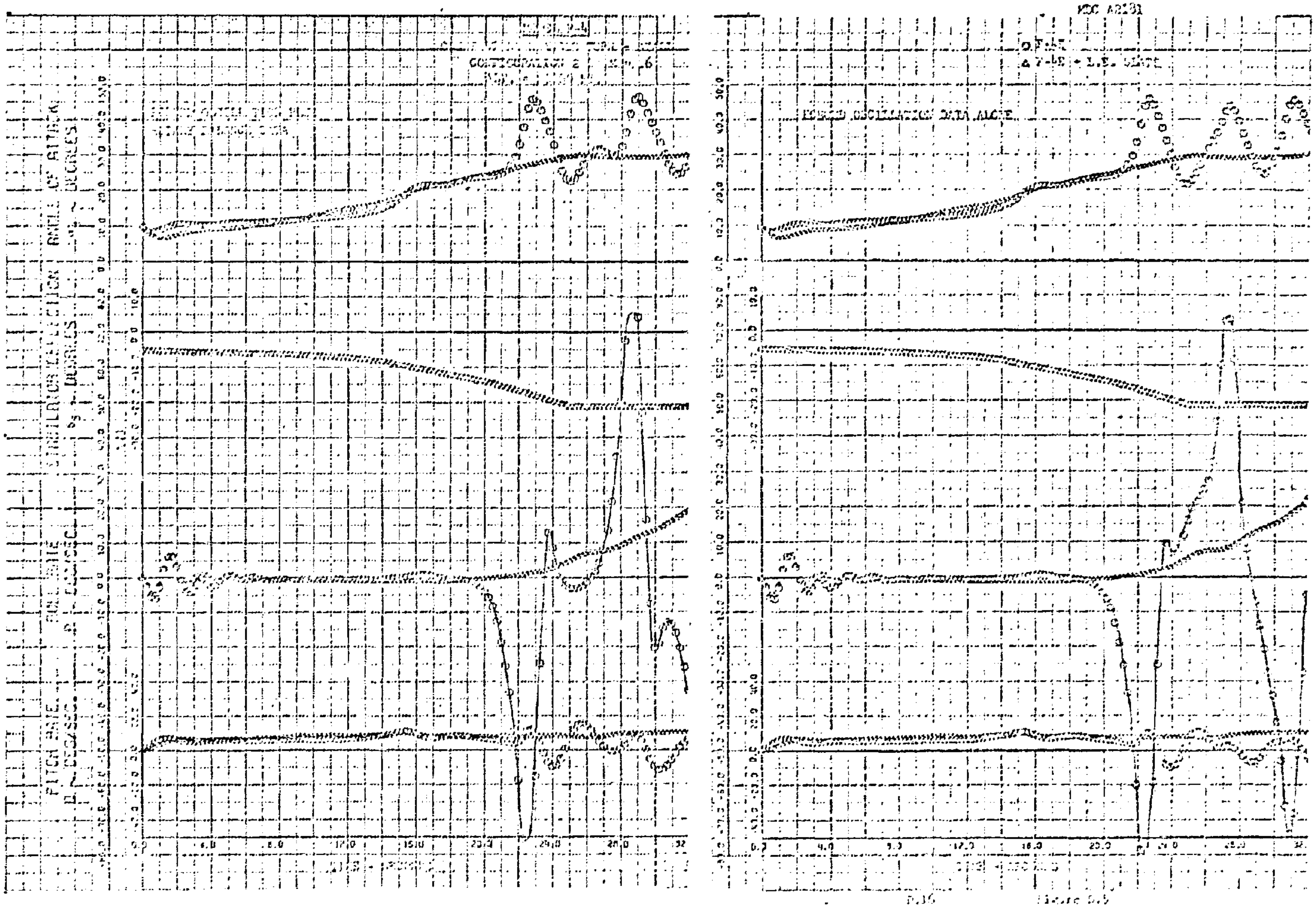
MDC A2131
○ F-15
△ F-15 + L.E. SLATS
FORCED OSCILLATION DATA ALONE
CONFIGURATION 2
ANGLE OF ATTACK
α ~ DEGREES
STABILATOR DEFLECTION
δs ~ DEGREES
ROLL RATE
p ~ DEG/SEC
PITCH RATE
q ~ DEG/SEC
0.0
4.0
8.0
12.0
16.0
20.0
24.0
28.0
32.
TIME ~ SECONDS

Figure D.5

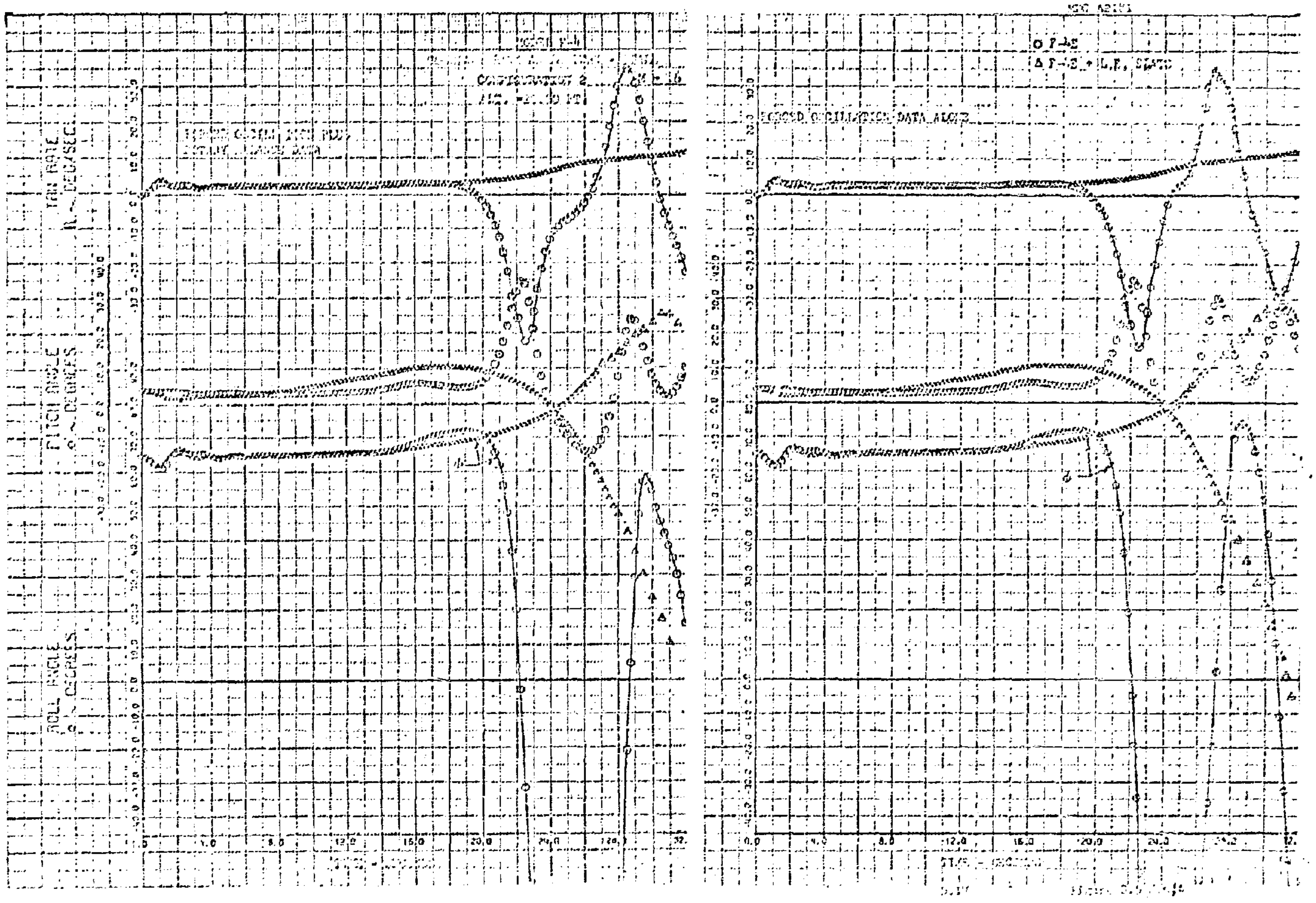
YAW RATE
R ~ DEG/SEC.
PITCH ANGLE
θ ~ DEGREES
ROLL ANGLE
φ ~ DEGREES
CONFIGURATION 2
SECOND OSCILLATION DATA ALONE
○ F-4E
Δ F-4E + L.E. SLATS
0.0
4.0
8.0
12.0
16.0
20.0
24.0
28.0
32.

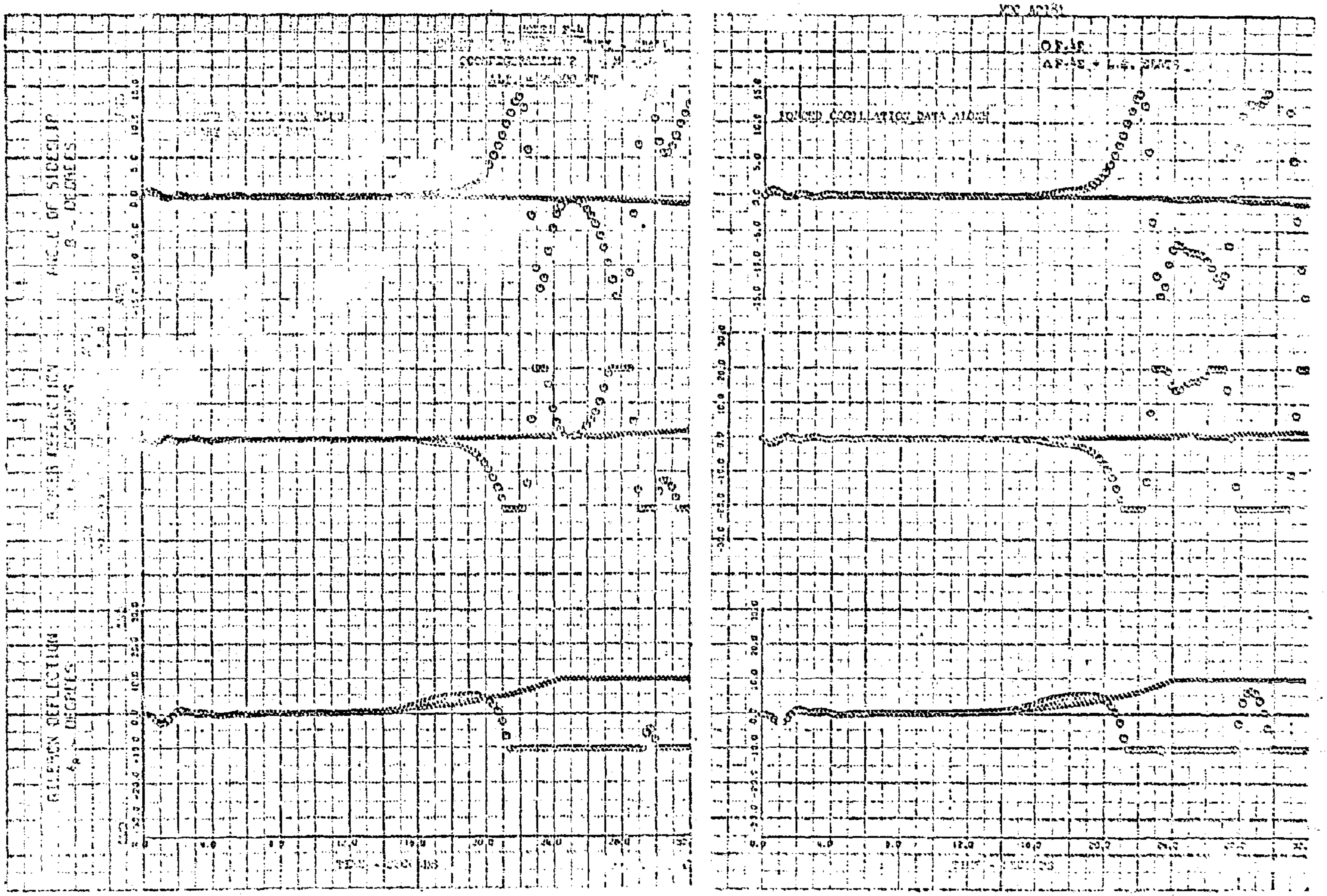

Figure 8.7 Cont'd